AD_____

Award Number: W81XWH-07-1-0193

TITLE: SPARKy-Spring Ankle with Regenerative Kinematics

PRINCIPAL INVESTIGATOR: Dr. Thomas Sugar

CONTRACTING ORGANIZATION: Arizona State University
Tempe, AZ 85287

REPORT DATE: September 2011

TYPE OF REPORT: Final

PREPARED FOR: U.S. Army Medical Research and Materiel Command
Fort Detrick, Maryland 21702-5012

DISTRIBUTION STATEMENT: Approved for public release; distribution unlimited

The views, opinions and/or findings contained in this report are those of the author(s) and should not be construed as an official Department of the Army position, policy or decision unless so designated by other documentation.

REPORT DOCUMENTATION PAGE

Form Approved
OMB No. 0704-0188

Public reporting burden for this collection of information is estimated to average 1 hour per response, including the time for reviewing instructions, searching existing data sources, gathering and maintaining the data needed, and completing and reviewing this collection of information. Send comments regarding this burden estimate or any other aspect of this collection of information, including suggestions for reducing this burden to Department of Defense, Washington Headquarters Services, Directorate for Information Operations and Reports (0704-0188), 1215 Jefferson Davis Highway, Suite 1204, Arlington, VA 22202-4302. Respondents should be aware that notwithstanding any other provision of law, no person shall be subject to any penalty for failing to comply with a collection of information if it does not display a currently valid OMB control number. **PLEASE DO NOT RETURN YOUR FORM TO THE ABOVE ADDRESS.**

1. REPORT DATE	2. REPORT TYPE	3. DATES COVERED *(From - To)*
September 2011	Final	1 FEB 2007 - 30 JUN 2011

4. TITLE AND SUBTITLE
SPARKy-Spring Ankle with Regenerative Kinematics

5a. CONTRACT NUMBER

5b. GRANT NUMBER
W81XWH-07-1-0193

5c. PROGRAM ELEMENT NUMBER

6. AUTHOR(S)
Dr. Thomas Sugar

E-Mail: thomas.sugar@asu.edu

5d. PROJECT NUMBER

5e. TASK NUMBER

5f. WORK UNIT NUMBER

7. PERFORMING ORGANIZATION NAME(S) AND ADDRESS(ES)
Arizona State University
Tempe, AZ 85287

8. PERFORMING ORGANIZATION REPORT NUMBER

9. SPONSORING / MONITORING AGENCY NAME(S) AND ADDRESS(ES)
U.S. Army Medical Research and Materiel Command
Fort Detrick, Maryland 21702-5012

10. SPONSOR/MONITOR'S ACRONYM(S)

11. SPONSOR/MONITOR'S REPORT NUMBER(S)

12. DISTRIBUTION / AVAILABILITY STATEMENT
Approved for Public Release; Distribution Unlimited

13. SUPPLEMENTARY NOTES

14. ABSTRACT

The goal is to design the Spring Ankle with Regenerative Kinetics (SPARKy) which seeks to develop a new generation of powered prosthetic devices based on the Robotic Tendon actuator. This actuator is a lightweight motor and transmission in series with a helical spring that significantly minimizes the peak power requirement of an electric motor and total system energy. The Robotic Tendon has kinetic advantages and stores and releases energy to provide SPARKy users with 100% of required push-off power and ankle range of motion comparable to able-bodied ankle motion while maintaining a form factor that is portable to the wearer. In the second year, we developed and tested a transtibial prosthesis that supports continuous unstructured walking for up to 2.8 hours. A pilot study with 2 subjects tested the device. All components are worn and are lightweight and portable. In the third year, jogging on a treadmill was demonstrated.

15. SUBJECT TERMS
Transtibial Prosthesis, regenerative, spring, wearable robot

16. SECURITY CLASSIFICATION OF:			17. LIMITATION OF ABSTRACT	18. NUMBER OF PAGES	19a. NAME OF RESPONSIBLE PERSON
a. REPORT	b. ABSTRACT	c. THIS PAGE			USAMRMC
U	U	U	UU	127	19b. TELEPHONE NUMBER *(include area code)*

Table of Contents

Introduction

"SPARKy – Spring Ankle with Regenerative Kinetics" to build a new generation of transtibial prostheses

Keywords: Transtibial Prosthesis, regenerative, spring, wearable robot

The goal is to design the *Spring Ankle with Regenerative Kinetics (SPARKy)* which seeks to develop a new generation of powered prosthetic devices based on the Robotic Tendon actuator. This actuator is a lightweight motor and transmission in series with a helical spring that significantly minimizes the peak power requirement of an electric motor and total system energy. The Robotic Tendon has kinetic advantages and stores and releases energy to provide SPARKy users with 100% of required push-off power and ankle range of motion comparable to able-bodied ankle motion while maintaining a form factor that is portable to the wearer.

Objective: The SPARKy Team using several unique technologies developed at Arizona State University's Human Machine Integration Lab will build a new generation of smart, active, energy-storing, transtibial prostheses that will support a Military amputee's return to active duty.

Military Relevance: Military amputees have unique requirements not found in the general amputee population. Military amputees are typically highly active and young. Their profession requires that they perform physically demanding dynamic tasks under severe conditions. Current state-of-the-art devices that are commercially available and in research do not address their unique requirements. SPARKy is the only device of its kind designed to address the technologically challenging requirements of the highly active Military amputees. SPARKy is very powerful and efficient. This will allow the amputee to carry heavy loads while walking at speeds up to 2 m/s. The mechanical design addresses the demanding nature of the service member's environment and conditions. For example, the complete electronics and power train package can easily be removed in the case of a malfunction in a field condition, so that the device transforms into a conventional prosthesis.

Public Purpose: A transtibial prosthetic device that satisfactorily mimics able-bodied gait can be used by the general public. Because of the prevalence of diabetes, the number of below-the- knee amputees will increase greatly. In the first year, we found that the subject's health improved because he was briskly walking on a treadmill with a powered prosthetic device.

Body

The **SPARKy** Project (Spring Ankle with Regenerative Kinetics)

Even today's most sophisticated microprocessor controlled foot-ankle prosthetic devices are passive. They lack internal elements that actively generate power, which is required during the "push-off" phase of normal able-bodied walking gait. Amputees must rely upon the limited spring-back available within the flexed elastic elements of their prostheses to provide power and energy and thus must modify their gait through compensation. Consequently, lower limb amputees expend 20-30% more metabolic power to walk at the same speed as able-bodied individuals. A key challenge in the development of an active foot-ankle prosthetic device is the lack of good power and energy density in current actuator technology. Human gait requires 250W of peak power and 36 Joules of energy per step (80kg subject at 0.8Hz walking rate). Even a highly efficient motor such as the RE75 by Maxon Precision Motors, Inc. rated for 250W continuous power with an appropriate gearbox would weigh 6.6 Kg. This significant weight is only the actuator and transmission. It does not include the electronics or the batteries.

In the first year, we designed the *Spring Ankle with Regenerative Kinetics (SPARKy)* which uses a new generation of powered prosthetic devices based on the Robotic Tendon actuator. This actuator is a lightweight motor and lead screw in series with a helical spring that significantly minimizes the peak power requirement of an electric motor and total system energy. The kinetic advantages of the Robotic Tendon will be shown along with the electro-mechanical design and analysis that will provide SPARKy users with 100% of required push-off power and ankle range of motion comparable to able-bodied ankle motion while maintaining a form factor that is portable to the wearer.

In the second year, we developed and tested a transtibial prosthesis that will support continuous unstructured walking for up to 2.8 hours. A pilot study with 2 subjects tested the device. All components are worn and are lightweight and portable.

In the third year, we developed a transtibial prosthesis that will transition from walking to jogging on a treadmill. We are designing new controllers this year studying different types of microprocessors.

SPARKy Project Overview

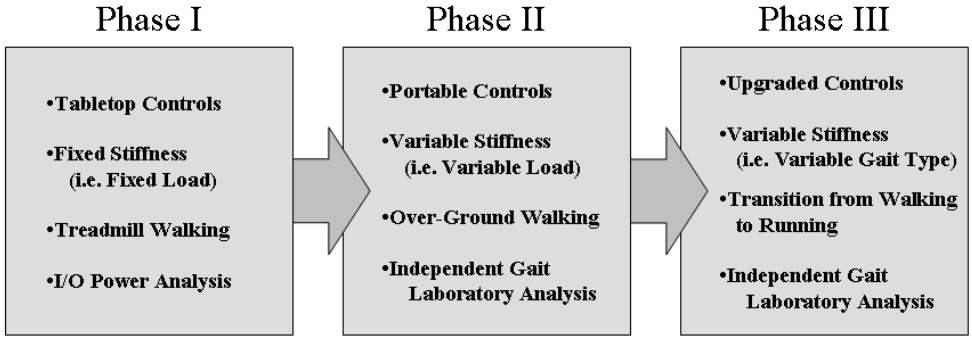

Phase 1. To develop, test and demonstrate a transtibial prosthesis based on our "Robotic Tendon" technology (Months 1-12):

a. Design and build SPARKy I with the capability to support walking on a treadmill. Sensor feedback will identify user intent to start, stop and change speed. The device will continue to passively support walking even in the event of battery failure. (Months 1-8).

This subtask has been completed. Sensor feedback allows the user to start, stop and adjust their speed when walking on a treadmill. When power is lost, the pylon is locked in place and the user will walk on the passive carbon fiber keel.

In our design considerations, we kept the passive carbon fiber keel to allow for walking in the event of battery failure.

b. Test and iterate the design with selected transtibial amputees. (Months 9-11).

We have recruited one subject and have tested the design. We are using a harness mounted above the treadmill for safety.

c. Demonstrate SPARKy I to MARP and TATRC. (Month 12).

Completed on November 2nd, 2007 at Brooke Army Medical Center.

Phase 2.To develop, test and demonstrate a transtibial prosthesis for over ground unstructured walking (Months 13-24):

a. Design and build SPARKy 2a with the capability to support continuous, unstructured walking for up to 2.8 hours. Mechanical tunability and sensor feedback will allow for variations in load, speed, and environment within the bounds of walking. All componentry will be lightweight, self-contained, and portable. (Months 13-20).

SPARKy 2a has been designed and built. Testing of the mechanical design is on going. A microprocessor has been chosen and code has been ported to the microprocessor. The microprocessor unit has been attached to the device and drives a brushed RE40 DC motor.

b. Bounds of walking (up to 2 m/s) will include walking on flat even surfaces, walking on inclines/declines, and ascending/descending stairs

We are able to walk continuously over ground and can walk up and down slopes and stairs. Walking up a slope and ascending stairs needs to be improved, adding extra propulsion. The propulsion walking down stairs needs to be reduced.

c. Test and iterate the design with two selected transtibial amputees at Arizona State University.

A second subject has been recruited and a new socket has been manufactured. The second subject has successfully worn SPARKy 2a.

d. Testing will include motion capture and oxygen consumption measures and will be independently conducted by another research team at Washington University, Saint Louis, MO. (Months 21-23).

SPARKY 1a has been delivered to Washington University on January 11, 2009 for initial fitting and testing.

e. Demonstrate SPARKy II to Brooke Army Medical Center. (Month 24). Demonstrated SPARKy II on October 22, 2009.

Phase 3. To expand the capabilities of SPARKy II so that the device supports treadmill jogging (Months 25-36):

a. Modify hardware and upgrade control software for SPARKy II, which will allow the device to support the transition from walking to jogging and permit continuous jogging (2.5 to 4 m/s for up to 1 hour). (Months 25-32).

We are working in conjunction with LTC Joseph Hitt to develop a jogging prosthesis. Jogging was first demonstrated on April 16th and April 23rd, 2010 at West Point.

b. Test and iterate the design with selected transtibial amputees. Again, the task will include independent motion capture and oxygen consumption tests at Saint Louis University Hospital, Saint Louis, MO. (Months 33-35).

In process

c. Demonstrate SPARKY III to MARP and TATRC. (Month 36).

Program Line Review on July 27th, 2010.

Phase 2 Deliverables

Deliverables:

1. Design and construction of SPARKy 2a - **Completed**
2. Develop a rate gyro based controller for over ground walking - **Completed**
3. Test able bodied subjects walking on flat even surfaces, inclines/declines, and ascending/descending stairs – **Completed**
4. Using able bodied test data, a controller will be developed for over ground walking that includes inclines/declines and ascending/descending stairs – **Completed**
5. Develop a compact microprocessor - **Completed**
6. Develop a compact brushless DC motor amplifier – **Stopped working on this item**
7. Port Matlab code to microprocessor **Completed**
8. Test SPARKy 2a on two transtibial amputees at Arizona State University **Completed**
9. Conduct and Independent Motion Capture and Oxygen Consumption Test. **In Process**

Phase 3 Deliverables

Deliverables:

10. Design and construction of SPARKy 3a
    a. Developing an ankle in conjunction with West Point **Completed**
11. Develop a rate gyro based controller for treadmill jogging
    a. Jogging was demonstrated at West Point on April 23rd, 2010 **Completed**
12. Develop a compact microprocessor
    a. Investigating new microprocessors **Completed**
13. Develop a compact brushless DC motor amplifier **Completed**
    a. Using AMC AZBE40A8
14. Port Matlab code to microprocessor **Completed**
    a. Using Matlab, Real Time Workshop, MPLAB from Microchip, and the Kerheul Toolbox
15. Test SPARKy 3a on two transtibial amputees at Arizona State University **Completed**
16. Conduct and Independent Motion Capture and Oxygen Consumption Test. **In process**

Background Material

Due to its repetitive nature, the discussion of gait is done in terms of percentages of a gait cycle. A gait cycle is defined for a single leg and begins with the initial contact of the foot with the ground or `heel strike', the conclusion of a cycle occurs as the same foot makes a second `heel strike'. To illustrate a typical pattern of gait, consider the kinematics and kinetics of a normal ankle, see Figures 1 and 2. Notice, the ankle moment (torque) data is normalized by body weight, kg. The gait data is based on inverse dynamic calculations.

In figure 1, peak ankle moment occurs at roughly 45% of the gait cycle and at a value of -1.25 Nm/kg or for an 80 kg person, -100 Nm. The negative sign represents the physiological direction for which the moment occurs; in this case, peak moment is acting to move the foot in a toes-down direction. As an interesting note, at the point at which the peak moment occurs, the ankle angle begins a rapid descent to its lowest overall value of -24° at 60% of the gait cycle. The region of gait approximately between 45% and 60% of the gait cycle is known as `push off'. At the conclusion of `push off', now considered `toe off', the leg initiates `swing' and the foot is then positioned for the next `heel strike'.

Use of the term **Robotic Tendon** implies an analogy to human physiology. The simple inclusion of a spring to a linear actuator can provide energy and power savings to the design of a wearable robotic device. The premise is that the human muscular system uses the advantages inherent in its elastic nature. Those advantages are a minimization of both work and peak power. In terms of an electric motor, *minimizing peak power* implies the reduction of requirements for motor size and thus *weight*. Minimizing work implies a *reduction of stored energy* supply or longer battery life.

A conceptual model of the Robotic Tendon can be seen in Figure 3. In the prosthetic system, the forces and displacements are based upon able body ankle gait patterns.

In contrast to a direct drive example, our spring based actuator design has very different characteristics. Using the simple model of the Robotic Tendon in Figure 3, comparisons to direct drive approaches can be seen. In a direct drive approach, the stiffness *K* can be considered nearly infinite, thus all of the environmental displacements must come from the linear actuator.

From Figure 3, a development of motor power requirements based upon stiffness *K* can be derived. The position of the environment, x_g, is given by converting the joint angles of gait to linear displacement using a simple *lever arm*. The motor position is thus a combination of the position of the environment, x_g, and the position of the spring, x_s.

Unlike other elastic robot designs, it is important to note that the motor is *position controlled* which is very simple and economical. The position of the motor is adjusted based on the desired gait kinematics and kinetics. The ankle does not interact directly with the motor but interacts directly with the spring. Repeating the previous statement, the motor controls the input side (proximal side) of the spring and the output side (distal side) of the spring is *not controlled*, but moves based on the user.

In 2007, we are the first to show that a SLIP model (Spring Loaded Inverted Pendulum model) works very well for walking. In the past, it was shown to work for running.

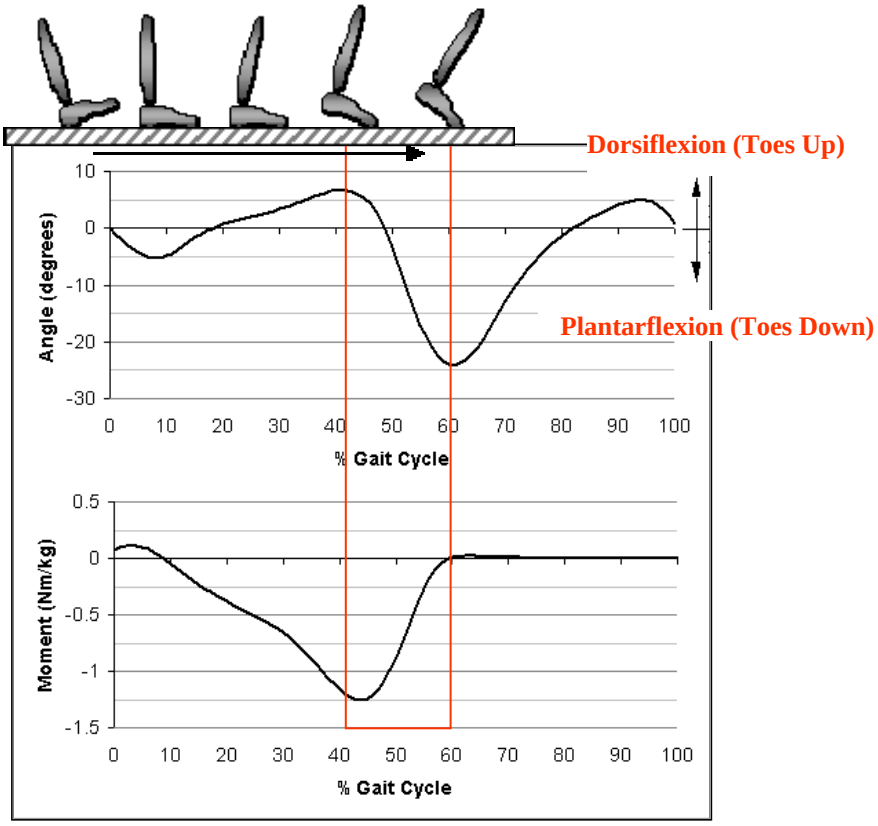

Figure 1: Normal ankle gait kinematics and kinetics.

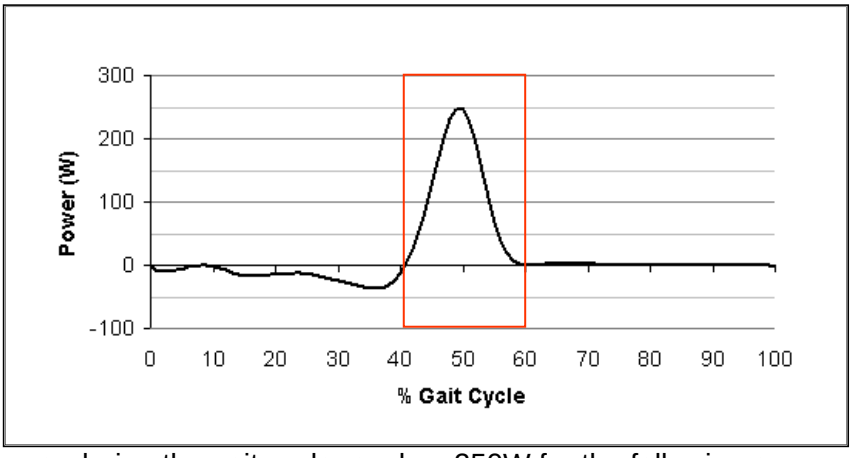

Figure 2: The power during the gait cycle reaches 250W for the following assumptions: 80 kg person, walking at 0.8 Hz (1.25 sec/cycle).

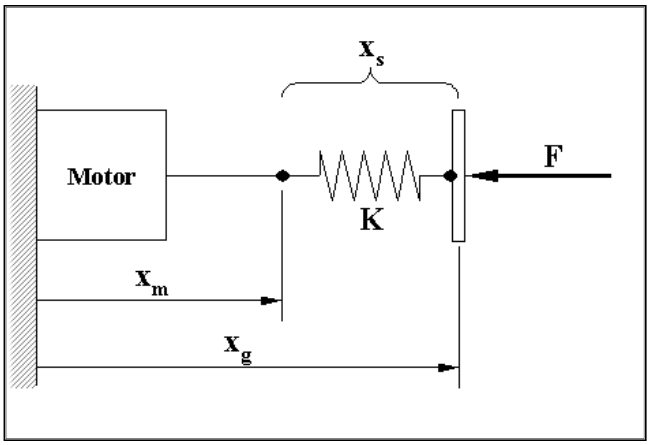

Figure 3: Robotic Tendon Model: A motor and spring in series (spring is tuned for proper gait). We use a position controller to place the spring at the correct location at the correct time. The motor controls the input side of the spring and the output side of the spring is *not controlled*, but moves based on the user.

Power Analysis

$$F = K(a_o - x_s)$$

$$x_m = x_g + \frac{F}{K} - a_o$$

$$\left(P_m\right)_{\text{peak}} = \max\left|F \cdot \dot{x}_g + \frac{F \cdot \dot{F}}{K}\right|$$

gait power spring power

Human ankle gait power, $F\dot{x}_g$, can be both negative and positive. When it is negative, a resistance motion is applied to the ankle and when it is positive a propelling motion is applied. A motor unit must provide power, P_m, to both resist and propel human motion. For this reason, a direct-drive solution is not energy efficient because the motor is used to resist the motion. Values for force, F, velocity, $\dot{x}_g$, and $\dot{F}$ can all be determined from human gait analysis data; thus stiffness, K, becomes the only design parameter to reduce the peak motor power.

To design an assistive robotic device for gait, understanding motor velocity and power requirements is fundamental. Consider the case where spring stiffness, K, is nearly infinite (i.e. direct drive). In this example the spring power term drops to zero and the motor must provide the absolute value of normal gait power. In the opposite case, consider a spring with stiffness near zero. In the second example, the power requirements tend toward infinity. If we were to assume a straight line between these two cases it would appear that one could never do any better than a direct drive scenario. Fortunately, this simplistic relationship is not the case. On the contrary, if a spring is properly selected both energy and peak power for a motor required to perform human gait can be drastically reduced compared to the direct drive analogy.

Basic System Principles:

The operating principles of SPARKy are shown in Figure 4. During the stance phase, the leg rolls over the ankle pulling on the output side (distal side) of the spring. The motor also pulls on the input side (proximal side) of the spring adding stored energy as well. The stored energy is then released quickly during powered plantarflexion.

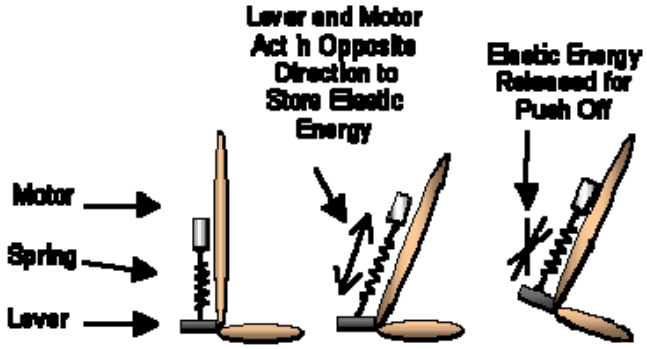

Figure 4: In our prosthetic ankle, the motor and spring are mounted behind the leg. We use springs to store and release the needed energy. As the leg rolls over the ankle, the motor attached to the proximal side of the spring and the lever attached to the keel and the distal side of the spring both pull on the spring in opposite directions. The stored energy is then released for powered plantarflexion.

In our design we chose springs because of the following reasons.

- Springs are Powerful
- Springs are Efficient
- Springs are Lightweight
- Springs are Economical
- Springs are Compliant

Our robotic tendon gives us the following benefits.

- Input Power reduced by 2/3
- Weight reduced by a factor of 7
- Input Energy is 1/2 of direct drive example

SPARKy Phase 1 Design

Figure 5:

1. A Robotic Tendon is mounted behind the leg.
2. Springs are used to store and release energy.
3. Very efficient and lightweight RE40 motor is used.
4. Efficient gearbox and lead screw design.
5. Rod ends are used to quickly adjust the lever arm length.
6. The sensors used include a motor encoder, ankle encoder, and a heel switch.
7. Energy efficient carbon fiber keel is integrated into the device.

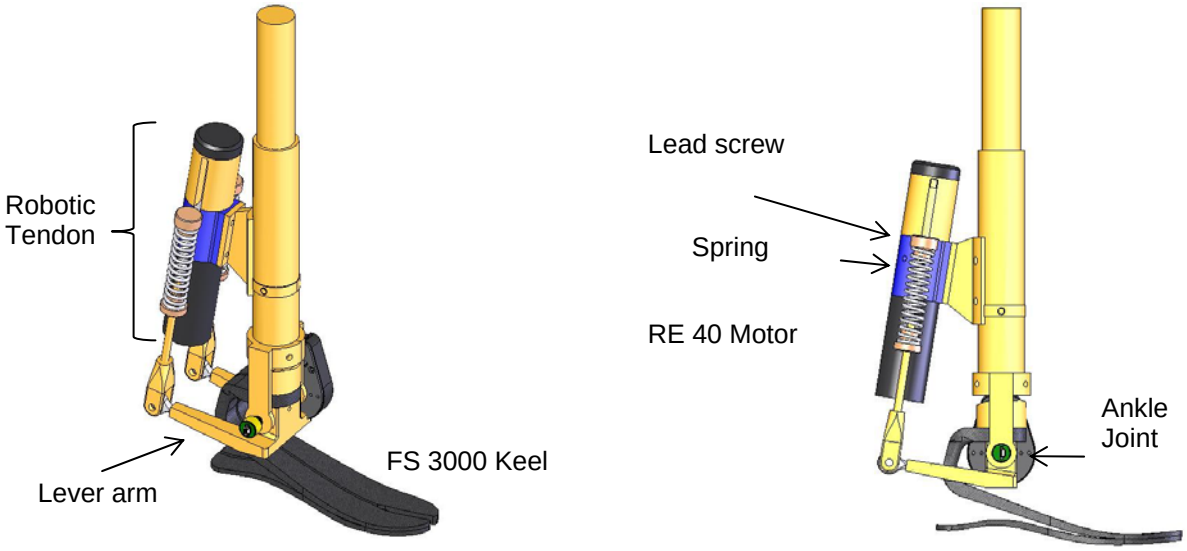

Figure 6: Isometric and side views of SPARKy Phase 1 as modeled in SolidWorks. The Robotic Tendon actuator provides a dynamic moment about the ankle joint.

SPARKy Phase 2 Design

Figure 7. SPARKy 2a: It weighs less than 3.0 kg and will use a RE40 DC motor along with a custom roller screw. The sole of the shoe to the top of the Robotic tendon measures 12.9 inches.

- The refined SPARKy design uses the RE40 motor, roller screw robotic tendon and FS3000 keel.
- Total Weight: 5 lbs not including socket
- Box Dimensions: 9.6 L x 3.7 W x 12.9 H (inches)
- Min. Clearance Height: 5.5 inches

Human Subject Data:

Our system provides ankle motion that is comparable to able-bodied gait. See Figure 8.

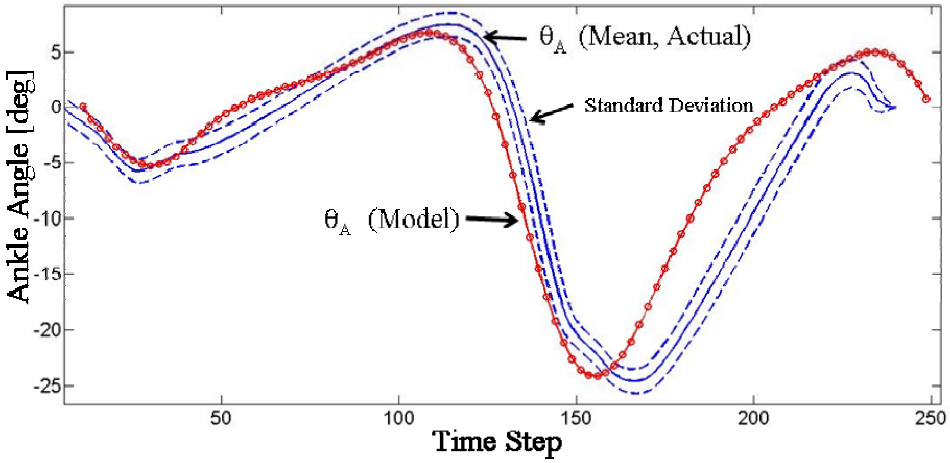

Figure 8: The subject walks on a treadmill at 2.2 mph. The ankle has 9 degrees of dorsiflexion and more importantly 23 degrees of plantarflexion based on the actual lever displacement. The user has complete control of the ankle motion because the output side of the spring is not controlled. The actual lever displacement fits the model extremely well.

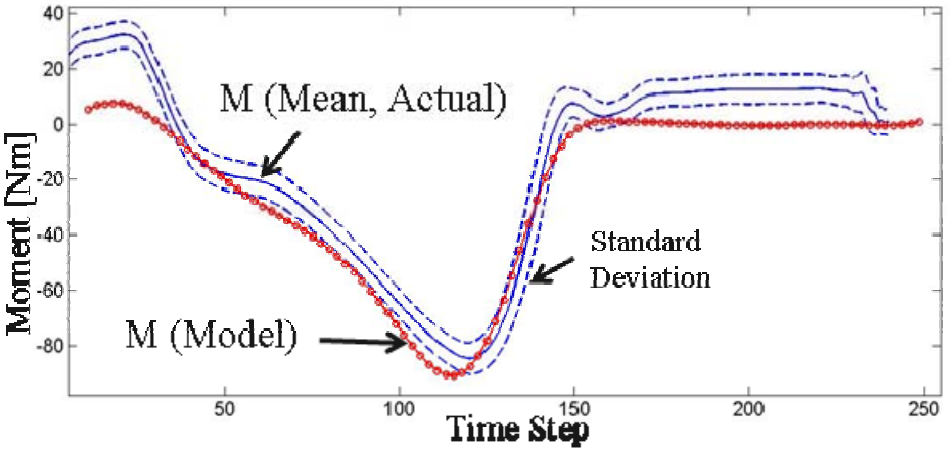

Figure 9: The subject walks on a treadmill at 2.2 mph. The ankle moment matches the model very well.

Our system provides 100% of required push-off power. See Figure 10. Our subject requires 250 Watts of push off power, but the motor supplies only 55 watts of power. How is this possible? A power amplification of 4.5 is achieved because the user stores energy in the spring as the leg rolls over the ankle in the stance phase. The motor stores additional energy in the stance phase, and then the spring quickly releases the energy during powered plantarflexion.

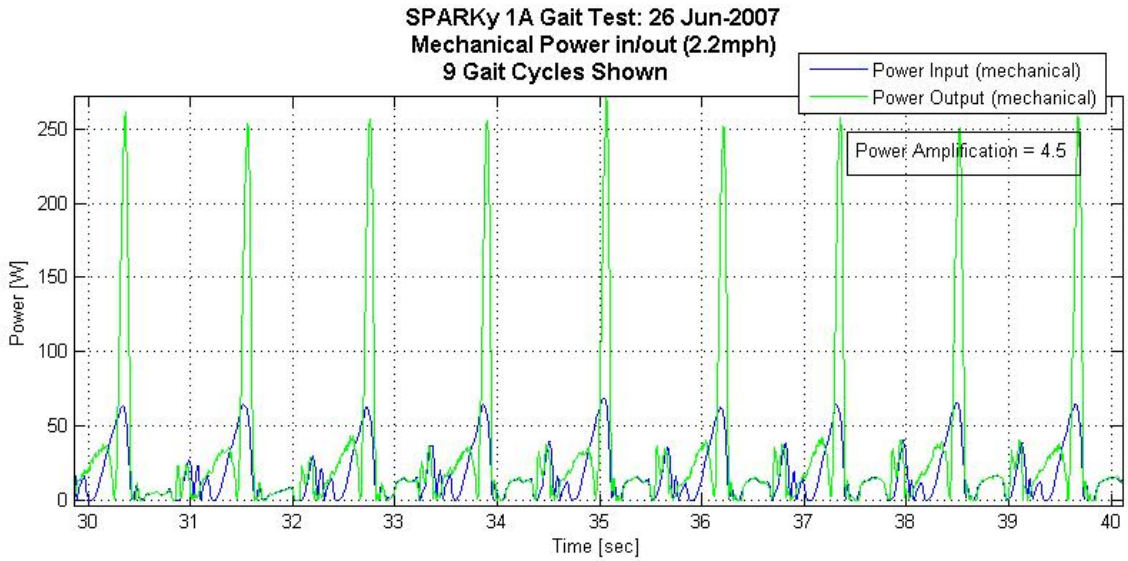

Figure 10: The subject walks on a treadmill at 2.2 mph. At push off, the motor supplies 55 watts of power to the input side of the spring. The output side of the spring supplies 250 watts of power to the subject allowing for powered plantarflexion. This is only possible if the spring stores energy during the stance phase and quickly releases the energy in a powerful burst at push-off.

In Figure 11, the true energy supplied to the device is shown. In real-time, the current and voltage to the motor are measured.

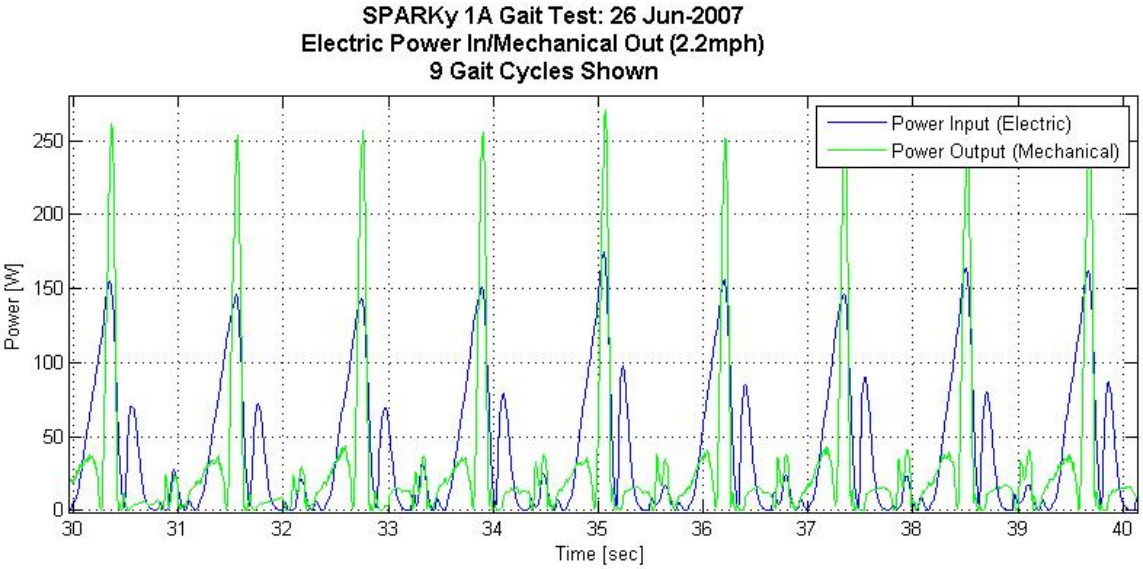

Figure 11: The subject walks on a treadmill at 2.2 mph. At push off, the motor supplies 55 watts of power to the input side of the spring. Because the gearbox, leadscrew, and motor are not perfectly efficient, the electrical input is 150 watts at push off. The output side of the spring supplies 250 watts of power to the subject allowing for powered plantarflexion.

The same data is repeated for the subject walking at 3mph. See Figures 12, and 13.

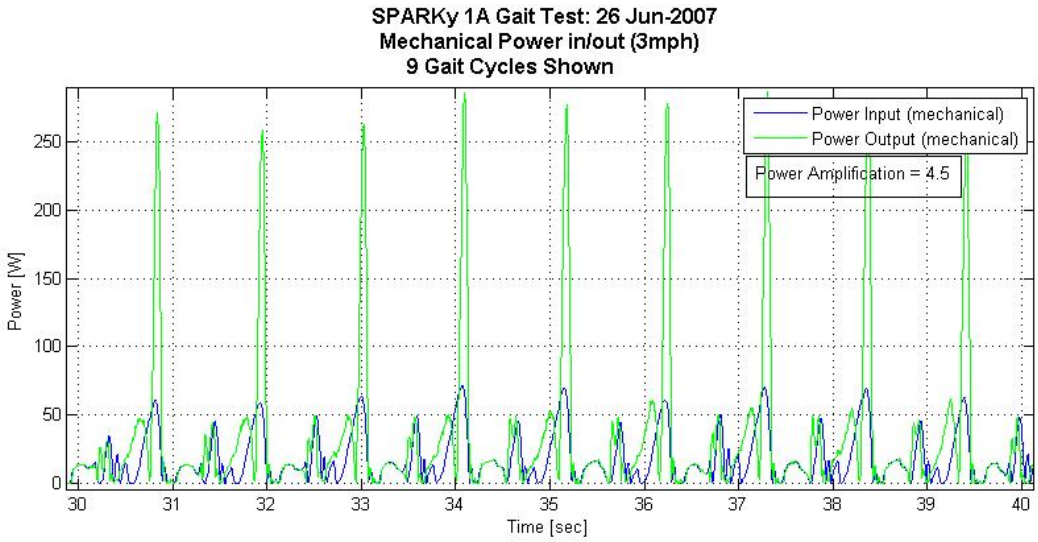

Figure 12: The subject walks on a treadmill at 3 mph. At push off, the motor supplies 60 watts of power to the input side of the spring. The output side of the spring supplies 270 watts of power to the subject allowing for powered plantarflexion. This is only possible if the spring stores energy during the stance phase and quickly releases the energy in a powerful burst at push-off.

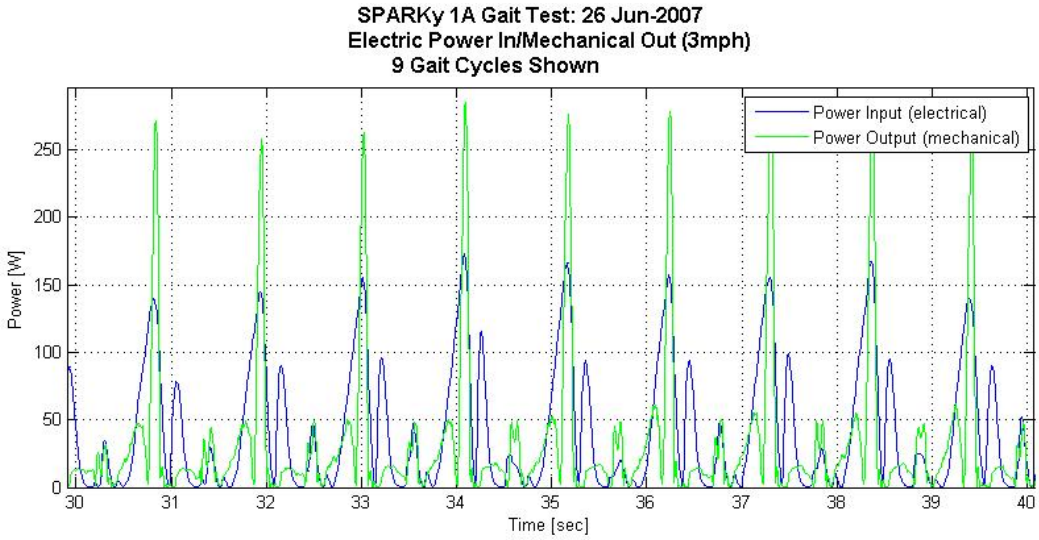

Figure 13: The subject walks on a treadmill at 3 mph. At push off, the motor supplies 60 watts of power to the input side of the spring. Because the gearbox, leadscrew, and motor are not perfectly efficient, the electrical input is 150-160 watts at push off. The output side of the spring supplies 270 watts of power to the subject allowing for powered plantarflexion.

In Figure 14, multiple gait cycles are averaged together. The peak of the mean output power curve is compared to the peak of the main motor input power curve and a power amplification of 3.7 was determined. A sophisticated model of the Robotic Tendon that includes motor inertia, gearbox dynamics, friction, and lead screw dynamics was created. Using this derived model, an output power curve and a motor power curve were simulated.

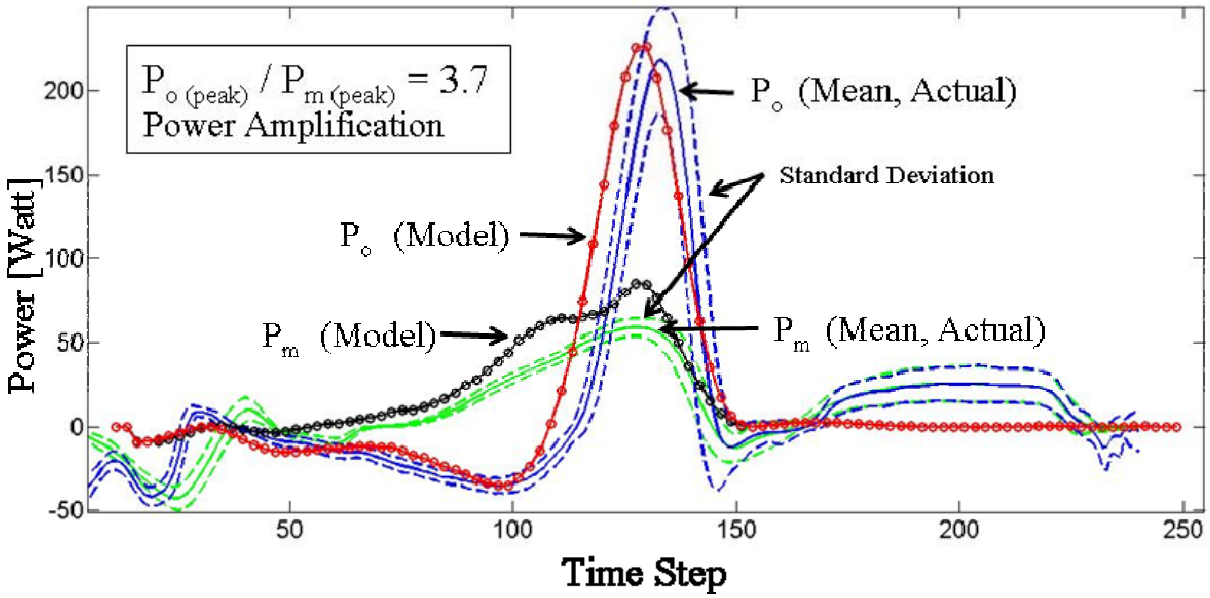

Figure 14: The subject walks at 2.2 mph. Measured power out, $P_{o,}$ and power at the nut, P_m, for the test series with a 36KN/m spring and a 9 cm lever at 1 m/s (2.2 mph). The figure shows the mean and standard deviation of the data and its corresponding models, as annotated. Note that the device achieves a very high level of power amplification of 3.7. This is the unique advantage of a Robotic Tendon. A sophisticated model was built to simulate a gait cycle and the model data matches the mean data well.

Testing of SPARKy Phase 2:

Sparky 2a has been designed and built. We are able to continuously walk over ground, walk up and down slopes and stairs, and walk forwards and backwards. See Figures 15, 16, and 17.

Figure 15: Subject is walking over ground on a flat surface.

Figure 16: Subject is walking on an inclined surface where the angle is constantly changing. Two small batteries are carried at the waist.

Figure 17: Subject is able to ascend and descend stairs.

Shank Based Controller

In the phase 2, we developed a tibia based controller or a "shank based controller." Our goal was to develop a continuous based controller for walking. We wanted to eliminate the need for state based control and heel strike sensors. In our phase 1 research, if the heel strike sensor was not pressed, then the motor pattern was not initiated. Also, the user can be tricked by a state based controller if each state is not initiated in the correct pattern. Lastly, it is tricky to formally test a state based controller because all of the different states must be tested in multiple scenarios. Testing 4 states in 4 scenarios could lead to testing 4 to the power 4 cases which equals 256 trials.

We measured the shank angle in world coordinates for different stride lengths, see Figure 18. Calculating the gait percent uniquely from this curve is not possible. For example, the angle 0 degrees corresponds to approximately 35% and 88% of gait.

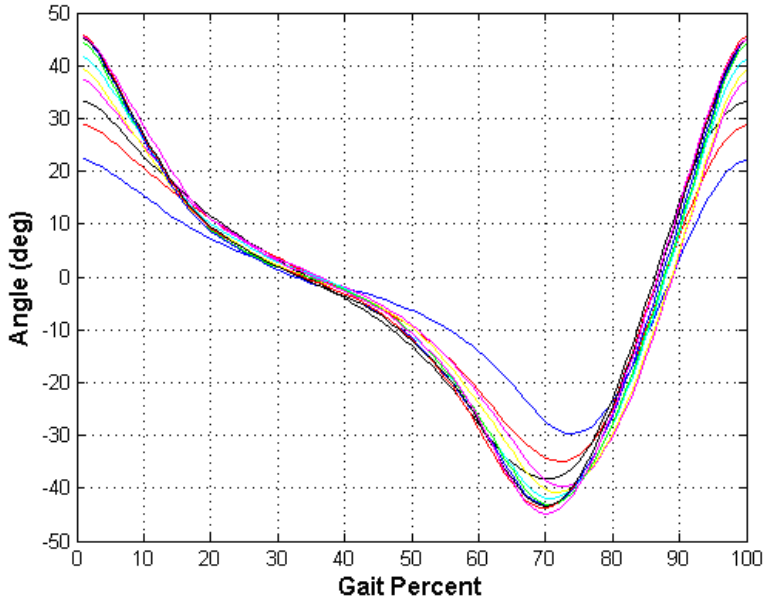

Figure18: Shank angle in world coordinates for different stride lengths.

We then decided to use phase angles which allowed for a unique one-to-one correspondence between shank phase angle and gait percent. The phase plot is constructed by plotting the shank angle versus shank angular velocity, see Figure 19. In this way, each point in Figure 18 is matched to its corresponding angular velocity. Continuous, oval shaped curves represent a particular gait cycle with a particular stride length. As the stride length is increased, the ovals become larger.

For a particular phase curve, the polar angle, Phi, and the polar radius, r, can be measured. In our analysis, the polar angle starts at 0 degrees, and the radius rotates in a clockwise fashion.

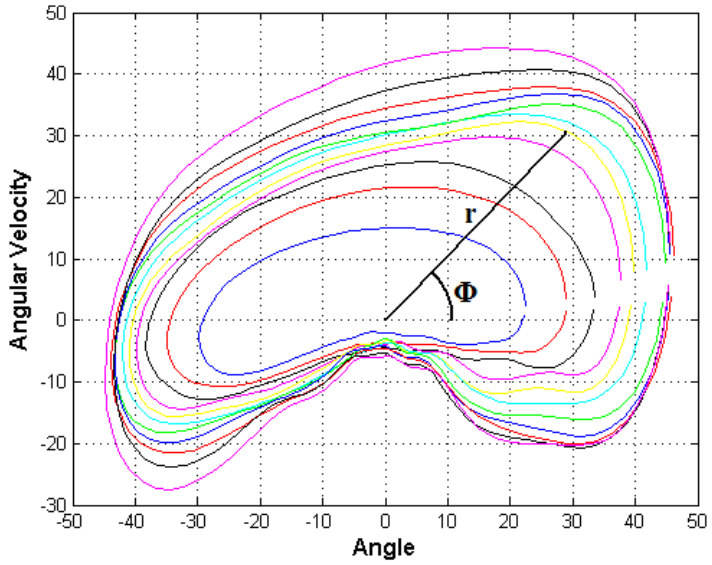

Figure 19: Phase plot of the shank angle versus shank angular velocity. The ovals become larger as the stride length increases. For a particular phase curve, the polar angle, Phi, and the polar radius, r can be measured.

The polar angle is measured as a function of gait percent and is shown in Figure 20. Two important results are shown. Firstly, for each polar angle, there exists one unique gait percent. Thus, if the polar angle is measured in real time on the robot, the gait percent can be calculated. Secondly, the curve of polar angle versus gait percent is invariant to the different stride lengths. We can then measure the polar angle and determine gait percent uniquely regardless of the stride length.

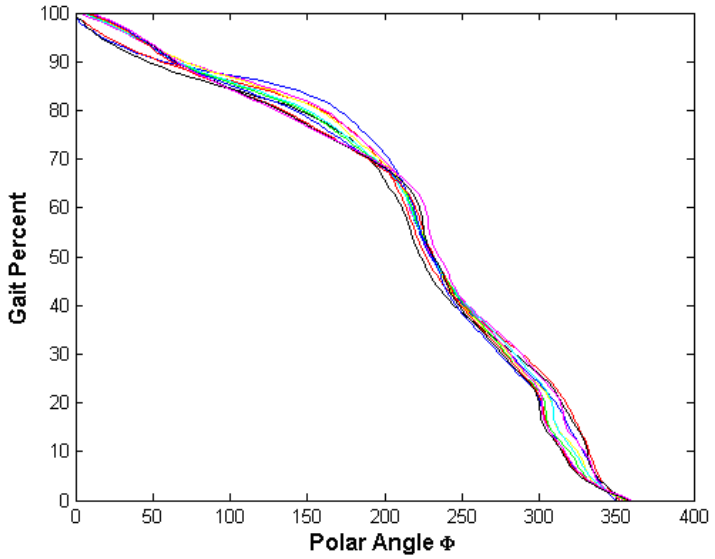

Figure 20: The polar angle is calculated as a function of gait percent. There is one unique polar angle for each gait percent. All of the curves lie on top of each other so that the polar angle is invariant to stride length.

To test our ability at calculating gait percent, a heel strike sensor and a rate gyro were measured while a subject wore the robotic ankle. A straight, diagonal dashed-line was drawn between heel strike sensors to determine a predicted gait percent. The gait percent calculated from the polar angle was drawn using a solid-line. Our method was able to calculate gait percent accurately, see Figure 21.

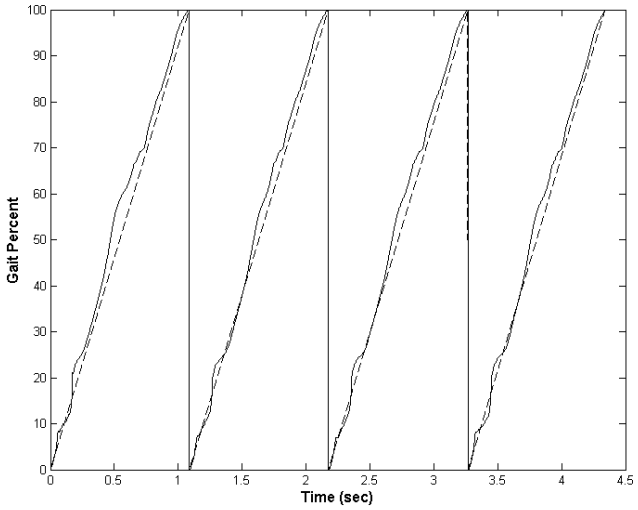

Figure 21: Gait percent is calculated using the polar angle.

The polar radius from Figure 19 is used to calculate the stride length. There was not a one-to-one function between polar radius and stride length. We used a look up table to determine stride length. The polar radius and polar angle are measured and then used to determine the stride length.

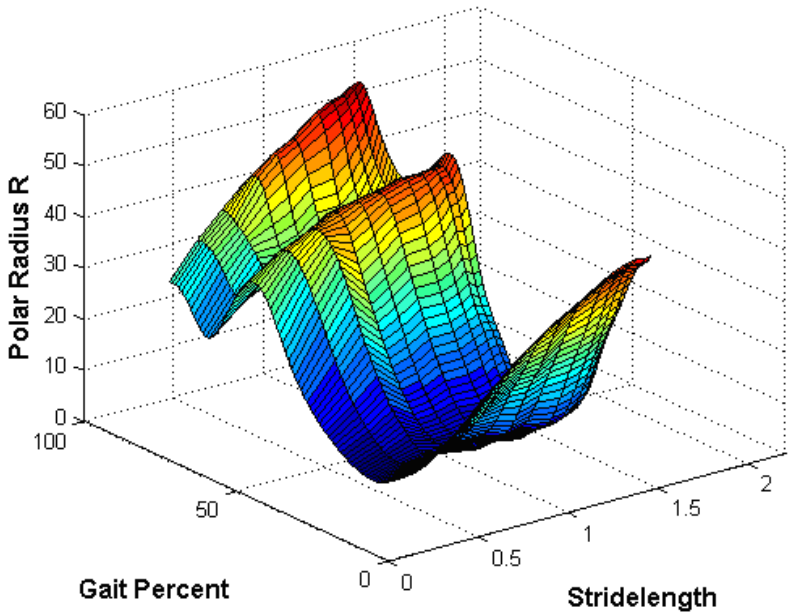

Figure 22: The polar radius and gait percent are used to calculate stride length.

Once the stride length and gait percent are determined, the speed of the user as well as where they are in the gait pattern can be determined. We used these two variables to determine the position of the motor. We used the robotic tendon analysis to determine the deflection of the spring for each gait cycle corresponding to different stride lengths. The deflection of the spring uniquely determines the motor position. We then use a position controller to drive the screw to the correct position.

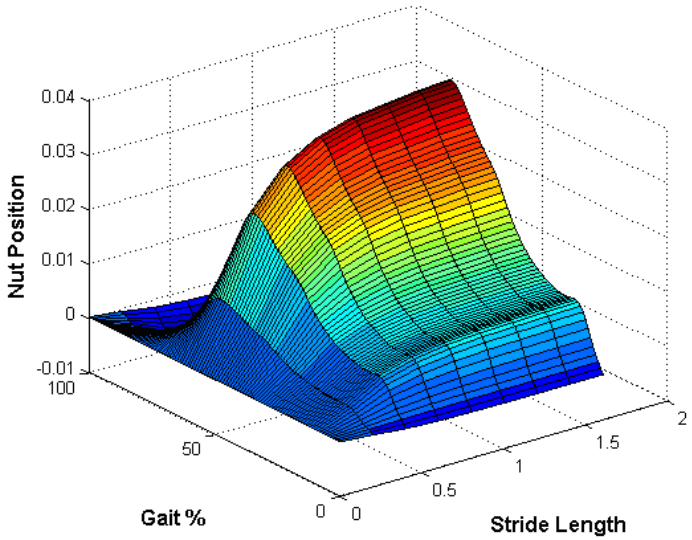

Figure 23: The stride length and gait percent are used to determine the motor position.

In summary, we are developing a continuous based controller based on the phase plot of the tibia angle. The phase angle determines gait percent regardless of stride length. The polar radius is a measure of the stride length. The stride length and gait percent determine the proximal position of the spring in the robotic tendon. We use a simple position controller to adjust the proximal position of the spring.

In our lab, we are now using gait surfaces instead of gait curves.

Key Research Accomplishments:

Our powered ankle devices include the following characteristics:

- User has full range of sagittal ankle motion comparable to able-bodied gait. (23 degrees of plantar-flexion, 7 degrees of dorsiflexion.)
- User has 100% of the required power for gait delivered at the correct time and magnitude.
- The peak output power is 3-4 times larger than the peak motor power allowing a reduction in motor size and weight.
- Provide the user the flexibility to easily remove and install the Robotic Tendon to allow SPARKy to be used as a “powered and computer controlled” prosthesis or a “standard” keel and pylon prosthesis
- Based on lightweight, energy storing springs
- Allows a highly active amputee to regain high functionality and gait symmetry
- A demonstration of a powered, transtibial prosthesis was performed on November 2nd, 2007 at The Center for the Intrepid, Brooke Army Medical Center.

Phase 2:

- Roller screw transmission was very robust and lightweight.
- A compact microprocessor was developed.
- Over ground walking was demonstrated.
- Walking on inclines and declines was demonstrated.
- Ascending and descending stairs was demonstrated.

SPARKy’s biggest advantage lies in the fact that we are storing energy in a spring uniquely chosen for an individual. If one chooses the correct stiffness, the spring can be adjusted by the motor to allow for a 3 to 4 times power amplification. Because we have a large power amplification, we can use a small motor allowing a very large sized user to walk slow or walk at a very fast pace. Currently, we are only using 55 Watts of a 150 Watt motor so that we can easily power large individuals and can power fast walking.

We are using a fully intact keel that will absorb the heel strike impact and allow for correct rocker motion over the heel. The Robotic Tendon can be detached so that it can

be easily removed reverting back to a standard, passive carbon fiber keel. This feature can provide an alternative if the electronics fail in a field condition.

We are focused on developing the most durable, versatile, and powerful walk/run prosthetic ankle that meets the goals of a highly functional Military amputee. Because of our power amplification, we can easily walk very fast and have confidence in building a jogging device.

Phase 3:

- Jogging was demonstrated on a treadmill at the United States Military Academy at West Point
- Walking forwards and backwards was demonstrated.
- Walking over a rocky or grass surface was demonstrated.

Reportable Outcomes

- Manuscripts
    - o two PhD dissertations,
    - o one MS thesis
    - o eleven conference papers were published
    - o four journal paper were published

- Popular Press – multiple web pages and newspaper articles discussed research

National Geographic Magazine, Issue on The Bionic AGE, January 2010

Dean of Invention: Introducing the Age of Bionic Limbs, October 19, 2010

- Presentations – presented research at Dynamic Walking 2007, 2008, 2009, and 2011

- Demonstrations – Brooke Army Medical Center, Center for the Intrepid, November 2007, October 22, 2009

Joseph Hitt Mechanical Engineering Graduated May. 2008.
Dissertation: A Robotic Transtibial Prosthesis with Regenerative Kinetics

Ryan Bellman Mechanical Engineering Graduated August 2008.
Mechanical and Conceptual Design of a Robotic Transtibial Prosthesis

Matthew Holgate Mechanical Engineering Graduated Dec. 2009.
Dissertation: Control of a Robotic Transtibial Prosthesis

Guest Editor

1. Vanderborght, B.; **Sugar**, T.; Lefeber, D., “Adaptable compliance or variable stiffness for robotic applications [From the Guest Editors]”, IEEE Robotics & Automation Magazine, vol. 15, Issue: 3, pp 8-9, 2008.

Guest paper

2. Exciting Benefits of Powered Prosthetic Systems, Lt. Col. Joseph K. Hitt, PhD; Kevin Hollander, PhD; and Thomas Sugar, PhD, The O&P EDGE, October 2010

Keynote Speaker

Keynote Speaker for the SPIE EAPAD conference, March 7, 2011 “Walking with Springs”

Keynote Speaker, Darmstadt, Germany: Proceedings of SIMPAR 2010 Workshops, Intl. Conf. on SIMULATION, MODELING and PROGRAMMING for AUTONOMOUS ROBOTS Darmstadt (Germany) November 15-16, 2010

Conclusion

Significant advances have been achieved towards creating a computer-controlled, powered transtibial prosthesis that can actively support a user in their normal environment and conditions. Low power, high energy consumption, and sophisticated control methodology are key challenges towards realizing a smart, powered prosthesis. In Phase 1, the SPARKy project was able to develop a prosthesis that could supply high peak power to the user at push off in a light weight and energy efficient device.

The key outcomes included:

1. the user has full range of sagittal ankle motion comparable to able-bodied gait. (23 degrees of plantar-flexion, 7 degrees of dorsiflexion, and
2. the user has 100% of the required power for gait delivered at the correct time and magnitude.

The device provides the user 100% of the ankle power and ankle joint movement similar to able-bodied gait. This unique device is one of the most powerful and efficient devices of its kind.

The analyses and test data show that the motor power can be amplified to provide the user 100% of the required power. We showed a power amplification of the output power compared to the input power of 3 to 4 times. This power amplification allows the downsizing of the actuator to a portable level. For example, a small 150 W motor in combination with a transmission and spring provides 200 W to 400 W during testing. This size and weight of the system is to a level that is comfortably portable to the user while powerful enough to support an 80 kg subject up to his maximum walking speed of 1.8 m/s (4 mph). The data suggests that there is enough power available to support even larger users at such speeds.

In Phase 2, the SPARKy project developed a very lightweight prosthesis that was used in over ground walking. The roller screw design was very successful because it provided a very robust and lightweight transmission. We ported all of the code to a dsPIC 33 microprocessor. Finally, this project exceeded our expectations in terms of the device performance. Our new control methodology and embedded microprocessor control allowed our Phase 2 device to move from the laboratory to the unstructured and highly dynamic environments that include stairs, inclines/declines and over ground walking.

In Phase 3, the SPARKy project developed a prosthesis that was able to allow a user to jog on a treadmill. We also demonstrated that the prosthesis could be used while walking on grass and rocky surfaces. A very functional robotic ankle was developed by the end of Phase 3; we demonstrated jogging, walking, walking over unstructured terrain, walking forwards and backwards, and walking up and down slopes and stairs.

The team would like to thank the support of Military Amputee Research Program and the help from our test subjects.

References

Popular Press:

1. Next generation of powered prosthetic devices based on lightweight energy storing springs. What's next network - Science and Technology - May 2, 2007

2. "Sparky;" the Ankle Prosthetic of the Future, Med Gadget - May 2, 2007

3. Researchers create next generation prosthetic devices - News-Medical.net - May 2, 2007

4. ASU researchers putting new spring into amputees' step, MSN Money, May 1, 2007

5. Smart Prosthesis of the future created, United Press International - May 3, 2007

6. Smart Prosthesis of the future created, Podiatry News, Foot News - May 3, 2007

7. The World's First Powered Ankle, Technology Review - By Emily Singer and Duncan Graham-Rowe - May 11, 2007

8. SPARKy the prosthetic ankle set to "revolutionize prosthetics"
Posted May 3rd 2007 by Paul Miller

9. ASU, Walter Reed researchers create prosthesis of the future, ASU Insight -May 11, 2007

10. Innovations Report -By Chris Lambrakis - May 03, 2007
EurekAlert - May 1, 2007
Brightsurf Science News - May 2, 2007
FusePress - May 2, 2007
Medical News Today - May 3, 2007
newsrx.com - May 1, 2007
ScienceDaily - May 2, 2007
VA News Flash - VA Watchdog dot Org By Larry Scott at -May 03, 2007
First Science News - May 1, 2007

11. Discovery News - By Tracy Staedter - May 31, 2007

12. Arizona researchers putting new spring into amputees' step
The Business Journal of Phoenix - May 1, 2007

13. Washington Business Journal -by Ty Young May 3, 2007
Researchers take step forward in design of new prosthesis

14. Creating a Future Prosthesis for Today's Military Amputees, Orthotics and Prosthetics, September 1, 2007

15. Discovery Channel, 2008, "Toad research could leapfrog to new muscle model", show was called "Toady Tendons", December 3, 2008, 8 minutes

16. National Geographic, January 2010, Applied Bionics

17. Robotic ankle only steps away from daily use, AZ Republic, December 21, 2009

18. Device reflects value of research for ASU, AZ Republic, December 21, 2009

19. SPARKy device helps amputees return to normal lives, ASU, December 2009

20. Mesa Talking with Scott Anderson, December 2009

21. Innovative prosthetic ankle to mobilize amputees, AZ State Press, January 22, 2010

22. Researchers develop new robotic prosthetic technology to aid amputees, College Times, January 21, 2010

23. Dean of Invention: Introducing the Age of Bionic Limbs, October 19, 2010

24. Sports Illustrated, August 8, 2011, "New and Improved" by Alexander Wolff

Conference Papers:

1. Ward, J., Sugar, T. G., Hollander, K. W., Optimizing the Translational Potential Energy of Springs for Prosthetic Systems, IEEE MSC 2011.

2. Sugar, T. G., Hollander, K. W., Hitt, J. K., "Walking with Springs, SPIE, EAPAD, 2011.

3. Hitt, J., Merlo, J., Boehler, A., Holgate, M., and Sugar, T., "Bionic Running for Unilateral Transtibial Military Amputees," 27th Army Science Conference, Orlando, Florida, Nov., 2010.

4. Hitt, J., and Sugar, T., "Load Carriage Effects on a Robotic Transtibial Prosthesis," International Conference on Control, Automation and Systems, Gyeonnggi-do, Korea, Oct, 2010.

5. M. Holgate, T G. Sugar, A. Boehler, "A Novel Control Algorithm for Wearable Robotics using Phase Plane Invariants, IEEE International Conference on Robotics and Automation (ICRA), 2009.

6. M. Holgate, J. K. Hitt, R. D. Bellman, T. G. Sugar, K. W. Hollander, "The SPARKy (Spring Ankle with Regenerative Kinetics) Project: Choosing a DC Motor Based Actuation Method," Biorobotics 2008.

7. R D. Bellman, T. G. Sugar, "SPARKy 3: Design of an Active Robotic Ankle Prosthesis with Two Actuated Degrees of Freedom Using Regenerative Kinetics," Biorobotics 2008.

8. M. A. Holgate, A. W. Boehler, T. G. Sugar, "Control Algorithms for Ankle Robots: A Reflection on the State-of-the-Art and Presentation of Two Novel Algorithms," Biorobotics 2008.

9. J. Hitt, R. Bellman, M. Holgate, T. Sugar, and K. Hollander, The SPARKy (Spring Ankle with Regenerative Kinetics) Project: Design and Analysis of a Robotic Transtibial Prosthesis with Regenerative Kinetics, ASME International Design Engineering Technical Conference, CD-ROM, pp. 1-10, 2007.

10. K. Hollander and T. Sugar, "A Robust Control Concept for Robotic Ankle Gait Assistance," IEEE International Conference on Rehabilitation Robotics (ICORR), Holland, 2007.

11. J. Hitt, A. Mehmet Oymagil, T. Sugar, K. Hollander, A. Boehler and J. Fleeger, "Dynamically Controlled Ankle-Foot Orthosis (DCO) with Regenerative Kinetics: Incrementally Attaining User Portability," IEEE International Conference on Robotics and Automation (ICRA), Roma, Italy, 2007.

Journal Papers:

1. Joseph K. Hitt, Thomas G. Sugar, Matthew Holgate, and Ryan Bellman , "An Active Foot-Ankle Prosthesis with Biomechanical Energy Regeneration", ASME Journal of Medical Devices, vol 4(1) 2010.
Number 1 downloaded paper for the journal in April and May 2010

2. Hitt, J, Holgate, M, Bellman, R, Sugar, TG, Hollander, KW, “Robotic Transtibial Prosthesis with Biomechanical Energy Regeneration”, Industrial Robot: An International Journal, vol 36(5), pp. 441-447, 2009.
Outstanding Paper Award Winner at the Literati Network Awards for Excellence 2010.

3. Ronald Van Ham, Thomas G. Sugar, Bram Vanderborght, Kevin W. Hollander, Dirk Lefeber, “Compliant Actuator Designs: Review of Actuators with Passive Adjustable Compliance / Controllable stiffness for Robotic Applications”, IEEE Robotics and Automation Magazine, vol 16(3), pp. 81-94, September 2009.
Top Ten downloaded paper for the Magazine
Our article is in top 10 download in February 2010
http://ieeexplore.ieee.org/xpl/topAccessedArticles.jsp?reload=true&punumber=100

4. **K. W. Hollander**, **Robert Ilg**, T. G. Sugar, and D. E. Herring, “An Efficient Robotic Tendon for Gait Assistance,” ASME Journal of Biomechanical Engineering, vol 128(5), pp. 788-791, October 2006.

Dissertation:
Dissertation: A Robotic Transtibial Prosthesis with Regenerative Kinetics, Joseph Hitt, Arizona State University, May 2008.

Dissertation: Control of a Robotic Transtibial Prosthesis, Matthew Holgate, Arizona State University, December 2009.

Thesis:
Thesis: Mechanical and Conceptual Design of a Robotic Transtibial Prosthesis, Ryan Bellman, Arizona State University, August 2008.

Appendices

Four journal papers and eleven conference papers are attached.

Journal Articles

1. Joseph K. Hitt, Thomas G. Sugar, Matthew Holgate, and Ryan Bellman , “An Active Foot-Ankle Prosthesis with Biomechanical Energy Regeneration”, ASME Journal of Medical Devices, vol 4(1) 2010.

2. Hitt, J, Holgate, M, Bellman, R, Sugar, TG, Hollander, KW, “Robotic Transtibial Prosthesis with Biomechanical Energy Regeneration”, Industrial Robot: An International Journal, vol 36(5), pp. 441-447, 2009.

3. Ronald Van Ham, Thomas G. Sugar, Bram Vanderborght, Kevin W. Hollander, Dirk Lefeber, “Compliant Actuator Designs: Review of Actuators with Passive Adjustable Compliance / Controllable stiffness for Robotic Applications”, IEEE Robotics and Automation Magazine, vol 16(3), pp. 81-94, September 2009.

4. **K. W. Hollander**, **Robert Ilg**, T. G. Sugar, and D. E. Herring, “An Efficient Robotic Tendon for Gait Assistance,” ASME Journal of Biomechanical Engineering, vol 128(5), pp. 788-791, October 2006.

Conference Papers

1. Ward, J., Sugar, T. G., Hollander, K. W., Optimizing the Translational Potential Energy of Springs for Prosthetic Systems, IEEE MSC 2011.

2. Sugar, T. G., Hollander, K. W., Hitt, J. K., “Walking with Springs, SPIE, EAPAD, 2011.

3. Hitt, J., Merlo, J., Boehler, A., Holgate, M., and Sugar, T., “Bionic Running for Unilateral Transtibial Military Amputees,” 27th Army Science Conference, Orlando, Florida, Nov., 2010.

4. Hitt, J., and Sugar, T., “Load Carriage Effects on a Robotic Transtibial Prosthesis,” International Conference on Control, Automation and Systems, Gyeonnggi-do, Korea, Oct, 2010.

5. M. Holgate, T G. Sugar, A. Boehler, “A Novel Control Algorithm for Wearable Robotics using Phase Plane Invariants, IEEE International Conference on Robotics and Automation (ICRA), 2009.

6. M. Holgate, J. K. Hitt, R. D. Bellman, T. G. Sugar, K. W. Hollander, “The SPARKy (Spring Ankle with Regenerative Kinetics) Project: Choosing a DC Motor Based Actuation Method,” Biorobotics 2008.

7. R D. Bellman, T. G. Sugar, “SPARKy 3: Design of an Active Robotic Ankle Prosthesis with Two Actuated Degrees of Freedom Using Regenerative Kinetics,” Biorobotics 2008.

8. M. A. Holgate, A. W. Boehler, T. G. Sugar, “Control Algorithms for Ankle Robots: A Reflection on the State-of-the-Art and Presentation of Two Novel Algorithms,” Biorobotics 2008.

9. J. Hitt, R. Bellman, M. Holgate, T. Sugar, and K. Hollander, The SPARKy (Spring Ankle with Regenerative Kinetics) Project: Design and Analysis of a Robotic Transtibial Prosthesis with Regenerative Kinetics, ASME International Design Engineering Technical Conference, CD-ROM, pp. 1-10, 2007.

10. K. Hollander and T. Sugar, “A Robust Control Concept for Robotic Ankle Gait Assistance,” IEEE International Conference on Rehabilitation Robotics (ICORR), Holland, 2007.

11. J. Hitt, A. Mehmet Oymagil, T. Sugar, K. Hollander, A. Boehler and J. Fleeger, “Dynamically Controlled Ankle-Foot Orthosis (DCO) with Regenerative Kinetics: Incrementally Attaining User Portability,” IEEE International Conference on Robotics and Automation (ICRA), Roma, Italy, 2007.

Walking with Springs

Thomas G. Sugar*[a], Kevin W. Hollander[b], Joseph K. Hitt[c]
[a]Arizona State University, 7231 E. Sonoran Arroyo Mall, Mesa, AZ, USA 85212;
[b]SpringActive, Inc, 2039 E Cedar Street, Suite 101, Tempe, AZ 85281;
[c]United States Military Academy, Dept. of Civil and Mechanical Engineering, West Point, NY

ABSTRACT

Developing bionic ankles poses great challenges due to the large moment, power, and energy that are required at the ankle. Researchers have added springs in series with a motor to reduce the peak power and energy requirements of a robotic ankle. We developed a "robotic tendon" that reduces the peak power by altering the required motor speed. By changing the required speed, the spring acts as a "load variable transmission." If a simple motor/gearbox solution is used, one walking step would require 38.8J and a peak motor power of 257 W. Using an optimized robotic tendon, the energy required is 21.2 J and the peak motor power is reduced to 96.6 W. We show that adding a passive spring in parallel with the robotic tendon reduces peak loads but the power and energy increase. Adding a passive spring in series with the robotic tendon reduces the energy requirements. We have built a prosthetic ankle SPARKy, Spring Ankle with Regenerative Kinetics, that allows a user to walk forwards, backwards, ascend and descend stairs, walk up and down slopes as well as jog.

Keywords: prosthetic ankle, spring, power, energy

1. INTRODUCTION

Within the US there are approximately 1.8 million people who have suffered limb loss, with about 100,000 new cases each year. Of those people affected, approximately 80% are lower limb amputees. Robotic technology offers great hope and promise to individuals coping with the lost functionality of a missing limb. Until recently, robotic technology for amputees has been limited, but functional, powered, walking-assistance devices have just begun to emerge.

Our mission is to develop a new generation of powered orthotic/prosthetic devices based on lightweight, energy storing springs that will create a natural, more functional gait. Very few researchers are addressing powered wearable robotic systems because they pose many crucial engineering challenges [1-7]. They must be lightweight, safe, compliant, and powerful, but also energy efficient. Engineers have struggled to meet all of these functional requirements in a single device. For example, the ankle poses a particularly difficult set of design parameters, including a very large power requirement (257W for an 80kg person) in addition to a very high cycle life (3 – 5 thousand steps daily translating to 44 to 73 million revolutions per year on our motor system).

Direct drive electric, hydraulic, and pneumatic systems have been proposed, but they are heavy [8, 9]. In contrast, we propose a radically different approach by storing and releasing energy in springs [4-6, 10-13]. A spring can have power to weight ratios of 300,000 W/kg versus 300 W/kg for DC motors. A small, lightweight, low power motor is used to adjust the position of the spring. A heavy, powerful motor is not necessary because it is not the "actuator". The actuator is a spring tuned and adjusted for an *individual*. Our robotic systems are a combination of safe, lightweight motors and powerful, compliant, energy storing helical springs.

The robotic tendon actuator is based on a helical spring that has shown significant results in supplying large power spikes using a low power motor [4, 5, 14]. Additionally, this actuator is optimized through the use of a unique, customized spring for each subject.

In section 2, a mathematical description of a lead screw actuator and a robotic tendon actuator will be presented. The main difference is that the varying load changes the input motor speed and input power in the robotic tendon actuator. In section 3, a description of the ankle position, moment and power during gait will be described. In section 4, models of the robotic tendon actuator with additional springs will be optimized to minimize input motor energy and a reduction of peak power.

*a. thomas.sugar@asu.edu; phone 1 480-727-1127; Human Machine Integration Laboratory

2. DESCRIPTION OF A ROBOTIC TENDON ACTUATOR

In a bionic ankle, an actuator system must convert the motor angular velocity and torque into a linear velocity and force. A standard lead screw model will be described first which will be used to highlight a motor/gearbox transmission. The robotic tendon actuator system will then be described which adds an additional spring at the end of the nut. In this system, the spring alters the input velocity and power.

2.1 Standard Model of a Lead/Ball Screw Actuator

In a lead screw or ball screw model, the motor rotates moving the nut position, *r*, inward and outward, Figure 1. To simplify the analysis, friction is not modeled. The output position, *x*, and force, *F*, describe the required movement and force to move the ankle during gait. In our research, standard gait data [15] is used to determine *x* and *F*.

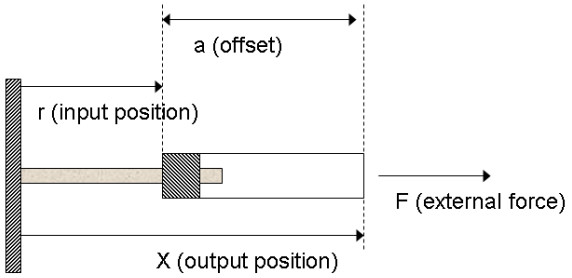

Figure 1. In a lead/ball screw model, the motor turns moving a nut inward or outward adjusting, *r*. The external force, *F*, and position, *x*, describe the desired outputs. The offset distance, *a*, is fixed.

In a quasi static analysis, the external force determines the toque on the lead screw where *l* describes the lead:

$$\tau = \frac{Fl}{2\pi} \tag{1}$$

The input position, *r*, is determined by the number of revolutions, *n*, that the motor spins and the lead, *l*:

$$r = l \cdot n \tag{2}$$

The output position, *x*, is determined by *r* and the constant offset *a*:

$$x = r + a \tag{3}$$

The input velocity is given by differentiating (2) and assuming the lead, *l*, is fixed:

$$\dot{r} = l \cdot \dot{n} \tag{4}$$

The output velocity is given by differentiating (3):

$$\dot{x} = \dot{r} \tag{5}$$

The motor angular velocity is given by:

$$\omega = \dot{\theta} = 2\pi \cdot \dot{n}$$
$$\dot{\theta} = \frac{2\pi \cdot \dot{r}}{l} \tag{6}$$

The input power is determined by multiplying the input torque and angular velocity. In this simple case, the input power equals the output power. The lead, *l,* can be used to adjust the motor speed and torque to fit the motor operating specifications. Typically a gearbox and a small lead are both needed to achieve the slow speeds and high torques needed

at the ankle. The problem with this method is that a large motor and gearbox combination is needed [6, 11, 16]. To be consistent with the standard gait literature, the power curves will be inverted and a negative sign is added.

$$\tau\dot{\theta} = -F \cdot \dot{r} = -F \cdot \dot{x} \tag{7}$$

2.2 Model of a Robotic Tendon Actuator

In a robotic tendon model, the motor rotates moving the nut position, *r*, inward and outward, Figure 2. The output position, *x*, and force, *F*, describe the required movement and force to move the ankle during gait. In this model, a spring with stiffness, *K*, is placed between the nut and the external force. The spring is a buffer which can store and release energy altering the power relationships.

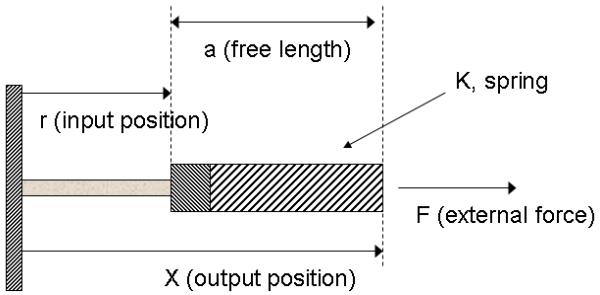

Figure 2. In a robotic tendon model, the motor turns moving a nut inward or outward adjusting, *r*. The external force, *F*, and position, *x*, describe the desired outputs. A spring is placed in between the nut and the external force. The free length of the spring is given by, *a*.

In a quasi static analysis ignoring friction, the external force determines the torque on the lead screw where *l* describes the lead. Ignoring acceleration or inertia at the output position by assuming they are both small, the external force is balanced by the spring force. We have modeled inertias in a separate model [5].

$$\tau = \frac{Fl}{2\pi} \tag{8}$$

$$F = K(x - r - a) \tag{9}$$

The input position, *r*, is determined by the number of revolutions, *n*, that the motor spins and the lead, *l*:

$$r = l \cdot n \tag{10}$$

The output position, *x*, is determined by *r*, *F*, and the constant offset *a*:

$$x = r + a + \frac{F}{K} \tag{11}$$

The input velocity is given by differentiating (10) and assuming the lead, *l*, is fixed:

$$\dot{r} = l \cdot \dot{n} \tag{12}$$

The output velocity is given by differentiating (11) assuming the spring stiffness is constant:

$$\begin{aligned} \dot{x} &= \dot{r} + \frac{\dot{F}}{K} \\ \dot{r} &= \dot{x} - \frac{\dot{F}}{K} \end{aligned} \tag{13}$$

The motor angular velocity is given by:

$$\omega = \dot{\theta} = 2\pi \cdot \dot{n}$$
$$\dot{\theta} = \frac{2\pi \cdot \dot{r}}{l} = \frac{2\pi}{l}(\dot{x} - \frac{\dot{F}}{K}) \tag{14}$$

The input power is determined by multiplying the input torque and angular velocity. In this case, the input power does not equal the output power. To be consistent with the standard gait literature, the power curves will be inverted and a negative sign is added.

$$\tau\dot{\theta} = -F \cdot \dot{r} = -F \cdot (\dot{x} - \frac{\dot{F}}{K}) \tag{15}$$

The term $\frac{F \cdot \dot{F}}{K}$ can increase or decrease the required input power. In the specific case for analyzing ankle gait, the maximum peak motor power and motor angular velocity are both reduced. The spring stores braking energy releasing it when needed. Because of the ability of the spring to store energy, the total input energy is kept to a minimum. This term corresponds to the storage of "translational potential energy."

It is interesting to note that the input speed shown in equation (14) is not only a function of the lead, *l*, but also the changing force. The slope of the external force or the slope of the load curve can speed up or slow down the required motor speed. In this sense, the spring acts as a "load variable transmission." In our work [17], we have been studying a dynamic stiffness defined by:

$$K = \frac{\dot{F}}{\dot{x}} \tag{16}$$

3. GAIT

Gait is the term used to describe the locomotion of legged animals. Gait is a recurring pattern of leg and foot movements, rotations, and torques. Due to its repetitive nature, the discussion of gait is done in terms of percentages of a gait cycle. A gait cycle is defined for a single leg and begins with the initial contact of the foot with the ground or 'heel strike', the conclusion of a cycle occurs as the same foot makes a second 'heel strike'. The end of one gait cycle is of course the beginning of another. The input motions are typically determined using a motion capture system and the torques are derived using an inverse dynamics calculation. The ankle gait data is digitized from Whittle [15].

The ankle position is shown in Figure 3. Initially after heel strike, the ankle plantarflexes or moves downward. After the foot is flat on the ground, the shank then rolls over the ankle, i.e. dorsiflexing. During this period, the spring in the robotic tendon stores energy. At 40% of the gait cycle, the foot rapidly plantarflexes , which propels the person forward. During powered push-off or powered plantarflexion the moments and angular speeds are high. In this phase of gait, the spring releases its energy aiding in push-off. At 60% of the gait cycle, the toe comes off of the ground and the ankle rapidly dorsiflexes to insure that the toe does not touch or skid on the ground during the next phase of gait. From 60% to 100% of the gait cycle, the foot is in the air during the swing phase. During this phase of gait the ankle moments are low.

The ankle moment is shown in Figure 4. The ankle moment data was scaled for an 80kg person. At 40% of the gait cycle, the moment is at its peak just as the angular velocity begins to increase rapidly. The combination of high forces and high velocities means that large powers are experienced in this region of the gait cycle, see Figure 5.

Figure 5 shows both positive and negative powers developed during a typical gait cycle. Utilizing a robot to aid in gait, sometimes the robot needs to aid the user (positive power) and sometimes for support the robot needs to resist the user (negative power) and in either case the robot is putting energy into the system. A tuned, spring-based system allows for a well timed energy storage when resisting the user and energy release when assisting the user.

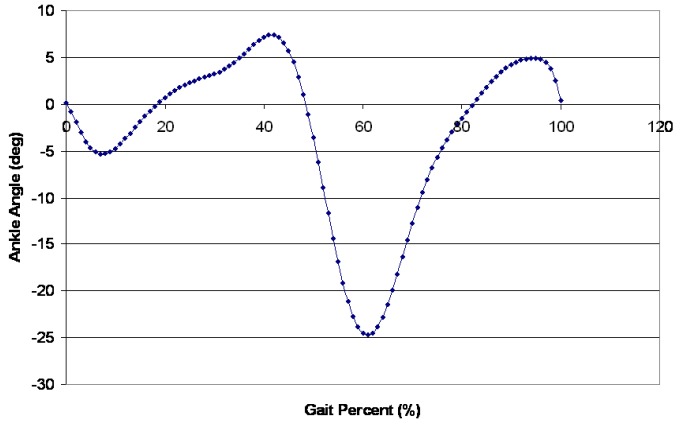

Figure 3. The ankle position in degrees as a percent of the gait cycle.

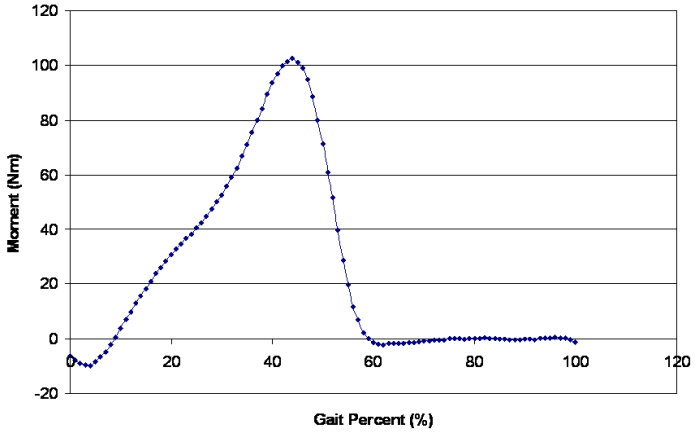

Figure 4. Ankle moment as a percentage of the gait cycle.

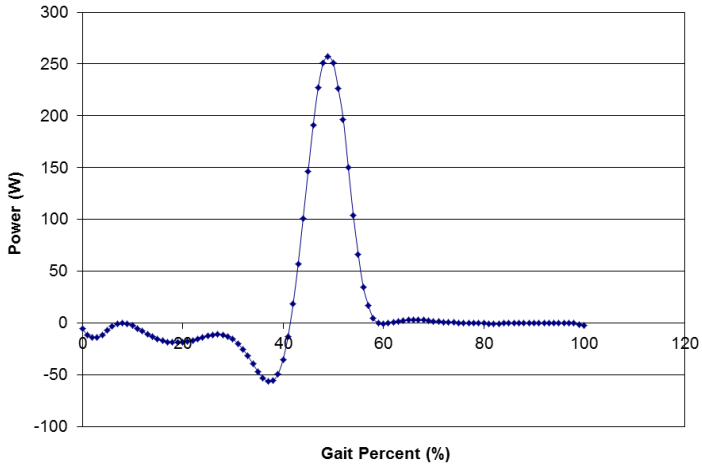

Figure 5. Ankle power as a percentage of the gait cycle, assumes a 0.8 Hz gait frequency.

4. SIMULATIONS

In this section, three scenarios of spring placement were modeled; 1) our typical robotic tendon configuration, with multiple spring stiffness choices, 2) a robotic tendon including a parallel spring and 3) a robotic tendon including a spring in series with the ankle joint.

4.1 Simulation of the Robotic Tendon model using gait data

In the ideal case (i.e. no friction) for one walking condition (Model 1 in Table 1), if one was to assume that energy can be stored and released properly, the peak motor power is 257.6 W and the energy required for each step is 19.4 J. In this ideal case, all of the braking energy is stored and used in push-off. We assumed an 80kg subject and the gait cycle duration is 1.25 seconds. The area underneath the power curve in Figure 5 is integrated to determine 19.4 J.

Table 1. Different springs are modeled to determine the required peak motor power and energy

Model	Spring Stiffness	Peak Motor Power	Input Motor Energy	Optimization Criteria
1		257.6 W	19.4 J	Ideal Case
2	infinite	257.6 W	38.8 J	Lead Screw Model with no additional spring
3	53,224 N/m	96.6 W	21.2 J	Robotic Tendon spring is optimized to reduce the peak power of the motor
4	43,658 N/m	106.9 W	22.1 J	Robotic Tendon spring is optimized to reduce the peak power of the motor to zero at push-off
5	51,627 N/m	97.9 W	21.2 J	Robotic Tendon spring is optimized to reduce the required input energy of the motor

A mechanical system based on the lead screw model is not adequate because peak power and energy required are both very high (Model 2 in Table 1). If a lead/ball screw system assuming 100% efficiency is used, the peak motor power equals 257.6 W and the energy equals 38.8 J. The energy is much larger because a motor must resist the load as the shank rolls over the ankle and must provide the push-off energy to propel the person forward. In this simulation, the absolute value of the input power was integrated to determine the 38.8 J.

Using a tuned spring in the simulation of the robotic tendon model (Model 3 in Table 1), the peak power and energy are both reduced. The peak input power is reduced to 96.6 W and the integration of the absolute value of the input power equals 21.2 J. This is a remarkable reduction in peak power and a large energy savings. In the model, the spring is optimized to reduce peak power. The spring stiffness is 53,224 N/m and a lever arm at the ankle is assumed to be 0.07 m. In Figure 6, the peak motor power is reduced and the spring supplies much of the push-off power.

The input power is drastically reduced because the motor velocity is reduced with the addition of the spring. In Figure 7, the velocity of the motor is shown for two cases. If there is a tuned spring, the velocity of the motor is low during 40-60% of the gait cycle. During the swing phase because the derivative of the force is close to zero, the velocity of the motor matches the lead screw model. If a spring is eliminated, the velocity of the motor must match the velocity of the gait cycle.

In Figure 8, the input position, r, and the output position, x, are determined from the gait data (equation 13). The deflection of the spring in the robotic tendon is determined by the desired force, F and the spring stiffness K (equation 9).

The robotic tendon actuator has been used to power our SPARKy prosthetic ankle [4, 5, 10, 18]. In Figure 9, the actual motor power and output power at the spring were determined as the user walked on a treadmill.

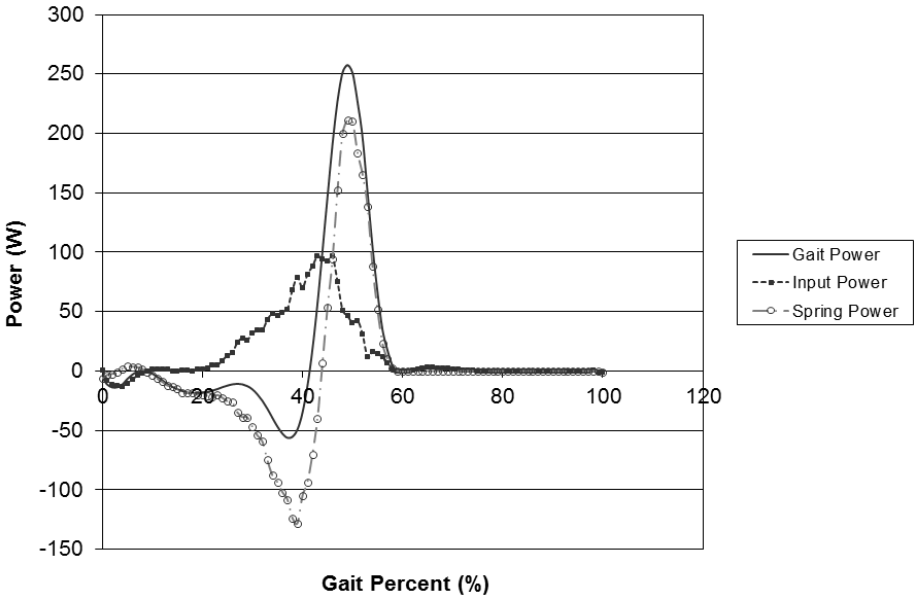

Figure 6. The spring power and the input power add together to match the output gait power.

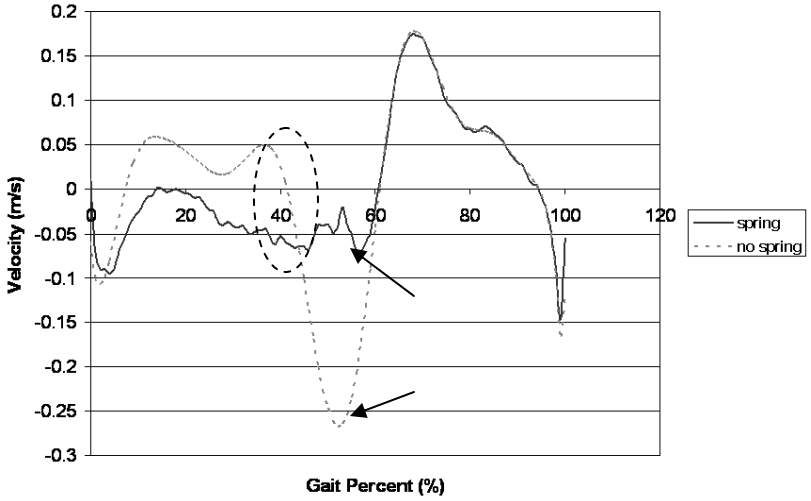

Figure 7. In the lead screw model without a spring, the velocity of the motor is determined by the ankle motion. In the robotic tendon model, the velocity of the motor is lowered during the push off phase of gait (40-60% of the cycle). More importantly, the motor does not change directions under high loads, see dashed oval.

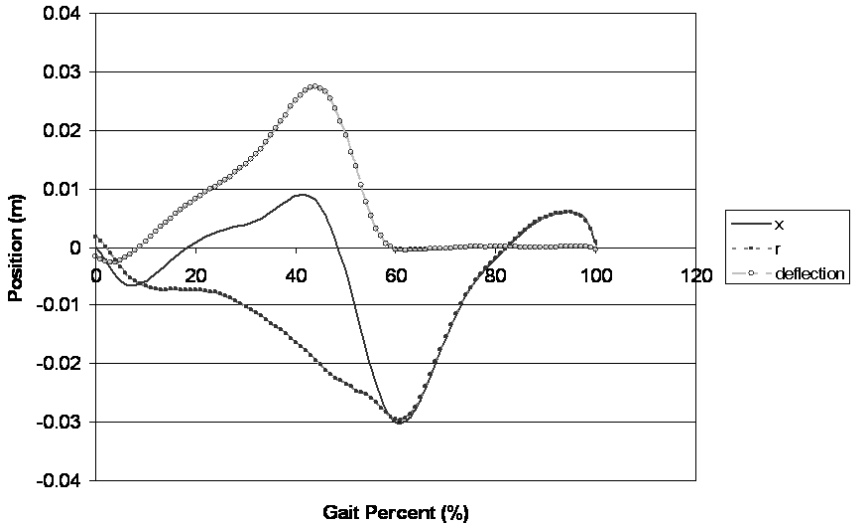

Figure 8. The output position, *x*, is determined by the gait data. The input position of the robotic tendon is determined by the position *x*, the desired force, *F*, and the spring stiffness *K*. The deflection of the spring in the robotic tendon is determined by the desired force, *F* and the spring stiffness *K*.

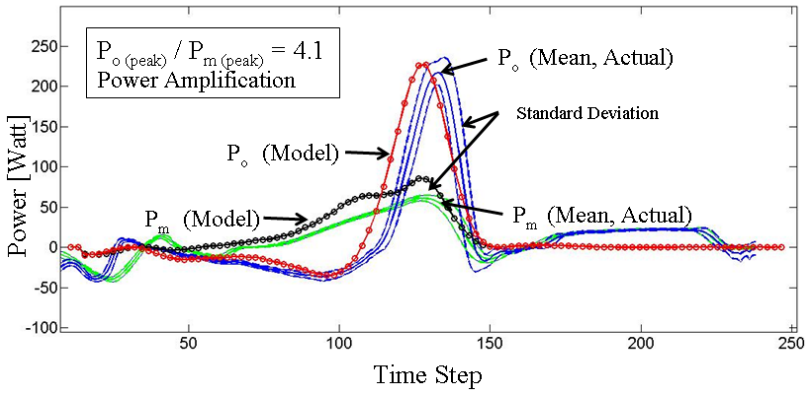

Figure 9. A robotic tendon actuator was used to power a prosthetic ankle. A powered push-off was achieved at 225 W with a 55 W peak motor power [4]. Pm (model) is the simulated power required by the motor. Pm (actual) is the mechanical power at the motor in the SPARKy ankle. Po (Model) is the output power required from published gait data. Po (actual) is the output power at the spring in the SPARKy ankle.

In a second example (Model 4 in Table 1), using the robotic tendon model, a spring can be optimized to reduce the push-off power at 49% of the gait cycle to zero, Figure 10. In this example choosing a spring stiffness of 43,658 N/m, the peak power increases to 106.9 W and the energy increases to 22.1 J. In this case, the spring is doing the work during push-off.

In a third example (Model 5 in Table 1), stiffness can be chosen to minimize energy. In this example choosing a stiffness of 51,627 N/m, the peak power is 97.9 W and the energy needed per step is reduced to 21.2 J. The energy in this case is just slightly lower than in Model 3 in Table 1.

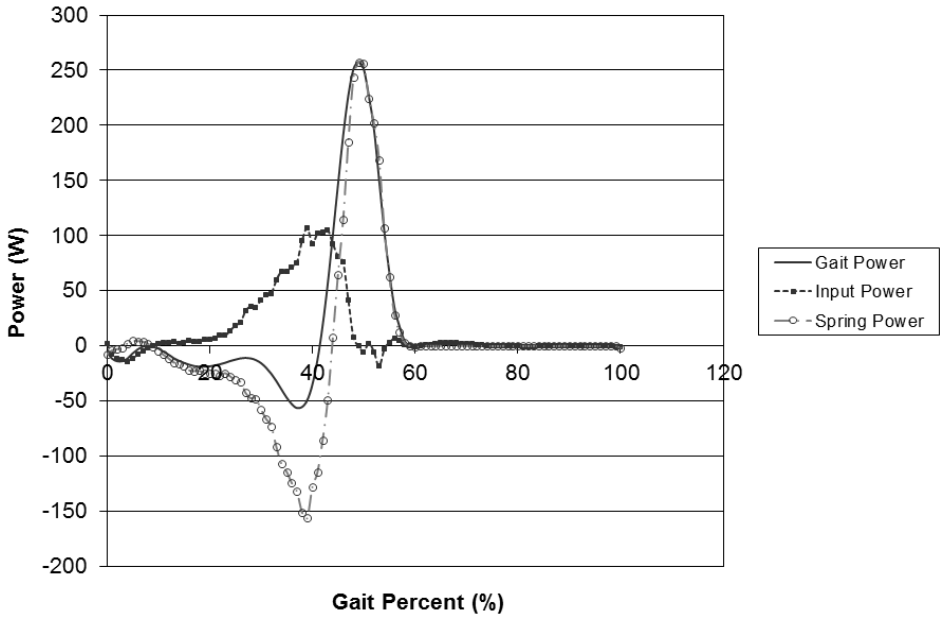

Figure 10. The robotic tendon model can be optimized so that the input power at 49% of the gait cycle is zero. In this example, energy is stored early in the spring so that it provides the push off power.

4.2 Simulation of the Robotic Tendon model with an additional parallel spring

A passive spring can be added in parallel to the robotic tendon to add an additional load path, Figure 11. The additional spring will lower the forces needed at the robotic tendon. In this model, the parallel spring can only be pushed and cannot be pulled. Thus, this spring will aid in reducing the forces during dorsiflexion at the peak loads from 35 to 48% of the gait cycle.

$$F_{external} = F_{gait} - K_{parallel} x \tag{17}$$

An additional parallel spring can be added to the model (Model 1 in Table 2). The maximum force is reduced from 1462 N to 1351 N. This will reduce the peak loads on the actuator. On the other hand, the peak power increases to 137.6 W and the energy increases to 22.0J, Figure 12. In this model, the robotic tendon stiffness is 51,627 N/m and the parallel spring stiffness is 14000 N/m. The problem is that the actuator must work against the parallel spring in the swing phase, Figures 13 and 14.

Table 2. A robotic tendon and an additional parallel spring are modeled to determine the required peak motor power and energy

Model	Spring Stiffness	Peak Motor Power	Input Motor Energy	Optimization Criteria
1	51,627 N/m and 14,000 N/m	137.6 W	22.0 J	A parallel spring is added to reduce the peak forces on the robotic tendon
2	51,627 N/m and 3,991 N/m	106.8 W	21.4 J	A parallel spring is added to reduce the peak forces on the robotic tendon by a small amount.
3	51,627 N/m and 3,991 N/m	106.8 W	21.2 J	A parallel spring is added to reduce the peak forces on the robotic tendon. The parallel spring is only functional during the stance phase of gait.

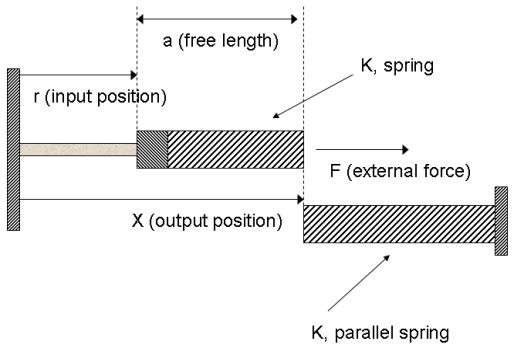

Figure 11. A parallel spring is added to reduce the loads during dorsiflexion (when the ankle position is greater than zero). The spring can only be compressed and cannot be pulled.

In a second example (Model 2 in Table 2), the robotic tendon stiffness is 51,627 N/m and the parallel spring stiffness is 3991 N/m. In this example the energy is reduced to 21.4 J and the peak power is reduced to 106.8 W. With the energy savings, there is a cost. The maximum force is only reduced from 1462 N to 1431 N.

In a third example (Model 3 in Table 2), a passive parallel spring is added only during the stance phase of gait. It could be imagined that a latch is activated when the foot is on the ground. In this example, the stiffness parameters are the same as in Model 2 in Table 2. The peak power remains at 106.8 W but the energy is reduced to 21.2 J.

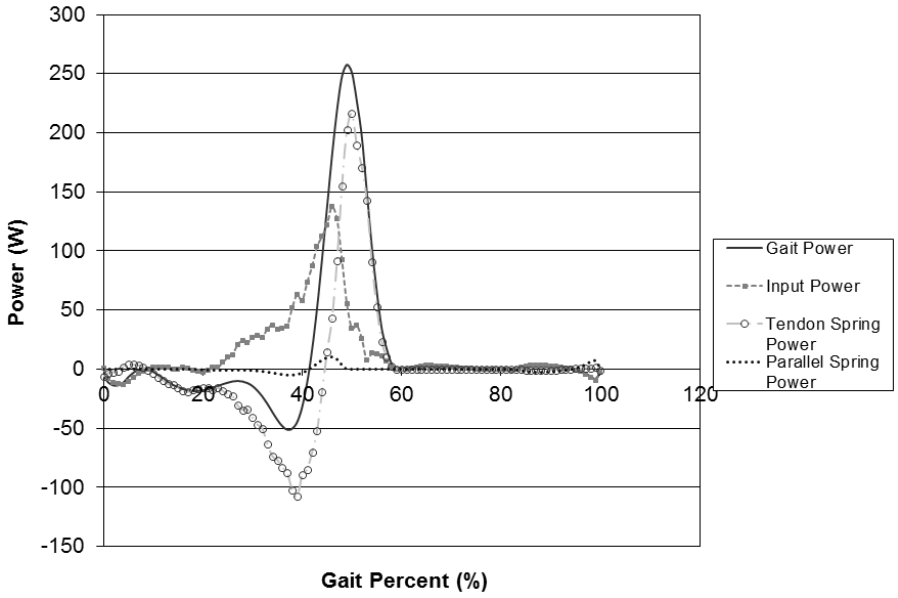

Figure 12. With the addition of a parallel spring the peak motor power does increase to 137.6 W.

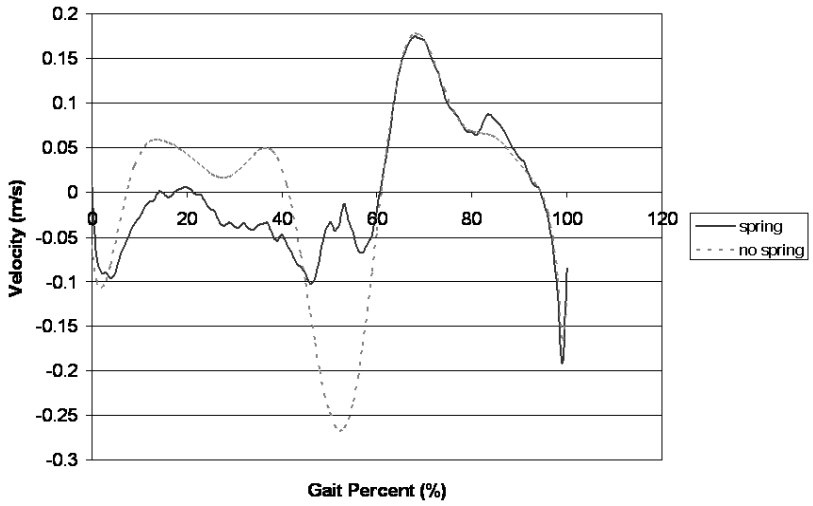

Figure 13. The motor velocity with the two springs is reduced during the stance phase but the velocity slightly increases during the swing phase because the motor must push against the parallel spring.

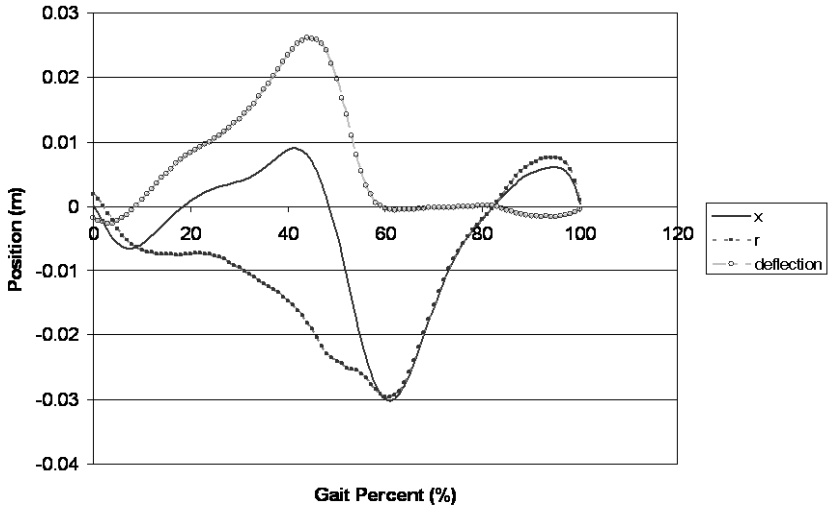

Figure 14. Additional parallel spring model. The motor position, *r*, and the deflection of the robotic tendon spring are shown. During the later part of the swing phase, 80-100%, the robotic tendon must push against the parallel spring.

4.3 Simulation of the Robotic Tendon model with an additional series spring

A passive spring can be added in series to the robotic tendon to reduce the overall stiffness, Figure 15. The additional spring will lower the stiffness of the entire system when the foot is on the ground. In this model, a spring is added to the forefoot of the shoe to act in series with the system from 8 to 41% of the gait cycle. Thus, this spring will aid in reducing the needed motion of the actuator from 8 to 41% of the gait cycle. The movement of the robotic tendon motor is reduced because the series spring will stretch or deform under load.

$$x = x_{gait} - \frac{F_{gait}}{K_{series}} \tag{18}$$

In this example, the robotic tendon stiffness is 51,627 N/m and a series spring is added underneath the ball of the foot with a stiffness value of 877,760 N/m (Model 1 in Table 3). The peak power is 97.9 W and the energy is reduced to 20.1

J, Figure 16. Using a series spring, there was a reduction of 1.1 J as compared to the other cases. One joule might not seem significant but over 3000 to 5000 steps per day, it will add up. The velocity and position of the robotic tendon motor are shown in Figures 17 and 18.

Table 3. A robotic tendon and an additional series spring are modeled to determine the required peak motor power and energy

Model	Spring Stiffness	Peak Motor Power	Input Motor Energy	Optimization Criteria
1	51,627 N/m and 877,760 N/m	97.9 W	20.1 J	A series spring is added to the robotic tendon to reduce the required input energy of the motor.

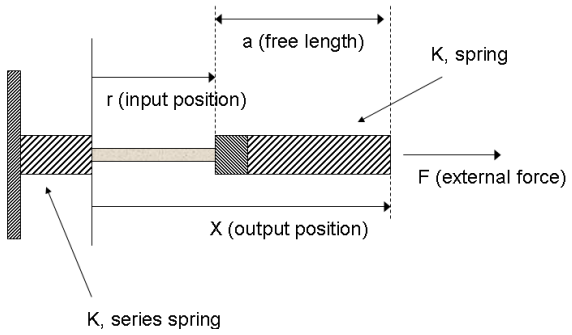

Figure 15 A series spring is added to reduce the stiffness when the forefoot is on the ground. The spring only acts when the foot is on the ground. For example, a spring mounted under the ball of the foot can be thought of as a series spring reducing the stiffness of the Achilles tendon.

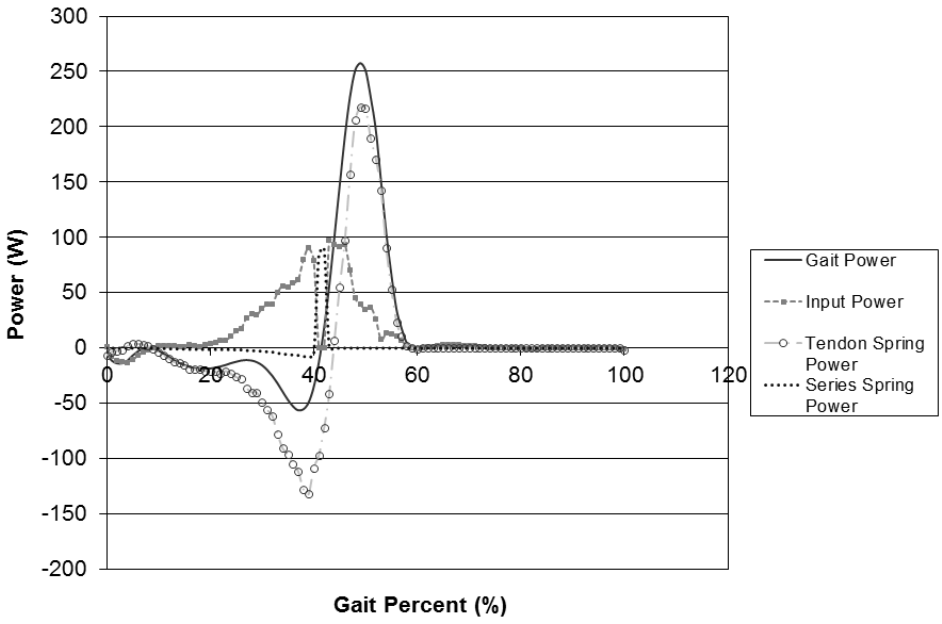

Figure 16. The input power is reduced significantly at the start of push off, 40% of the gait. At this point, the series spring releases its energy and the overall stiffness increases from 48,759 to 51,627.

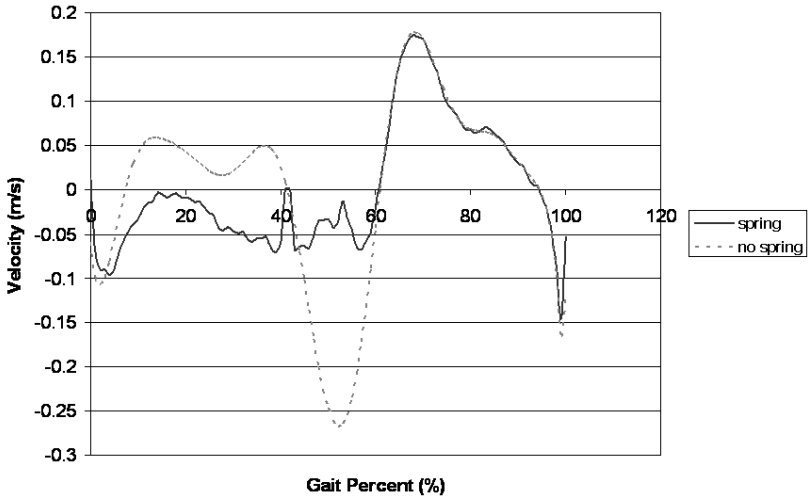

Figure 17. The velocity of the motor using a series spring and a robotic tendon is reduced at 40% of the gait cycle.

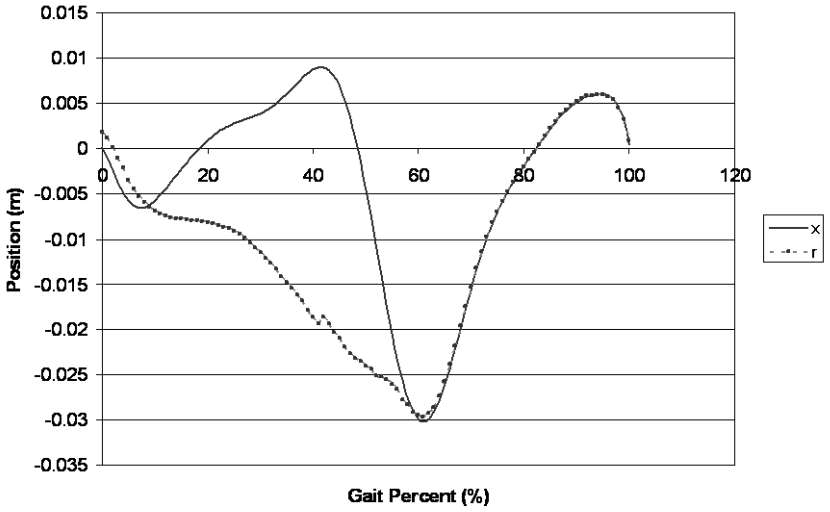

Figure 18. The motor position, *r*, is shown with a discontinuity when the system increases stiffness at 40% of the gait cycle.

We have been actively studying actuators that can change stiffness and developed a Jack Spring actuator [19]. In this actuator, the spring is used as a lead screw and the motor adds and subtracts coils of the spring. As more coils are added, the stiffness is reduced and vice versa. Changing stiffness is not always beneficial because the input velocity is altered when K varies. If one were to build a robotic tendon actuator that can change stiffness as well as change the input position of the spring, the input velocity will be different than equation (13). In this new case, a third term is added.

$$\dot{r} = \dot{x} - \frac{\dot{F}}{K} + \frac{F\dot{K}}{K^2} \tag{19}$$

The input power becomes:

$$F\dot{r} = F\dot{x} - \frac{F\dot{F}}{K} + \frac{F^2\dot{K}}{K^2} \tag{20}$$

5. PROTOTYPE ANKLE

Figure 19. Using a robotic tendon actuator, a user is able to walk over ground, walk up and down inclines, and ascend and descend stairs.

Our research has been able to show the following characteristics. The user has full range of sagittal ankle motion comparable to able-bodied gait (23 degrees of plantarflexion and 7 degrees of dorsiflexion.) They have 100% of the required power for gait delivered at the correct time and magnitude. The peak output power is 3-4 times larger than the peak motor power allowing a reduction in motor size and weight [4, 5]. The design provides the user the flexibility to easily remove and install the Robotic Tendon to allow SPARKy to be used as a "powered and computer controlled" prosthesis or a "standard" keel and pylon prosthesis.

In our second year, a roller screw transmission was purchased that is very robust and lightweight. The system is completely portable allowing the user to walk over ground, Figure 19 [4, 5, 20, 21].

SPARKy's biggest advantage lies in the fact that we are storing energy in a spring uniquely chosen for an individual. If one chooses the correct stiffness, the spring can be adjusted by the motor to allow for a 3 to 4 times power amplification. Because we have a large power amplification, we can use a small motor allowing a user to walk. Currently, we are only using 55 Watts of a 150 Watt motor so that we can easily power large individuals and can power fast walking.

We are focused on developing the most durable, versatile, and powerful walk/run prosthetic ankle that meets the goals of a highly functional Military amputee. Because of our power amplification, we can easily walk very fast and have confidence in building a jogging device [18].

6. CONCLUSIONS

Significant advances have been achieved towards creating a computer-controlled, powered transtibial prosthesis that can actively support a user in their normal environment and conditions. Low power, high energy consumption, and sophisticated control methodology are key challenges towards realizing a smart, powered prosthesis. The SPARKy project was able to develop a prosthesis that can supply high peak power to the user at push-off in a light weight and energy efficient device.

The analyses and test data show that the motor power can be amplified to provide the user 100% of the required power. We showed a power amplification of the output power compared to the input power of 3 to 4 times. This power amplification allows the downsizing of the actuator to a portable level. For example, a small 150 W motor in combination with a transmission and spring provides 200 W to 400 W during testing. This size and weight of the system is to a level that is comfortably portable to the user while powerful enough to support an 80 kg subject up to his maximum walking speed of 1.8 m/s (4 mph). We show that adding a passive spring in parallel to the robotic tendon reduces peak loads but both the power and energy increase. Adding a passive spring in series to the robotic tendon reduces the energy requirements.

The SPARKy project developed a very lightweight prosthesis that is used in over ground walking. Our new control methodology and embedded microprocessor control allows the device to move from the laboratory to the unstructured and highly dynamic environments that include stairs, inclines/declines, and over ground walking.

REFERENCES

[1] Au, S., Berniker, M., and Herr, H., "Powered ankle-foot prosthesis to assist level-ground and stair-descent gaits," Neural Networks, 21(4), 654–666 (2008).

[2] Au, S. K., and Herr, H., "Powered ankle-foot prosthesis," IEEE Robotics & Automation Magazine, 15(3), 52-59 (2008).

[3] Au, S. K., Weber, J., and Herr, H., "Powered Ankle-Foot Prosthesis Improves Walking Metabolic Economy," IEEE Transactions on Robotics, 25(1), 51-66 (2009).

[4] Hitt, J., Sugar, T., Holgate, M. *et al.*, "Robotic transtibial prosthesis with biomechanical energy regeneration," Industrial Robot: An International Journal, 36(5), 441–447 (2009).

[5] Hitt, J. K., Sugar, T. G., Holgate, M. *et al.*, "An Active Foot-Ankle Prosthesis With Biomechanical Energy Regeneration," ASME Journal of Medical Devices, 4(1), 011003 (2010).

[6] Hollander, K. W., Ilg, R., Sugar, T. G. *et al.*, "An Efficient Robotic Tendon for Gait Assistance," ASME Journal of Biomechanical Engineering, 128(5), 788-791 (2006).

[7] Sup, F., Varol, H. A., Mitchell, J. *et al.*, "Design and control of an active electrical knee and ankle prosthesis," 2nd IEEE RAS & EMBS International Conference on Biomedical Robotics and Biomechatronics, BioRob 2008, 523-528 (2008).

[8] Kawamoto, H., Kanbe, S., and Sankai, Y., "Power assist method for HAL-3 estimating operator's intention based on motion information," The 12th IEEE International Workshop on Robot and Human Interactive Communication, ROMAN 2003. , 67 (2003).

[9] Kazerooni, H., Racine, J. L., Lihua, H. *et al.*, "On the Control of the Berkeley Lower Extremity Exoskeleton (BLEEX)," Proceedings of the 2005 IEEE International Conference on Robotics and Automation, ICRA 2005, 4353 (2005).

[10] Hitt, J., Bellman, R., Holgate, M. *et al.*, "The SPARKy (Spring Ankle with Regenerative Kinetics) Project: Design and Analysis of a Robotic Transtibial Prosthesis with Regenerative Kinetics," ASME International Design Engineering Technical Conference, (2007).

[11] Hollander, K. W., and Sugar, T. G., "Design of Linear Actuators for Wearable Robotic Applications," ASME Journal of Mechanical Design, 128(3), 644-648 (2006).

[12] Sugar, T. G., "A Novel Selective Compliant Actuator," Mechatronics Journal, 12(9-10), 1157-1171 (2002).

[13] Sugar, T. G., and Kumar, V., "Design and control of a compliant parallel manipulator for a mobile platform," Proceedings of the 1998 ASME Design Engineering Technical Conferences and Computers in Engineering Conference, CD-ROM (1998).

[14] Hollander, K. W., Ilg, R., and Sugar, T. G., "Design of the Robotic Tendon" Design of Medical Devices, (2005).

[15] Whittle, M. W., [Gait Analysis: An Introduction] Butterworth-Heinemann, Oxford (1996).

[16] Hollander, K. W., and Sugar, T. G., "Design of Lead Screw Actuators for Wearable Robotic Applications " ASME International Design Engineering Technical Conference, (2005).

[17] Ward, J. A., [Design, Control, and Data Analysis for Rehabilitation Robotics] Arizona State University, Tempe (2009).

[18] Hitt, J., Merlo, J., Johnston, J. *et al.*, "Bionic Running for Unilateral Transtibial Military Amputees," Army Science Conference, (2010).

[19] Hollander, K. W., Sugar, T. G., and Herring, D., "A Robotic Jack Spring for Ankle Gait Assistance" ASME International Design Engineering Technical Conference, (2005).

[20] Holgate, M. A., Boehler, A. W., and Sugar, T. G., "Control algorithms for ankle robots: A reflection on the state-of-the-art and presentation of two novel algorithms," 2nd IEEE RAS & EMBS International Conference on Biomedical Robotics and Biomechatronics, BioRob 2008, 97-102 (2008).

[21] Holgate, M. A., Sugar, T. G., and Boehler, A. W., "A novel control algorithm for wearable robotics using phase plane invariants," IEEE International Conference on Robotics and Automation, ICRA '09. , 3845-3850 (2009).

Using the Translational Potential Energy of Springs for Prosthetic Systems

Jeffrey A. Ward, Thomas G. Sugar, *Member, IEEE,* and Kevin W. Hollander
Special Session: "Robotics in Medicine - Advances and Challenges"

***Abstract*—A robotic tendon is modeled and the stiffness of the spring is tuned so that the spring power reduces the peak motor power and energy required for ankle gait. When determining stiffness from gait literature, it is usually assumed that one side of the spring is fixed. We assume that the spring is translating to derive a second method to calculate stiffness.**

By choosing a tuned spring based on a "dynamic stiffness", the motor velocity was shown to be constant during the loading phase of ankle gait. We simulated this system and showed that energy was reduced and peak power was dramatically reduced.

The constant velocity controller was implemented on a powered ankle foot orthosis and test data was correlated with the simulation.

I. Introduction

One of the key challenges in wearable robotic systems is the ability to supply high power with low energy in a very lightweight actuator. Sometimes wearable exoskeletons must behave in a soft and compliant manner and sometimes they must behave in a stiff and rigid manner. The human body can effortlessly switch between a fast rigid position control scheme and a soft compliant, force control scheme. Researchers including us have developed actuators such as the series elastic actuator [1] and the robotic tendon actuator [2-6]. We also developed a Jack Spring actuator [7, 8] that uses a spring as a lead screw to dynamically adjust stiffness. Exoskeletons designed for gait are being developed [9-11].

In this paper, we focus on one method that the human could use to control the power and energy at a joint. We hypothesize that the human controls muscle/tendon springs to achieve high power when needed and to store and release energy. Instead of focusing on a spring that is fixed on one side, we focus on springs that translate and the relative velocity between the input and output sides of the spring determines the power and energy storage. Instead of focusing on the relationship between force and velocity (impedance control), we focus on the relationship between the derivative of force and velocity.

In the first section, we derive our robotic tendon model [4, 5] to emphasize the input and output power of a spring based actuator. In the next section, we study the ankle gait kinematics and kinetics applying the actuator to a bionic ankle. In the last section, we study "dynamic stiffness" which allows the input velocity of the actuator to be constant. We implemented the control scheme on a powered ankle foot orthosis and describe the results.

Manuscript received February 11, 2011. This work was supported in part by the Military Amputee Research program administered by TATRC Telemedicine and Advanced Technology Research Center.

Jeffrey A. Ward is with SpringActive Inc., Tempe, AZ 88281 USA

Thomas G. Sugar is with Arizona State University, Mesa, AZ 85212, (corresponding author: 480-727-1127; e-mail: Thomas.sugar@asu.edu).

Kevin W. Hollander is with SpringActive, Inc., Tempe, AZ 85281, USA.

II. Model of a Robotic Tendon

In a robotic tendon model, the motor rotates moving the nut position, *r*, inward and outward, Fig. 1. The output position, *x*, and force, *F*, describe the required movement and force to move the ankle during gait. A spring with stiffness, *K*, is placed between the nut and the external force. The spring is a buffer which can store and release energy altering the power relationships. In our case, the spring deflection is determined by the relative position between *x* and *r*.

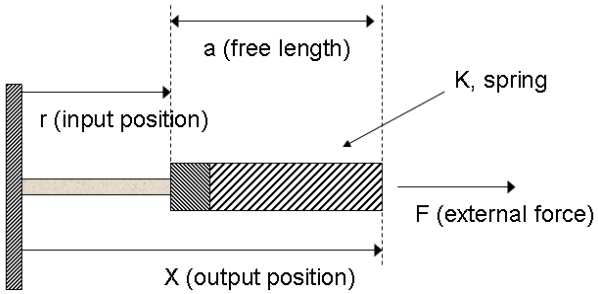

Fig. 1. In a robotic tendon model, the motor turns moving a nut inward or outward adjusting, *r*. The external force, *F*, and position, *x*, describe the desired outputs. A spring is placed in between the nut and the external force. The free length of the spring is given by, *a*

In a quasi static analysis ignoring friction, the external force determines the torque on the lead screw where *l* describes the lead. Assuming an ideal spring, the external force is balanced by the spring force.

$$\tau = \frac{Fl}{2\pi} \tag{1}$$

$$F = K(x - r - a) \tag{2}$$

The input position, *r*, is determined by the number of revolutions, *n*, that the motor spins and the lead, *l*:

$$r = l \cdot n \tag{3}$$

The output position, *x*, is determined by *r*, *F*, and the constant offset *a*:

$$x = r + a + \frac{F}{K} \tag{4}$$

The input velocity is given by differentiating (3) and assuming the lead, *l*, is fixed:

$$\dot{r} = l \cdot \dot{n} \tag{5}$$

The output velocity is given by differentiating (4) assuming the spring stiffness is constant:

$$\dot{x} = \dot{r} + \frac{\dot{F}}{K}$$

$$\dot{r} = \dot{x} - \frac{\dot{F}}{K}$$

$$\dot{x} - \dot{r} = \frac{\dot{F}}{K} \tag{6}$$

The relative velocity between the ends of the spring determines the power stored in the spring.

The spring power is defined:

$$\frac{F \cdot \dot{F}}{K} \tag{7}$$

The spring power is defined for a translating spring where both ends are moving. This term is not found in common textbooks because it is usually assumed that one side of the spring is fixed.

The motor angular velocity is given by:

$$\omega = \dot{\theta} = 2\pi \cdot \dot{n}$$

$$\dot{\theta} = \frac{2\pi \cdot \dot{r}}{l} = \frac{2\pi}{l}(\dot{x} - \frac{\dot{F}}{K}) \tag{8}$$

The input power is determined by multiplying the input torque and angular velocity. In this model, the input power does not equal the output power. To be consistent with the standard gait literature, the power curves will be inverted and a negative sign is added.

$$\tau\dot{\theta} = -F \cdot \dot{r} = -F \cdot (\dot{x} - \frac{\dot{F}}{K}) \tag{9}$$

The spring power can increase or decrease the required input power. In the specific case for analyzing ankle gait, the maximum peak motor power and motor angular velocity are both reduced. The spring stores braking energy releasing it when needed. Because of the ability of the spring to store energy, the total input energy is kept to a minimum. This term corresponds to the storage of "translational potential energy."

It is interesting to note that the input speed, $\dot{r}$, shown in (6) is not only a function of the lead, *l*, but also the changing force. The slope of the external force or the slope of the load curve can speed up or slow down the required motor speed. In this sense, the spring acts as a "load variable transmission." In our work [12], we have been studying a dynamic stiffness defined by:

$$K = \frac{\dot{F}}{\dot{x}} \tag{10}$$

In an ideal case, the input velocity would be zero if $(\dot{x} - \frac{\dot{F}}{K}) = 0$ at all points during the gait cycle. In the actual ankle gait cycle, positive work is performed so that this term will not always equal 0. It is interesting to study the dynamic stiffness to determine if a simple controller can be designed.

III. Ankle Gait Data

Gait is the term used to describe the locomotion of legged animals. Gait is a recurring pattern of leg and foot movements, rotations, and torques. Due to its repetitive nature, the discussion of gait is done in terms of percentages of a gait cycle. A gait cycle is defined for a single leg and begins with the initial contact of the foot with the ground or 'heel strike', the conclusion of a cycle occurs as the same foot makes a second 'heel strike'. The end of one gait cycle is of course the beginning of another. The input motions are typically determined using a motion capture system and the torques are derived using an inverse dynamics calculation. The ankle gait data used in our analysis has been digitized from Whittle [13].

The ankle position is shown in Fig. 2. Initially after heel strike, the ankle plantarflexes or moves downward. After the foot is flat on the ground, the shank then rolls over the ankle, i.e. dorsiflexing. During this period, the spring in the robotic tendon stores energy. At 40% of the gait cycle, the foot rapidly plantarflexes, which propels the person forward. During powered push-off or powered plantarflexion the moments and angular speeds are high. In this phase of gait, the spring releases its energy aiding in push-off. At 60% of the gait cycle, the toe comes off of the ground and the ankle rapidly dorsiflexes to insure that the toe does not touch or skid on the ground during the next phase of gait. From 60% to 100% of the gait cycle, the foot is in the air during the swing phase. During this phase of gait the ankle moments are low.

The ankle moment is shown in Fig. 3. The ankle moment data was scaled for an 80kg person. At 40% of the gait cycle, the moment is at its peak just as the angular velocity begins to increase rapidly. The combination of high forces and high velocities means that large powers are experienced in this region of the gait cycle, see Fig. 4.

Fig. 4 shows both positive and negative powers developed during a typical gait cycle. Utilizing a robot to aid in gait, sometimes the robot needs to aid the user (positive power) and sometimes for support the robot needs to resist the user (negative power) and in either case the robot is putting energy into the system. In our system, the spring stores energy when resisting the user and energy is released when assisting the user.

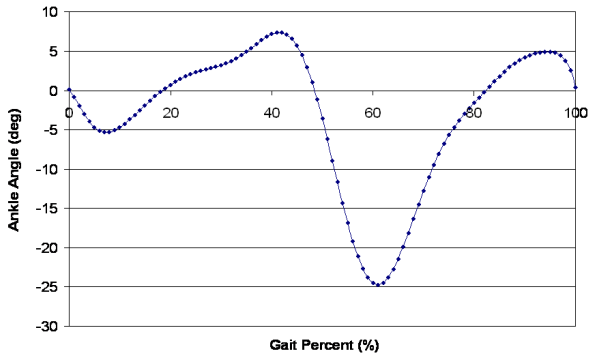

Fig. 2. Ankle angle as a percentage of the gait cycle. If the foot moves in a downward direction, it is plantarflexed and if the foot moves in an upward motion, it is dorsiflexed.

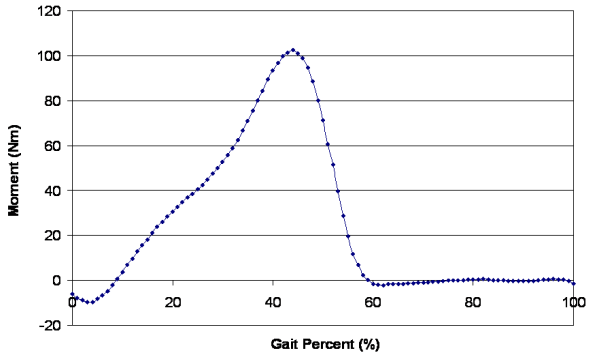

Fig. 3. The moment at the ankle as a percentage of the gait cycle.

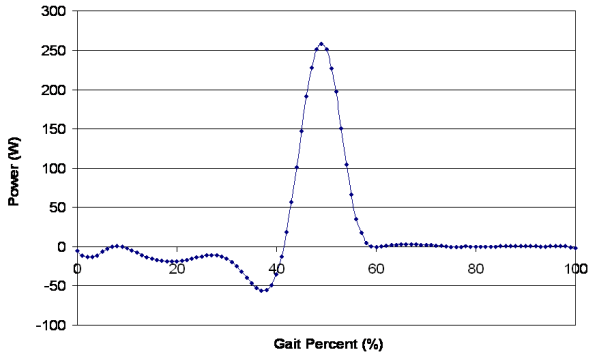

Fig. 4. The power at the ankle assuming a 0.8 Hz cycle and an 80 kg subject.

IV. Determining the Ankle Stiffness

It would seem that the stiffness at the ankle joint should be simple to calculate, but two different methods to calculate stiffness will be analyzed. In gait literature, the slope of the force/position curve is used to determine the stiffness, Fig. 5. For example, K is determined by the common Hooke's Law relationship.

$$F = K \cdot x \tag{11}$$

The stiffness is calculated at every point in the gait cycle using (11) and is shown in Fig. 6. The stiffness swings between very large negative and positive values.

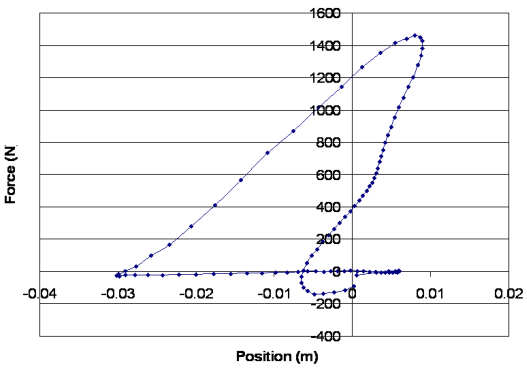

Fig. 5. The slope of the force versus deflection curve is used to determine stiffness. The force and position are derived from the moment and ankle position curves using a 0.07 m lever arm.

In a second method, the stiffness can be determined from (10). This method can be more relevant because the spring is not fixed but is moving relative to a fixed point. The dynamic stiffness is calculated for every point in the gait cycle and is shown in Fig. 6. In this case, the stiffness values are not as large and are not negative between 10 and 20% of the gait cycle.

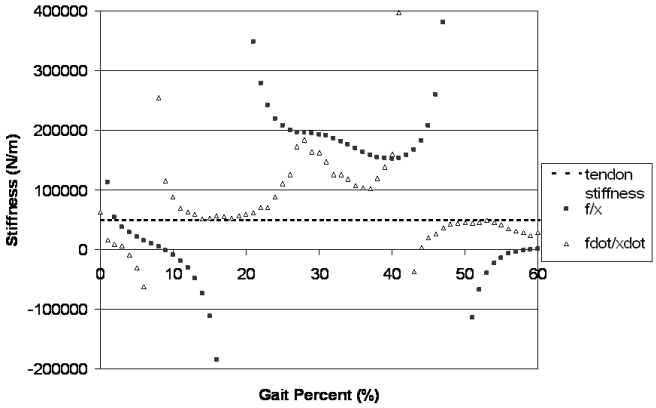

Fig. 6. Different methods of calculating stiffness. The standard method is to calculate F/x. A second method to calculate stiffness is to determine the ratio of the derivative of force vs. velocity. In one of the simulations, we use a fixed tendon stiffness of 48,587 N/m which matches the dynamic stiffness at 15% and 50% of the gait cycle.

A more interesting question arises, "Is there a relationship between velocity, $\dot{x}$, and the slope of the external force?" In this case, the impedance, which relates the velocity to the force, is not interesting. The relationship between velocity and the derivative of force is shown in Fig. 7. Data points only during the loading phase of stance, 9% to 60% of the gait cycle are used for the fit. A linear fit captures 96% of the variance.

$$\dot{F} = 48{,}587 \frac{N}{m} \cdot \dot{x} + 1750.6 \frac{N}{s} \tag{12}$$

The offset determines the speed that the motor must travel. If the offset was zero, then the input power would be zero.

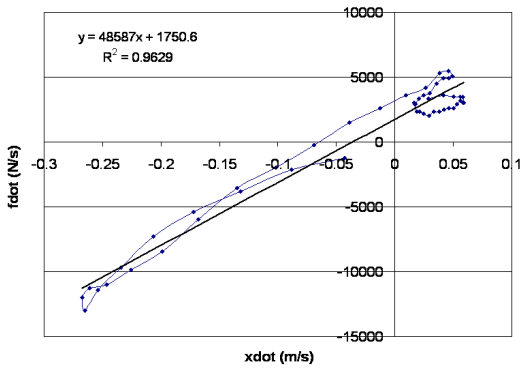

Fig. 7. The derivative of the force versus velocity. The relationship is used to determine a dynamic stiffness.

Fig 8. shows the ankle position curve and ankle force curve during the loading phase of gait. The slopes of each curve are similar. There is a gradual upward slope from 9 to 43% of the gait cycle for the force and a sharp downward slope from 46 to 60% of the gait cycle. The ankle position has a gradual upward slope from 9 to 42% of the gait cycle and then a sharp downward slope from 45% to 60% of the gait cycle. A tendon stiffness of 48,587 N/m is shown in Fig. 6.

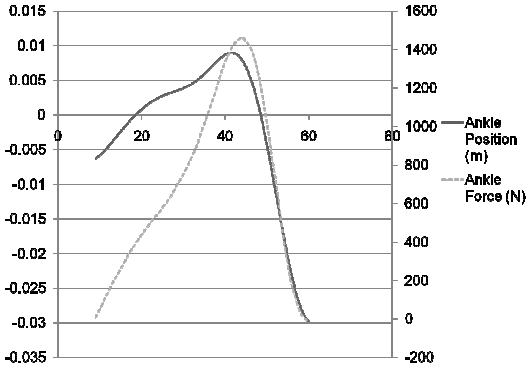

Fig. 8. The ankle position, x, and the ankle force, F are shown on the same graph during the stance phase of gait.

V. Simulations of the Robotic Tendon

In this section, the robotic tendon model is simulated to determine the input position, force, and power.

A. Choosing a stiffness to minimize power

In the ideal case, if one was to assume that energy can be stored and released properly, the peak motor power is 257.6 W and the energy required for each step is 19.4 J. In this ideal case, all of the braking energy is stored and used in push-off. We assumed an 80kg subject and the gait cycle duration is 1.25 seconds. The area underneath the power curve in Fig. 4 is integrated to determine 19.4 J.

A mechanical system without a spring is not adequate because peak power and energy required are both very high. If a motorized system assuming 100% efficiency is used without a spring, the peak motor power equals 257.6 W and the energy equals 38.8 J. The energy is much larger because a motor must resist the load as the shank rolls over the ankle and must provide the push-off energy to propel the person forward. In this simulation, the absolute value of the power curve in Fig. 4 was integrated to determine 38.8 J.

Using a tuned spring in the simulation of the robotic tendon model, the peak power and energy are both reduced. The peak input power is reduced to 96.6 W and the integration of the absolute value of the input power equals 21.2 J. This is a remarkable reduction in peak power and a large energy savings. In the model, the spring is optimized to reduce peak power. The spring stiffness is 53,224 N/m and a lever arm at the ankle is assumed to be 0.07 m. In Fig. 9, the peak motor power is reduced and the spring supplies much of the push-off power.

The input power is drastically reduced because the motor velocity is reduced with the addition of the spring. In Fig. 10, the velocity of the motor is shown for two cases. If there is a tuned spring, the velocity of the motor is low during 40-60% of the gait cycle. During the swing phase because the derivative of the force is close to zero, the velocity of the motor matches the gait data. If a spring is not added to the system, the velocity of the motor must match the velocity of the gait cycle.

In Fig. 11, the input position, *r*, and the output position, *x*, are determined from the gait data using equation (4). The deflection of the spring in the robotic tendon is determined by the desired force, *F* and the spring stiffness *K* using equation (2).

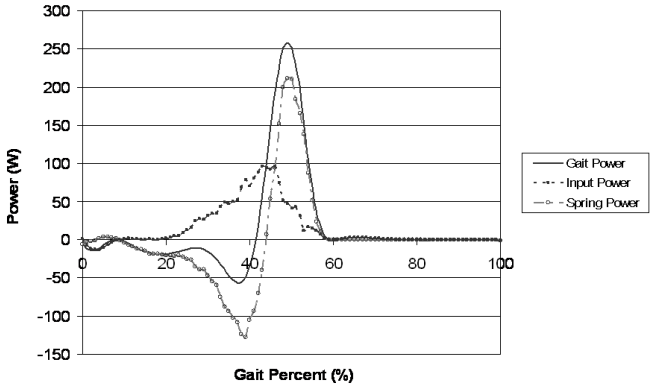

Fig. 9. The input power of the robotic tendon is determined using equation (9). The spring power is determined using equation (7).

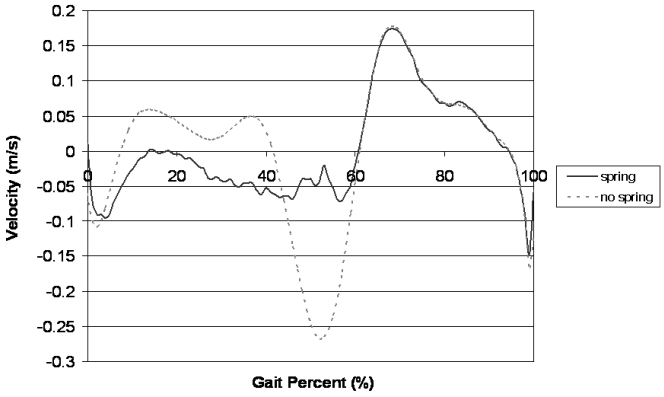

Fig. 10. When there is not a spring in the system, the motor velocity matches the gait velocity. When there is a spring, the motor velocity is reduced by the slope of the force curve using the second formula in equation (6).

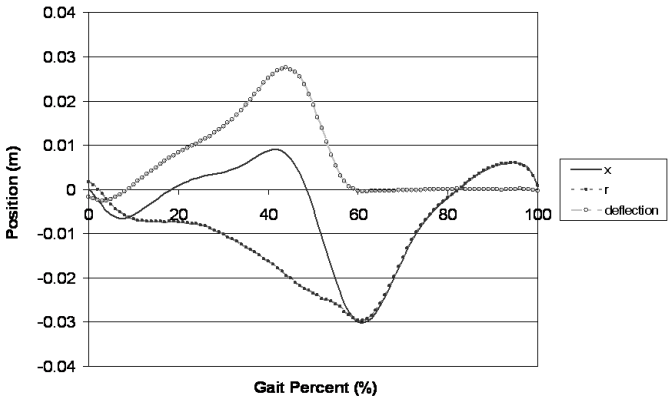

Fig. 11. The output position, x, is determined from the gait data. The ankle moment directly determines the force in the spring and its deflection. The motor position is determined by the output position, force, and spring constant using equation (4).

B. Choosing a Dynamic Stiffness

The stiffness of the system can be chosen so that it matches the dynamic stiffness calculated from the gait data.

$$\dot{r} = \dot{x} - \frac{\dot{F}}{K}$$

$$\dot{r} = \dot{x} - \frac{48587\dot{x} + 1750.6}{K}$$

It makes sense to choose a spring stiffness in the robotic tendon that matches the dynamic stiffness of 48,587 N/m. Using this method, the input velocity is no longer dependent on the output velocity. The input velocity equals a constant value.

$$\dot{r} = \dot{x} - \frac{48{,}587\dot{x} + 1750.6}{48{,}587}$$

$$\dot{r} = \frac{-1750.6}{48{,}587} m/s$$

In the second simulation, the spring in the robotic tendon equals 48,587 N/m and the input velocity is constant between 9% and 60% of the gait cycle, see Fig 12. A constant velocity command to a motor is very efficient because motors are inherent velocity sources.

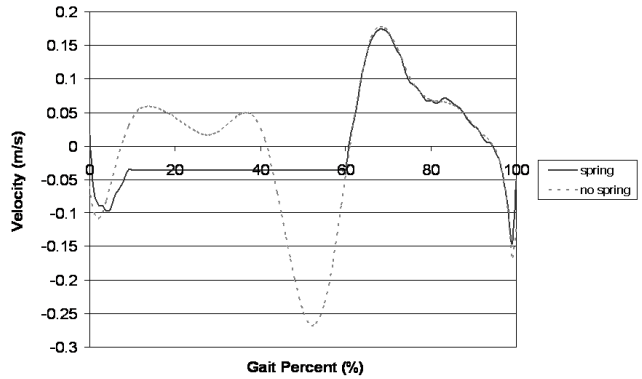

Fig. 12. When there is no spring in the system, the motor must match the gait velocity. When there is a spring in the system, the motor velocity is determined using equation (6). From 9% to 60% of the gait cycle, the motor velocity is constant.

In this simulation, the spring force is slightly altered from 9% to 60% of the gait cycle, Fig 13. Because the input velocity is constant, it can be easily integrated to determine the input position. The gait position and the new input position determine the spring deflection and new spring force. The spring force is slightly too large between 20 and 40% of the gait cycle resulting in extra energy storage.

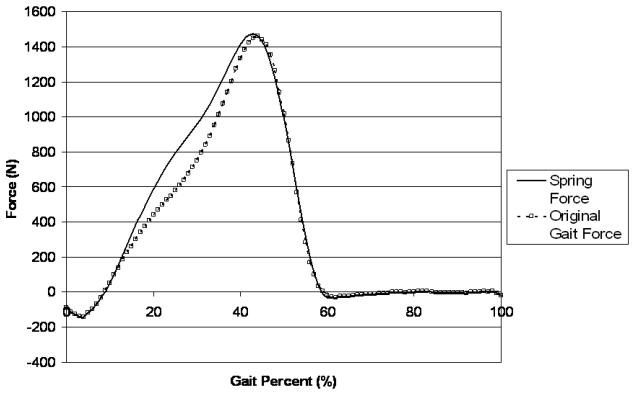

Fig. 13. The spring force is slightly too large between 20% and 40% of the gait cycle.

In this second simulation, the output gait power is slightly altered between 9% and 60% of the gait cycle because the constant velocity was not a perfect match, see Fig 14. The new gait force multiplied by the original gait velocity slightly alters the gait power. In this example, the peak power is 251 W and the required gait energy equals 17.5 J. The energy is less in this example, because there is slightly more braking energy. If the spring was eliminated from the system, the peak power is 251 W and the energy required is 40.3 J.

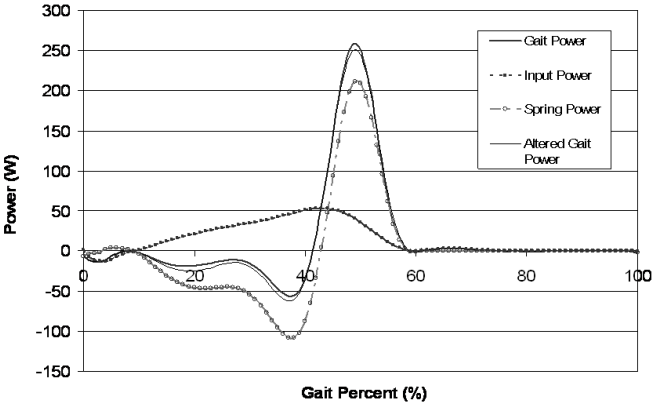

Fig. 14. The gait power curve is the same as the original data. The input power is determined by multiplying the new spring force with the new input velocity. The spring power is determined using equation (7). The altered gait power is determined by multiplying the new spring force with the original gait velocity.

Using a tuned spring and a constant velocity, the robotic tendon peak power is 53 W and the required energy is 19.3 J. The required energy is calculated by integrating the absolute value of the input power in Fig 14. The motor peak power, 53 W, was amplified by 4.7 in this case to achieve a fully powered push-off of 251 W. In the original tendon case, the power amplification was only 2.7. The output position, x, is

calculated from the original gait data using a 0.07 m lever arm. The input position, r, is a straight line between 9% and 60% of the gait cycle, Fig 15.

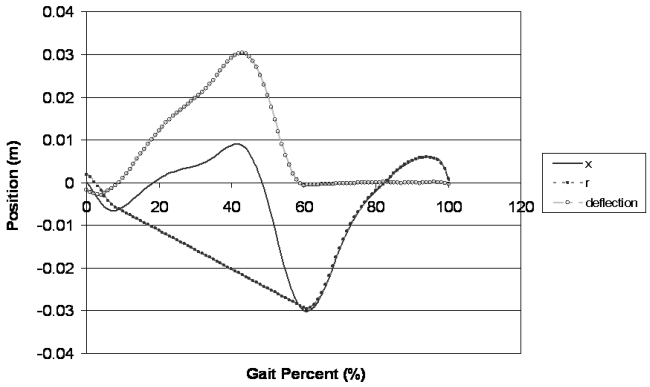

Fig. 15. The output position is determined from gait data. The input position is a straight line from 9% to 60% of the gait cycle.

VI. Testing on a Powered Orthosis

A powered ankle foot orthosis was designed and built based on the robotic tendon model [12, 14]. See Fig. 16. The custom lead screw moves the input position of the spring, *r*. Two helical springs mounted symmetrically on each side of the motor store and release energy. The springs are attached to a lever arm to provide the output moment and position of the ankle. A motor incremental encoder measures the input position and an absolute encoder measures the output ankle position. A prosthetist manufactured the custom foot bed, ankle joint, and plastic shell.

As the shank rolls over the ankle, the lever arm pulls down on the springs. At the same time, the motor pulls up on the springs storing energy in the spring. During push off, the spring contracts and the motor pulls up, pushing the foot downward to propel the person forward.

A simple servo position-controller is used to control the input side of the spring.

A constant velocity controller, CV Controller, was implemented on the powered exoskeleton, see Fig 17. The motor velocity was constant from 0 to 61% of the gait cycle. The ankle position (m) is shown with a small dorsiflexion pattern from 12 to 25% of the gait cycle. A fast plantarflexion pattern is shown from 50 to 60% of the gait cycle. The ankle position curve differs from Fig. 2 because the exoskeleton alters the gait pattern. This is true even for a passive orthosis without the robotic tendon assistance. Data we collected showed that while wearing a passive orthosis a longer dorsiflexion phase from 20 to 50% of the gait cycle occurred. The plantarflexion phase (50 to 69% of gait) was late as compared to able body gait.

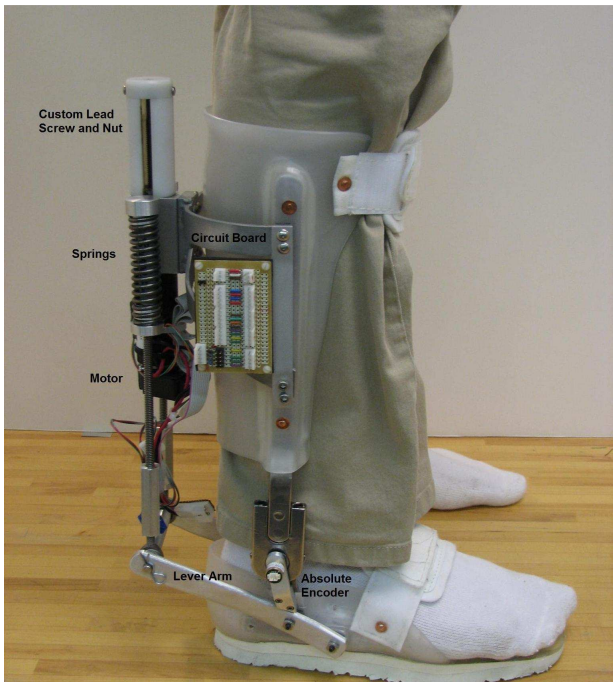

Fig. 16. A custom powered ankle foot orthosis was manufactured. The robotic tendon is mounted in the rear of the leg and is used to pull on the input side of the springs.

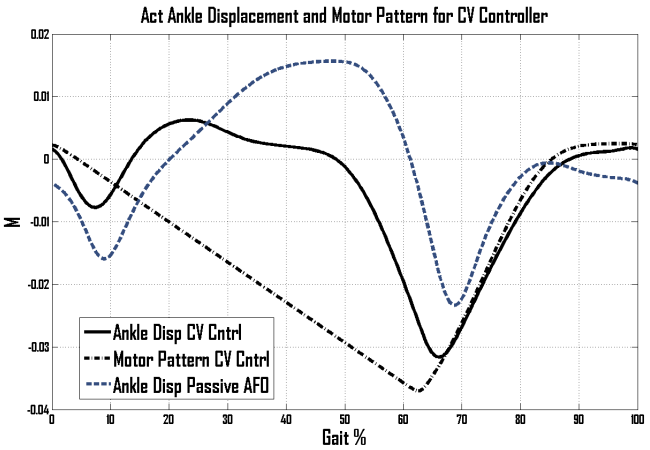

Fig. 17. The motor pattern for the Constant Velocity (CV) controller is shown. The ankle position is shown in solid. An ankle position curve wearing a non-powered exoskeleton is shown dashed. The exoskeleton causes the ankle motion to be altered as compared to able body gait.

The controller achieves a very good dynamic stiffness, see Fig 18. A plot of the derivative of force versus ankle velocity is shown. It should be noted that the output position of the spring is *not controlled*. The human being places their foot on the ground, loads the spring, and pushes off. During this time, if the output position *x* diverges from "normal" values, then the spring force, the derivative of the force, and the ankle velocity also diverge. During the trial, *x*, despite being controlled open loop, still tracked "normal" values quite well. This is demonstrated by the linear fit of the $\dot{F}$ versus $\dot{x}$ data shown in Fig. 18.

The stiffness differs because the weight of the individual and the length of the lever arm are different as compared to the simulation in Section V.

The graph of the average $\dot{F}$ versus $\dot{x}$ is shown in Fig 18. 110 steps were used to determine the average. This figure demonstrated the tight grouping of the data $\dot{F} = 15{,}361 \cdot \dot{x} + 688$. In this experiment, the user was only given 50% gait assistance. Half of the weight of the user is used as the input to the gait force and the ankle position remains the same. A motor pattern is then calculated as described in section V. In simulation, we expected to find an equation, $\dot{F} = 14{,}285 \cdot \dot{x} + 743$. This equation is a close match to the CV controller's data.

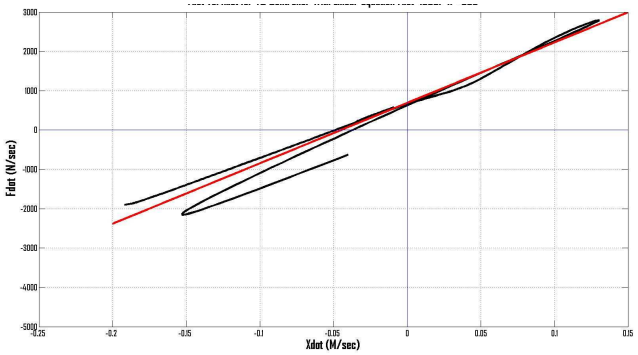

Fig. 18. Rate change of force versus rate change of ankle displacement from able bodied Powered Ankle Foot Orthosis, PAFO data.

VII. Conclusion

We derived our robotic tendon model to emphasize that the relative velocity between the input and output sides of the spring determines the spring power. The stiffness of the spring is tuned so that the spring power reduces the peak motor power and energy required for ankle gait.

When determining stiffness from gait literature, it is usually assumed that one side of the spring is fixed. Again, we assumed that the spring is translating and used the spring power term to derive a second dynamic method to calculate stiffness.

By choosing a tuned spring based on a "dynamic stiffness", the motor velocity was shown to be constant during the loading phase of ankle gait. We simulated this system and showed that energy was reduced and peak power was dramatically reduced.

The constant velocity controller was implemented on a powered ankle foot orthosis and test data correlated with the simulations.

References

[1] S. K. Au and H. Herr, "Powered ankle-foot prosthesis," *IEEE Robotics & Automation Magazine*, vol. 15, pp. 52-59, 2008.

[2] J. Hitt, T. Sugar, M. Holgate, R. Bellman, and K. Hollander, "Robotic transtibial prosthesis with biomechanical energy regeneration," *Industrial Robot: An International Journal*, vol. 36, pp. 441–447, 2009.

[3] J. K. Hitt, T. G. Sugar, M. Holgate, and R. Bellman, "An Active Foot-Ankle Prosthesis with Biomechanical Energy Regeneration," *ASME Journal of Medical Devices*, vol. 4, p. 011003, 2010.

[4] K. W. Hollander, R. Ilg, and T. G. Sugar, "Design of the Robotic Tendon " in *Design of Medical Devices*, 2005.

[5] K. W. Hollander, R. Ilg, T. G. Sugar, and D. Herring, "An Efficient Robotic Tendon for Gait Assistance," *ASME Journal of Biomechanical Engineering*, vol. 128, pp. 788-791, 2006.

[6] T. G. Sugar, "A Novel Selective Compliant Actuator," *Mechatronics Journal*, vol. 12, pp. 1157-1171, 2002.

[7] K. W. Hollander, T. G. Sugar, and D. Herring, "A Robotic Jack Spring for Ankle Gait Assistance " in *ASME International Design Engineering Technical Conference*, 2005.

[8] K. W. Hollander, T. G. Sugar, and D. E. Herring, "Adjustable robotic tendon using a 'Jack Spring'," in *9th International Conference on Rehabilitation Robotics, ICORR 2005*, 2005, p. 113.

[9] S. K. Agrawal, A. G. Erdman, "Biomedical Assist Devices and New Biomimetic Machines - A Short Perspective," *Journal of Mechanical Design*, vol. 127, p. 799-801, 2005.

[10] S. K. Banala, S. H. Kim, S. K. Agrawal, and J. P. Scholz, " Robot assisted gait training with active leg exoskeleton (ALEX)," *IEEE Transactions on Neural Systems and Rehabilitation Engineering*, vol. 17, pp. 2-8, 2009.

[11] J. A. Blaya and H. Herr, "Adaptive control of a variable-impedance ankle-foot orthosis to assist drop-foot gait," *IEEE Transactions on Neural Systems and Rehabilitation Engineering*, vol. 12, pp. 24-31, 2004.

[12] J. A. Ward, "Design, Control, and Data Analysis for Rehabilitation Robotics," in *Mechanical Engineering*. vol. PhD Tempe: Arizona State University, 2009.

[13] M. W. Whittle, *Gait Analysis: An Introduction*, 2 ed. Oxford: Butterworth-Heinemann, 1996.

[14] J. Ward, T. Sugar, J. Standeven, and J. R. Engsberg, "Stroke survivor gait adaptation and performance after training on a Powered Ankle Foot Orthosis," in *2010 IEEE International Conference on Robotics and Automation (ICRA)*, 2010, pp. 211-216.

International Conference on Control, Automation and Systems 2010
Oct. 27-30, 2010 in KINTEX, Gyeonggi-do, Korea

Load Carriage Effects on a Robotic Transtibial Prosthesis

Joseph Hitt[1] and Thomas Sugar[2]

[1] Department of Civil & Mechanical Engineering, United States Military Academy, West Point, New York, USA
(Tel : 845-938-2665; E-mail: joseph.hitt@usma.edu)
[2] Department of Engineering, Arizona State University, Mesa, Arizona, USA
(Tel : 460-727-1127; E-mail: thomas.sugar@asu.edu)

Abstract: The purpose of this study was to investigate the kinetic and kinematic effects of load carriage while wearing a robotic transtibial prosthesis. Nine separate tests were conducted with a unilateral transtibial amputee test subject wearing the robotic foot-ankle prosthesis. The subject walked on a treadmill at 1.3 m/s with a back pack weighing 0 kg, 4.5 kg and 9 kg. Direct measurement of the kinematics and kinetics of the robotic prosthesis at varying loads and ankle joint stiffness using embedded sensors is presented. The test data suggest that the coping strategy for load carriage is one of kinetic variance and kinematic invariance for subjects using a powered, computer controlled foot-ankle prosthesis. The finding suggests that modulation of the spring stiffness as a function of load condition may reduce system energy expenditure by 10%.

Keywords: Bionics, Biorobotics, Powered Prosthesis, Load Carriage, SPARKy.

1. INTRODUCTION

The implications of load carrying are primarily due to the overall increase in weight supported by the prosthesis. A passive prosthetic device that is optimized for the user weight and level of activity is not functionally designed for significant weight increases. One of the Nation's leading prosthetic companies suggests that 10lbs or more of added weight will cause undesirable gait changes and discomfort [1]. Holt et al in their study found a strong relationship between loading, walking speed and leg stiffness [2]. 11 health subjects walked at speeds ranging from 0.6 m/s to 1.6 m/s in combination with and without a backpack weighing 40% of their body weight. They found that "stiffness showed significant increases as a function of both speed and load." Harman et al. examined gait kinematics and gait kinetics of 16 able-bodied subjects who also carried various loads in a backpack [3]. They showed that as the load was increased, the ankle, knee and hip kinematics did not change. However, the joint torques increased considerably with increase in load. Selles, extended this thought to transtibial amputees. He found that a "kinematic invariance" strategy was likely used by persons using transtibial prostheses when weights were added to their prostheses [4]. In another study by Hansen, Childress et al, 2005 [5], they strongly support the hypothesis that the strategy is one of kinetic variance and not kinematic. They suggest that the "quasi-stiffness" of the ankle, knee and hip joints may increase to accommodate the change in load and speed while the kinematics such as the roll-over rocker remains unchanged. They surmise that this strategy best maintains the vertical profile of the center of mass of the body and consequently minimizes energy consumption.

2. ROBOTIC PROSTHESIS

The robotic prosthesis, SPARKy, Fig. 1, used in this study utilizes the Robotic Tendon, a DC motor in series with helical springs, to regenerate energy [6]. The dynamics of the user stores energy in the spring and the spring returns that energy to the user in a cyclical and highly efficient regenerative manner [7-9].

Fig. 1. Isometric view and photograph of SPARKy on a male transtibial amputee test subject.

A Robotic Tendon actuator is employed in this device to minimize the peak motor power requirement by correctly positioning a uniquely tuned helical spring so that the spring provides most of the peak power required for gait. The Robotic Tendon is a small and lightweight actuator that features a low power motor that is used to adjust the position of the helical spring using a very robust position controller. The controller achieves the desired spring deflection and, consequently via Hooke's Law, the desired force and ankle moment is realized using a spring in series with a motor. As the ankle rotates over the foot during the stance phase, as illustrated in Fig. 2 by the inverted pendulum model, the spring is extended by the falling center of mass of the body. Additional deflection in the spring is achieved

by correctly positioning the motor so that the desired ankle joint angle and moment is realized. A heavy, powerful motor is not needed because the Robotic Tendon, similar to the biological tendon-muscle complex, stores a portion of the stance phase kinetic energy and additional motor energy within the spring. The spring releases its stored energy to provide most of the peak power required during "push off." Therefore, the power requirement on the motor is significantly reduced. As described in [6], peak motor power required is 77W compared to 250W for a direct drive system in the 80 kg subject at a 0.8 Hz example. Consequently, the weight of the Robotic Tendon, at just 0.95 kg, achieves a power density that in essence is 7 times greater than a direct drive approach.

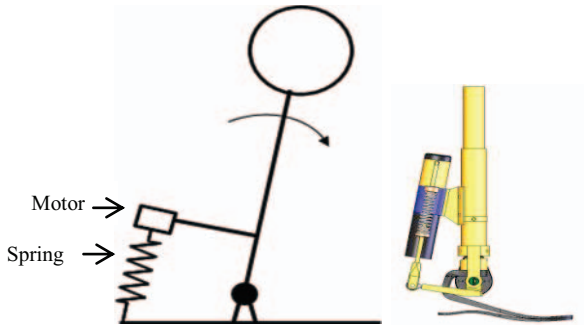

Fig. 2. Desired spring deflection is achieved by controlling the motor position and capitalizing on the cyclical nature of gait. As the tibia rotates over the stance foot, springs are extended. Simultaneously, the motor extends the springs to achieve the desired spring deflection and the forces required to generate the required ankle moment for walking. This inverted pendulum with a lumped mass illustrates the regeneration energy with use of a spring in series with a motor. Computer aided design model of the prototype is illustrated on the right.

3. METHODS

Nine separate tests were conducted with one unilateral transtibial amputee test subject, who weighs 80 kg. The subject walked on a treadmill at 1.3 m/s (3 mph) with a back pack weighing 0 kg, 4.5 kg and 9 kg. 9 kg (11.25% of body weight) was the limit for the test subject even though a heavier load may have provided for a better test range and stronger indication of the load effect. The spring stiffness on the device was set at 33 KN/m, 36 KN/m and 40 KN/m for each loading condition, accounting for the 9 tests. All other parameters remained constant. The true power model, Eq. (1), developed in [10] was used to predict the system energy requirement.

$$P_e = P_j + \frac{P_m}{\eta_m \eta_g \eta_{ls}} + P_s \quad (1)$$

where P_j is the power required to overcome the inertia effects, P_m is the power required at the nut for gait and P_s is the power required to overcome the system mechanical power sinks. The denominator of P_m is the product of the motor, gear box and lead screw efficiency. P_j is the angular velocity at the motor times the torque required to overcome the motor rotor and gear box inertia.

Direct measurement of voltage and current to the motor was used to determine the actual energy usage. An incremental encoder at the robot ankle joint and at the motor provided position information. Via Hooke's Law, product of the spring deflection and stiffness was used to determine the moment at the robot ankle joint. Statistically, load and stiffness were considered separate factors each with three levels (treatments) in the 2 Factor ANOVA.

4. RESULTS

The variance in mean of each level of both factors, load and stiffness, was determined using a two factor ANOVA. The results of the ANOVA indicate that the loading and spring stiffness factors significantly affect data mean in terms of ankle joint moment and input energy. The ANOVA also indicates a strong interaction between spring stiffness and loading. The results do not show a significant relationship between the factors and ankle joint angle.

The data, Table 1, suggests that ankle joint moment increase with increase in loading. The variance in mean of each level of both factors (load and stiffness) was determined using a two factor ANOVA. The p-value for the loading factor is $<10^{-12}$. The p-value for the stiffness factor is 10^{-10}. The p-value for the factor interaction is 10^{-12}. Therefore, the results of the ANOVA indicate that the loading and spring stiffness factors significantly affect data mean. The ANOVA also indicates a strong interaction between spring stiffness and loading.

The data and its analysis confirm what is found in literature that ankle joint moment increases with load. However, the data in this testing is unique since it is from direct measurements at the ankle joint rather than indirect methods such as inverse dynamics. In addition, it provides a unique observation that there is a relationship between ankle joint moment and spring stiffness.

Table 1. Mean and STD Peak Ankle Joint Moment for Stiffness and Loading Variation.

Mean Peak Ankle Joint Moment [Nm] (STD)			
	0 kg	4.5 kg	9 kg
33 KN/m	70.4 (3.4)	72.7 (2.9)	80.2 (1.6)
36 KN/m	74.4 (1.7)	75.6 (1.5)	75.2 (1.3)
40 KN/m	76.0 (3.4)	75.0 (1.3)	83.6 (1.9)

Table 2 provides the ankle joint angle measurements for both factors (load and stiffness) and its three

treatments. Inspection of the data in the table horizontally, with varying load, or vertically, with varying stiffness, shows that the ankle joint angle does not indicate a trend. Rather, the only variability seems to be caused by unknown factors (nuisance factors). This is consistent with literature that the strategy with loading is one of kinetic not kinematic variance.

The data are from an independent sample with normal distribution. The variance in mean of each level of both factors (load and stiffness) was determined using a two factor ANOVA. The p-values for both the loading and stiffness factors and their interactions were not significant.

Table 2. Mean Peak Ankle Joint Angle for Stiffness and Loading Variation.

Mean Peak Ankle Joint Angle [deg]			
	0 kg	4.5 kg	9 kg
33 KN/m	25.0	25.1	24.4
36 KN/m	23.9	25.0	25.1
40 KN/m	22.5	25.2	24.0

Table 3 is the mean input energy at each treatment and its associated input energy value from the model, numerical integration of Eq. (1), is parenthetically included. The mean values show that input energy increases with both load and stiffness. The lowest value is at (33 KN/m, 0 kg) and the highest value is at (40 KN/m, 9 kg). The model and the data correlate very well for every treatment. However, the model, which follows the test results very well, predicts that at 20 kg, the stiffest spring is optimal. This is consistent with even literature on passive devices. A heavier person requires a stiffer prosthesis for a given level of activity. In the same manner, as the user increases the load he carries, the spring stiffness must increase. The data here provides support to that notion in a very direct approach. At low loading ranges, such as the case in our testing (0 to 9 kg), there may not be a need to change spring stiffness. However, if the loading becomes significant, i.e., 20 kg, increasing the stiffness on the device will decrease input energy.

Both data and model indicates that the optimal stiffness is the 33 KN/m stiffness at every loading condition. It also shows that input energy increases with increase in loading. The data and the model are in very good agreement.

The input energy data are from an independent sample with normal distribution. The variance in mean of each level of both factors (load and stiffness) was determined using a two factor ANOVA. The p-value for the loading factor, in terms of the input energy, is 0.02. The p-value for the stiffness factor is 0.02. The p-value for the factor interaction is 0.9. Therefore, the results of the ANOVA indicate that the loading and spring stiffness factors significantly affect data mean. The ANOVA indicates a very slim interaction between spring stiffness and loading in terms of input energy.

Table 3. Input Energy Under Stiffness and Loading Variation. The model results are in parentheses.

Input Energy: Test and (Model) [J/s]				
	0 kg	4.5 kg	9 kg	20 kg
33 KN/m	49.5 (39.8)	51.3 (41.2)	53.2 (42.9)	(53.5)
36 KN/m	52.6 (40.5)	52.5 (41.8)	54.7 (43.2)	(52.9)
40 KN/m	51.9 (42.2)	54.2 (43.2)	55.0 (44.3)	(52.5)

The data, Tables 1-3, and its analysis support literature in that a person will change his ankle joint moment to compensate for the change in load while maintaining a similar ankle joint angle. It extends this observation further by demonstrating that input energy at the ankle joint must also increase with load. The testing also showed that there is an optimal stiffness for a given load. For example, 33 KN/m is optimal at 0 to 9 kg. However, the model predicts that at 20 kg, 40 KN/m is optimal. In terms of future design, if the loading condition of the user increases significantly, such as a Military amputee carrying a heavy backpack, which can weigh in excess of 30 kg, simply dialing away one or two active coils in the helical springs may equate to 5-10% energy savings and an additional half to one kilometer walking distance.

4. CONCLUSION

The test results support the findings in literature that the strategy may be one of kinetic variance and not kinematic. It also suggest that energy efficiency can improve with change in spring stiffness. The significance of this study is that direct measurements of the ankle joint kinetics and kinematics was possible with embedded sensors while the studies in literature are predominately one of inverse dynamics based on motion capture and force plate data which adds significant accuracy challenges. In addition, this is most likely the first study of its kind for powered transtibial prosthesis in literature today. In addition, in this study, the effective ankle joint stiffness was varied by changing the spring stiffness from 33KN/m to 40 KN/m. This is also very unique since a physical change in ankle joint stiffness is not possible in able-bodied subjects and difficult in amputee subjects using passive, unchangeable prostheses.

5. FUTURE STUDIES

The team has developed several overground, powered, walking transtibial prostheses since this study, Fig. 3. These prototypes leverage the regenerative kinetics and compliance inherent in the Robotic Tendon design. The newest prototype, Fig. 4, supported an amputee running at 3.6 m/s on a treadmill [11]. Future

versions of the walking and running capable powered transtibial prostheses will dynamically modulate the spring stiffness as a function of loading to improve energy efficiency and performance as this study suggests.

Fig. 3. Transtibial amputee subjects during metabolic and gait studies using two of the newer prototypes.

Fig. 4. Computer aided design view of the newest prototype with two DC motors demonstrated by a unilateral amputee at 3.6 m/s running.

REFERENCES

[1] Patient Information (2007) Ohio Willow Wood Prosthetic Company. [Online]. Available: http://www.owwco.com/

[2] K. Holt, R. Wagenaar, M. LaFiandra, M. Kubo, J. Obusek, "Increased musculoskeletal stiffness during load carriage at increasing walking speeds maintains constant vertical excursion of the body center of mass," *Journal of Biomechanics*, vol. 36(4), pp. 465-71, 2003.

[3] E. Harman, K. Han, P. Frykman, C. Pandorf, "The effects of backpack weight on the biomechanics of load carriage," *Technical Report T00/17, United States Army Research Institute of Environmental Medicine*, pp. 1–62, 2000.

[4] R. Selles, "Weighing weight: effect of below-knee prosthetic inertial properties on gait," PhD Dissertation, Erasmus University, Rotterdam, The Netherlands, 2002.

[5] A. H. Hansen, D. S. Childress, "Effects of adding weight to the torso on roll-over characteristics of walking," *Journal of Rehabilitation Research & Development*, Vol. 42 Issue 3, p381, 10p, Jun 2005.

[6] K. W. Hollander, Robert Ilg, T. G. Sugar, and D. E. Herring, "An Efficient Robotic Tendon for Gait Assistance," *ASME Journal of Biomechanical Engineering*, vol 128(5), pp. 788-791, 2006.

[7] J. Hitt, M. Holgate, R. Bellman, T. Sugar, K. Hollander, "The SPARKy (Spring Ankle with Regenerative Kinetics) Project : Design and Analysis of a Robotic Transtibial Prosthesis, " ASME International Design Engineering Technical Conference & Computers and Information in Engineering Conference, Las Vegas, NV, 2007.

[8] J. Hitt, A. Oymagil, T. Sugar, et al. "Dynamically Controlled Ankle-Foot Orthosis with Regenerative Kinetics: Incrementally Attaining User Portability," Proceedings of the 2007 IEEE International Conference on Robotics and Automation, Roma, Italy, 2007.

[9] J. Hitt, M. Holgate, T. Sugar, R Bellman and K. Hollander, "Robotic Transtibial Prosthesis with Biomechanical Energy Regeneration," Journal of Industrial Robots, vol. 36, issue 5, pp. 441-447, 2009.

[10] J. Hitt, Holgate, M., Bellman, R., and Sugar, T., "Building an Energy Efficient Robotic Transtibial Prosthesis," *ASME Journal of Medical Devices*, vol. 4, issue 1, 2010.

[11] Discovery Channel documentary "Kamen Code: Bionics," airing Jan, 2011.

BIONIC RUNNING FOR UNILATERAL TRANSTIBIAL MILITARY AMPUTEES

Joseph Hitt, James Merlo, and Jonathan Johnston
United States Military Academy
West Point, NY 10996

Matthew Holgate, Alex Boehler, Kevin Hollander, and Thomas Sugar
SpringActive, Inc.
Tempe, AZ 85281

ABSTRACT

A team from the United States Military Academy and Walter Reed Medical Center, in collaboration with private industry partner, SpringActive, Inc., have designed, built, and demonstrated a first of its kind motor powered, single board computer controlled, running prosthesis for military transtibial amputees. This paper presents the design and initial results of the new prototype, which includes successful testing with one unilateral transtibial Military amputee running at 3.6 m/s (8 mph) on a treadmill. The 2011 prototype described in this paper is intended to support a unilateral transtibial Military amputee on an Army Physical Fitness Test which includes a 2 mile timed run on a level ground.

1. INTRODUCTION

A team of faculty, staff, and cadets from the United States Military Academy, with support from the clinicians at Walter Reed Medical Center, in collaboration with private industry partner, SpringActive, Inc., have designed, built, and demonstrated a first of its kind motor powered, single board computer controlled, running prosthesis for military transtibial amputees.

Despite several versions of passive and active transtibial prostheses in various stages of technological readiness levels, none currently provide the military transtibial amputees a single component solution for returning to full duty. The desired outcome is to develop a robust walk-run, all terrain, all-weather, quiet device that requires one battery charge per day and with a total weight less than the replaced limb. The device must be metabolically efficient and kinematically beneficial. The device will integrate with individual soldier equipment. The design will allow simple removal of active components, such as the computer and the motor, for occasions when a passive device provides sufficient performance or when Military operations such as airborne and waterborne operations dictate.

1.1 Passive Prostheses

The limitation of passive prostheses ultimately stems from their constant stiffness characteristics and inability to supplement the potential energy stored during the stance phase of the gait cycle.

The prevalence of activity-specific foot-ankle prosthetics highlights the consequences of the constant stiffness characteristics for passive devices. These purpose-built passive prosthetics are optimized for a desired level of energy efficiency and stability for a given activity, in a given environment, and under the constraint of the mechanics properties for the components that store and release potential energy during the stance phase of the gait cycle. Varying the design constraints is critical to transitioning between various gait speeds and conditions because they affect the overall compliance and energy regeneration capabilities of the prosthetic limb. The amount of compliance or effective stiffness of the limb is effectively a compromise between metabolic efficiency and stability for a given condition of user biometrics, gait speed, and running surface (Daley and Usherwood, 2010). The transtibial amputee is often thus confronted with the decision to interchange between several prosthetic feet or use one, likely suboptimal for several environments. These decisions become more challenging for Military amputees who may be in austere environments under unpredictable operational conditions.

There exist unique solutions using active controls to vary the kinematics of the lower limb prosthesis. One such example is the Propio ankle by Ossur, which uses a computer based motor to control ankle angle based on position in gait cycle, gait, and other external conditions (Proprio Technical Manual, 2009). Unfortunately, it does not provide any additional power to the gait cycle, which is a limitation of all passive prostheses. The human gait cycle has an energy deficit for a 70kg person ranging from 36J/step while walking, to 100J/step while running, which is provided in non-amputees by the lower limb muscle network (Hitt et al., 2010). This energy deficit attributes to greater energy consumption while walking

and running for transtibial amputees, with tests indicating that they can expend up to 35% more energy while walking (Rao et al., 1998).

1.2 Active Prostheses

Active prostheses serve to replicate the lower limb muscle-tendon system in the sagittal plane with a combination of a linear springs and actuators. The linear springs regenerate energy during the stance phase, while the actuator effectively decreases the equilibrium length of the spring after dorsi-flexion of the stance phase to supplement the amount of potential energy it stores and releases. Decreasing the effective equilibrium length of the spring increases the displacement of the spring from equilibrium during dorsi-flexion, which by Hooke's Law, stores additional energy in the spring equal to the product of the spring rate and difference in the squares of the effective displacements. Brushless (Blaya and Herr, 2004) and brushed motors (Hitt et al., 2010), in addition to pneumatic muscles (Kao et al., 2010; Versluys et al., 2008; Hitt et al., 2010) provide the energy required to increase the spring potential in the stance phase of both prostheses and orthotics. The benefit of storing the potential energy during dorsi-flexion is it effectively provides a motor power multiplication factor of up to 3. That is, the muscle-tendon system is able to maintain a 450W power output while using a 150W motor while walking (Hitt et al., 2010).

1.3 Transitioning from Walking to Running

As previously discussed, there is nearly a threefold increase in energy required during the gait cycle to transition from walking to running. In addition, the stride frequency nearly doubles, necessitating close to six times the power output from the muscle-tendon complex while running when compared to walking. What further exacerbates this power requirement is the increased effort required to overcome actuator inertial characteristics, which were found to account for a significant 18% (80W) of the muscle-tendon output simply during walking (Hitt et al., 2010). Not only does the gait cycle frequency increase in the transition to running, but the acceleration of actuator components within each gait cycle increases as a result of the changes in kinematics between walking and running. While walking, the stance phase accounts for 62% of the gait cycle, which decreases to 36% as the gait transitions from walking to running (Novacheck, 1998). The effect of an increased gait cycle frequency and reduced time for storing and releasing energy per cycle is a dramatic elevation in the power required to overcome the inertial effects of the actuators and supply the needed quick power spike at push-off.

Another important consideration in the transition to running is the biped's natural neuromuscular adaptation while changing gait from walk to run. Comparisons between gait speed and leg stiffness indicated a positive correlation between the two. However, clinical trials determined that increases in gait speed caused solely by increases in stride length had little effect on the leg stiffness (Farley and Gonzales, 1996). Additional trials determined a strong correlation between stride frequency and leg stiffness (Farley and Ferris, 1998).

When comparing leg stiffness to surface compliance at constant speeds in human subjects (Ferris et al., 1998) and guinea fowl (Daley and Biewener., 2006; Daley and Usherwood, 2010; Biewener, 2007), results demonstrated that biped neuromuscular control maintains a constant effective leg stiffness, which accounts for the leg stiffness in series with the surface stiffness. While some experiments determined that the majority of the neuromuscular stiffness adjustments occurred at the knee joint (Burdett, 1982), there exists convincing evidence that neuromuscular adaption exists at the ankle as well. Active transtibial prosthesis testing of subjects loaded with different weights at a specified gait demonstrated that tendon stiffness adjustments affected actuator efficiency (Hitt and Sugar, 2010). Clinical trials conducted to determine the reduction in muscle-tendon loading using an active orthosis demonstrated that human subjects were also likely to reduce leg stiffness (Ferris and Farley, 1998) when supplemented by an actuator. However, most interesting was the change in ankle kinematics when using an active orthosis. Research suggests that the neuromuscular response at the ankle seeks to maintain a specified moment within the joint, to the point that the subject will change his or her gait to maintain that ankle moment (Kao et al., 2009). Thus, in order to prevent disruption to the transtibial amputee's running gait, the actuation of the active ankle prosthesis must accurately mimic the kinematics and kinetics of the ankle. This requires a robust control system that allows the active prosthesis to properly mimic the ankle moment profile for given user-specific gait kinematics.

1.4 Tendon-Muscle Control Schemes

Finite state machine control systems exist for active transtibial prosthesis in various levels of robustness. Single state control schemes estimate the start and frequency of a specified gait cycle, and control the effective length of the spring based on an assumed gate profile (Oymagil et al. 2007). However, due to the variability in gait profile under realistic conditions, the limitations of this simple state machine overcome the inherent stability of the compliance offered by series actuator spring muscle tendon system. This limitation is particularly critical when transitioning from walking to running as the magnitude and timing of dorsi and plantar flexion differ significantly between the two gaits.

Robust finite state control systems adapt to changes in the gait by controlling invariant parameters within different portions of the gait. One implementation (Bohler et al., 2008) divides the stance phase into five zones based on the ankle angular position, and controls either ankle torsional stiffness or angular velocity within each zone. This method seeks to control angular velocity when the ankle is plantarflexing, and stiffness when the ankle is dorsiflexing during the stance phase. The optimal angular velocity and stiffness parameters vary based on the position within the gait cycle, which the control method addresses by defining specific parameters for three separate plantarflexion zones and two separate dorsiflexion zones, accounting for five unique parameters for a given gait cycle. As the optimal angular ankle angular velocity and stiffness profiles also vary under realistic conditions, this control system uses state logic to determine the amputee activity given the conditions, and maps the five optimal parameters to that specific activity.

Impedance Control methods (Shaeffer and Hirzinger, 2002) provide actuator inputs to change the effective inertia, damping, and stiffness characteristics of the robotic limb. Though this method requires knowledge of the reaction forces and moments on the ankle, it offers flexibility within the system to adapt to changing environmental conditions. Applications in active ankle foot orthotics use state logic to determine different zones within the stance and swing phases to vary the effective impedance of the limb (Blaya and Herr, 2004). Such applications have been effective in stabilizing plantarflexion during the beginning of the stance phase to prevent toe slap, while still allowing sufficient dorsiflexion during the beginning of the swing phase to prevent toe drag, thereby reducing hip circumduction.

The critical function within finite state control methods is properly estimating the dynamic state. Unfortunately, robust state estimation algorithms are increasingly complex and computationally expensive, potentially limiting their effectiveness during real time control. One simplification to state estimation algorithms is to measure the amputee's electromyographic (EMG) signals directly. Studies suggest there is a correlation between the amputee's EMG signals and the desired actuator function (Ferris, 2006; Novacheck, 1998). However, the dominant factor in the effectiveness of myoelectric-based control is the system's ability to reliably acquire and process an accurate EMG signal, which still remains a significant challenge (Holgate et al., 2009).

A novel approach to overcome the limitations of finite state machine controls is to define gait parameters invariant of amputee activity in a continuous control system. One implementation couples tibia angular velocity and angular position in the sagittal plane to identify the desired ankle angle and moment, adaptive to any gait kinematic (Holgate et al., 2009). Using a single rate gyro, this method captures tibia velocity in the inertial earth fixed reference frame, determines an angular position, and identifies the corresponding stride length and position within the gait cycle. The challenge in the tibia based control system is integrating the rate gyro's angular velocity signal, which is prone to offset and drift. Rather than augment the rate gyro with an accelerometer to perform complementary or Kalman filtering, the tibia based control method implements a novel analog signal processing technique that tenuates the drift. This method is more robust than the aforementioned dual signal processing techniques, as it provide a variable neutral reference based on gait kinematics rather than constant neutral reference defined in the direction of acceleration due to gravity. Thus, the neutral tibia position is referenced in the center of the stance phase which directs more in line with the normal to the walking surface. This allows the system to adapt to uneven terrain and varying amputee activities without state logic.

2. IMPLEMENTATION

2.1 Mechanical Design

The running prosthesis was essentially a redesign of the SPARKy walking active ankle prosthesis (Hitt et al., 2010). Refining the walking prosthesis for running required component modification to resist the increased dynamic loads on the structural components and provide the increased actuator power necessary for running. Refer to Fig. 1 for an illustration of the embodiment design and Fig. 5 for a comparison of the walking and running feet designs.

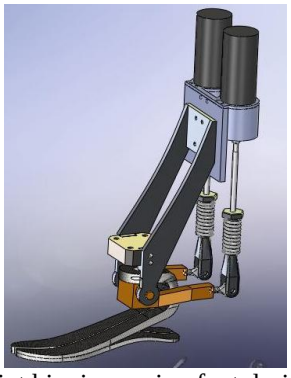

Fig. 1. West Point bionic running foot design incorporates a dual actuator, dual spring muscle-tendon system

Simulation and testing revealed 4200N as the objective peak load on the robotic muscle-tendon system for a specified foot-ankle configuration.

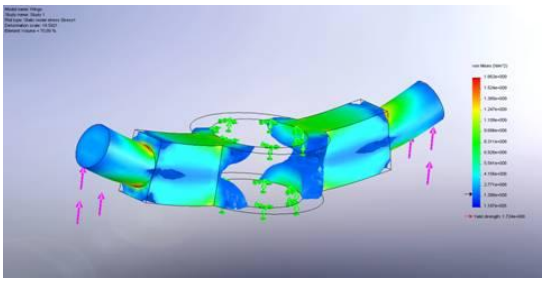

Fig 2. Finite element analysis of the muscle-tendon interface component revealed excessive internal stresses, necessitating redesign for the running foot.

Finite element analysis of the components indicated three critical areas for redesign: the robotic muscle-tendon interface; the tibia-ankle interface; and the tendon-ankle interface. The robotic muscle-tendon interface originally transmitted inputs from the single linear actuator to both springs, resulting in significant internal moments and shear loads in the interface component. Refer to Fig. 2 for a depiction of internal stresses of the muscle-tendon interface component. To mitigate the excessive normal and shear stresses at the interface surfaces, the team included a second actuator such that each actuator interfaced with a single spring.

Increased external moments exerted on the revolute joint at the ankle caused excessive shear loads on the bolted tibia-ankle interface adjacent to the ankle joint. To mitigate the risk of failure at the revolute joint, the team replaced the bolted connection with a unitary, solid component. Refer to Fig. 3 for a comparison of the tibia-ankle interface component for the walking and running feet.

With increased internal moments in the ankle-tendon interface component, the team removed the stress concentrations in the component, with emphasis near the revolute ankle joint. The redesign also incorporates an increased second area of moment of the interface component in the direction of the applied moment.

Fig. 3. Comparison of critical system interfaces between the running foot (foreground) and the walking foot.

The 300-400W actuator power requirement mandated replacement of the Maxon RE40 based actuator system rated up to 150W. The team evaluated three alternatives with similar power characteristics: a single Maxon RE75 brushed motor actuator; a dual Maxon RE40 actuator system; and a single EC40 brushless motor actuator system. Evaluation parameters included the complexity of the motor control required, the overall weight and inertial characteristics of the components, and the clearance provided for the lower limb socket. The RE75 allowed for the simplest motor control algorithm, but provided less than optimal socket clearance due to the large diameter of the motor casing. In addition, the RE75's rotating inertia was double to quadruple of the inertia of the other two alternatives, which would have limited its efficiency. Furthermore, the single actuator system would have generated excessive internal moments in the muscle-tendon interface component. The dual actuator system required additional control requirements to synchronize the two motors, but mitigated risk of muscle-tendon component failure. Additionally, though inertial power requirements were significantly less than the RE75 system, they were double the EC40 brushless motor actuator power requirements. However, the EC40 brushless motor system control had inherent instabilities during actuator direction reversal, and tested methods proved unreliable at that particular transition in the gait cycle. Therefore, the RE40 dual system proved the best compromise between motor control requirements, efficiency, and compatibility with the amputee.

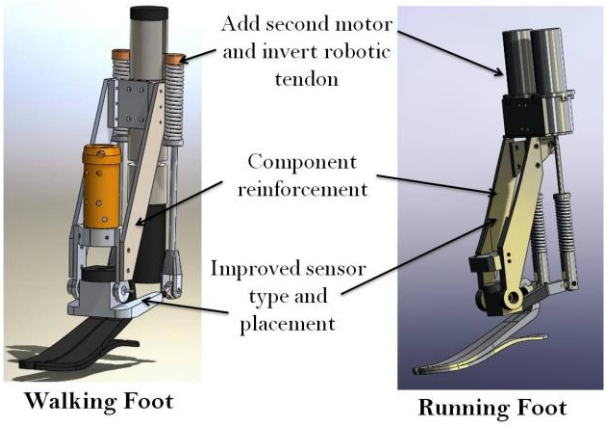

Fig 5. Additional power and load requirements mandated component redesign at the muscle-tendon, tendon-ankle, and tibia-ankle interfaces.

2.2 Control System Design

The controller hardware is composed of a PC104 microprocessor with a Sensoray DAQ unit attached. Utilizing control code downloaded from MalLab, the PC104 drives two custom brushed motor position controllers, see Fig. 6.

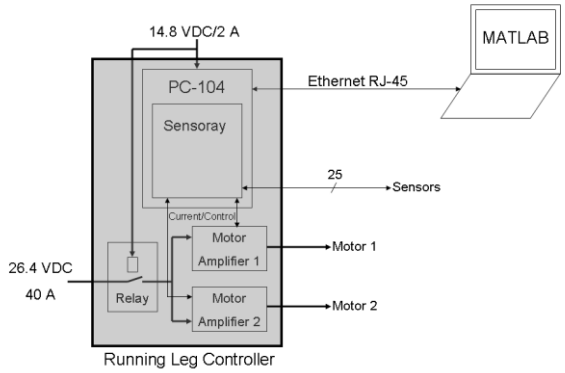

Fig. 6. Control Hardware Diagram.

The electronics are portable and are powered by a 26.4V battery pack. An Ethernet connection to the Matlab PC is used to download the control code as well as collect the data measured from the robot.

The controller software logic for running is based strongly on the team's prior work with walking gait, and the tibia controller (Holgate et al., 2009). The advantages of this control approach for both walking and running are that its modeling is not based upon time, and is inherently continuous, i.e. no state base decision logic is used. In addition, the method detects user movement intent 1000 times every second.

Although based upon the same methods used in development of the original tibia based control model, the development of the running controller required significant modification for the task of running. Due to these distinctive differences in coordinated motion, a modified motor reference pattern distinctive to running gait was required. Refer to Fig. 7 and Fig. 8 for a sample ankle-gait profile and ankle moment-gait profile determined by stride length, respectively. Statistical analysis of running gait kinematics determined an appropriate ankle angle and ankle moment for a given position in the gait cycle, where the position is defined as a percent within the gait cycle.

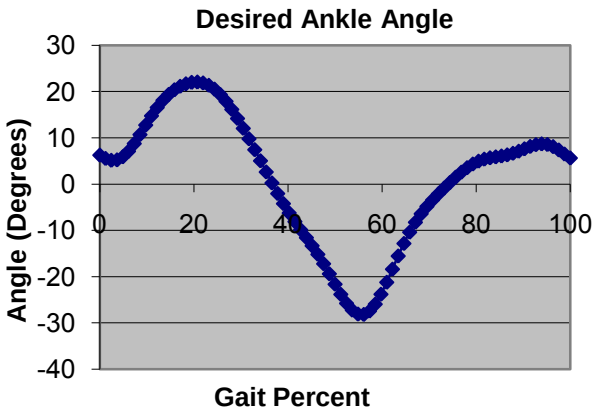

Fig. 7. Desired ankle kinematics as a function of the position within the gait cycle for a specified stride length.

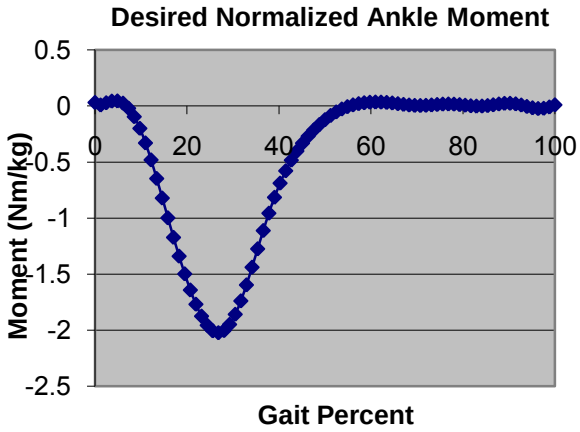

Fig. 8. Desired ankle kinetics as a function of the position within the gait cycle for a specified stride length.

Using a rate gyro to measure the motion of the tibia, percent gait and stride length can be determined. Corresponding gait percentage and stride lengths determine the current desired moment at the ankle, which is reflected in the displaced length of the spring. The position of the actuator nut determines the effective equilibrium length of the spring, which is controlled to maintain the appropriate spring displacement. The lever position is a measure of the ankle angle, and indicates the vertical displacement of the tendon-ankle interface from neutral, i.e., an ankle angle of 90 degrees. See Fig. 9 for a sample motor position-gait profile.

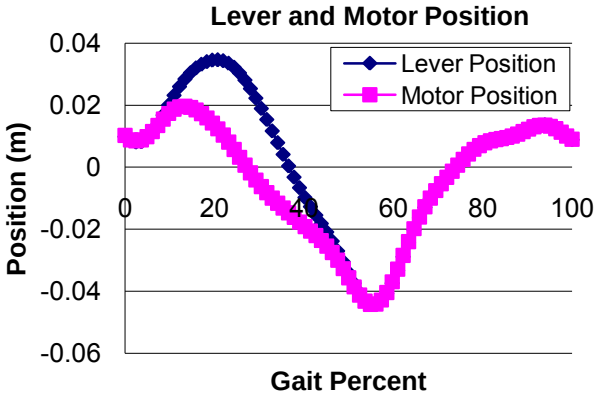

Fig 9. Desired motor position and tendon-ankle interface (lever) position in the gait cycle for a specified stride length.

The team then developed a two dimensional mapping of the motor position as a function of stride length and position within the gait cycle. See Fig. 10 for a sample look-up map. This two dimensional array is stored within the control system memory, providing a lookup table for the desired motor position indirectly as a function of the measured tibia angular rate and calculated tibia angular position.

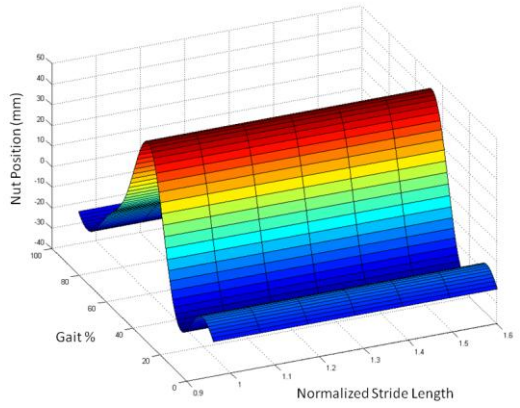

Fig. 10: Displacement of the spring attachment nut (mm) as a function of stride length and gait percent.

3. RESULTS

The team conducted clinical tests with an 80kg unilateral transtibial amputee at the United States Military Academy 13-25 April 2010. See Fig. 11 for the testing apparatus. IRB approval was obtained from the United States Military Academy.

Fig. 11. Single subject treadmill running tests 13-25 April.

During tests, the amputee, a United States Army Special Operations noncommissioned officer, sustained a moderate running gait speed up to 3.6 m/s (8 mph), see Fig. 12. In one test, after reaching a speed of 3.6 m/s, the subject jumped off the moving treadmill coming to an abrupt stop. The continuous tibia-based control effectively adapted to the significant and rapid change in gait kinematics and kinetics within one sampling cycle.

Fig. 12. Subject running on a treadmill.

The clinical trials validated the tibia-based control algorithm for running and allowed the team to refine simulation models for accurate analysis of required actuator power input in future designs. Though the running foot proved effective for gaits speeds up to 3.6 m/s, testing also highlight key areas of emphasis for the next iterative design process with the objective of sustained overground running. Visual inspection of the subject's gait indicated hip circumduction likely caused by an underpowered actuator system. Model refinement based on the test results indicated that the actuators delivered up to 550W of the 590W peak power required for the subject's weight and gait speed. See Fig. 13 for the refined power requirement analysis based on gait position. See Fig. 14 for the measured (current and voltage) motor input power. Thus, future redesign efforts will focus on reducing the power required to overcome inertial characteristics of the actuator system and structural components, as well as increase the power capacity of the actuator system. The solution emphasis for the next design is incorporating a brushless motor actuator system that halves the actuator inertial properties and more than doubles the actuator's nominal power capacity to 800W.

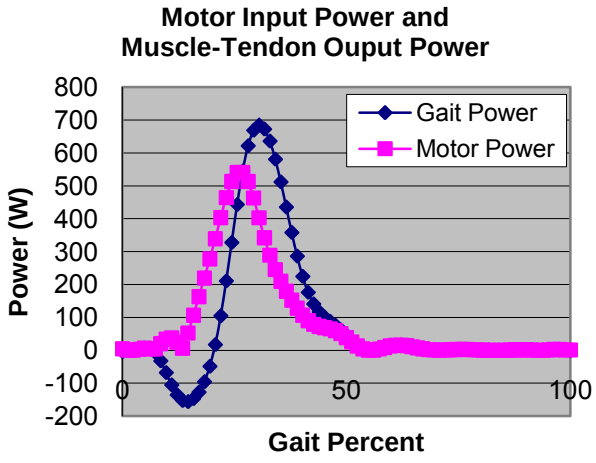

Fig. 13. Motor and muscle-tendon power capacities for 80kg subject running at 3.6 m/s.

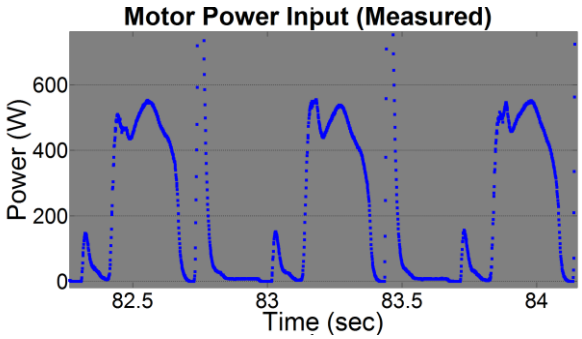

Fig. 14. Motor power input determined as the product of the measured voltage and current for 80kg subject running at 3.6 m/s. Note that the spike in power is due to reversal of the motor between stance and swing.

Testing also indicated service life challenges with the lead screw assembly in the actuator. The lead screw assembly is required to convert the rotational motion of the electric motors to translation with a high enough mechanical advantage to limit the size of the electric motors used. Therefore, as second emphasis of the next redesign is incorporation of a roller screw assembly in place of the lead screw, and elimination of any external moments not exerted axially on the roller screw. See Fig. 15 for a rendering of the future design concept.

Fig. 15**.** Conceptual design of next running foot iteration includes a single brushless motor actuator, reduced overall weight, and isolated roller screw assembly.

4. CONCLUSION

Preliminary testing indicates that it is possible to use a series actuator-spring system to mimic the tendon-muscle power amplification strategy for running. Overground tests continue with full system portability, see Fig. 16. However, running gait kinematics, particularly the reduced stance phase within a gait cycle, increases the importance of component inertial characteristics, thereby generating a requirement to use brushless motor systems in future designs and complex manufacturing techniques that facilitate significant weight reduction. As ancillary efforts to develop battery systems with increasing energy density continue, the development of a feasible robust foot capable of replacing limb functions under any activity and environmental condition becomes a more realizable goal.

Fig 16. Unilateral transtibial amputee conducting overground walking tests with fully portable tibia-based controller.

ACKNOWLEDGEMENTS

The authors would like to thank the Center for the Intrepid at the Brooke Army Medical Center, the U.S. Army Medical Research and Material Command's Telemedicine and Advanced Technology Research Center (TATRC), and the Army Research Laboratory for their sponsorship. The authors would also like to thank our Wounded Warrior test subject for his invaluable help and dedication during testing.

REFERENCES

Biewener, A.A. and Daley, M.A., 2007, "Unsteady locomotion: integrating muscle function with whole body dynamics and neuromuscular control," *The Journal of Experimental Biology*, **210**, 2949-2960.

Blaya, J.A. and Herr, H.M., 2004, "Adaptive Control of a Variable-Impedance Ankle-Foot Orthosis to Assist Drop-Foot Gait," *IEEE Transactions on Neural Systems and Rehabilitation Engineering*, **12**, 24-31.

Bohler, A.W., Hollander, K.W., Sugar, T.G., and Shin, D., 2008, "Implementation and Test Results of a Robust Control Design Concept for a Powered Ankle-Foot-Orthosis (AFO)," *Proceedings of the 2008 IEEE International Conference on Robotics and Automation (ICRA).*

Burdett, R.G., 1982, "Forces predicted at the ankle during running," *Medicine & Science in Sports & Exercise*, **14(4)**, 308-316.

Daley, M.A. and Biewener, A.A., 2006, "Running over rough terrain reveals limb control for intrinsic stability," *Proceedings of the National Academy of Sciences of the United States of America*, **103**, 15681-15686.

Daley, M.A. and Usherwood, J.R., 2010, "Two explanations for the compliant running paradox: reduced work of bouncing viscera and increased stability in uneven terrain," *Biology Letters*, **6**, 418-421.

Farley, C.T. and Ferris, D.P., 1998, "Biomechanics of Walking and Running: Center of Mass Movements to Muscle Action," *Exercise and Sports Sciences Reviews*, **26**, 253-285.

Farley, C.T., Glasheen, J., and McMahon, T.A., 1993, "Running Springs: Speed and Animal Size," *Journal of Experimental Biology*, **185**, 71-86.

Farley, C.T. and Gonzalez, O., 1996, "Leg Stiffness and Stride Frequency in Human Running, " *Journal of Biomechanics*, **29(2)**, 181-186.

Ferris, D.P., Louie, M., and Farley, C.T., 1998, "Running in the real world: adjusting leg stiffness for different surfaces," *Proceedings of the Royal Society B: Biological Sciences*, **265**, 989-994.

Ferris, D.P., Gordon, K.E., Sawicki, G.S., and Peethambaran, A., 2006, "An Improved Powered Ankle-Foot Orthosis Using Proportional Myoelectric Control," *Gait and Posture*, **23**, 425-428.

Hitt, J.K., Sugar, T.G., Holgate, M.A., and Bellman, R., 2010, "An Active Ankle-Foot Prosthesis With Biomechanical Energy Regeneration", *Transactions of the ASME Journal of Medical Devices*, **4**, 0011003-1 – 0011003-9.

Hitt, J.K. and Sugar, T.G., 2010, "Load Carriage Effect on a Robotic Transtibial Prosthesis," *2010 International Congress on Control, Automation, and Systems*, Oct 2010.

Holgate, M.A., Sugar, T.G., and Bohler, A.W., 2009, "A Novel Control Algorithm for Wearable Robotics using Phase Plane Invariants", *2009 IEEE Conference on Robotics and Automation (ICRA)*, 3845-3850.

Kao, P.C., Lewis, C.L., and Ferris, D.P., 2010, "Invariant ankle moment patterns when walking with an without a robotic ankle exoskeleton," *Journal of Biomechanics*, **43**, 203-209.

Kerdok, A.E., Biewener, A.A., McMahon, T.A., Weyand, P.G., and Herr, H.M., 2002, "Energetics and mechanics of human running on surfaces of different stiffnesses," *The Journal of Applied Physiology*, **92**, 469-478.

Novacheck, T.F., 1998, "The biomechanics of running," *Gait and Posture*, **7**, 77-95

2009, Proprio Technical Manual, Ossur Orthopaedic Products and Services Company, http://www.ossur.com

Oymagil, M.A., Hitt, J.K., and Sugar, T.G., 2007, "Control of a Regenerative Braking Powered Ankle Foot Orthosis, " *2007 IEEE 10th International Conference on Rehabilitation Robotics (ICORR)*, 28-34.

Rao, S.S, Boyd, L.A., Mulroy, S.J., Bontrager, E.L., Gronley, J.K., and Perry, J., 1998, "Segment Velocities in Normal and Transtibial Amputees: Prosthetic Design Implications," *IEEE Transactions on Rehabilitation Engineering*, **6-2**, 219-226.

Shaeffer, A.A. and Hirzinger, G., 2002, "Cartesian Impedance Control Techniques for Torque Controlled Light-Weight Robots," *Proceedings of the 2002 IEEE International Conference on Robotics and Automation (ICRA).*

Versluys, R., Desomer, A., Gerlinde, L., Pareit, O., Vanderborght, B., Van der Perre, G., Peeraer, L., and Lefeber, D., 2008, "A Biomechanical Transtibial Prosthesis Powered by Pleated Pneumatic Artificial Muscles," *Model Identification and Control*, **4**, 394-405.

Joseph K. Hitt
Department of Civil and Mechanical Engineering,
West Point, New York, NY 10996
e-mail: Joseph.Hitt@usma.edu

Thomas G. Sugar
e-mail: thomas.sugar@asu.edu

Matthew Holgate
e-mail: matthew.holgate@asu.edu

Ryan Bellman
e-mail: Ryan.Bellman@asu.edu

Mechanical and Aerospace Engineering,
P. O. Box 876106,
Tempe, AZ 85283

An Active Foot-Ankle Prosthesis With Biomechanical Energy Regeneration

A unique, robust, robotic transtibial prosthesis with regenerative kinetics was successfully built and a 6-month human subject trial was conducted on one male below-the-knee amputee under linear walking conditions. This paper presents the quasistatic system modeling, DC motor and transmission modeling and analyses, design methodology, and model verification. It also outlines an approach to the design and development of a robotic transtibial prosthesis. The test data will show that the true power and energy requirement predicted in the modeling and analyses is in good agreement with the measured data, verifying that the approach satisfactorily captures the physical system. The modeling and analyses in this paper describes a process to determine an optimal combination of motors, springs, gearboxes, and rotary to linear transmissions to significantly minimize the power and energy consumption. This kinetic minimization allows the downsizing of the actuation system and the battery required for daily use to a self-portable level. [DOI: 10.1115/1.4001139]

1 Introduction

One of the primary challenges in the development of a truly biomimetic, foot-ankle, prosthetic device is prohibitively low power and energy density in traditional actuation schemes. The ankle joint requires considerable power and energy, and applying a traditional approach with a DC motor and gearbox at the ankle joint would force the system to become too heavy and bulky.

A portable, daily use powered prosthesis requires both high power to weight ratio (power density) and energy to weight ratio (energy density) in an actuator. Without these limitations, one could take, for example, a RE75 DC Motor from Maxon Precision Motors, Inc., rated for 250 W continuous power to provide the 250 W peak power required in human gait (80 kg subject at 0.8 Hz walking) [1]. But this motor, in combination with a gearbox in a traditional approach, would weigh 6 kg to 7 kg, which exceeds the weight of a typical, biological, below-knee limb. In addition, the size of the batteries needed to power the system would become too large and heavy, making the system unmanageable.

There have been significant improvements in prosthetic and orthotic technologies in recent years. Energy storage and return (ESAR) devices allow faster walking velocity and better terrain negotiation [2–4]. They have an increased range of motion, store and return energy, and reduce the needed metabolic requirements [5–9].

Even with these improvements, current ankle-foot prosthetic devices are passive. They typically use rubber like springs or leaf springs made from carbon composite materials. They do not contain powered elements that assist in locomotion. Amputees must rely on the spring-back passive devices to provide and adjusted gait to help propel them forward.

In an effort to develop active lower-limb prostheses, researchers are investigating alternatives to traditional actuation schemes. Several researchers [10–14] developed quite mature novel prototypes, while many others are at varying stages of research and development. The Proprio ankle by Ossur is the first commercially available motorized and computer controlled ankle device that modulates ankle angle, based on the environment, gait, and conditions, to better mimic the kinematics of the lost limb, however, without the functionality to actively generate power [15].

Manuscript received August 19, 2009; final manuscript received January 22, 2010; published online March 26, 2010. Assoc. Editor: Just Herder.

The purpose of this paper is to describe the development and testing of a motorized foot-ankle prosthetic device that utilizes biomechanical energy regeneration to reduce the electric motor and battery to self-portable weight and volume. Energy regeneration is typically thought of as the capture and conversion of negative mechanical work to electric energy, as is done in electric cars with regenerative braking. In this paper, biomechanical energy regeneration is the storage of negative mechanical work in springs, to be used as mechanical energy without the need to undergo the inefficient energy conversion process from mechanical to electrical, and back to mechanical.

2 The Robotic Tendon

A robotic tendon [1] actuator, Fig. 1, is utilized in this device to minimize the peak motor power requirement by correctly positioning a uniquely tuned helical spring so that the spring provides most of the peak power required for gait. The robotic tendon is a small and lightweight actuator that features a low power motor that is used to adjust the position of the helical spring using a very robust position controller. Figure 1 illustrates how the desired spring deflection and consequently via Hooke's law the desired force and ankle moment is achieved using a spring in series with a motor. As the ankle rotates over the foot during the stance phase, as illustrated in Fig. 1 by the inverted pendulum model, the spring is extended by the falling center of mass of the body. Additional deflection in the spring is achieved by correctly positioning the motor so that the desired ankle joint angle and moment is realized. A heavy, powerful motor is not needed because the robotic tendon, similar to the biological tendon-muscle complex, stores a portion of the stance phase kinetic energy and additional motor energy within the spring. The spring releases its stored energy to provide most of the peak power required during "push off." Therefore, the power requirement on the motor is significantly reduced. As described in Ref. [1], the peak motor power required is 77 W, compared with 250 W for a direct drive system in the 80 kg subject at a 0.8 Hz example. Consequently, the weight of the robotic tendon, at just 0.95 kg, achieves a power density that in essence is seven times greater than a traditional approach.

3 The Simple Series Quasistatic System Model

What combination of actuator, robotic tendon spring stiffness, ESAR keel stiffness, ankle joint motion, and control scheme is

 Copyright © 2010 by ASME

Downloaded 26 Mar 2010 to 149.169.104.18. Redistribution subject to ASME license or copyright; see http://www.asme.org/terms/Terms_Use.cfm

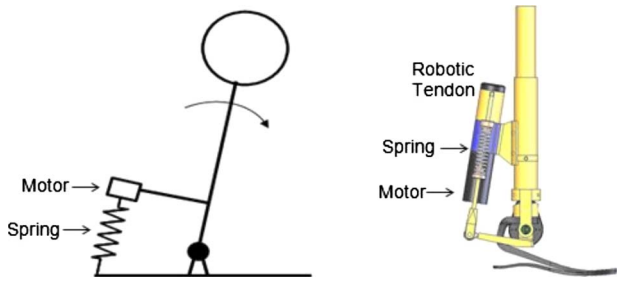

Fig. 1 Desired spring deflection is achieved by controlling the motor position and capitalizing on the cyclical nature of gait. As the tibia rotates over the stance foot, springs are extended. Simultaneously, the motor extends the springs to achieve the desired spring deflection and the forces required to generate the required ankle moment for walking. This inverted pendulum with a lumped mass illustrates the regeneration energy with use of a spring in series with a motor. Computer aided design model of the prototype is illustrated on the right.

optimal in terms of power and energy? To answer these questions, multiple models were derived, each with varying combinations of these design parameters [16]. The ankle joint angle and moment data used in the simulation are from able-bodied data, generated by the inverse dynamics of motion capture and force plate test data published by Whittle in Ref. [17]. The remaining kinetic and kinematic analysis is derived using a quasistatic approach. MATLAB simulation of the models showed that a power amplification (P_{out} peak/P_{in} peak) of up to 6 may be possible. P_{out} is the power out of the system (prosthesis). P_{in} is the power out of the motor. Presented here is the simple series model selected for its simplicity and robustness in terms of hardware design. Simulation of the model showed that a power amplification of 3.25 is possible while maintaining gait kinematics and kinetics similar to able-bodied persons.

In the simple series model, the keel and the robotic tendon springs are in series; therefore, the moment in the keel is equal to the moment in the robotic tendon. The moment in the ankle joint is from published able-bodied data [17]. The motor position is controlled so that the moment of the robotic tendon matches that of the able-bodied moment data, Eq. (1). As illustrated in Fig. 2, K_a is the keel stiffness, K_s is the spring stiffness, B is the radius of the keel deflection (0.17 m for the FS 3000 Keel used in this

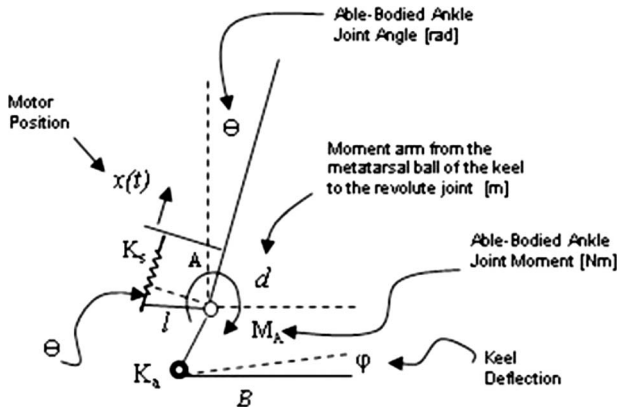

Fig. 2 A two degrees-of-freedom model with a seismic excitation representing the motor excitation, a torsion spring for the keel, and a helical (linear) spring between the lever and the motor is shown. The moment due to the keel is a function of $\varphi(t)$ and the moment due to the spring is a function of $\Theta(t)l - x(t)$. The moment at the ankle is from published information determined using inverse dynamics of motion capture and force plate test data as published in Ref. [17].

project), d is the moment arm (0.125 m from the metatarsal ball of the keel to the revolute joint at the ankle) due to the keel deflection, and l is the lever length (0.09 m). Small angle approximation is assumed as

$$M_A(t) = M_{\text{keel}}(t) = M_{\text{RT}}(t)$$

$$M_{\text{keel}}(t) = K_a B d \varphi(t) \tag{1}$$

$$M_{\text{RT}}(t) = K_s(l\theta_A(t) - x(t))l$$

Solving Eq. (1) for motor position $x(t)$ determines the expression

$$x(t) = l\theta_A(t) - \frac{K_a B d}{K_s l}\varphi(t) \tag{2}$$

The assumed force in the robotic tendon is given by

$$F(t) = \frac{M_A(t)}{l} \tag{3}$$

The ideal power generated by the motor to move to position $x(t)$ is given by the product of the force and velocity in the tendon

$$P_m(t) = F(t)\frac{dx(t)}{dt} \Rightarrow P_m(t) = \frac{M_A(t)}{l}\left[l\frac{d\theta_A(t)}{dt} - \frac{K_a B d}{K_s l}\frac{d\varphi(t)}{dt} \right] \tag{4}$$

The expression in Eq. (4) represents the power required by the motor to generate the desired moment and ankle angle of able-bodied gait published in Ref. [17], given that the spring provides the majority of the required peak power. The optimization of Eq. (4), varying keel stiffness K_a and spring stiffness K_s, showed that a minimum peak motor power profile is achieved by varying K_s. The analysis showed that a spring stiffness of 36,000 N/m is optimal in terms of the minimum peak motor power. At this spring stiffness, the peak motor power is at its lowest value of 80 W. The simulation of this model showed that with a peak input power of 80 W from the motor, together with the power stored in the spring through regeneration, the system can deliver the required 260 W of peak gait power, which is a power amplification of 3.25. Note that Eq. (4) is fully developed and validated in Ref. [18]; this paper represents a major extension of Ref. [18] with the development of the true power equation, Eq. (10), and the modeling and testing presented in the following sections.

4 Power and Energy Efficiency

Literature is replete with discussions about power and energy input and output as it relates to transtibial prostheses. However, there is very little discussion and analyses outside of the idealized system. Providing the idealized 36 J (summing the absolute value of the power curve) of energy per step [1] becomes an issue because one must consider the efficiency of the motor, gearbox, and other transmission mechanisms, friction, and inertia, and the consumption of energy by the sensors and electronics if a system is to be designed and to be portable. The mechanism inefficiency alone can double the energy requirement. For example, a DC motor with an average efficiency of 70%, connected to a ball screw at 90% and a gearbox at 80%, multiplies to produce a 50% efficiency actuation system. This would suggest a doubling of the energy input requirement to 72 J/step to provide the necessary 36 J/step at the output end. This is still an optimistic estimate because this does not include several other factors such as: the energy consumed to counter motor/actuator inertia, which tests show, is considerable in a highly cyclical gait pattern where the motor rapidly changes direction several times per step, friction in the mechanism or energy required by the microprocessor, sensors, motor controller, etc., see Fig. 3. In addition, the efficiency of the motor varies significantly during a gait cycle as a function of motor torque and angular velocity; therefore, the use of a constant motor efficiency is an invalid assumption for our cyclic gait research. One can easily see that the actual energy requirement could grow to three

Downloaded 26 Mar 2010 to 149.169.104.18. Redistribution subject to ASME license or copyright; see http://www.asme.org/terms/Terms_Use.cfm

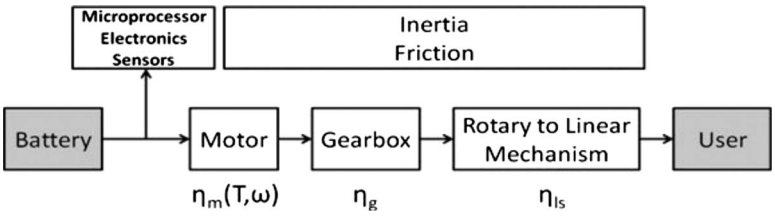

Fig. 3 This diagram illustrates the flow of power and energy from the battery to the user. Significant amount of energy is lost due to inefficiency in the mechanisms, motor, inertia, friction, etc. Proper selection and design can drastically improve overall system efficiency. Note that the system efficiency is defined as average output power to the user/average input power from the battery. The inertia and friction box is assumed to be linked to all of the mechanical elements.

or fourfold of the idealized number of 36 J/step in a traditional approach, and consequently increasing the battery requirement proportionately in size and weight to nonportable levels. Also, under these circumstances, slow running, which may quadruple the peak power requirement as compared with normal walking (1000 W for heel to toe running as compared with 250 W, for walking) would send power and energy density requirements beyond what can be achieved today.

In this section, multiple effects will be investigated, focusing on several DC motors, rotary to linear transmission mechanisms, gear boxes, spring stiffness, and lever lengths on energy efficiency of the robotic transtibial prosthesis. Using MATLAB simulations of kinetic and kinematic models, the best combination of these variables will be predicted in terms of system energy reduction and efficiency. Later, these results will be compared with human subject test data.

4.1 Regenerative Energy. Using a spring in series with a motor allows regeneration of energy. Figure 4, in comparison with Fig. 3, illustrates the addition of regenerative power and energy made possible with the robotic tendon. The figure illustrates the energy cycle that occurs between the user and the spring. The dynamics of the user stores energy in the spring, and the spring returns that energy to the user in a cyclical and highly efficient regenerative manner.

4.2 DC Motors and Transmission. DC motor efficiency: A significant aspect of energy density is motor efficiency. For example, the RE 40 DC Motor by Maxon, Inc., currently used in the device, is one of the most efficient motors commercially available for this application. However, its rated efficiency of 91% is only achieved at a very small range of motor torque and rpm near 7000 rpm at 0.1 Nm. Below 2000 rpm and above 0.2 Nm, motor efficiency quickly drops below 50%. A 3D plot is shown in Fig. 5 as a function of motor torque and motor rpm [18]. Motor efficiency is mechanical power out/electrical power in

$$\eta_m = \frac{\text{mechanical power}}{\text{electrical power}} = \frac{\tau\omega}{Vi} \tag{5}$$

where V is voltage in volts, i is current in amperes, ω is the angular velocity in rad/s, and τ is torque in Nm.

The 3D plot in Fig. 5, which is determined by the evaluation of Eq. (5), shows that there is a narrow range of motor efficiency above 70%. Once the motor slows below 2000 rpm, or the motor torque exceeds 0.2 Nm, the motor efficiency degrades exponentially. Therefore, the motor should be properly matched with an appropriate gearing mechanism that maintains high motor speed and low torque for its given tasks.

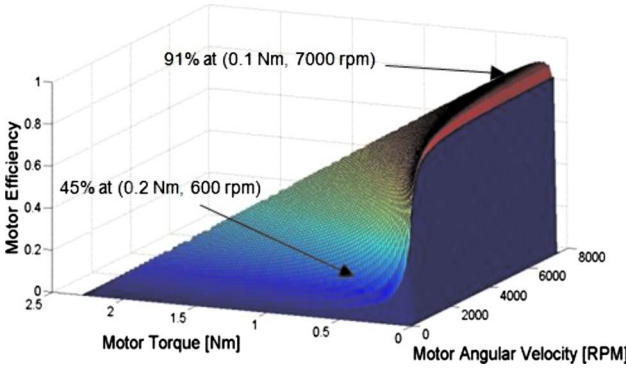

Fig. 5 3D plot of the RE40 motor efficiency as a function of motor torque (Nm) and motor angular velocity (rpm) [18]. Notice that the highest efficiency of 91% is only achieved at a narrow range of torque and angular velocity. Operating the RE40 at speeds lower than 2000 rpm or torque above 0.2 Nm will significantly degrade the motor efficiency. Illustrated in the figure are two points on the mesh.

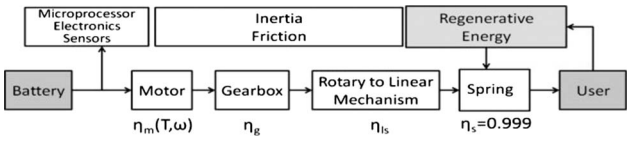

Fig. 4 This diagram illustrates the flow of energy from the battery to the user for the robotic tendon model. Even though significant amount of energy is lost due to inefficiency in the mechanisms, motor, inertia, friction, etc., the spring and the regenerative energy that it harnesses is nearly 100% efficient and accounts for the main share of the output energy. This method also allows for a smaller motor, battery, and transmission system.

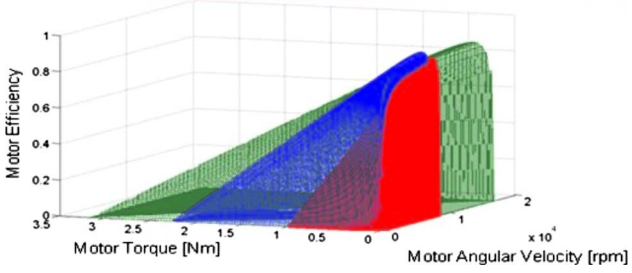

Fig. 6 The three motor efficiency 3D plots overlapped. The blue is the RE 40, the red is the RE 30, and the green is the EC 30. The red surface ends at 1.02 Nm on the horizontal axis describing torque. The vertical axis measures efficiency.

Downloaded 26 Mar 2010 to 149.169.104.18. Redistribution subject to ASME license or copyright; see http://www.asme.org/terms/Terms_Use.cfm

Motor efficiency analyses of other motors can be accomplished using the same method. Figure 6 shows the motor efficiency 3D plots of the Maxon RE 40, Maxon RE 30, and the brushless Maxon EC Power Max 30. The RE 30 motor is a 60 W nominal motor that is half the size and weight of the RE 40 motor with a rotor inertia that is $\frac{1}{4}$ of that of the RE 40 motor. The RE 30 motor is much more desirable if the peak motor power requirement can be reduced below 60 W. The EC 30 motor is a 200 W nominal motor that is half the size and weight of the RE 40 motor with a rotor inertia that is $\frac{1}{4}$ of that of the RE 40 motor. The EC 30 motor may be the best performing of the three motors since it is as small as the RE 30, and is even more powerful than the RE 40 motor. However, because it is a brushless motor, it requires a much more sophisticated motor controller and it operates at a much higher rpm.

In Fig. 6, the three motor efficiency plots are overlapped. This highlights the similarities and differences of the three motors. The blue surface plot is the RE 40, the red is the RE 30, and the green is the EC 30. It illustrates that the EC 30 has a significantly higher range of torque and speed while maintaining a similar efficiency profile. The red surface, hidden in view by the blue surface, is the smallest ending at 1.02 Nm on the torque side. Also, notice that the blue surface reaches the highest point at 0.91, while the red surface reaches 0.87, and the green surface reaches 0.88. However, all three surfaces reach their maximum points near their maximum speed and minimum torque point, and the shape of the surfaces are very similar.

Rotational to linear motion mechanisms: A mechanical element is required in our design that will convert the rotation of the DC motor to a linear motion that can be used to adjust the position of the helical spring in the robotic tendon. Typical solutions are power screws, such as lead screws and ball screws. Lead screws are capable of large mechanical advantages by modifying the pitch of the lead screw threads. The motorized lead screw translates the nut to provide the rotary to linear motion. However, in typical lead screw applications, the efficiency is very low, due to the significant friction between the lead screw and nut interface. In contrast, a ball screw, with its rolling contact, achieves high efficiency because of the minimal frictional losses between the rolling ball and screw interface. Unfortunately, the ball bearings within the nut assembly wear quickly in high dynamic load applications, and the weight and volume of the ball screw is much higher than that of the lead screw. The lead screw performance can be enhanced by reducing the friction between the nut and screw, and by selecting the best lead screw angle. By careful design selection, lead screw efficiency can be increased from its typical range of 0.2–0.3 to 0.7–0.8. Equation (6) is the lead screw efficiency from Ref. [19], where it is only a function of μ, coefficient of friction, and α, lead angle

$$\eta_{\text{ls}} = \frac{1 - \mu \tan(\alpha)}{1 + \mu \cot(\alpha)} \tag{6}$$

The inertia effect: The motor, gear box, lead screw, and the load have inertia that resists the applied torque as a function of angular acceleration; therefore, the system requires additional power and energy from the batteries to counter the effects of inertia. The motor and the gear box, which accelerates and decelerates at very high rates in this application, consume significant power. The other elements contribute to the total inertia to a much lesser degree, as the speed reduction from the motor to the load has a $(\omega_{n+1}/\omega_n)^2$ reduction factor. For example, the gear box with a 4.3:1 gear ratio has a gear box reduction factor of $(1/4.3)^2$ or 0.054. The lead screw, which rotates at the reduced rate reflects only 5.4% of its inertia back to the motor in this example. In addition, the small lead screw radius makes the inertia effects of the lead screw low in the first place. Therefore, the primary cause of the system inertia effect is the motor's equivalent rotor inertia and the gear box equivalent inertia. The total mass moment of inertia about the axis of rotation for the motor, gearbox, and lead screw system is simply

$$J_{\text{total}} = J_m + J_g + \left[J_{\text{ls}} + \frac{M}{(2\pi l_d)^2} \right] \left(\frac{\omega_g}{\omega} \right)^2 \tag{7}$$

where J_m is the equivalent motor rotor inertia from published specifications, J_g is the equivalent gear box inertia from published specifications, and J_{ls} is the lead screw inertia. The lead screw is assumed to be a slender rod with an inertia equal to one-half of the mass of the lead screw times the radius squared, $J_{\text{ls}} = 1/2mr^2$. The lead screw nut inertia is given by $M/(2\pi l_d)^2$, where M is the mass of the nut assembly and l_d is the lead of the lead screw. Finally, because the lead screw is rotating at a reduced rate, a reduction factor of $(\omega_g/\omega)^2$ is used. ω_g is the angular velocity after the gearbox and ω is the angular velocity after the motor.

4.3 The True Power. The true power is the electric power, as defined by the product of the input voltage and current. This is the power required by the battery to provide the required mechanical power in our application. Significant amount of power is consumed as this electric power is converted and delivered to the nut as mechanical power. Accounting for these losses in power, due to mechanism inefficiency and inertia effects, together with the mechanical power required at the nut, determines the electric power requirement. In addition, frictional losses, damping, heating, structural deflection, and other power sinks not accounted for in the efficiency calculations must be included in the true power requirement. This system mechanical power loss is determined experimentally. Equation (8) is the expression for electric power P_e

$$P_e = P_j + \frac{P_m}{\eta_m \eta_g \eta_{\text{ls}}} + P_s \tag{8}$$

where P_j is the power required to overcome the inertia effects, P_m is the power required at the nut for gait, and P_s is the power required to overcome the system mechanical power sinks. The denominator of P_m is the product of the motor, gear box, and lead screw efficiency. P_j is the angular velocity at the motor times the torque is required to overcome the motor rotor and gear box inertia

$$P_j = \tau_j \omega = \left[(J_m + J_g) \frac{d\omega}{dt} \right] \omega \tag{9}$$

Combining these power, Eqs. (8), (9), and (4) gives

$$P_e = \left[(J_m + J_g) \frac{d\omega}{dt} \right] \omega + \frac{\frac{M_A}{l} \left[l\omega_A - \frac{K_a B d}{K_s l} \omega_{\text{keel}} \right]}{\eta_m \eta_g \eta_{\text{ls}}} + P_s \tag{10}$$

where the motor and lead screw efficiency, derived in the above sections, are given by Eqs. (5) and (6).

Inspection of Eq. (10) and the separate efficiency equations point out the parameters that can be varied to minimize the true power requirement. P_j is *a* function of $d\omega/dt$ and ω, which are the angular acceleration and angular velocity of the motor, and $(J_m + J_g)$ are the rotor and gear box inertia. P_m, in our simple series model optimization, is a function of the spring stiffness K_s and lever length l, since all other variables such as the ankle joint moment and ankle joint angle are assumed to be set as inputs to the system. The efficiencies are functions of motor torque τ, and motor angular velocity ω, μ, and α, which are the coefficient of friction and lead angle for the lead screw. Therefore, the parameters that can be varied to determine an optimal combination that minimizes electric power (true power), termed as "system efficiency parameters," are as follows:

(1) motor torque (τ)
(2) motor angular velocity (ω)

Downloaded 26 Mar 2010 to 149.169.104.18. Redistribution subject to ASME license or copyright; see http://www.asme.org/terms/Terms_Use.cfm

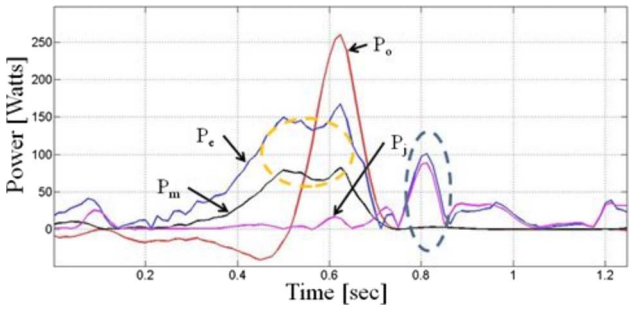

Fig. 7 Shown for one gait cycle are the electric power P_e, blue, power at the nut P_m, black, the output power P_o, red, and the power consumed due to rotor and gear inertia P_j. The area in the blue circle highlights the inertia effect and its power curve. The area in the yellow circle highlights the efficiency effect and the larger electric power curve.

(3) motor angular acceleration ($d\omega/dt$)
(4) rotor inertia (J_m)
(5) gear box inertia (J_g)
(6) spring stiffness (K_s)
(7) lever arm length (l)
(8) lead screw lead angle (α)
(9) lead screw friction coefficient (μ)

Integration of Eq. (10), which is done numerically in the model, is the true energy required to power gait. Minimization of the true energy is the primary goal in mechanical system design for this application. Shown in Fig. 7 is the electric power P_e, blue, required to deliver 80 W peak power at the nut P_m, black, as determined in the optimized simple series model described earlier. The power required for gait, the output power P_o, is in red. Also shown in the figure, in lavender, is the power consumed due to rotor and gear inertia P_j. The electric power is determined by evaluation of Eq. (10) with full implementation of the efficiency models for the motor, gear box, and lead screw. Highlighted in the blue dotted circle is the main inertia effect. Approximately 80 W peak power is consumed to counter inertia here. The area under the power curve is the energy drain on the system due to inertia. This point coincides with high angular velocity and angular acceleration as the foot quickly changes direction from plantarflexion to dorsiflexion as it leaves the ground at the start of the swing phase. The difference between P_e and P_m near the area highlighted in the yellow circle is the result of system efficiency near 50%. Fortunately, when the efficiency is at its lowest, P_m is near zero and the efficiency effects become negligible. Otherwise, high power requirement and low motor efficiency could lead to malfunction of the motor as the motor current reaches unacceptable levels as the motor draws increasing amounts of current to achieve high motor torque under low efficiency.

5 Methods and Analyses in Actuation Efficiency

The DC motor, transmission, and spring in the series design is a complex electromechanical system in terms of its physics. In practical terms, what this suggests is that one should select each mechanism and component on the basis of the system efficiency parameters, and more importantly, their interactions. For example, in this application, motor selection should include a careful evaluation of Eq. (10). From Fig. 6, the motor efficiency surfaces of three different motors have a similar shape if scaled for torque and angular velocity. The real differences are in the allowable torque and angular velocity ranges and their rotor inertia. The differences in torque and angular velocity range would force a change in mechanical advantage by changing the gear box and lead screw combination. Also, this would change the moment of inertia of the motor and gear box and all of the efficiency calculations. Therefore, the motor type has compounding effects on the system and its selection cannot be made without a system level evaluation.

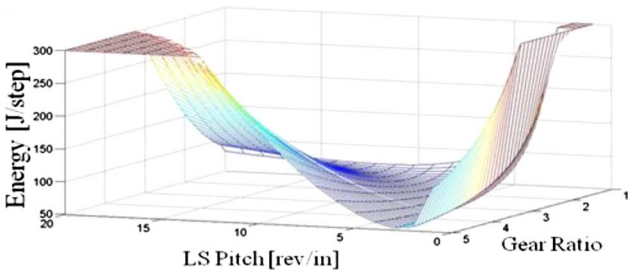

Fig. 8 Energy surface plots for the RE 40 motor in combination with different lead screw pitch and gear ratio. The best result, 53.1 J/step, is at 4.6 GR and 3 rev/in. lead screw.

System simulations are evaluated using MATLAB simulations of Eq. (10) and associated efficiency models. They are fully derived in Ref. [16]. The spring stiffness, lever length, keel stiffness, ankle joint moment, and angle are as described and selected in the simple series model. Three motor combinations, the RE 40, two RE 30s in parallel, and the EC 30 are analyzed. For each motor, different gear box ratios from 1:1 (no gear box) to 5:1 are evaluated, and the lead is adjusted from 1 rev/in. to 20 rev/in. The diameter of the lead screw remains unchanged at $\frac{1}{4}$ in.. The output of the simulation is based on the total electric input energy. This is determined by the numeric integration of P_e. The lead screw pitch is limited to 20 rev/in. because beyond that, the threading becomes too fine and delicate for this application. Gear ratios above 5:1 usually require additional stages of gears, and therefore, decrease gear box efficiency significantly (additional simulations of ratios above 5:1 did not show better results).

Each point in the surface plot in Fig. 8 represents one iteration of Eq. (10), varying the gear ratio and the lead screw pitch for the RE 40 motor. The surface represents the input energy requirement per step. Notice that there is only a narrow range of acceptable transmission combinations. The best results are near the high pitch and high gear ratio combinations. For this simulation, the best parameters are 53.1 J/step at 4.6 GR and 3 rev/in. for the lead screw. If we compare 53.1 J/step to the integration of the gait power curve, 19.5 J/step, rather than the absolute output energy of the gait power curve, 36 J/step, the system efficiency is 37%. The best solution without a gearbox is 69.4 J/step at 13 rev/in. Table 1 is the summary for all three motors and their transmission combination.

The motor and transmission analysis show that all three motors (RE40, two RE30s, and the brushless EC30) with their unique optimal combination of gear box and lead screw result in similar energy efficiency levels of approximately 53 J/step (37% energy efficiency), with gear box ratios near 5 and lead screw pitch near 3 rev/in.

The final step is to select the best motor and transmission combination and reevaluate Eq. (10), varying the spring stiffness and lever length to identify the best combination in terms of energy efficiency. In a second optimization routine, the selected system fixed the following parameters: the RE 40 and transmission combination of a 4.6:1 gear box and a 3 rev/in. lead screw. The spring stiffness was varied from 10 KN/m to 700 KN/m. The lever length

Table 1 Input energy requirement for motor and transmission combinations (spring stiffness=36 kN/m, lever length=9 cm)

Motors	Lead screw and gearbox	Lead screw only
RE 40	53.1 J/step, 4.6GR, 3 rev/in.	69.4 J/step, 13 rev/in.
EC 30	52.9 J/step, 5GR, 4 rev/in.	76.9 J/step, 18 rev/in.
2 RE 30	53.3 J/step, 5GR, 3 rev/in.	73 J/step, 15 rev/in.

Downloaded 26 Mar 2010 to 149.169.104.18. Redistribution subject to ASME license or copyright; see http://www.asme.org/terms/Terms_Use.cfm

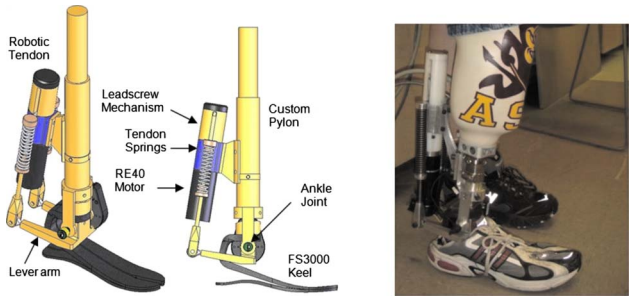

Fig. 9 Left figure is the isometric and side views of current design as modeled in SOLIDWORKS. The RE40 motor coupled with the robotic tendon provides a dynamic moment about the ankle joint. The right figure is a photograph of SPARKy on a male transtibial amputee test subject.

was varied from 3.5 cm to 35 cm. The best result is 52.3 J/step at 31 KN/m and a 9 cm lever length. This is a slight improvement from 53.1 J/step using 36 KN/m spring stiffness and a 9 cm lever length combination determined in the peak P_m optimization calculations in the simple series model. Efficiency improves from 36.5% to 37% by selecting a slightly less stiff spring and the same lever length. These slight improvements may fall within the error margin of the model.

6 Design and Build

The final design was based on several factors. The primary factors were the power and energy analyses described earlier, and user safety assessment followed by technical risk mitigation assessment, year 1 deliverables to our army sponsors, manufacturability, and commercial component availability. The design is based on the simple series model with the Maxon RE 40 motor. A planetary gear box, Maxon GP42, with 1:4.3 gear ratio was selected. A $\frac{1}{4}-4$ lubricated steel lead screw with bronze nut was selected as the rotational to linear transmission. A custom helical spring with sufficient dynamic load capability was designed at the lab and fabricated off site. The target stiffness was 30 kN/m to 40 kN/m, based on the analysis. The lever arm length is 9 cm. Recall that the analysis showed that the most energy efficient RE 40 design, 52.3 J/step input energy was a 1:4.6 gear box with a $\frac{1}{4}-3$ lead screw, 31 KN/m spring stiffness, 9 cm lever length. However, due to component availability, the final selection of the gear box and lead screw was based on a best match with commercial components.

Figure 9 shows two perspective views of the spring ankle with regenerative kinetics (SPARKy) and a side view photograph. A parallel, two-spring robotic tendon is attached to a custom aluminum pylon and to a commercial FS3000 keel from freedom innovations via a lever. The lever is rigidly attached to the keel. Note that the aluminum pylon was cut to size, and a socket was mounted for proper limb interface. The computer and electronics are currently worn as a fanny pack.

SPARKy is controlled in real time using Real Time Workshop and SIMULINK from Mathworks. The SIMULINK model is compiled on to the embedded target PC running the xPC target operating system. An encoder at the motor, an encoder at the ankle joint, and an optical switch embedded at the heel provides the necessary sensor feedback. Advantech's 650MHZ PC-104 with 512MB on board memory is selected to run the system. A multifunctional I/O board from Sensoray Co., Model 526, which is connected to the PC104 via an ISA bus, controls a RE-40 Maxon DC motor with encoder feedback. Future prototypes will make use of a computing system fully contained in the prosthesis.

The SPARKy controller, as described in Refs. [16,20–22], has a predetermined gait pattern, which is based on able-bodied gait data from Ref. [17] and kinetic analysis from Ref. [16], expressed as a time-based function embedded in the controller, which drives the motor controller, and thus, the system. Gait is initiated at heel strike with activation of an optical switch embedded in the heel. As the user initiates gait, the motor drives the lead screw nut through a pattern predetermined for each subject with closed loop feedback. The ankle, however, is not forced to follow the specific pattern because the compliant spring is between the motor and user, safely absorbing environmental irregularities such as a rock under foot or user errors. This inherent compliance not only provides for a safer interface, but also allows for a much simpler control scheme because high-bandwidth, high-precision force control is not required.

7 The Subject Testing

The collected data in this investigation are primarily the measurements of the kinetics and kinematics of the device, based on embedded sensor information, motor current, and voltage. The data was collected during 40 separate test dates over a 6-month period. The tests were conducted at Arizona State University. All of the measurements were taken while the subject was walking on a Lite Gait harnessed treadmill. The tests were conducted under varying speeds of up to 1.8 m/s (4 mph), which is at the upper end of normal walking speeds. The testing was approved by the Institutional Review Boards at Arizona State University and the sponsoring organization. The data show that power amplification of over 3 is possible over many walking speeds and conditions, and was shown consistently throughout the trials. The energy input requirement is at a level that a portable amount of lithium ion polymer batteries can support daily powered walking with a single charge of the batteries. The data also show that the device provides ankle joint motion and ankle power that is comparable to able-bodied persons. In terms of user benefit, the device has increased the self selected pace of the user from 0.45 m/s (1 mph) with his passive prosthesis, to 1 m/s (2.2 mph) with SPARKy. 1 m/s is more consistent with able-bodied persons. In addition, the one test subject, who has used the device for over 6 months, feels very strongly about the effectiveness of this device and its benefit. Prototype testing with three additional users is underway. Initial observations with the newest users are consistent with the detailed findings from our initial user reported in this paper.

Finally, in terms of the models used to design the device and predict its performance, the data shows that the models compare very well with the actual results. This indicates that the models have adequately captured the physical system.

7.1 SPARKy Performance Data. The following series of figures illustrate the actual electric power P_e, power out P_o, power at the nut P_m, ankle joint angle θ_A, and ankle joint moment M_A, compared with the model results. Electric power is determined by the direct measurement of voltage and current input to the motor. Since the measurements are continuous, the electric power is synchronized with the heel switch signal to identify the start and end of each step. Therefore, the captured data can be binned into separate gait cycles, based on the heel switch data. Figure 10 is the illustration of that methodology. Note that the energy input per step is merely the summation of the area under the electric power curve.

Figure 11 is the same data set shown in two dimensions. It provides a better indication of the range of variability, standard deviation, and mean. The predicted P_e is determined by evaluating Eq. (10) from the model. This figure clearly shows good agreement between measured data and the model. The higher level of noise in the model is due primarily to the errors generated by the numerical derivatives used to determine the angular velocity and angular acceleration components for the inertia effect. Filtering and smoothing can reduce the noise, the amplitude of the inertia effect, and consequently, the accuracy of the data, even further. Note that the models are shifted in time for better alignment with the test data.

Downloaded 26 Mar 2010 to 149.169.104.18. Redistribution subject to ASME license or copyright; see http://www.asme.org/terms/Terms_Use.cfm

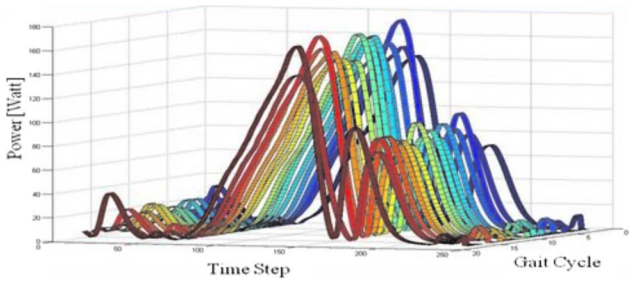

Fig. 10 Electric power, determined from voltage and current input readings, for the test subject on a treadmill at 1 m/s with 9 cm lever arm and 36 KN/m spring stiffness. Note that there is variability in each step, even though the subject is on a treadmill that is set at 1 m/s (2.2 mph).

Figure 12 is the measured power at the nut P_m and measured power out P_o, compared with the model. P_m is determined by the product of the measured nut velocity and the force at the nut. The force at the nut is determined by the measured spring deflection, times the spring stiffness. P_o is determined by the product of the measured angular velocity of the lever, effective lever length, and the same spring force. The power amplification $P_{o\ \mathrm{peak}}/P_{m\ \mathrm{peak}}$ is approximately 218 W/59 W in this data set. This is an amplification of 3.7. This level of amplification could potentially allow an even smaller Maxon RE 30 motor to power gait. Note that there seems to be a negative power recorded at heel strike. Part of this is the compression or even slight buckling in the spring during loading. Also, power is required during the swing phase to counter friction, control system delay, etc. These initial and swing phase conditions are not included in the model.

Figure 13 is the ankle joint angle versus the model, and Fig. 14 is the ankle joint moment versus the model for the same test as above. As mentioned earlier, a large portion of the differences between the model and test data for the ankle joint moment can be attributed to the compression or even slight buckling in the spring during loading and the friction in the system during the swing phase. These initial and swing phase conditions are not included in the model. The ankle joint angle is determined by the encoder at the ankle joint, and the ankle joint moment is determined by the product of the effective lever length and the spring force. The data clearly shows that the device provides full ankle motion. This is a unique achievement because today's commercially available devices do not provide any plantarflexion during push off, and only have limited dorsiflexion. The ankle joint moment achieved by SPARKy is also much closer to user requirements, and it is an improvement, as compared with today's state of the art passive device where the magnitude of the moment is decreased and delayed [16].

As illustrated in Figs. 12–14, the device provided 100% of ankle joint power, moment, and ankle joint motion required in gait while maintaining a power amplification of 3.7. This meets every goal for phase 1 of the SPARKy project.

8 Conclusion

This research presented the modeling, design, analyses, and testing of SPARKy 1. We are developing SPARKy 2 to reduce energy consumption and create more sophisticated control systems for unstructured walking. In this paper, human subject test data shows that our approach gains kinetic advantages by leveraging the elastic energy potential in uniquely tuned helical springs. It does this while providing the user the ankle power and ankle joint movement similar to able-bodied gait.

The analyses focused on a simple series quasistatic system model. The model provides a process to use springs in series with motors in designing devices such as SPARKy. It lays out a methodology of selecting the spring stiffness and lever lengths to de-

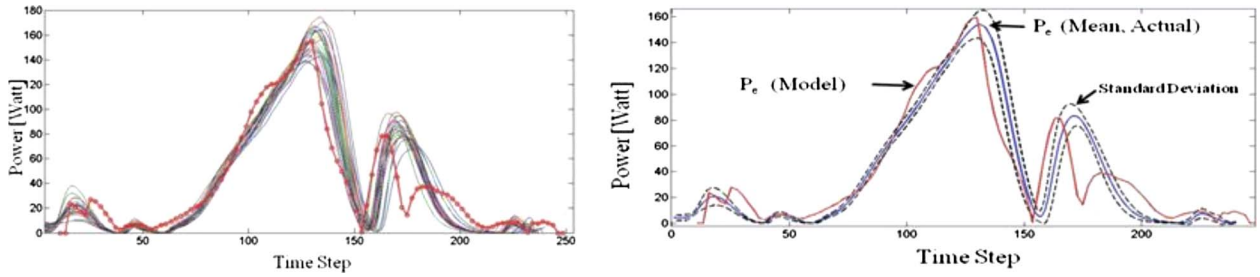

Fig. 11 The same electric power data set as in Fig. 10. The dotted line, left figure, is the predicted P_e from Eq. (10), and the solid lines are the raw measurements. The right figure shows the mean and standard deviation of the P_e data and the model, as annotated.

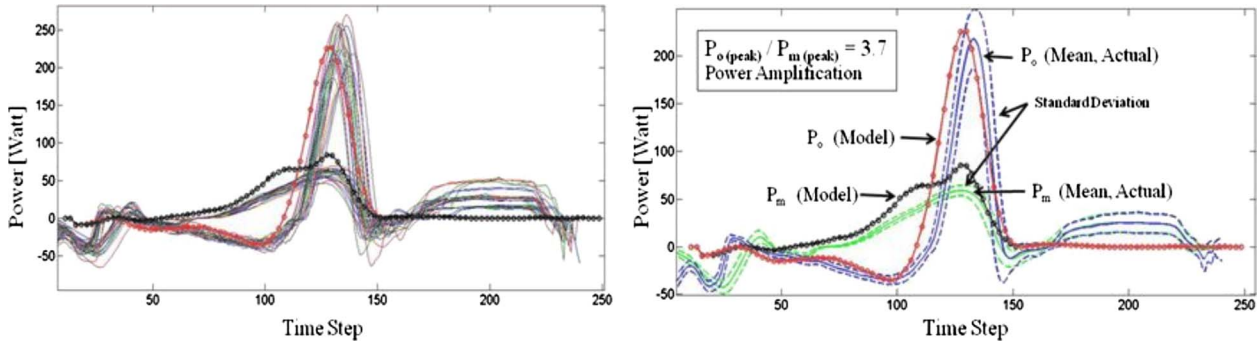

Fig. 12 Measured power out P_o and power at the nut P_m with 36 KN/m spring, 9 cm lever at 1 m/s (2.2 mph). The left figure shows the raw data for the P_o and the P_m for multiple gait cycles. The right figure shows the mean and standard deviation of the data and its corresponding models, as annotated. Note that the device achieves a very high level of power amplification of 3.7. This is the unique advantage of a robotic tendon.

Downloaded 26 Mar 2010 to 149.169.104.18. Redistribution subject to ASME license or copyright; see http://www.asme.org/terms/Terms_Use.cfm

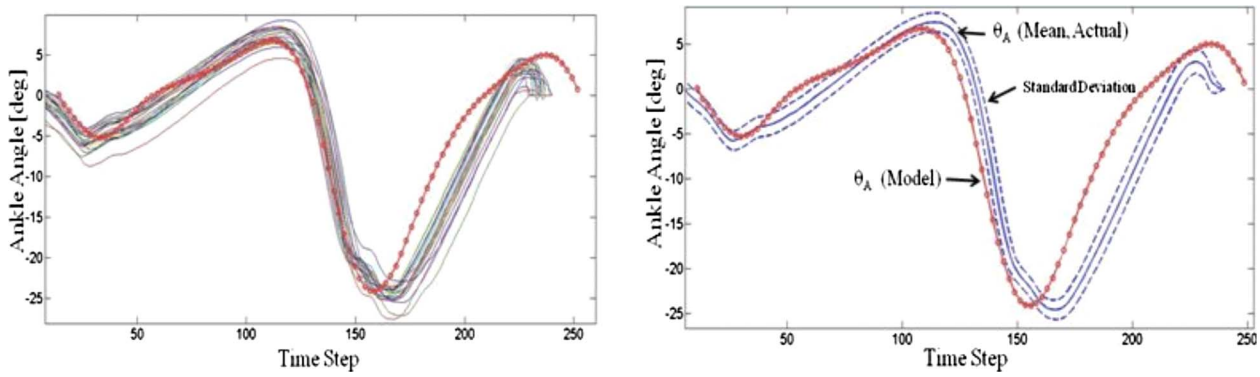

Fig. 13 Measured ankle joint angle for the same test series: 9 cm lever arm, 36 KN/m spring, and 1 m/s (2.2 mph). The left figure shows the raw data for the ankle joint angle for multiple gait cycles and the model. The right figure shows the mean and standard deviation of the data and the model, as annotated. Note that the device provides ankle joint motion that is comparable to able-bodied gait.

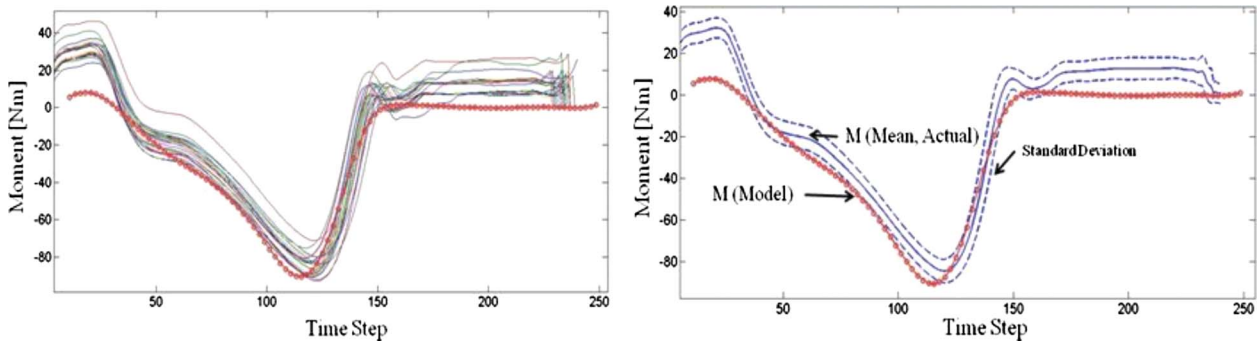

Fig. 14 Measured ankle joint moment: 9 cm lever arm, 36 KN/m spring, and 1 m/s (2.2 mph). The left figure shows the raw data for the ankle joint moment for multiple gait cycles and the model. The right figure shows the mean and standard deviation of the data and the model, as annotated. Note that the device provides ankle joint moment that is comparable to able-bodied gait.

termine the minimum peak motor power. This allows the peak motor power to decrease while providing the user the required power. The model predicted a power amplification of 3.25. This power amplification allows the downsizing of the actuator to a portable level. The test data showed a power amplification between 3 to 4 consistently, and reaching a power amplification of 6 during the testing phase.

In the analysis of determining the electric power, the research includes efficiency models for several different DC motors, lead screws, and gear boxes. It includes the inertia models for the motor and transmission combination. All of these models together formed Eq. (10), which is the electric power (true power) required for walking gait. Evaluating Eq. (10) as a function of several efficiency parameters: lever length, spring stiffness, lead screw pitch, and gear ratio narrowed the design space and became the primary factor in the final design of SPARKy 1. Testing suggests that the model adequately characterized the physical system to include changes in lever length, spring stiffness, and loading.

As such, the modeling allowed a small 150 W motor in combination with an optimized transmission and set of springs to provide 200–400 W during testing. This size and weight of the system is to a level that is comfortably portable to the user while powerful enough to support this 80 kg subject up to his maximum walking speed of 1.8 m/s (4 mph). The data suggests that there may be enough power available to support even larger users at such speeds.

Acknowledgment

The authors would like to thank the Center for the Intrepid at the Brooke Army Medical Center and the U.S. Army Medical Research and Material Command's Telemedicine and Advanced Technology Research Center (TATRC) for their sponsorship. The authors would also like to thank our team members, Arise Prosthetics and Robotics Group Inc., for their expertise and participation, and to our test subject for his invaluable help and dedication during testing.

References

[1] Hollander, K. W., Ilg, R., Sugar, T. G., and Herring, D. E., 2006, "An Efficient Robotic Tendon for Gait Assistance," J. Biomech. Eng., **128**(5), pp. 788–791.
[2] Casillas, J., Dulieu, V., and Cohen, M., 1995, "Bioenergetic Comparison of a New Energy-Storing Foot and SACH Foot in Traumatic Below Knee Vascular Amputations," Arch. Phys. Med. Rehabil., **76**, pp. 39–44.
[3] Rao, S., Boyd, L., and Mulroy, S., 1998, "Segment Velocities in Normal and Transtibial Amputees: Prosthetic Design Implications," IEEE Trans. Rehabil. Eng., **6**, pp. 219–226.
[4] Torburn, L., Perry, J., Ayyappa, E., and Shanfield, S., 1990, "Below-Knee Amputee Gait With Dynamic Elastic Response Prosthetic Feet: A Pilot Study," J. Rehabil. Res. Dev., **27**, pp. 369–384.
[5] van der Linden, M. L., Solomonidis, S. E., Spence, W. D., Li, N., and Paul, J. P., 1999, "A Methodology for Studying the Effects of Various Types of Prosthetic Feet on the Biomechanics of Trans-Femoral Amputee Gait," J. Biomech., **32**, pp. 877–889.
[6] Lehmann, J., Price, R., Boswell-Bessette, S., Dralle, A., Questad, K., and Delateur, B., 1993, "Comprehensive Analysis of Energy Storing Prosthetic Feet: Flex-Foot and Seattle Foot Versus Standard SACH Foot," Arch. Phys. Med. Rehabil., **74**, pp. 1225–1231.
[7] MacFarlane, P., Nielsen, D., Shurr, D., and Meier, K., 1991, "Gait Comparisons for Below-Knee Amputees Using a Flex-Foot Versus a Conventional Prosthetic Foot," Prosthet. Orthot Int., **3**, pp. 150–161.
[8] Postema, K., Hermens, H., de Vries, J., Koopman, H., and Eisma, W., 1997, "Energy Storage and Release of Prosthetic Feet. Part 1: Biomechanical Analysis Related to User Benefits," Prosthet. Orthot Int., **21**, pp. 17–27.
[9] Postema, K., Hermens, H., de Vries, J., Koopman, H., and Eisma, W., 1997, "Energy Storage and Release of Prosthetic Feet. Part 2: Subjective Ratings of

Downloaded 26 Mar 2010 to 149.169.104.18. Redistribution subject to ASME license or copyright; see http://www.asme.org/terms/Terms_Use.cfm

2 Energy Storing and 2 Conventional Feet, User Choice of Foot and Deciding Factor," Prosthet. Orthot Int., **21**, pp. 28–34.
[10] Klute, G., Czerniecki, J., and Hannaford, B., 2002, "Artificial Muscles: Actuators for Biorobotic Systems," Int. J. Robot. Res., **21**(4), pp. 295–309.
[11] Au, S., Berniker, M., and Herr, H., 2008, "Powered Ankle-Foot Prosthesis to Assist Level-Ground and Stair-Descent Gaits," J. Neural. Netw. Comput., **21**, pp. 654–666.
[12] Sawicki, G., and Ferris D. P., 2008, "Mechanics and Energetics of Level Walking With Powered Ankle Exoskeletons," J. Exp. Biol., **211**, pp. 1402–1413.
[13] Fite, K., Withrow, T. J., Shen, X., Wait, K. W., Mitchell, J. E., and Goldfarb, M., 2008, "A Gas-Actuated Anthropomorphic Prosthesis for Transhumeral Amputees," IEEE Trans. Rob., **24**(1), pp. 159–169.
[14] Versluys, R., Desomer, A., Gerlinde, L., Pareit, O., Vanderborght, B., Van der Perre, G., Peeraer, L., and Lefeber, D., 2008, "A Biomechantronical Transtibial Prosthesis Powered by Pleated Pneumatic Artificial Muscles," Model. Identif. Control, **4**(4), pp. 394–405.
[15] 2009, Proprio Technical Manual, Ossur Orthopaedic Products and Services Company, http://www.ossur.com
[16] Hitt, J., 2008, "A Robotic Transtibial Prosthesis With Regenerative Kinetics," Ph.D. thesis, Arizona State University, Tempe, AZ.
[17] Whittle, M. W., 1996, *Gait Analysis: An Introduction*, 2nd ed., Butterworths, London.
[18] Hitt, J., Holgate, M., Sugar, T., Bellman, R., and Hollander, K., 2009, "Robotic Transtibial Prosthesis With Biomechanical Energy Regeneration," Ind. Robot, **36**(5), pp. 441–447.
[19] Norton, R., 2005, *Machine Design: An Integrated Approach*, 2nd ed., Prentice-Hall, Englewood Cliffs, NJ.
[20] Ward, J., Hitt, J., Sugar, T., and Bharadwaj, K., 2006, "Dynamic Pace Controller for the Robotic Gait Trainer," Proceedings of the ASME International Design Engineering Technical Conference and Computers and Information in Engineering Conference, Philadelphia, PA.
[21] Hitt, J., Oymagil, A., Sugar, T., Hollander, K., Boehler, A., and Fleeger, J., 2007, "Dynamically Controlled Ankle-Foot Orthosis With Regenerative Kinetics: Incrementally Attaining User Portability," Proceedings of the 2007 IEEE International Conference on Robotics and Automation, Roma, Italy.
[22] Hitt, J., Holgate, M., Bellman, R., Sugar, T., and Hollander, K., 2007, "The SPARKy (Spring Ankle With Regenerative Kinetics) Project: Design and Analysis of a Robotic Transtibial Prosthesis," Proceedings of the ASME International Design Engineering Technical Conference and Computers and Information in Engineering Conference, Las Vegas, NV.

Downloaded 26 Mar 2010 to 149.169.104.18. Redistribution subject to ASME license or copyright; see http://www.asme.org/terms/Terms_Use.cfm

Research article

Robotic transtibial prosthesis with biomechanical energy regeneration

Joseph Hitt
Department of Civil and Mechanical Engineering, United States Military Academy, West Point, New York, USA

Thomas Sugar
Department of Engineering, Arizona State University, Tempe, Arizona, USA

Matthew Holgate and Ryan Bellman
Department of Mechanical and Aerospace Engineering, Arizona State University, Tempe, Arizona, USA, and

Kevin Hollander
Augspurger-Komm Engineering, Phoenix, Arizona, USA

Abstract
Purpose – The purpose of this paper is to describe a project which seeks to develop a new generation of powered prostheses based on lightweight, uniquely tuned, energy-storing elastic elements in series with optimal actuator systems that will significantly reduce the peak power requirement of the motor and the total system energy requirement while providing the amputee 100 percent of required "push-off" power and ankle sagittal plane range-of-motion comparable to able-bodied gait.
Design/methodology/approach – This paper presents the design, power, and energy-efficiency analyses, and the results of a five-month trial with one trans-tibial amputee subject as part of the first phase of the Spring Ankle with Regenerative Kinetics project.
Findings – The data show that by leveraging uniquely tuned springs and transmission mechanisms, motor power is easily amplified more than four fold and the electric energy requirement is cut in half compared with traditional approaches.
Originality/value – This paper describes an energy efficient, powered transtibial prosthesis currently unavailable commercially. Motor power and energy requirements are reduced with use of a unique design that employs regenerative kinetics.

Keywords Rehabilitation, Robotics, Prosthetic devices, Limbs, Mechanical systems, Control technology

Paper type Research paper

1. Introduction

There have been significant improvements in prosthetic and orthotic technologies in recent years. Several prosthetic companies have produced devices that are more comfortable, provide life-like cosmeses, provide significant energy return, and are now even computer controlled. Energy storage and return (ESAR) devices allow faster walking velocity and better terrain negotiation (Casillas *et al.*, 1995; Rao *et al.*, 1998; Torburn *et al.*, 1990). They have increased range of motion; they store and return energy; and they reduce the needed metabolic requirements (van der Linden *et al.*, 1999; Lehmann *et al.*, 1993; MacFarlane *et al.*, 1991; Postema *et al.*, 1997a, b).

Hydraulic, pneumatic, motor/gearbox, series-elastic, electroactive polymer-based, chemical-based and many other actuation schemes are also at varying stages of research and development (Klute *et al.*, 2002; Au *et al.*, 2008; Sawicki and Ferris, 2008; Fite *et al.*, 2008; Versluys *et al.*, 2008). Other researchers are working on wearable robot control. From the highly publicized neuro-controlled bionic arm (*Popular Magazine*, 2005) to embedded gait pattern control (Ward *et al.*, 2006), electromyography (EMG) motion control (Au *et al.*, 2005; Ferris *et al.*, 2005) and state-based control (Pappas *et al.*, 2001), they are all producing positive results. The Proprio Ankle by Ossur is the first commercially available motorized and computer-controlled ankle device that modulates ankle angle based on the environment, gait, and conditions to better mimic the kinematics of the lost limb, however, without the functionality to actively generate power (Ossur Orthopaedic Products and Services Company, 2009).

2. Power and energy density

A portable, daily-use powered prosthesis such as Spring Ankle with Regenerative Kinetics (SPARKy) requires both high power to weight ratio (power density) and energy to weight ratio (energy density) in an actuator (Hitt, 2008). Without these limitations, one could take, for example, a RE75 DC Motor from Maxon Precision Motors, Inc. rated for 250 W

The current issue and full text archive of this journal is available at
www.emeraldinsight.com/0143-991X.htm

Industrial Robot: An International Journal
36/5 (2009) 441–447
© Emerald Group Publishing Limited [ISSN 0143-991X]
[DOI 10.1108/01439910910980169]

continuous power to provide the 250 W peak power required in human gait (80 kg subject at 0.8 Hz walking; Hollander and Sugar, 2006; Hollander *et al.*, 2006). But this motor in combination with a gearbox in a traditional approach would weigh 6-7 kg, which exceeds the weight of a typical biological below knee limb. Providing the idealized 36 J of energy per step (Hollander and Sugar, 2006; Hollander *et al.*, 2006) also becomes an issue because one must consider the efficiency of the motor, gearbox and other transmission mechanisms, friction and inertia, and the consumption of energy by the sensors and electronics. Just the mechanism inefficiency alone can double the energy requirement. For example, a DC motor with an average efficiency of 70 percent, connected to a ball screw at 90 percent and a gearbox at 80 percent multiply to produce a 50 percent efficiency actuation system. This would suggest a doubling of the energy input requirement to 72 J/step to provide the necessary 36 J/step at the output end. This is an optimistic estimate because this does not include several other factors such as: the energy consumed to counter motor/actuator inertia, which our tests show, is considerable in a highly cyclical gait pattern where the motor rapidly changes direction several times per step, friction in the mechanism or energy required by the microprocessor, sensors, motor controller, etc. (Figure 1). One can easily see that actual energy requirement could grow to three- or fourfold of the idealized number of 36 J/step in a traditional approach and consequently increasing the battery requirement proportionately to non-portable levels. Also under these circumstances, slow running which may quadruple the peak power requirement as compared to normal walking (1,000 W for heel to toe running as compared to 250 W for walking) would send power and energy density requirements beyond what can be achieved.

3. Motor power requirement

SPARKy utilizes the Robotic Tendon (Hollander and Sugar, 2006; Hollander *et al.*, 2006) actuator to minimize the peak motor power requirement by correctly positioning a uniquely tuned helical spring so that the spring provides most of the peak power required for gait. The Robotic Tendon is a small and lightweight actuator that features a low energy motor that is used to adjust the position of the helical spring using a very simple position controller. The work differs from the series elastic actuator because the proximal side of the spring is controlled using position feedback, and the distal side of the spring is not controlled. Figure 2 shows how the desired spring deflection and consequently via Hooke's law the desired force and ankle moment is achieved using a spring. As the ankle rotates over the foot during the stance phase, a lever position profile as shown in Figure 2 is obtained. By correctly positioning the motor, a desired spring deflection as shown in the shaded area of Figure 2 is obtained. A heavy, powerful, impedance-controlled motor is not needed because the Robotic Tendon stores a portion of the stance phase kinetic energy and additional motor energy within the spring. The spring releases its stored energy to provide most of the peak power required during "push off." Therefore, the power requirement on the motor is significantly reduced. As described in Hollander and Sugar (2006) and Hollander *et al.* (2006), peak motor power required is 77 W compared to 250 W for a motor/gearbox system in the 80 kg subject at a 0.8 Hz example. Consequently, the weight of the Robotic Tendon, at just 0.95 kg, is seven times less than an equivalent direct drive motor and gearbox system that is required to provide the necessary peak power. In other words, the Robotic Tendon achieves a power density that in essence is seven times greater than a traditional approach. Figure 3, in comparison with Figure 1, shows the addition of regenerative

Figure 1 Illustration of the flow of power and energy from the battery to the user

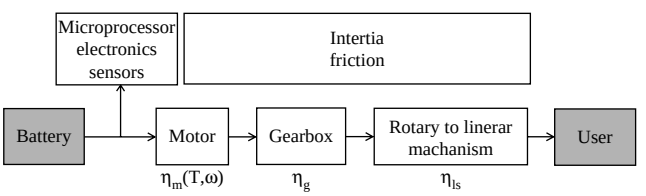

Notes: Significant amount of energy is lost due to inefficiency in the mechanisms, motor, inertia, friction, etc. Proper selection and design can drastically improve overall system efficiency. The system efficiency is defined as average output power to the user/average input power from the battery

Figure 2 Desired spring deflection, shaded area, is achieved by controlling the motor position and capitalizing on the cyclical nature of gait

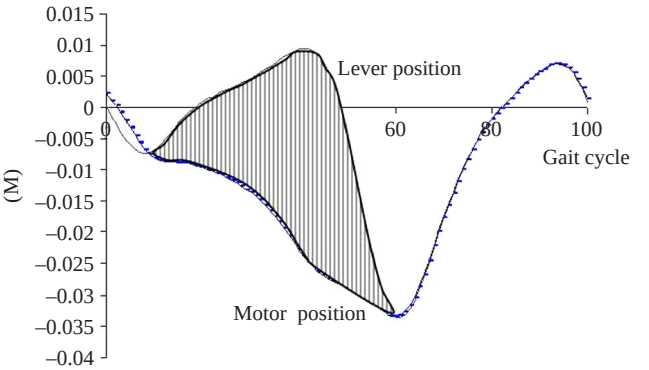

Notes: As the tibia rotates over the stance foot, the lever extends the springs. Simultaneously, the motor extends the spring in the opposite direction to achieve the desired spring deflection and via Hooke's Law the forces required to generate the required ankle moment for walking

Figure 3 Illustration of the flow of energy from the battery to the user for the Robotic Tendon model

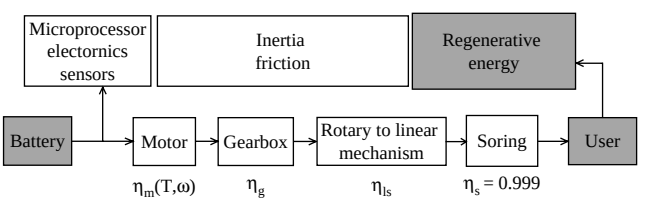

Notes: Even though significant amount of energy is lost due to inefficiency in the mechanisms, motor, inertia, friction, etc., the spring and the regenerative energy that it harnesses is nearly 100% efficient and accounts for the main share of the output energy. This method also allows for a smaller motor, battery and transmission system

power and energy made possible with the spring in series with the motor.

4. Motor energy requirement

SPARKy increases energy density of the actuation system by using the spring, which is almost 100 percent efficient, to provide most of the energy. Additionally, ideal motor energy requirement, as determined by the integration of the power curves, is reduced from nearly 36 J in the 250 W peak power case to 21 J/step in the 77 W peak power case described above (80 kg subject walking at 0.8 Hz). This significantly reduces the energy input burden of the motor and it allows the much more efficient helical spring to store and release energy.

Another significant aspect of energy density is motor efficiency. The RE40 DC Motor by Maxon Precision Motors, Inc. (2009) currently used in the Phase I SPARKy is one of the most efficient motors commercially available for this application. However, its rated efficiency of 90 percent is only achieved at a very small range of motor torque and angular velocity – near 7,000 rpm at 0.1 N m. Below 2,000 rpm and above 0.2 N m, motor efficiency quickly drops below 50 percent. The motor efficiency 3D plot is shown in Figure 4 as a function of motor torque and motor rpm.

Figure 4 shows that there is a narrow range of motor efficiency above 70 percent. Once the motor slows below 2,000 rpm or motor torque exceeds 0.2 N m, the motor efficiency degrades exponentially. Therefore, the motor should be properly matched with an appropriate gearing mechanism that maintains high motor speed and low torque.

On Phase I SPARKy, a 4.3 gear ratio gearbox from Maxon rated at 90 percent efficiency, 1/4 in.-16 turns/in. ACME 4 start lead screw and an adjustable length lever are used to achieve high motor efficiency. A lead screw was selected over other rotation to translation mechanisms such as a ball screw or a roller screw for several reasons. A ball screw is highly efficient because of its rolling contact but is limited in terms of the dynamic load rating. Roller screws are also very efficient and they have high dynamic load ratings but the price can be prohibitive.

The efficiency of a typical lead screw is low compared to the other transmission mechanisms mentioned above. By using a small diameter lead screw with a proportionately large lead, one can achieve a lead angle that allows for maximum efficiency. By selecting a lubricated steel lead screw and bronze nut, one can achieve a coefficient of friction below 0.1. The efficiency of our lead screw is 0.7 as determined by the method outlined in Hollander and Sugar (2006) and Hollander *et al.* (2006).

Figure 4 3D plot of the RE40 motor efficiency as a function of motor torque (Nm) and motor angular velocity (rpm)

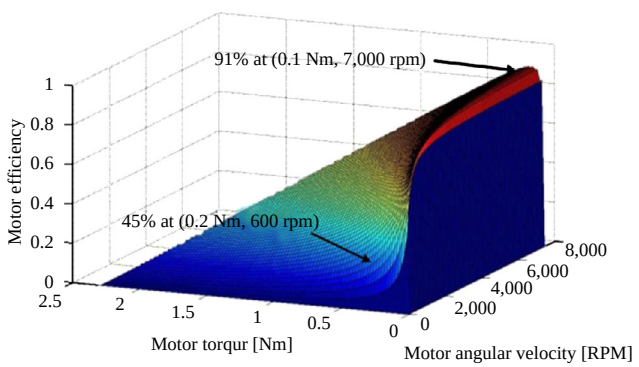

Notes: Notice that the highest efficiency of 90 percent is only achieved at a narrow range of torque and angular velocity. Operating the RE40 at speeds lower than 2,000 rpm or torque above 0.2 Nm will significantly degrade the motor efficiency. Illustrated in the figure are two points on the mesh

5. SPARKy design

5.1 Mechanical design

The mechanical design of SPARKy has presented several obstacles that needed to be overcome to maximize the energy output without limiting the comfort, capability and safety of the robot. Figure 5 shows two perspectives of the modeled prosthetic ankle. A new parallel two spring Robotic Tendon is attached to a custom aluminum pylon and to a commercial FS3000 Keel from Freedom Innovations via a lever. The three sensors that provide closed loop feedback are not shown in these illustrations. The computer and electronics are packaged in a portable 5 × 7 in. case worn at the hip for the current phase of SPARKy I.

The mechanical design includes two safety features. First, the threading of the lead screw is removed at both ends to allow for free spin of the lead screw nut so that the ankle cannot over extend in plantarflexion or dorsiflexion directions. Additionally, the ankle joint is mechanically limited to normal ankle joint ranges as a secondary counter-measure for over-extension.

5.2 Electronics, sensors and computing

SPARKy is controlled in real time using Real Time Workshop and Simulink from Mathworks. The Simulink model is compiled on to the embedded target PC running the xPC Target Operating System. An encoder at the motor, an encoder at the ankle joint and an optical switch embedded at the heel provides the necessary sensor feedback. Advantech's 650 MHz PC-104 with 512 MB on-board memory is selected to run the system. A multifunctional I/O board from Sensoray Co., Model 526, which is connected to the PC104 via an ISA bus, controls a RE40 Maxon DC motor with encoder feedback. Future prototypes will make use of a computing system fully contained in the prosthesis.

Figure 5 Isometric and side views of current design as modeled in Solid Works

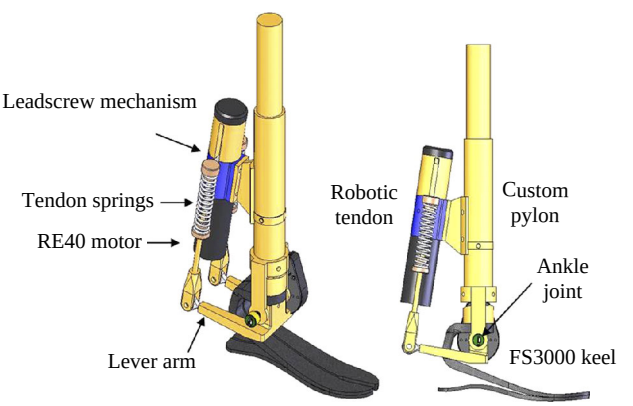

Note: The RE40 motor coupled with the robotic tendon provide a dynamic moment about the ankle joint

Two safety features are designed into the electronics of the prototype. A handheld dead man's switch must remain engaged to maintain power to the motor. An emergency stop is incorporated into the power system that an investigator can use to cut the power to the entire system.

5.3 Control

Together with power and energy density, computer control of prostheses remains a significant challenge. Efforts towards control methodology that produce biologically realistic movement in prostheses and orthoses began in the early 1960s with work such as the Belgrade Hand. However, even after a half century of work, achieving human-like control is proving to be very difficult. Work by Au *et al.* (2005) and Ferris *et al.* (2005) in EMG position control and by Pappas *et al.* (2001) in state-based control seems promising because of its simplicity. Sugar's (2002) effort to reduce the control problem using compliant simple force control is a key finding towards simplifying control methodology and served as our starting point with the Robotic Tendon.

The SPARKy controller, as described in Hitt *et al.* (2007a, b), has a predetermined gait pattern, which is based on able-bodied gait data (Whittle, 1996) and kinetic analysis (Hollander and Sugar, 2006; Hollander *et al.*, 2006), expressed as a time-based function embedded in the controller, which drives the motor controller and thus the system. Gait is initiated at heel strike with activation of an optical switch embedded in the heel. As the user initiates gait, the motor drives the lead screw nut through a pattern predetermined for each subject with closed loop feedback. The ankle, however, is not forced to follow the specific pattern because the compliant spring is between the motor and user, safely absorbing environmental irregularities such as a rock under foot or user errors. This inherent compliance not only provides for a safer interface, but allows for a much simpler control scheme because high-bandwidth, high-precision force control is not required.

6. SPARKy modeling

Ankle joint angle and moment data used in the simulation are from able-bodied data generated by inverse dynamics of motion capture and force plate test data and published by Whittle (1996). The remaining kinetic and kinematic analysis is derived using a quasi-static approach. MATLAB simulation of the models showed that a power amplification of up to six may be possible. Presented here is one of those models selected for SPARKy Phase I for its simplicity and robustness in terms of mechanical design and control. Simulation of this model showed that a power amplification of more than three is possible while maintaining gait kinematics and kinetics similar to able-bodied persons.

In the simple series model, the keel and the Robotic Tendon springs are in series; therefore, the moment in the keel is equal to the moment in the Robotic Tendon. Motor position is controlled so that the moment of the Robotic Tendon matches that of the able-bodied moment data (equation (1)). K_a is the keel stiffness in N/m; K_s is the spring stiffness in N/m; B is the radius of the keel deflection in meters; d is the moment arm due to the keel deflection in meters; and l is the lever length in meters (Figure 6). Note that the derivation applies small angle approximations:

Figure 6 A two degrees-of-freedom model with a seismic excitation representing the motor excitation, a torsional spring for the keel and a helical spring between the lever and the motor is shown

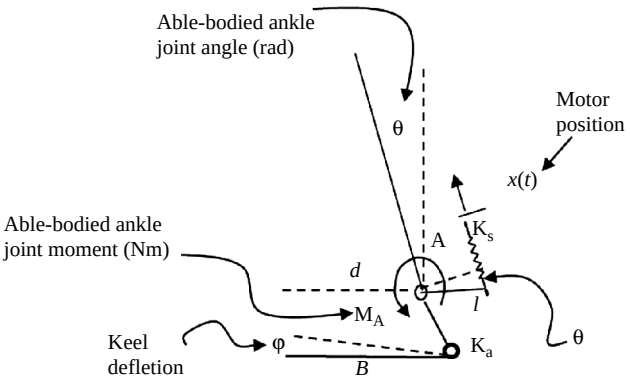

Notes: The moment due to the keel is a function of ?(t) and the moment due to the spring is a function of x(*t*)–/θ(*t*). The moment at the ankle is from published information determined using inverse dynamics of motion capture and force plate test data as published in Whittle (1992)

$$M_A(t) = M_{keel}(t) = M_{RT}(t) \tag{1}$$

where:

$$M_A, \quad \text{from published } AB \text{ data [24]}$$

$$M_{keel}(t) = -K_a B d\varphi(t) \quad M_{RT}(t) = K_s(x(t) - l\theta(t))l$$

Solving equation (1) for motor position, $x(t)$, determines the expression in equation (2):

$$x(t) = l\theta(t) - \frac{K_a B d}{K_s l}\,\varphi(t) \tag{2}$$

The assumed force in the Robotic Tendon is given by equation (3):

$$F(t) = \frac{M_A(t)}{l} \tag{3}$$

The ideal power generated by the motor to move to position $x(t)$ is given by the product of the force and velocity in the tendon, equation (4):

$$\begin{gathered} P_m(t) = F(t)\frac{dx(t)}{dt} \\ \Rightarrow P_m(t) = \frac{M_A(t)}{l}\left[l\frac{d\theta(t)}{dt} - \frac{K_a B d}{K_s l}\,\frac{d\varphi(t)}{dt}\right] \end{gathered} \tag{4}$$

The expression in equation (4) represents the power required by the motor to generate the desired moment and ankle angle of able-bodied gait (Whittle, 1996) given that the spring provides the majority of the required peak power.

Optimization of equation (4) varying keel stiffness, K_a, and spring stiffness, K_s, showed that a minimum peak motor power profile is achieved by varying K_s as shown in Figure 7. This figure is a surface plot of the peak power at a given spring and keel stiffness. It shows that a spring stiffness of 32,000 N/m is optimal in terms of minimum peak motor power. At this spring stiffness, the peak motor power is at its lowest value of 80 W. As the tendon spring becomes rigid, required motor power reaches that of a rigid system. As the tendon spring

Figure 7 A surface plot of the peak power from equation (4) varying K_a and K_s

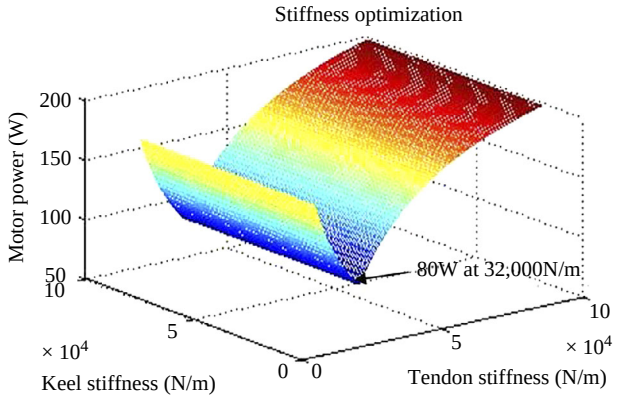

Notes: Notice that at a spring stiffness of 32,000 N/m, the minimum peak motor power of 80 W is achieved. Keel stiffness does not greatly influence the design in this optimization

stiffness reaches zero, required motor power becomes asymptotically large.

The results are significant because it shows that SPARKy with use of a keel and Robotic Tendon can achieve significant kinetic advantages. With an input power of 80 W from the motor, this simulation illustrates that SPARKy, with use of springs, can deliver the required 260 W of peak gait power, which is a power amplification of 3.25. Figure 8, generated from the simulation, shows the motor, gait and keel power profiles. Notice that the motor power peaks at 80 W and the gait power peaks at 260 W. The keel power profile is not additive because the system is in series. However, the keel power profile is similar to what is found in literature describing the power of ESAR keels.

This series model achieves 100 percent of the required peak gait power with less than one-third of the peak input power (motor power) by harnessing the energy storage potential of springs. In addition, because the system's joint motion is controlled only by the counter moments of the tendon spring and keel, kinematics of the system is almost identical to the desired able-bodied gait (Figure 9). This total motion of SPARKy provides its user with kinematics similar to able-bodied gait kinematics representing a significant improvement from today's state of the art.

Figure 8 The power profiles for able-bodied gait (system output power), required motor power and power from the keel (from simulations)

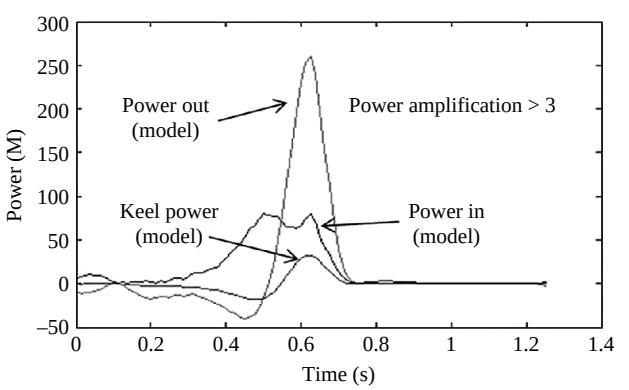

Figure 9 The ankle joint angle, the keel deflection angle, and the sum of both angles (from simulations)

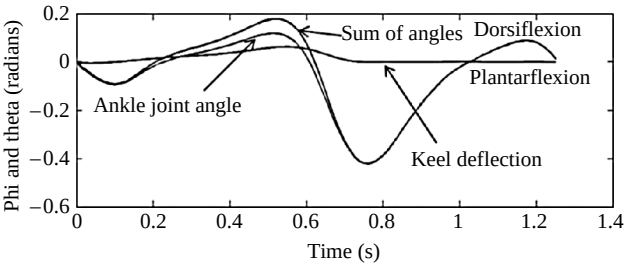

7. SPARKy testing

SPARKy Phase I device was tested on a single transtibial amputee male subject for a period of five months walking on a treadmill. Embedded sensor data such as motor and ankle encoder information were recorded at varying walking speeds with varying spring stiffness, lever lengths, and loading condition. In addition, direct measurements of motor current and voltage information were recorded. This information was used to determine the ankle kinematics and kinetics of the user on the SPARKy device. Figure 10 is a picture of a transtibial amputee test subject, 80 kg, walking over level ground using SPARKy.

Figure 11 shows the desired ankle position as modeled previously and the actual ankle position measured using the ankle encoder. Testing shows that SPARKy achieves full ankle sagittal plane range of motion. The ankle position is quite accurate and smooth even though the distal side of the spring is not controlled.

Figure 12 shows the desired motor and gait output powers determined from our simple series model described earlier. Using measured spring deflection to determine the force at the spring and ankle and motor encoder information to determine the velocity at the motor and at the ankle, motor and output powers are determined using the product of force and velocity. The measured powers are in very good agreement with the modeled powers. Figure 13 shows the measured motor power and the measured output power for a series of nine gait cycles of our subject walking at 1.3 m/s (3 mph). The power amplification is consistently above 4.5 (peak output power/peak motor power). The motor only outputs 60 W peak but

Figure 10 A picture of a transtibial amputee using SPARKy overground

Figure 11 The desired ankle movement and the actual ankle movement for one walking gait cycle

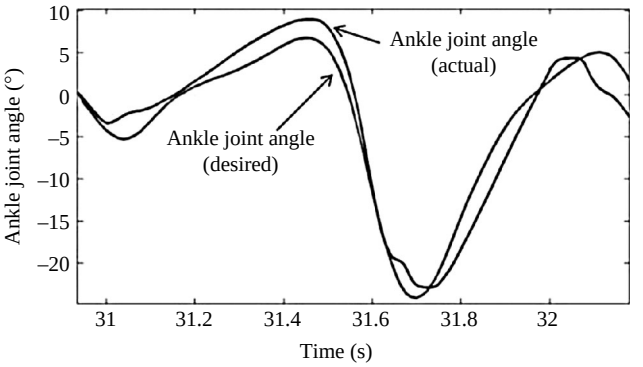

Note: The subject was walking at 1 m/s (2.2 mph) on a treadmill

Figure 12 The ideal output and motor power determined by the simple series model versus the measured output and motor power

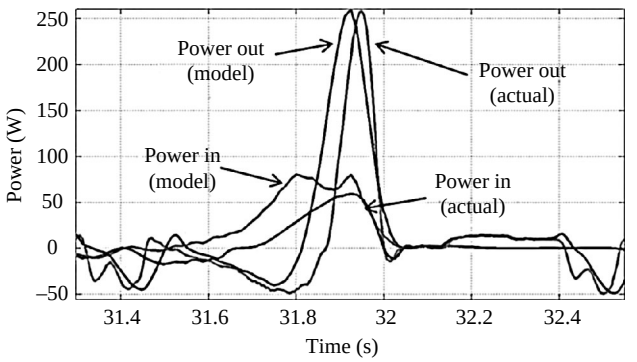

Figure 13 The measured motor power and output power for nine gait cycles

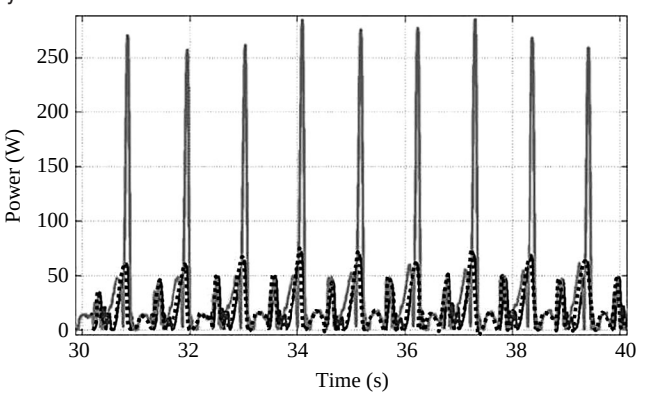

Notes: The power amplification is consistently above 4.5 (270W peak/ 60Wpeak). Our test data has shown amplifications of six and eight are possible

SPARKy with the use of springs delivers 270 W of peak power to the user. Figure 14 shows the measured power from the motor and spring. Notice that the spring provides the majority of the power required during push off.

Electric power used by the motor is determined using the direct measurement of current and voltage to the motor (Figure 15). Integration of the electric power provides the energy input requirement for SPARKy at 1.3 m/s (3 mph) as 43 J/s or 43 W. Output power is the product of the measured ankle velocity and force. Integration of the output power

Figure 14 The motor power and the spring power sum to the output power

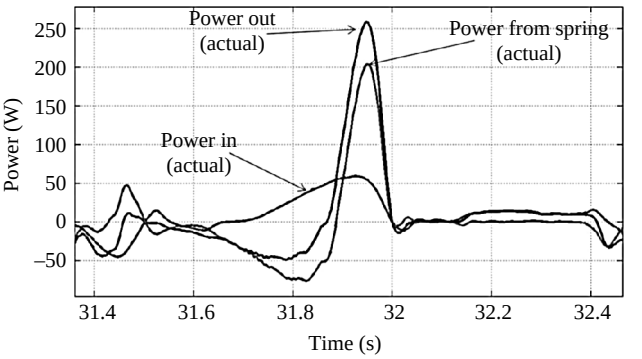

Note: The spring provides the majority of the push-off power required in gait

Figure 15 The dashed line is the electric power input as determined by the measured current and voltage to the motor. The solid line is the same output power shown in Figure 13

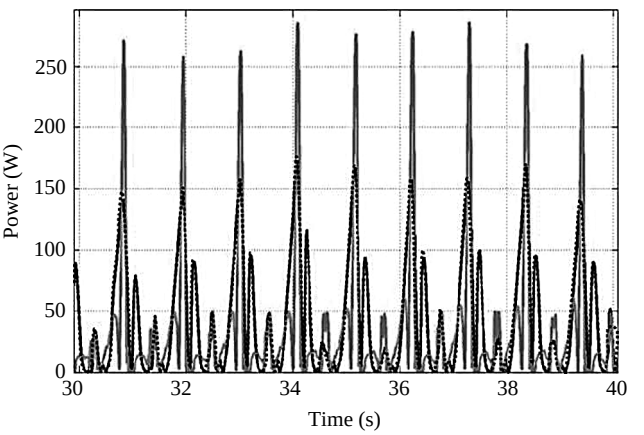

provides the energy output by SPARKy at 1.3 m/s (3 mph) as 35 J/s or 35 W. Therefore, the system efficiency in terms of average power in and out is 0.81. This level of efficiency is possible because majority of the work is done by the springs. We have similar data and results with the subject walking at 0.5, 1, 1.3 and 1.8 m/s.

8. Conclusion

We presented in this paper the design, analysis and testing of the Phase I SPARKy. We showed that this approach gains kinetic advantages by leveraging elastic energy potential in uniquely tuned helical springs. As the tibia rotates over the stance foot ankle during walking gait, we position the spring to maximize elastic energy storage. We presented the synergistic benefits of the Robotic Tendon in terms of motor efficiency and power and energy reductions. We presented test data to show that we achieved a power amplification of 4.5 consistently with the motor providing a peak of 60 W and the spring providing the remaining 210 W so that the user had a peak of 270 W at push off while walking at 1.3 m/s (3 mph). We showed that the system is 81 percent efficient in terms of the average electric power into the motor (43 W) and average mechanical power out to the user (35 W). This level of efficiency is possible because the springs perform the majority of the work. We also

show that SPARKy can provide 100 percent of the push-off power required in walking gait while maintaining gait kinematics similar to able-bodied gait.

References

Au, S., Berniker, M. and Herr, H. (2008), "Powered ankle-foot prosthesis to assist level-ground and stair-descent gaits", *Neural Networks*, Vol. 21, pp. 654-66.

Au, S., Bonato, P. and Herr, H. (2005), "An EMG-position controlled system for an active ankle-foot prosthesis: an initial experimental study", *Proceedings of the 2005 IEEE 9th International Conference on Rehabilitation Robotics, Chicago, IL, June 28-July 1*, pp. 379-375.

Casillas, J.M., Dulieu, V., Cohen, M., Marcer, I. and Didier, J.P. (1995), "Bioenergetic comparison of a new energy-storing foot and SACH foot in traumatic below knee vascular amputations", *Archives of Physical Medicine and Rehabilitation*, Vol. 76 No. 1, pp. 39-44.

Ferris, D.P., Gordon, K.E., Sawicki, G.S. and Peethambaran, A. (2005), "An improved powered ankle-foot orthosis using proportional myoelectric control", *Gait & Posture*, Vol. 23 No. 4.

Fite, K., Withrow, T.J., Shen, X., Wait, K.W., Mitchell, J.E. and Goldfarb, M. (2008), "A gas-actuated anthropomorphic prosthesis for transhumeral amputees", *IEEE Transactions on Robotics*, Vol. 24 No. 1.

Hitt, J. (2008), "Design and control of a robotic transtibial prosthesis with regenerative kinetics", PhD dissertation, Arizona State University, Tempe, AZ.

Hitt, J., Bellman, R., Holgate, M., Sugar, T. and Hollander, K. (2007a), "The SPARKy (Spring Ankle with Regenerative Kinetics) project: design and analysis of a robotic transtibial prosthesis", paper presented at the ASME International Design Engineering Technical Conference & Computers and Information in Engineering Conference, Las Vegas, NV.

Hitt, J., Oymagil, A., Sugar, T., Hollander, K., Boehler, A. and Fleeger, J. (2007b), "Dynamically controlled ankle-foot orthosis with regenerative kinetics: incrementally attaining user portability", *Proceedings of the 2007 IEEE International Conference on Robotics and Automation, Roma*, pp. 1541-6.

Hollander, K. and Sugar, T.G. (2006), "Design of lightweight lead screw actuators for wearable robotic applications", *ASME Journal of Mechanical Design*, Vol. 128 No. 3, pp. 644-8.

Hollander, K., Ilg, R., Sugar, T.G. and Herring, D.E. (2006), "An efficient robotic tendon for gait assistance", *ASME Journal of Biomechanical Engineering*, Vol. 128 No. 5, pp. 788-91.

Klute, G., Czerniecki, J. and Hannaford, B. (2002), "Artificial muscles: actuators for biorobotic systems", *The International Journal of Robotics Research*, Vol. 21 No. 4, pp. 295-309.

Lehmann, J.F., Price, R., Boswell-Bessette, S., Dralle, A., Questad, K. and deLateur, B.J. (1993), "Comprehensive analysis of energy storing prosthetic feet: Flex-Foot and Seattle foot versus standard SACH foot", *Archives of Physical Medicine and Rehabilitation*, Vol. 74, pp. 1225-31.

MacFarlane, P., Nielsen, D., Shurr, D. and Meier, K. (1991), "Gait comparisons for below-knee amputees using a Flex-Foot versus a conventional prosthetic foot", *Journal of Prosthetics and Orthotics*, Vol. 3, pp. 150-61.

Maxon Precision Motors (2009), *RE40 Motor Specifications*, Maxon Motor, Fall River, MA, available at: www.maxonmotor.com

Ossur Orthopaedic Products and Services Company (2009), *Proprio Technical Manual*, Ossur Orthopaedic Products and Services Company, Aliso Viejo, CA, available at: www.ossur.com

Pappas, I., Popovic, M., Keller, T., Dietz, V. and Morari, M. (2001), "A reliable gait phase detection system", *IEEE Transaction on Neural Systems and Rehabilitation Engineering*, Vol. 9 No. 2, pp. 113-25.

Popular Magazine (2005), "Neuro-controlled bionic army", *Popular Magazine*, November.

Postema, K., Hermens, H., de Vries, J., Koopman, H.F. and Eisma, W.H. (1997a), "Energy storage and release of prosthetic feet. Part 1: biomechanical analysis related to user benefits", *Prosthetics and Orthotics International*, Vol. 21 No. 1, pp. 17-27.

Postema, K., Hermens, H., de Vries, J., Koopman, H.F. and Eisma, W.H. (1997b), "Energy storage and release of prosthetic feet. Part 2: subjective ratings of 2 energy storing and 2 conventional feet, user choice of foot and deciding factor", *Prosthetics and Orthotics International*, Vol. 21, pp. 28-34.

Rao, S., Boyd, L., Mulroy, S., Bontrager, E., Gronley, J.K. and Perry, J. (1998), "Segment velocities in normal and transtibial amputees: prosthetic design implications", *IEEE Transactions on Rehabilitation Engineering*, Vol. 6 No. 2, pp. 219-26.

Sawicki, G. and Ferris, D.P. (2008), "Mechanics and energetics of level walking with powered ankle exoskeletons", *The Journal of Experimental Biology*, Vol. 211 No. 9, pp. 1402-13.

Sugar, T. (2002), "A novel selective compliant actuator", *Mechatronics Journal*, Vol. 12 Nos 9/10, pp. 1157-71.

Torburn, L., Perry, J., Ayyappa, E. and Shanfield, S. (1990), "Below-knee amputee gait with dynamic elastic response prosthetic feet: a pilot study", *Journal of Rehabilitation Research and Development*, Vol. 27 No. 4, pp. 369-84.

van der Linden, M.L., Solomonidis, S.E., Spence, W.D., Li, N. and Paul, J.P. (1999), "A methodology for studying the effects of various types of prosthetic feet on the biomechanics of transfemoral amputee gait", *Journal of Biomechanics*, Vol. 32 No. 9, pp. 877-89.

Versluys, R., Desomer, A., Gerlinde, L., Pareit, O., Vanderborght, B., van Der Perre, G., Peeraer, L. and Lefeber, D. (2008), "A biomechantronical transtibial prosthesis powered by pleated pneumatic artificial muscles", *International Journal of Modelling, Identification and Control*, Vol. 4 No. 4, pp. 394-405.

Ward, J., Hitt, J., Sugar, T. and Bharadwaj, K. (2006), "Dynamic pace controller for the robotic gait trainer", paper presented at the ASME International Design Engineering Technical Conference & Computers and Information in Engineering Conference, Philadelphia, PA.

Whittle, M. (1996), *Gait Analysis: An Introduction*, 2nd ed., Butterworth-Heinemann, Oxford.

Corresponding author

Joseph Hitt can be contacted at: joseph.hitt@usma.edu

To purchase reprints of this article please e-mail: **reprints@emeraldinsight.com**
Or visit our web site for further details: **www.emeraldinsight.com/reprints**

2009 IEEE International Conference on Robotics and Automation
Kobe International Conference Center
Kobe, Japan, May 12-17, 2009

A Novel Control Algorithm for Wearable Robotics using Phase Plane Invariants

Matthew A. Holgate, Thomas G. Sugar, Alexander W. Böhler

Dept. of Engineering
Human Machine Integration Laboratory
Arizona State University
Mesa, Arizona 85212-0180

Abstract— **With microprocessing power greatly increasing, hardware is no longer a hurdle in the development of controllers for wearable robotic systems, specifically lower limb robots. The challenge remains in developing smart algorithms that are able to detect which task a person is about to perform and then determine the correct desired movements for the robotic system. This paper reflects on four existing control algorithms for the task of level ground walking, and then presents theory and test results of a novel control algorithm based on phase plane invariants. The goal of this paper is to produce the correct motor reference command in a continuous fashion rather than based on determining distinct states for a given task.**

I. Introduction

Many people will benefit from a powered ankle. There are approximately 1.35 million people in the U.S. who are living with an amputation of the lower limbs and it is estimated that this number will more than double by the year 2050 [1], [2]. Moreover, there are about 4.7 million stroke survivors alive today in the United States, with about 700,000 additional cases each year [3]. Many of these stroke survivors could benefit from repetitive task training using a powered ankle foot orthosis. These numbers do not include other groups of people such as the weak or elderly who need a gait assistance device or other groups who suffer from a different neurological injury.

When building these robots, the current challenge is to develop sophisticated controllers since the mechanical systems in many cases have been (or are being) refined [4], [5], [6], [7]. In controls, it is no longer the hardware that is a bottleneck, but determining the user's intention is a very difficult challenge. One must determine smart and sophisticated algorithms that are able to sense which task a person is about to perform and then generate the the correct robotic movements. There are numerous tasks that a person performs during every day life, ranging from normal walking, to climbing stairs, walking up or down a slope, or even just balancing their legs while they are standing and talking to another person.

This paper firstly will reflect on some existing control methods and then present the theory and test results for a novel control concept based on phase plane invariants for wearable ankle robotics.

Matthew A. Holgate is with Arizona State University, Tempe Campus, matthew.holgate@asu.edu
Thomas G. Sugar is with Arizona State University, Polytechnic Campus, thomas.sugar@asu.edu
Alexander W. Böhler is with Arizona State University, Tempe Campus, alexander.boehler@asu.edu

II. Existing Control Algorithms

Over the past couple of years, several different control algorithms have been developed to control wearable robots for lower limbs. In this section some of the existing controllers are shown and briefly analyzed. The control algorithms presented in the first three sections have a structure shown in Fig. 1, where a DC motor is controlled in series with a transmission and linear spring that is attached to the ankle.

A. Basic Nut Control

One possibility to control a robot with the structure in Fig. 1 is to control the position y which in this case is the position of the nut on the lead screw. In this case, the proximal or input side of the spring is controlled. The actual nut position y_a can easily be measured with a motor encoder and then subtracted from a given reference command r.

The advantages of the system are that the input side of the spring is robustly controlled and small disturbances at the distal side (output side) of the spring are ignored by the controller.

However, limitations are reached with a fixed nut pattern as soon as optimization of the controller for certain stages during gait is desired, or if the reference command, which essentially is a gait pattern, must be adjusted for different walking speeds or different activities such as walking versus stair climbing. Oymagil et al. [8] have developed a controller that adjusts a pattern *only* in its duration in time; however, there are limitations since the amount of plantarflexion varies with speed as well. For example, when walking slowly, less plantarflexion is needed. In further refinement, a dynamic pace controller is described that adjusts the nut pattern both in time and in shape.

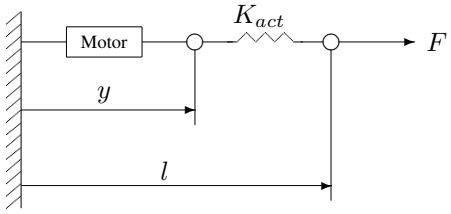

Fig. 1. Model for an actuator for the lower limbs

Authorized licensed use limited to: Arizona State University. Downloaded on November 10, 2009 at 12:36 from IEEE Xplore. Restrictions apply.

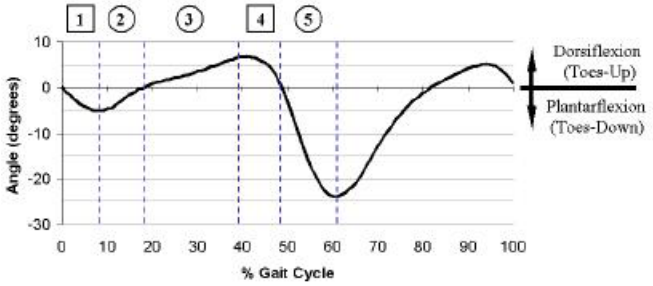

Fig. 2. The stance phase of gait split into 5 distinct zones.

B. Robust Control

In [9] the authors describe an algorithm, which combines velocity and stiffness control. The stance phase of gait is split into five different zones and each zone is governed by velocity or stiffness control as shown in Fig. 2. For *zone 1*, which starts at heel strike, Hollander suggests to use velocity control to keep the motor velocity constant and at a level proportional to the speed of the previous swing phase.

Zone 2 starts when the ankle angular velocity, $\dot{\theta}$, crosses through zero. For this zone it is suggested to maintain a constant stiffness which is 1.35 times the actual spring stiffness.

For, *zone 3*, which starts when the foot is flat and occupies most of the loading phase, again a constant stiffness should be applied which is 3 times the actual stiffness of the spring.

Zone 4 starts when the heel lifts off the ground. It is suggested to maintain a constant velocity during this zone that is equal to the motor velocity in the previous zone.

Zone 5 starts as the body can no longer resist the energy that was stored in the spring and therefore the energy is released which propels the body forward. For this phase it is important for the motor to just "hold position", hence allowing the energy to be released. The end of this zone is when all the stored energy of the spring has been released and the swing phase begins.

Promising test results have been achieved with this method and this algorithm is currently being optimized and tested in more detail. What is really interesting about this approach is that the shape of the motor profile is determined by only a few (five) numbers. These are the velocities and stiffness values that need to be set for each zone. By "tuning" these numbers, curves with different shapes can be produced, hence, one can use this basic control structure to produce profiles for different activities, such as climbing stairs or walking on different types of ground, simply by changing these parameters in an appropriate way.

C. Impedance Control

In this control method a mass-damper-spring relationship between a position x and force f is established as shown in (1).

$$f = m_d\ddot{x} + b_d\dot{x} + K_d x \tag{1}$$

Herein m_d, b_d and K_d denote desired or virtual inertia, damping and stiffness values of the system or plant. The advantage of this control method is its flexibility. It allows one to change the effective dynamics of the robot, hence, the resistance of the robot to variations in its environment, such as different types of surfaces. This requires, however, that the force f that the robot experiences with its environment is known [10]. This control method can use much energy if the dynamics of the robot are greatly different than the desired dynamics.

Blaya and Herr have shown that impedance control can assist patients with drop-foot gait. Two drop-foot patients were tested with their AAFO with zero, constant and variable impedance control strategies. They found that constant impedance control eliminated the occurrence of foot slap at slow and self-selected speeds. Furthermore, their variable impedance control strategy was able to increase the amount of swing dorsiflexion which helps with toe drag reducing hip circumduction [11].

D. Myoelectric Control

As mentioned before, one of the main challenges with controlling artificial limbs is to detect which activity the person is about to perform. All algorithms presented to this point measure positions, forces, states, etc. and then try to find a unique shape in these curves that enables the algorithm to make a decision. Hence, the question arises, why not measure the EMG signals of the muscles. EMG signals are measured by electrodes, filtered and used as reference commands.

Ferris et al. [12], [13] have used EMG signals from the soleus and tibialis anterior to control their pneumatically powered AFO. The raw EMG signals were firstly passed through a second order high-pass filter to remove movement artifacts. Then the signals were full-wave rectified and passed through a second order low-pass filter to obtain a smooth control signal. A threshold is used to eliminate background noise and the signal is scaled by an adjustable gain to calculate the final control signal.

Test results with their powered AFO showed that the person was able to walk immediately after turning on the proportional myoelectric control. The pneumatic muscles supplied 36% of the needed plantar flexor torque and 123% of the needed dorsi flexor torque.

Challenges that remain with this control approach are the process of obtaining a robust control signal from the raw EMG signals and there are many factors that influence the correlation between surface electromyography amplitude and biological muscle force.

III. Tibia Based Controller

The tibia based controller seeks to find a measurable variable to determine a mathematical relationship between the tibia angle and ankle angle. The tibia global angular position (world based coordinates) was chosen for this relationship because of its simple shape (Fig. 3). Looking at the different curves shown in Fig. 3, it is important to notice that each different stride length produces an almost identical curve, only scaled by some function of stride length. It is also of note that if the curve is divided into two parts at the minimum point, 70% of the gait cycle, each resulting half becomes an invertible function of gait percent. Each half can also be distinguished from one another by the slope of each

Authorized licensed use limited to: Arizona State University. Downloaded on November 10, 2009 at 12:36 from IEEE Xplore. Restrictions apply.

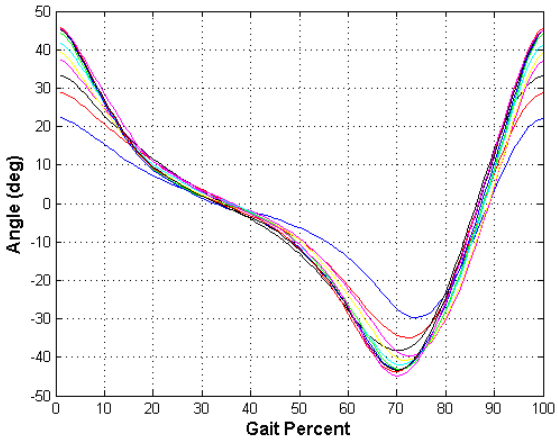

Fig. 3. Tibia angle profile for able bodied human gait. Each curve represents a different stride length. The closer the curve is to the zero degree axis, the shorter the stride length.

curve, which is negative for the first half and positive for the second half. Measurement of the tibia angle can also be accomplished with a sensor attached to the prosthetic device and requires no additional measurements or sensors on other parts of the body. The aforementioned characteristics make the tibia global angle a wise choice for a prosthetic controller.

Since our previous controllers have shown that using logic to make gait decisions can create situations in which the controller is fooled, it is desired that the tibia based controller be completely continuous. To develop a continuous controller, a relationship between the tibia angle and desired ankle angle is required. As previously mentioned, the tibia angle versus gait percent curve (Fig. 3) is not invertible as a whole. To make a function that is solvable, the tibia angular velocity dimension is added and the curve is plotted with tibia angle on the horizontal axis and tibia angular velocity multiplied by a scaling factor on the vertical axis. We are borrowing phase plane analysis from control theory. The resulting curves shown in Fig. 4, are for increasing stride length as the curves get larger. The coordinates in Fig. 4, instead of being represented in Cartesian coordinates of angle and angular velocity, will be represented by polar coordinates Φ and r.

From Fig. 4, it is apparent that the polar angle Φ must be related to gait percent by some function for each different stride length curve. The relationship between Φ and gait percent is plotted for each different stride length in Fig. 5. Of note is the fact that for each different stride length curve, the function relating Φ to gait percent is very close, and is invertible. Also shown in Fig. 5, gait percent is plotted versus polar angle Φ. A fit to this function means that for any stride length, if tibia global angle and angular velocity are measured and the polar angle is calculated, the result can be used as an input to the fitted function, giving an explicit relationship between tibia angle and gait percent. In our work, this explicit function is invariant to stride length.

With the new function, calculating gait percent is a straightforward operation, but ankle angles also depend on stride length. From Fig. 4, it can be seen that in general, the longer the stride length, the longer the polar radius r. However, it must also be noted that any function that relates stride length to r must also be a function of polar angle Φ. The result of plotting polar radius r versus stride length and gait percent is shown in Fig. 6.

A surface plot or function that relates radius r to stride length and gait percent can be found; however, the inverted relationship of stride length as a function of gait percent and radius r is needed. From Fig. 6, at 25% in the gait cycle, the inverted relationship is not one-to-one because the resulting surface will be near vertical and will have multiple values for a single point (gait percent, radius). The reason for this problem is shown in Fig. 3 at 25% in the gait and Fig. 4 at the bottom and middle of the curves where they are bunched up together.

Again from Fig. 4, the problem area occurs at angular velocity -5 and angle 0. At this point each stride-length curve enters the bunched area with a different approach. If a simple first order filter is used on radius r, the curves can be separated. Fig. 7 shows the result of such an approach. The resulting surface is flattened out, and for every combination of radius and gait percent, there is one value of stride length. It must also be understood that when using an aggressive first order filter, there will be some attenuation and phase lag. This lag can be reduced by comparing the measured and filtered r not to the actual radius surface (shown as before filter in Fig. 7), but to the expected filtered surface (shown as after filter in Fig. 7).

By implementing the previously discussed method of calculating gait percent and stride length, an ankle angle is generated using motion capture data from the literature. The ankle angle as a function of stride length and gait percent can be easily measured. The resulting surface can then be fit with a function or a look up table. Depending on what robot is being controlled, the controller will generate a desired position, an example of which is shown in Fig. 8.

In our research group, we no longer use gait curves, but develop and manipulate gait surfaces such as Fig. 8.

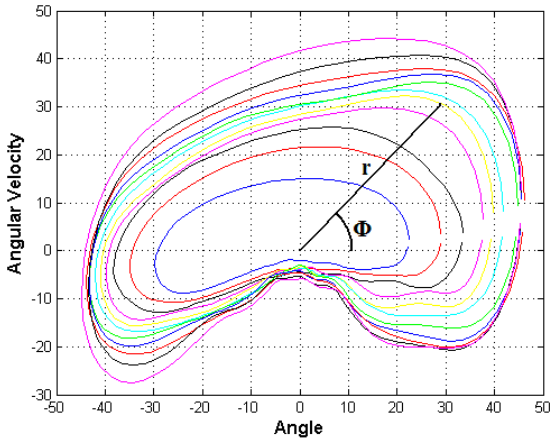

Fig. 4. Tibia angular velocity multiplied by a scaling factor versus tibia angle. The closer the curve is to the origin, the shorter the stride length. Polar angle Φ represents the progression around the curve based on gait percent. r is the polar radius and is related to the stride length of the particular curve.

Authorized licensed use limited to: Arizona State University. Downloaded on November 10, 2009 at 12:36 from IEEE Xplore. Restrictions apply.

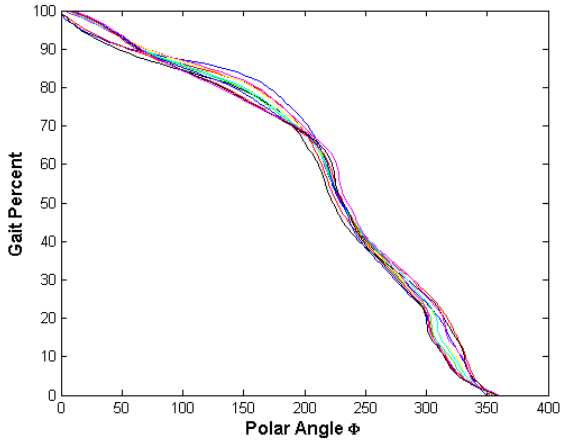

(a) Gait percent of each curve versus the polar angle Φ

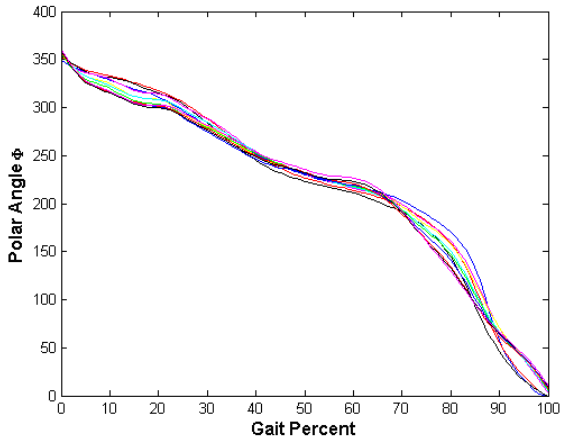

(b) Inverted curves, polar angle Φ versus gait percent

Fig. 5. Note the close relation between all of the curves. The relation between polar angle and gait percent is very close for all stride lengths.

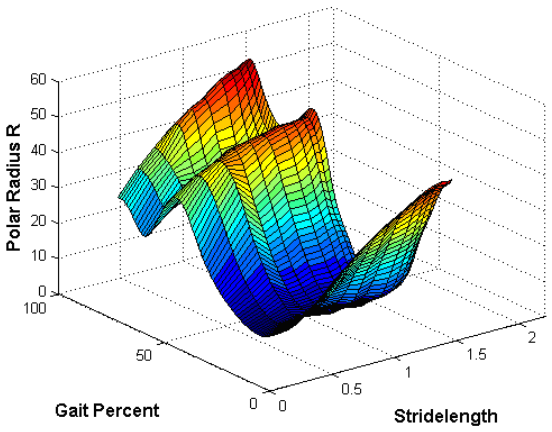

Fig. 6. Polar radius r versus gait percent and stride length. Unlike Φ, r is different for different stride lengths. At 25% in the gait cycle, the surface is flat along the stride length axis. This flatness creates a problem when trying to invert this surface to obtain stride length as a function of gait percent and polar radius.

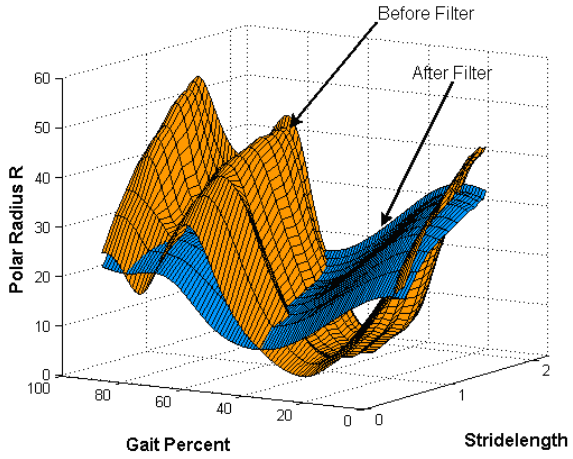

Fig. 7. Same plot shown in Fig. 6 (orange). The blue surface is the result of filtering the polar radius with a first order filter. This new surface can be inverted to find a function that relates stride length as a function of gait percent and polar radius.

IV. Implementation and Results

An interesting problem associated with the implementation of such a controller is accurately measuring the tibia global angle and angular velocity. In our experimental measurements, an angular rate sensor was used. This sensor outputs a voltage proportional to the rate at which it turns. To determine an angle from an angular velocity sensor, it is necessary to integrate the output. However, since the sampling is discrete; the sensor outputs noise; and the integration is numerical, the angle will drift. If the angle drifts away from its true value, the reference ankle angle generated will be completely wrong. To correct this problem methods such as strap down integration were considered, but were not employed due to the necessity of additional sensors and physical system complexity. A Kalman filter was also considered. The Kalman filter was not used again because of the necessity of additional sensors. Both methods could have been employed to get an accurate measure of the tibia angle. However, when looking at test data of tibia angles from multiple subjects, it is apparent that they are all unique. Curves from different subjects will vary in shape and will be shifted in angular units. The shape difference is mostly due to the individual's gait pattern. The shifted angle is due to the angle that the leg is at when the discrete integration begins. Both of these properties will cause difficulties for the tibia controller calculations.

The solution employed was to use a transfer function in place of a simple integrator. The form of the function is shown in (2).

$$\frac{\tau^2 s}{(\tau s + 1)^2} \tag{2}$$

It can be seen that for frequencies above τ the transfer function (2) approximates an integration in magnitude very well and phase sufficiently well (see Fig. 9). For frequencies above τ the magnitude is very close to that of an integrator,

Authorized licensed use limited to: Arizona State University. Downloaded on November 10, 2009 at 12:36 from IEEE Xplore. Restrictions apply.

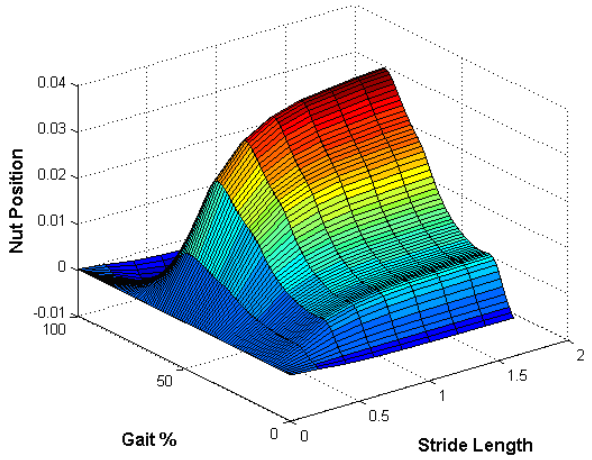

Fig. 8. Position of the nut in meters as a function of stride length and gait percent. Once gait percent and stride length are known, it is simply a matter of looking up the corresponding nut position.

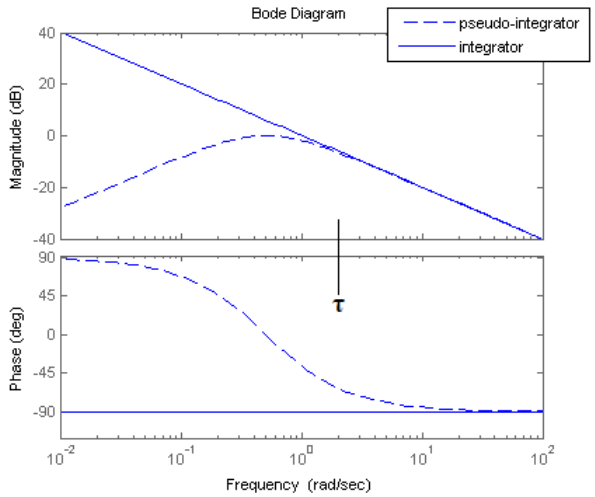

Fig. 9. Bode plot of the pseudo-integrating transfer function along with an integrator.

any differences are caused by the phase lag that is introduced. Depending on what value is chosen for τ, the lag is not significant for frequencies which arise from gait patterns. Also, the small amount of lag is not a problem because the controller can be tuned to expect this as an input. An integrator naturally has 90° of phase lag and is not a problem because it is expected. Also, the physical meaning of the exact angular input is not important, only that it uniquely corresponds to the output that is desired. Another desirable property of the pseudo-integration method is the removal of the integration drift. An integrator has a pole on the imaginary axis, which makes it marginally stable and therefore the output is able to drift. The pseudo-integration transfer function (2) has two stable poles, which eliminate the drift. By choosing τ one can choose how fast are the poles. This has the effect of constantly pulling the output toward the input, which is the angular velocity. Since the angular velocity is always centered around 0, the pseudo-angle will also be approximately centered around 0 since it is stable and attracted to the input.

The choice of τ is a compromise. First τ can be chosen to adjust the phase lag. Some lag is reasonable as previously discussed, but it is also important that the pseudo-angle be kept approximately 90° out of phase with the angular velocity because of the way Fig. 4 is constructed. If not, the ”bean” shape will become a diagonal line and the polar coordinate strategy will be foiled.

Secondly the value of τ has an effect on how fast are the poles of the transfer function. By choosing faster poles the output is more stable. This has two desirable effects, drift is lower, and the initial condition of the angle is less important. The initial condition of the leg or orientation of the sensor when the controller is started would be an enormous problem if other methods of integration were employed. Since the pseudo-integrator is stable, initial conditions are not a problem. The output is always trying to center itself around 0, and it is self correcting even for large deviations in the initial condition. By choosing an appropriate value for τ the controller can correct itself quickly while keeping acceptable amounts of lag.

Thirdly, the pseudo-integrator has the characteristic of deindividualization of the output between unique subjects. Notice in Fig. 9 that for frequencies smaller than τ; there is heavy attenuation. The value for τ also has an effect on which frequencies are attenuated. If τ is chosen correctly, the shape of the curves from different individuals are pulled together so that they are similar. The result is a much more robust controller which can be tuned on one individual and will work well for many.

It was thought at first that this was not a desirable method because it does not give the true tibia global angle, but in experiments, it does not matter what the input is to the controller calculations, as long as the calculations are expecting this input. An added benefit to the filtering method is that it makes actual tibia global angle curves which are slightly different between multiple subjects almost indistinguishable. The result is that the controller can be configured for one person and it will work for almost any user. (Filtered data was calculated when four people walked on a treadmill and over ground.)

For testing the controller, the functions and fits were conducted using data from an able bodied subject. The controller was implemented on the SPARKy robot. An amputee subject walked with stride lengths ranging from very slow to as fast as the subject could walk. The gait percent detection of the controller was always within 5 percent, a very encouraging result shown in Fig. 10. The stride length calculated oscillated smoothly with an error of about 10%. The overall result is a controller that operates smoothly for any stride length or gait percent. An example controller output is shown in Fig. 11.

Advantages of the controller include the ability to update the ankle position as fast as the sampling time of the sensors. The controller is never committed to one state of operation looking for another event to decide what to do. For example, the user can take a slow step, and in the middle of push off, they can quickly accelerate to a fast walk and the controller

Authorized licensed use limited to: Arizona State University. Downloaded on November 10, 2009 at 12:36 from IEEE Xplore. Restrictions apply.

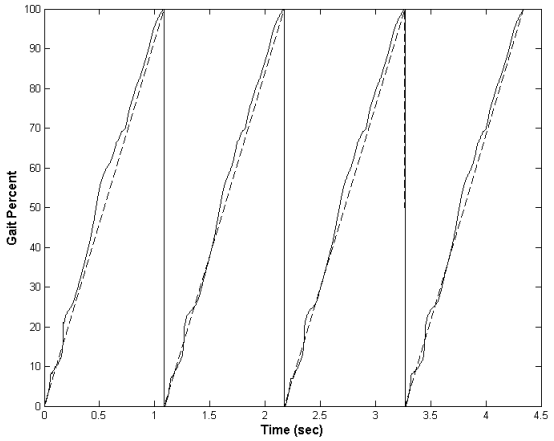

Fig. 10. Gait percent results walking at 2.5 mph. Dotted line is the target value and solid line is gait percent as calculated by the tibia controller.

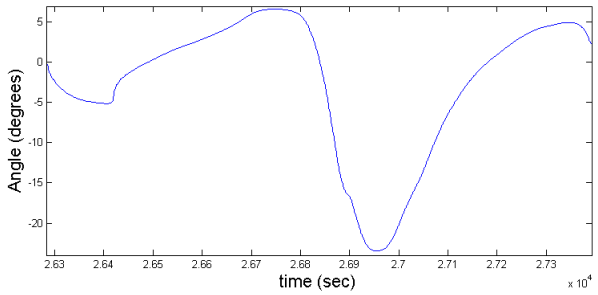

Fig. 11. Gait percent results walking at 2.5 mph. Ankle angle as calculated by the tibia based controller. Compare to Fig. 2.

will accelerate the ankle. The tibia based controller can also be configured on able bodied persons and operate well on a wide range of users. Another advantage, the details of which are not discussed here, is the ability of this controller to work while walking backwards. In initial tests, the subject was able to take backwards steps using SPARKy while the controller gave a correct ankle motion.

V. Conclusion

This paper has presented existing controllers for prosthetic and orthotic foot-ankle devices. The tibia controller based on phase plane invariants is introduced. It has been shown that the controller can calculate the necessary reference command. Already in earlier papers [4] and [5], our lab has shown that this reference command achieves the requirements to allow a transtibial amputee to walk at different speeds on a treadmill. The tibia controller has the advantage of not relying on logic to switch between states while only requiring one sensor. This type of controller is much more stable and adaptive to the user. This new controller is functionally superior to our existing controllers.

Most importantly, we showed an invariant phase-plane relationship for the tibia angular velocity and position. In our phase plane analysis, the phase angle, Φ, was invariant to small or large changes in stride length. Using one variable, Φ, we are able to determine gait percent for slow, normal, and fast walking. We also showed a more complicated relationship between the polar angle and radius to determine stride length. We believe that this continuous method of determining gait percent, stride length, and thus forward velocity is a very important step in our wearable robotics research.

VI. Acknowledgments

The authors would like to acknowledge the grant that was awarded and administered by the U.S. Army Medical Research & Material Command (USAMRMC), under Contract Number: W81XWH-0710193. The views, opinions, findings, information and presentations made do not necessarily reflect the position of the government and no official endorsement should be made.

References

[1] Ziegler-Graham, K., MacKenzie, E.J., Ephraim, P.L., Travison, T.G., Brookmeyer, R. “Estimating the prevalence of limb loss in the United States: 2005 to 2050”. *Archives of Physical Medicine and Rehabilitation 89 (2008)*, pp. 422-429.

[2] Amputee Coalition (2008). [Online]. Available: http://www.amputee-coalition.org

[3] Stroke Center (2008). [Online]. Available: http://www.strokecenter.org

[4] Hitt, J.K., Oymagil, M.A., Sugar, T.G., Hollander, K.W., Boehler, A.W., and Fleeger, J. “Dynamically Controlled Ankle Foot Orthosis (DCO) With Regenerative Kinetics: Incrementally Attaining User Portability”, *2007 IEEE Conference on Robotics and Automation (ICRA)*, pp. 1541-1546.

[5] Hitt, J., Bellman, R., Holgate, M., Sugar, T., and Hollander, K., ”The SPARKy (Spring Ankle with Regenerative Kinetics) Project: Design and Analysis of a Robotic Transtibial Prosthesis with Regenerative Kinetics”, ASME International Design Engineering Technical Conference, CD-ROM, pp. 1-10, 2007.

[6] Dollar, A. M. and Herr, H. “Active Orthoses for the Lower-Limbs: Challenges and State of the Art”, *2007 IEEE* 10^{th} *International Conference on Rehabilitation Robotics (ICORR)*, pp. 968-977.

[7] Au, S. K., Weber. J., and Herr, H., ”Biomechanical design of a powered ankle-foot prosthesis,” Proc. IEEE Int. Conf. On Rehabilitation Robotics, Noordwijk, The Netherlands, pp. 298-303, June 2007.

[8] Oymagil, M.A., Hitt, J.K., and Sugar, T.G., “Control of a Regenerative Braking Powered Ankle Foot Orthosis”, *2007 IEEE* 10^{th} *International Conference on Rehabilitation Robotics (ICORR)*, pp. 28-34.

[9] Böhler, A. W., Hollander, K. W., Sugar, T.G., Shin, D. “Design, Implementation and Test Results of a Robust Control Concept for a Powered Ankle-Foot-Orthosis (AFO)”. *2008 IEEE International Conference on Robotics and Automation (ICRA)*.

[10] Schaeffer, A.A., and Hirzinger, G., “Cartesian Impedance Control Techniques for Torque Controlled Light-Weight Robots”, *Proceedings of the 2002 IEEE International Conference on Robotics and Automation (ICRA)*, pp. 657-663, 2002.

[11] Blaya, J.A., Herr, H., “Adaptive Control of a Variable-Impedance Ankle-Foot Orthosis to Assist Drop-Foot Gait,” *IEEE Transactions on Neural Systems and Rehabilitation Engineering*, vol. 12(1), pp. 24-31, 2004.

[12] Ferris, D.P., et al., “An Improved Powered Ankle-Foot Orthosis Using Proportional Myoelectric Control,” *Gait & Posture*, vol. 23, pp. 425-428, 2006.

[13] Ferris, D.P., Czerniecki, J.M., Hannaford, B., “An Ankle-Foot Orthosis Powered by Artificial Muscles,” *Journal of Applied Biomechanics*, vol. 21, pp. 189-197, 2005.

Authorized licensed use limited to: Arizona State University. Downloaded on November 10, 2009 at 12:36 from IEEE Xplore. Restrictions apply.

Control Algorithms for Ankle Robots: A Reflection on the State-of-the-Art and Presentation of Two Novel Algorithms

Matthew A. Holgate, Alexander W. Böhler, Thomas G. Sugar

***Abstract*— With computer speeds greatly increasing, hardware is no longer a hurdle in the development of controllers for wearable lower limb robots. The challenge remains in developing smart algorithms that are able to detect which task a person is about to perform and then supply the robot with the correct desired movements. This paper reflects on some existing control algorithms and then presents theory and test results of two novel concepts. The goal of this paper is to show that the two new concepts are capable of producing the correct motor profile.**

I. Introduction

Many people could benefit from a powered ankle. There are approximately 1.35 million people in the U.S. who are living with an amputation of the lower limbs and it is estimated that this number will more than double by the year 2050 [1], [2]. Moreover, there are about 4.7 million stroke survivors alive today in the United States, with about 700,000 more cases each year [3]. Many of these stroke survivors could use a powered ankle foot orthosis. These numbers do not include other groups of people such as the elderly or people who suffered from a different neurological injury, who could also benefit from a powered ankle.

When building these robots, the challenge now is to develop sophisticated controllers since the mechanical systems in many cases have already been refined [4], [5], [6], [7]. In controls, it is no longer the hardware that is a bottleneck, but determining the user's intention is a very difficult challenge. One must determine smart and sophisticated algorithms that are able to sense which task a person is about to perform and then generate the the correct robotic movements. There are numerous tasks that a person performs during every day life, ranging from normal walking, to climbing stairs, walking up or down a slope, or even just balancing their legs while they are standing and talking to another person.

This paper firstly will reflect on some of our existing control methods and then present the theory and test results for two novel control concepts for wearable ankle robots.

II. Existing Control Algorithms

Over the past couple of years, several different control algorithms have been developed to control wearable robots for the lower limbs. In this section some of the existing controllers are shown and briefly analyzed. The control algorithms presented in the first three sections have a structure shown in Fig. 1, where a DC motor is controlled in series with a transmission and linear spring that is attached to the ankle.

A. Basic Nut Control

One possibility to control a robot with the structure in Fig. 1 is to control the position y (which in this case is the position of the nut on the lead screw), which is the backside of the spring. The actual nut position y_a can easily be measured with a motor encoder and then subtracted from a given reference command r.

However, limitations are reached with a fixed nut pattern as soon as optimization of the controller for certain stages during gait is desired, or if one wants the reference command, which essentially is a gait pattern, to adjust itself for different walking speeds or different activities such as walking versus stair climbing. Oymagil et al. [8] have shown the adjustment of a pattern *only* in its duration in time; however, there are limitations since the amount of plantarflexion varies with speed as well. For example, when walking slowly, the behavior of the robot feels unnatural. A dynamic pace controller is described in this paper to adjust the nut pattern both in time and in shape.

B. Robust Control

In [9] the authors describe an algorithm, which combines velocity and stiffness control. The stance phase of gait is split into five different zones and each zone is governed by velocity or stiffness control as shown in Fig. 2. For *zone 1*, which starts at heel strike, the author suggests to use velocity control to keep the motor velocity constant and at a level proportional to the speed of the previous swing phase.

Zone 2 starts when the ankle angular velocity, $\dot{\theta}$, crosses through zero. For this zone it is suggested to maintain a constant stiffness which is 1.35 times the actual spring stiffness.

For, *zone 3*, which starts at flat foot and occupies most of the loading phase, again a constant stiffness should be applied which is 3 times the actual stiffness of the spring.

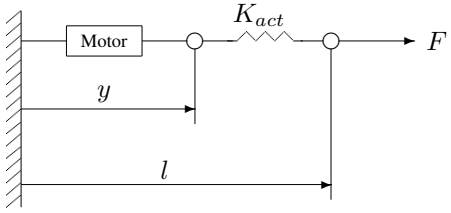

Fig. 1. Model for an actuator for the lower limbs

Manuscript received April 23, 2008.

Matthew A. Holgate is with Arizona State University, Tempe Campus, matthew.holgate@asu.edu

Alexander W. Böhler is with Arizona State University, Tempe, Arizona 85287-6106 alexander.boehler@asu.edu

Thomas G. Sugar is with Arizona State University, Polytechnic Campus, thomas.sugar@asu.edu

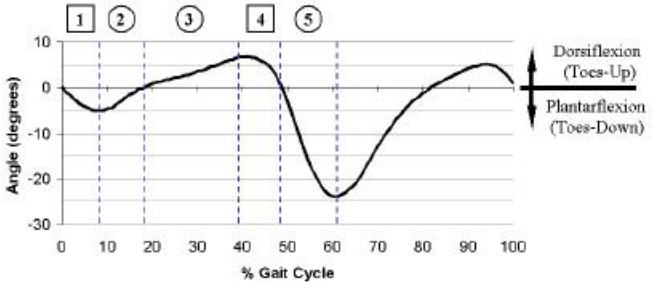

Fig. 2. The stance phase of gait split into 5 distinct zones.

Zone 4 starts when the heel lifts off the ground. It is suggested to maintain a constant velocity during this zone that is equal to the motor velocity in the previous zone.

Zone 5 starts as the body can no longer resist the energy that was stored in the spring and therefore the energy is released which propels the body forward. For this phase it is important for the motor to just "hold position", hence allowing the energy to be released. The end of this zone is when all the stored energy of the spring has been released and the swing phase begins.

Good first test results have been achieved with this method and this algorithm is currently being optimized and tested in more detail. What is really promising about this approach is that the shape of the motor profile is determined by only a few (five) numbers. These are the velocities and stiffnesses that need to be set for each zone. By "tuning" with these numbers, curves with different shapes can be produced, hence, our hope is that we can use this basic controller structure to produce profiles for different activities, such as climbing stairs or walking on different types of ground, simply by changing these parameters in an appropriate way.

C. Impedance Control

In this rather extensive control method a mass-damper-spring relationship between a position x and force f is established as shown in (1).

$$f = m_d\ddot{x} + b_d\dot{x} + K_d x \tag{1}$$

Herein m_d, b_d and K_d denote desired or virtual inertia, damping and stiffness of the system. The advantage of this control method is its flexibility. It allows one to change the effective dynamics of the robot, hence, the resistance of the robot to variations in its environment, such as different types of ground. This requires, however, that one knows the force f that the robot experiences with its environment [10].

Blaya and Herr have shown that impedance control can assist patients with drop-foot gait. Two drop-foot patients were tested with their AAFO with zero, constant and variable impedance control strategies. They found that constant impedance control eliminated the occurrence of foot slap at slow and self-selected speeds. Furthermore, their variable impedance control strategy was able to increase the amount of swing dorsiflexion which helps with toe drag, a second major complication that drop-foot patients experience [11].

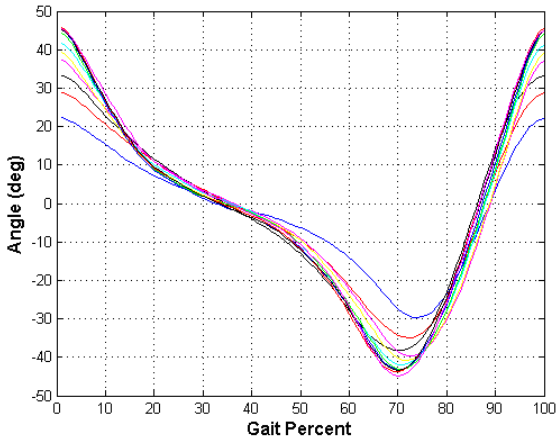

Fig. 3. Tibia angle profile for able bodied human gait. Each curve represents a different stride length. The closer the curve is to the zero degree axis, the shorter the stride length.

D. Myoelectric Control

As mentioned before, one of the main challenges with controlling artificial limbs is to detect which activity the person is about to perform. All algorithms presented to this point measure positions, forces, states, etc. and then try to find a unique shape in these curves that enables the algorithm to make a decision. Hence, the question arises, why not measure the EMG signals. EMG signals are measured by electrodes, filtered and used as reference commands.

Ferris et al. [12], [13] have used EMG signals from the soleus and tibialis anterior to control their pneumatically powered AFO. The raw EMG signals were firstly passed through a second order high-pass filter to remove movement artifacts. Then the signals were full-wave rectified and passed through a second order low-pass filter to obtain a smooth control signal. A threshold is used to eliminate background noise and the signal is scaled by an adjustable gain to calculate the final control signal.

Test results with their improved powered AFO showed that the person was able to walk immediately after turning on the proportional myoelectric control. The pneumatic muscles supplied 36% plantar flexor torque and 123% dorsi flexor torque.

Challenges that remain with this controls approach are the process of obtaining a robust control signal from the raw EMG signals and that there are many factors that influence the correlation between surface electromyography amplitude and biological muscle force.

III. Novel Controllers

A. Tibia Based Controller Theory

The tibia based controller seeks to find a measurable variable to determine a mathematical relationship between the tibia angle and ankle angle. The tibia global angular position (world based coordinates) was chosen for this relationship because of its simple shape (Fig. 3). Looking at the different curves shown in Fig. 3, it is important to notice that each different stride length produces an almost identical curve, only scaled by some function of stride length. It is also

of note that if the curve is divided into two parts at the minimum around 70% gait cycle, each resulting half becomes an invertible function of gait percent. Each half can also be distinguished from one another by the slope of each curve, which is negative for the first half and positive for the second half. Measurement of the tibia angle can also be accomplished with a sensor attached to the prosthetic device and requires no additional measurements or sensors on other body parts. The aforementioned characteristics make the tibia global angle a wise choice for a prosthetic controller.

Since previous controllers have shown that using logic to make gait decisions can create situations in which the controller is fooled, it is desired that the tibia based controller be completely continuous. To accomplish this, a relationship between the tibia angle and desired ankle angle is required. As previously mentioned, the tibia angle versus gait percent curve (Fig. 3) is not invertible as a whole. To make a function that is solvable, the tibia angular velocity dimension is added and the curve is plotted with tibia angle on the horizontal axis and tibia angular velocity multiplied by a scaling factor on the vertical axis. The resulting curves shown in Fig. 4, are for increasing stride length as the curves get larger. The coordinates in Fig. 4, instead of being represented in Cartesian coordinates of angle and angular velocity, will be represented by polar coordinates Φ and r.

Looking at Fig. 4, it is apparent that the polar angle Φ must be related to gait percent by some function for each different stride length curve. The relationship between Φ and gait percent is plotted for each different stride length in Fig. 5. Of note is the fact that for each different stride length curve, the function relating Φ to gait percent is very close, and is invertible. Also shown in Fig. 5 is gait percent plotted versus polar angle Φ. A fit to this function means that for any stride length, if tibia global angle and angular velocity are measured and the polar angle calculated, the result can be used as an input to the fitted function, giving an explicit relationship between tibia angle and gait percent.

Calculating gait percent is a straightforward operation, but

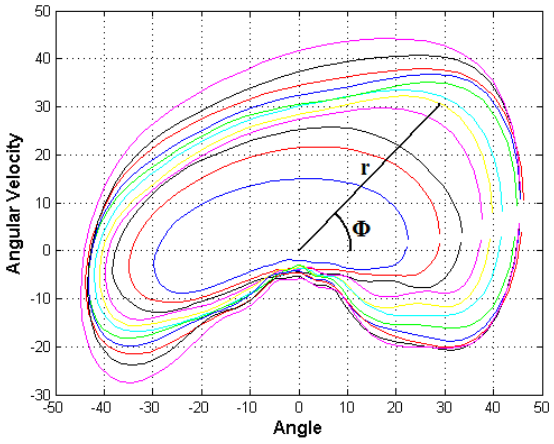

Fig. 4. Tibia angular velocity multiplied by a scaling factor versus tibia angle. The closer the curve is to the origin, the shorter the stride length. Polar angle Φ represents the progression around the curve based on gait percent. r is the polar radius and is related to the stride length of the particular curve.

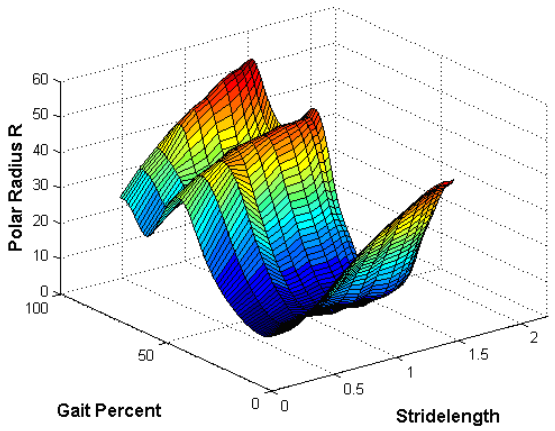

Fig. 6. Polar radius r versus gait percent and stride length. Unlike Φ, r is different for different stride lengths. Note that around 25% of gait cycle the surface is flat along stride length. This creates problems when trying to invert this surface to obtain stride length as a function of gait percent and polar radius.

ankle angles also depend on stride length. Looking back at Fig. 4 it can be seen that in general, the longer the stride length, the longer the polar radius r. However, it must also be noted that any function that relates stride length to r must also be a function of polar angle Φ. The result of plotting polar radius r versus stride length and gait percent is shown in Fig. 6.

It is easy to find how radius r is related to stride length and gait percent; however, the needed relationship is stride length as a function of gait percent and radius r, the two known variables. Looking at Fig. 6 it is obvious that this will be a problem around 25% of gait because the resulting surface will be near vertical and will have multiple values for a single point (gait percent, radius). The reason for this is shown in Fig. 3 at around 25% of gait and Fig. 4 at the bottom middle of the curves where they are bunched up together.

Looking again at Fig. 4 around the problem area at about angular velocity -5 and angle 0, it can be seen that each curve enters the bunched area with a different approach. If a simple first order filter is used on radius r, the curves can be separated. Fig. 7 shows the result of such an approach. The resulting surface is flattened out and for every combination of radius and gait percent there is one value of stride length. It must also be understood that when using an aggressive first order filter, there will be some attenuation and phase lag. This is taken care of by comparing the measured and filtered r not to the actual radius surface (shown as before filter in Fig. 7), but to the expected filtered surface (shown as after filter in Fig. 7).

By implementing the previously discussed method of calculating gait percent and stride length, generating an ankle angle is a simple matter. The ankle angle as a function of stride length and gait percent can be easily measured. The resulting surface can then be fit with a function or a look up table. Depending on what robot is being controlled, the controller will generate a desired position, an example of which is shown in Fig. 8.

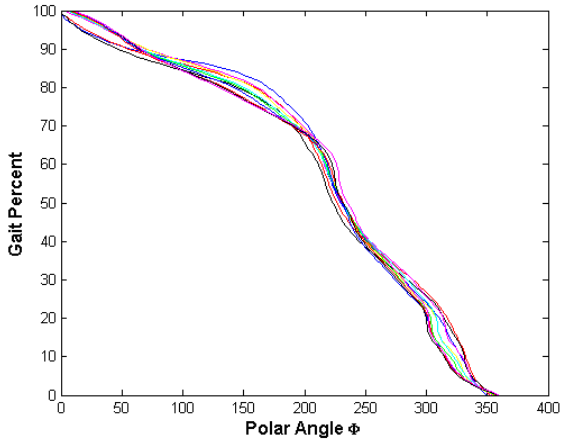

(a) Gait percent of each curve versus the polar angle Φ

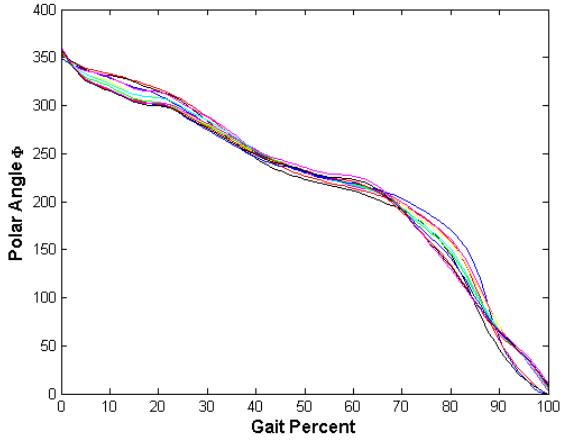

(b) Inverted curves, polar angle Φ versus gait percent

Fig. 5. Note the close relation between all of the curves. The relation between polar angle and gait percent is very close for all stride lengths.

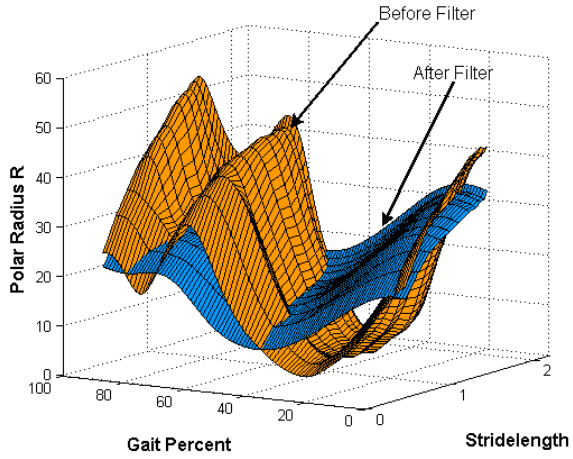

Fig. 7. Same plot shown in Fig. 6 (orange). The blue surface is the result of filtering the polar radius with a first order filter. Note how the new surface can be easily changed to be stride length as a function of gait percent and polar radius.

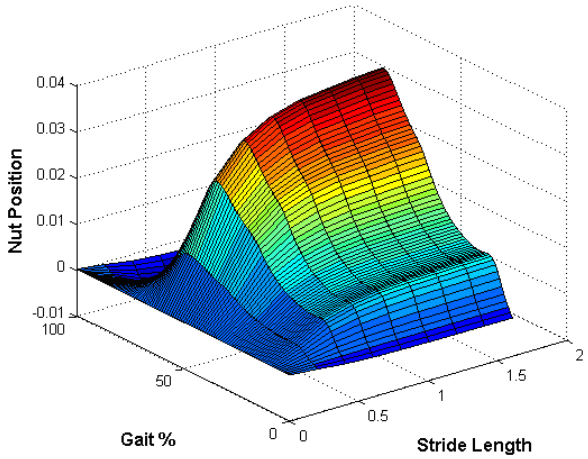

Fig. 8. Position of the nut in meters as a function of stride length and gait percent. Once gait percent and stride length are known, it is simply a matter of looking up the corresponding nut position.

B. Dynamic Pace Control

A second controller being developed in our lab will be discussed next.

Generally, it can be said that the amplitudes of plantarflexion and dorsiflexion become smaller with lower speeds and grow with larger speeds respectively. The latest approach concerning this problem is to adjust the nut profile not only in its duration in time but also in its amplitude.

For the dynamic pace controller firstly a standard motor curve for a stride time of 1 s is calculated. The amount of plantarflexion that this curve provides is then scaled up and down for faster and slower walking. This yields five different nut profiles for five different stride times. To obtain a continuous spectrum of nut profiles depending on the stride time the Fourier coefficients of each profile are calculated using a Fast Fourier Transform (FFT) as shown below, note that the symbols in boldface are matrices. **R** is a 5xn matrix of points describing the five different nut profiles as a percentage of gait.

$$\mathbf{F}_\omega = \text{fft}\,(\mathbf{R}) \tag{2}$$

These coefficients are then fit with a 2^{nd} order polynomial of the form

$$\mathbf{F}_\omega = \mathbf{AT} \tag{3}$$

with the matrices **A** being the coefficient matrix and **T** being the independent variable matrix based on the time duration of each gait cycle. Since **T** is not square we need to multiply (3) with the transpose of **T** first before we can take the inverse and multiply from the right to obtain **A**.

$$\mathbf{A} = \mathbf{F}_\omega \mathbf{T}^T \cdot \left(\mathbf{T}\mathbf{T}^T\right)^{-1} \tag{4}$$

Now, given the matrix **A** and a desired stride time t_s, equation (3) can be used to calculate the Fourier coefficient vector f_ω for the desired stride time. Note that the matrix **T** will become a vector because we are only looking at one

distinct stride time. Taking the inverse Fourier transform then yields the function for the motor reference command.

$$r(t) = \text{ifft}\,(f_\omega) \tag{5}$$

Fig. 9 shows the polynomial fit for the Fourier coefficients and Fig. 10 shows a 3D plot of nut profiles for different stride times, generated with the presented algorithm. It can be seen that time and amplitude of the profiles is adjusted.

Note that the generated nut profiles are also fit with a spline interpolation. This yields a smooth, high quality reference command, which is easy to follow and reduces the overall noise of the motor. As will be seen in IV very good results have been obtained with this method in terms of wearer comfort and power output to input ratios. However, there a few difficulties that remain.

Firstly, one still needs to compute different nut profiles for persons with different weights. Secondly, the controller cannot be optimized for different stages during gait or for different situations. One can easily imagine that, as soon as a person is walking over uneven ground instead of on a treadmill, the whole profile will change as well. Thirdly, this method will always be one gait cycle too late, since it uses the stride time of the last gait cycle to adjust the current gait cycle. These difficulties will be addressed in our future work.

IV. Test Results

A. Tibia Based Controller Implementation and Results

An interesting problem associated with the implementation of such a controller is accurately measuring the tibia global angle and angular velocity. To accomplish this, an angular rate sensor was used. This sensor outputs a voltage proportional to the rate at which it turns. To determine an angle from an angular velocity sensor, it is necessary to integrate the output. However, since the sampling is discrete; the sensor outputs noise; and the integration is numerical, the angle will drift. If the angle drifts away from its true value, the reference ankle angle generated will be completely wrong.

To correct this problem methods such as strap down integration were considered, but were not employed due to the necessity of additional sensors and physical system

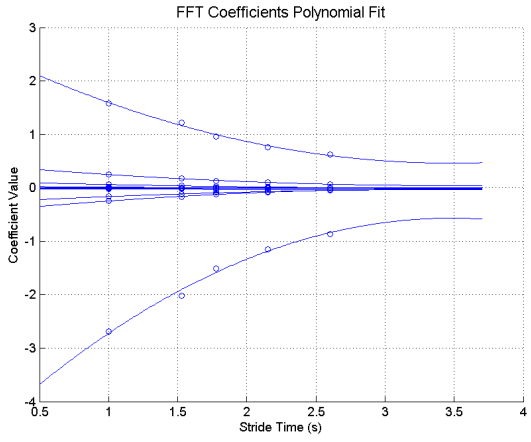

Fig. 9. Polynomial fit for the Fourier coefficients

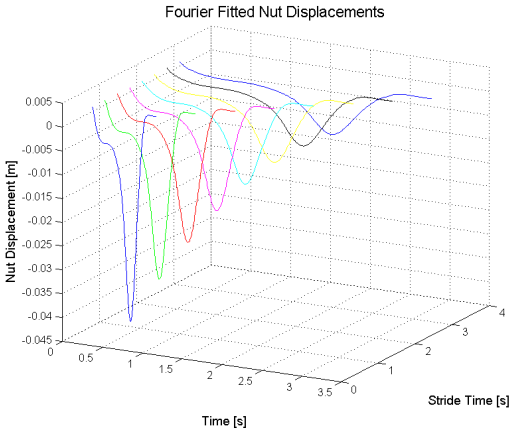

Fig. 10. Nut profiles for nine different stride times

complexity. A digital filter was used to integrate the signal but pulls the resulting signal towards zero. The result is a curve similar to the actual tibia global angle in shape Fig. 3, but centered on the horizontal axis.

It was thought at first that this was not a desirable method because it does not give the true tibia global angle. But in reality, it does not matter what the input is to the controller calculations, as long as the calculations are expecting this input. An added benefit to the filtering method is that it makes actual tibia global angle curves which are slightly different between multiple subjects almost indistinguishable. The result is that the controller can be configured for one person and it will work for almost any user. (Filtered data was calculated when four people walked on a treadmill and over ground.)

For testing the controller, the functions and fits were conducted using data from an able bodied subject. The controller was implemented on the SPARKy robot. An amputee subject walked with stride lengths ranging from very slow to as fast as the subject could walk. The gait percent detection of the controller was always within 5 percent, a very encouraging result shown in Fig. 11. The stride length calculated oscillated smoothly with an error of about 10%. The overall result is a controller that operates smoothly for any stride length or gait percent.

Advantages of the controller include the ability to update the ankle position as fast as the sampling time of the sensors. The controller is never committed to one state of operation looking for another event to decide what to do. For example, the user can take a slow step and in the middle of push off quickly accelerate to a fast walk and the controller will accelerate the ankle. The tibia based controller can also be configured on able bodied persons and operate well on a wide range of users. Another advantage, the details of which are not discussed here, is the ability of this controller to work while walking backwards. In initial tests, the subject was able to take backwards steps using SPARKy while the controller gave a correct ankle motion.

B. Dynamic Pace Test Results

The dynamic pace controller presented in section III-B has been tested several times using an AFO on able bodied

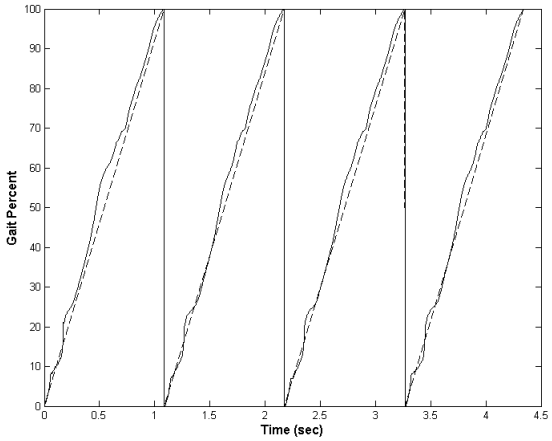

Fig. 11. Gait percent results walking at 2.5 mph. Dotted line is the target value and solid line is gait percent as calculated by the tibia controller.

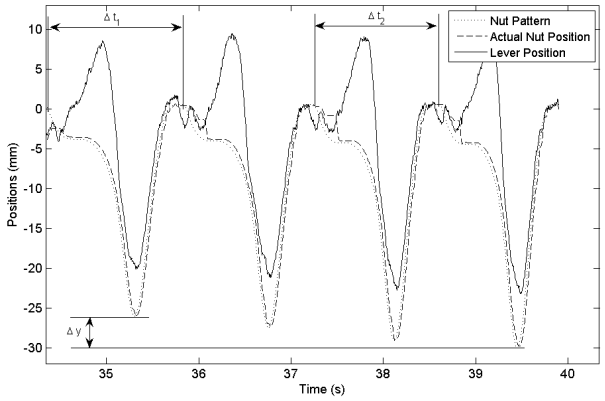

Fig. 12. Kinematics for four consecutive gait cycles

subjects and is currently being tested on stroke survivors. The following results have been obtained from tests on a treadmill with a 70 kg able bodied subject. The first plot in Fig. 12 shows the kinematic curves for four consecutive gait cycles. It can be seen that the amplitudes are adjusted (note Δy) and that the time between two heel strikes is adjusted as well, i.e. note that Δt_1 is greater than Δt_2.

V. Conclusion

This paper has presented existing controllers for prosthetic and orthotic foot-ankle devices. The tibia based and dynamic pace controllers are introduced. It has been shown that both controllers can calculate the necessary reference command. Already in earlier papers [4], [5] our lab has shown that this reference command achieves the requirements for human gait. The tibia controller has the advantage of not relying on any kind of logic to switch between states while only requiring one sensor. This type of controller is much more stable and adaptive to the user. The dynamic pace controller has the ability to change the duration and amplitude of the gait curve simultaneously. A combination of the two controllers is functionally superior to existing controllers.

VI. Acknowledgments

The authors would like to acknowledge the grant that was awarded and administered by the U.S. Army Medical Research & Material Command (USAMRMC), under Contract Number: W81XWH-0710193. The views, opinions, findings, information and presentations made do not necessarily reflect the position of the government and no official endorsement should be made.

References

[1] Ziegler-Graham, K., MacKenzie, E.J., Ephraim, P.L., Travison, T.G., Brookmeyer, R. "Estimating the prevalence of limb loss in the United States: 2005 to 2050". *Archives of Physical Medicine and Rehabilitation 89 (2008)*, pp. 422-429.

[2] Amputee Coalition (2008). [Online]. Available: http://www.amputee-coalition.org

[3] Stroke Center (2008). [Online]. Available: http://www.strokecenter.org

[4] Hitt, J.K., Oymagil, M.A., Sugar, T.G., Hollander, K.W., Boehler, A.W., and Fleeger, J. "Dynamically Controlled Ankle Foot Orthosis (DCO) With Regenerative Kinetics: Incrementally Attaining User Portability", *2007 IEEE Conference on Robotics and Automation (ICRA)*, pp. 1541-1546.

[5] Hitt, J., Bellman, R., Holgate, M., Sugar, T., and Hollander, K., "The SPARKy (Spring Ankle with Regenerative Kinetics) Project: Design and Analysis of a Robotic Transtibial Prosthesis with Regenerative Kinetics", ASME International Design Engineering Technical Conference, CD-ROM, pp. 1-10, 2007.

[6] Dollar, A. M. and Herr, H. "Active Orthoses for the Lower-Limbs: Challenges and State of the Art", *2007 IEEE* 10^{th} *International Conference on Rehabilitation Robotics (ICORR)*, pp. 968-977.

[7] Au, S. K., Weber. J., and Herr, H., "Biomechanical design of a powered ankle-foot prosthesis," Proc. IEEE Int. Conf. On Rehabilitation Robotics, Noordwijk, The Netherlands, pp. 298-303, June 2007.

[8] Oymagil, M.A., Hitt, J.K., and Sugar, T.G., "Control of a Regenerative Braking Powered Ankle Foot Orthosis", *2007 IEEE* 10^{th} *International Conference on Rehabilitation Robotics (ICORR)*, pp. 28-34.

[9] Böhler, A. W., Hollander, K. W., Sugar, T.G., Shin, D. "Design, Implementation and Test Results of a Robust Control Concept for a Powered Ankle-Foot-Orthosis (AFO)". *2008 IEEE International Conference on Robotics and Automation (ICRA)*.

[10] Schaeffer, A.A., and Hirzinger, G., "Cartesian Impedance Control Techniques for Torque Controlled Light-Weight Robots", *Proceedings of the 2002 IEEE International Conference on Robotics and Automation (ICRA)*, pp. 657-663, 2002.

[11] Blaya, J.A., Herr, H., "Adaptive Control of a Variable-Impedance Ankle-Foot Orthosis to Assist Drop-Foot Gait," *IEEE Transactions on Neural Systems and Rehabilitation Engineering*, vol. 12(1), pp. 24-31, 2004.

[12] Ferris, D.P., et al., "An Improved Powered Ankle-Foot Orthosis Using Proportional Myoelectric Control," *Gait & Posture*, vol. 23, pp. 425-428, 2006.

[13] Ferris, D.P., Czerniecki, J.M., Hannaford, B., "An Ankle-Foot Orthosis Powered by Artificial Muscles," *Journal of Applied Biomechanics*, vol. 21, pp. 189-197, 2005.

SPARKy 3: Design of an Active Robotic Ankle Prosthesis with Two Actuated Degrees of Freedom Using Regenerative Kinetics.

Ryan D. Bellman, Matthew A. Holgate, Thomas G. Sugar

Abstract— **The goal of modern prosthetics is to replicate the function of the replaced limb or organ in the most capable and discreet fashion possible. However, even the most advanced, commercial, transtibial prostheses available today only passively adjust the position of the ankle during the swing phase of gait and return a portion of the user's own gravitational input. To greatly improve the quality of life of a transtibial amputee, new technologies and approaches must be used to create a cutting-edge robotic ankle prosthesis which can perform on par with, if not outperform, the equivalent able-bodied human ankle. Initial attempts by us and others have had great success in providing the natural gait power and motion through all ranges of walking speeds. A new design is presented which governs both the coronal and sagittal angles and moments of the ankle joint to potentially provide unprecedented levels of athleticism and agility among transtibial amputees.**

I. INTRODUCTION

The SPARKy Project, short for Spring Ankle with Regenerative Kinetics, began with the goal of bringing full able-bodied ankle function to transtibial amputees, particularly those injured serving in the military who wish to be able to return to active duty. The first of three planned phases culminated in a highly successful product in SPARKy 1, Fig. 1. Six months of thorough subject testing ensued, and a follow-up design was created to improve on the form and function of SPARKy 1. SPARKy 2, Fig. 2, incorporates more efficient linear transmission options using a ball screw or a roller screw, a smaller and more powerful brushless motor without the need for a gearbox and a significant overall decrease in size and weight. Both designs use the proven technology of the Robotic Tendon of Hollander[1], the elastic energy storing ability of helical springs, and an advanced carbon, composite keel. Additionally, they are both capable of permitting walking speeds in excess of 4 miles per hour, with plenty of power in reserve [2], [3]. When subject testing starts for SPARKy 2, it may even reveal to be capable of light or moderate jogging as well. Herr is developing a similar spring based ankle with motion in the sagittal plane [4].

Both ankles by Hitt et al. and Au et al. though more advanced than any technology on the market, still do not compare to the functionality of the human ankle. A more robust and agile robotic prosthesis is needed to fulfill the more demanding and athletic movements needed for an active duty soldier or an active individual. The two previous designs are limited to active motion only in the sagittal plane, but the complex movements of the human ankle also require actuation in the coronal body plane, empowering transverse body movements as well as dorso-ventral and elevational movements. The SPARKy 3 design has two degrees-of-freedom without sacrificing the size and weight precedents set by the first phase.

The initial designs for the three versions of the SPARKy ankles are shown in in Fig. 3. The size of the second version was greatly decreased using a smaller motor and shorter lever arms. SPARKy 3 added a 2nd motor and two joints without increasing overall volume.

A. Intention and Goals

SPARKy 3 has taken a unique approach to providing two degrees-of-freedom to the prosthetic ankle seeking to revolutionize powered transtibial prosthesis design. While the average amputee may not need the ability to perform agile movements, many would prefer the ability to lead a more active lifestyle without being limited by their robotic ankle; some have expressed this desire directly to us. Military amputees in particular may benefit the most from such a device, as they must

This work was supported by the U.S. Army Medical Research & Materiel Command (USAMRMC)

R. Bellman is with the Department of Mechanical and Aerospace Engineering, Arizona State University, Tempe, Arizona ryan.bellman@asu.edu

M. Holgate is with the Department of Mechanical and Aerospace Engineering, Arizona State University, Tempe, Arizona matthew.holgate@asu.edu

T. Sugar is with the Department of Engineering, Arizona State University, Polytechnic Campus, Arizona thomas.sugar@asu.edu

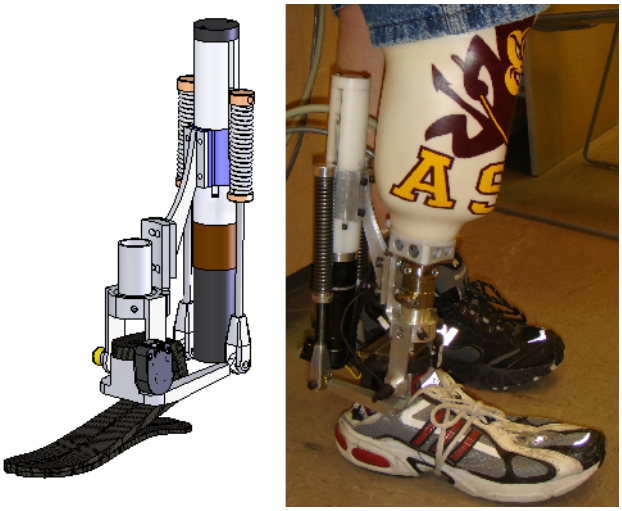

Fig. 1. The first built and tested robotic ankle prosthesis of the SPARKy Project, SPARKy 1 uses regenerative kinetics[2] to accurately and efficiently reproduce the human gait cycle. This design weighs under 2.7 kg (6 pounds) (not including the molded socket), comparable to the weight of the amputee's limb.

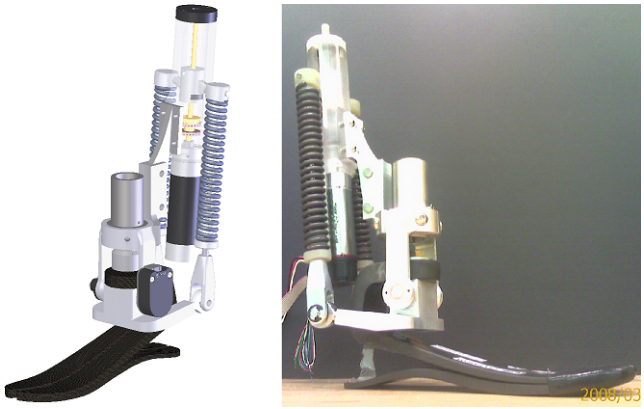

Fig. 2. The refined version of the first design evolved into SPARKy 2, incorporating a shorter lever arm, roller screw/ball screw interchangeable transmission, and the Maxon EC Powermax 30 motor[5], a high output brushless DC motor. It weighs approximately 2.0 kg (4.5 pounds) and is significantly reduced in size from its predecessor.

perform tasks such as running, jumping and passing their PT test returning to active duty service if they so desire. Our goal for the future is to allow an individual to return to active duty with increased athletic ability using two very powerful, lightweight motors.

The chief goal of this third phase of the SPARKy Project is to build a more dynamic robotic ankle without sacrificing size, weight or performance compared to the previous versions. Naturally, some compromises will have to be made to achieve these goals.

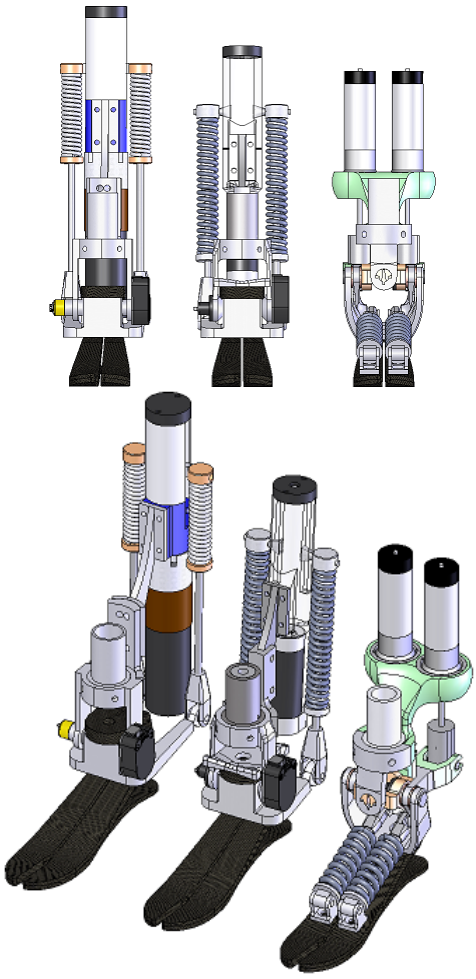

Fig. 3. The three initial designs of SPARKy 1, 2, and 3. SPARKy 2 reduces in size and weight while SPARKy 3 adds an additional degree-of-freedom.

II. Design Phase

A. *Pre-design and Sketching*

Intially, the design objectives were to achieve only running and jumping which requires two EC Powermax 30 motors to increase power capacity. The additional motor prompted investigation into adding an additional degree-of-freedom. We then focused on the idea of using both motors in unison for powered running, and controlling each individual motor to power the additional rotational degree-of-freedom.

Another desire of the design was to move the springs to a location above the keel but still in the envelope of the foot so that an unmodified shoe can still be worn over the device. This would allow for a lower profile device and remove much of mechanism from behind the leg. To additionally minimize the volume of

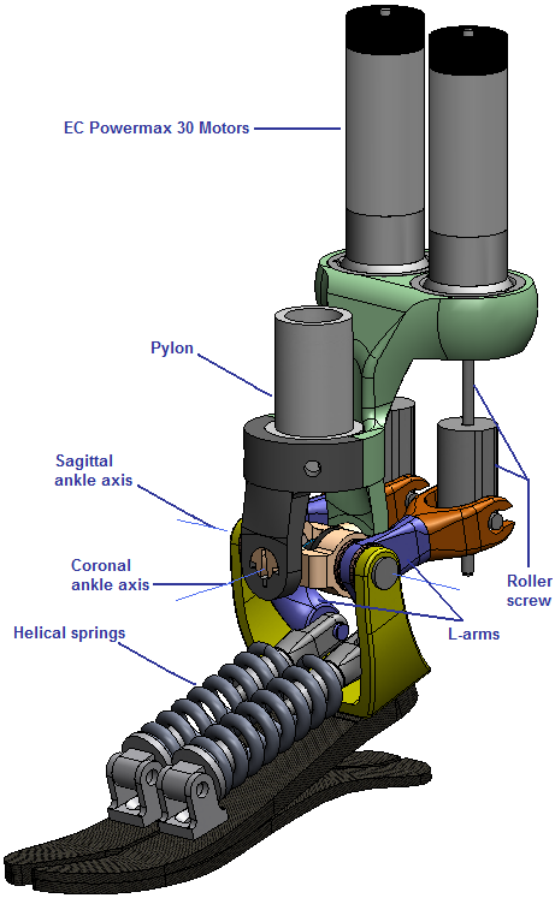

Fig. 4. SPARKy 3, the first fully actuated 2 DOF robotic prosthesis.

the design, a new low-profile foot replaces the FS3000 foot[6]. While the low-profile version of the same foot, the Pacifica FS4000[6], was considered initially, the eventual choice became Ossur's LP Vari-Flex foot [7] shown in Fig. 5. The Vari-Flex line was preferred by many users, and the design incorporates two bolts intended to hold the heel piece to the rest of the keel. These bolts proved a key factor in the decision, as they provide a perfect mounting point for the springs in our new configuration.

B. Functionality and Performance of SPARKy 3

In the primary operation of walking, the two motors work together either compressing or extending the two helical springs. For example during the stance phase, as the ankle rolls over the sagittal or primary ankle axis, the springs are extended and the motor extends the springs as well adding additional energy. During powered push-off, the motors move together releasing the energy in the springs. The combined motion has the added benefit of dividing the workload of each

Fig. 5. The low profile of the LP Vari-Flex foot by Ossur provides a low clearance keel and opens up room for a more complicated joint above it. The portion of the keel that low-profile version removes is not needed in a device with an active ankle joint, as its only purpose is to add flexibility of the ankle in a passive prosthesis.

motor. Analyzing the efficiency curve of the Maxon EC Powermax motor in Fig. 6, efficiency is greatly increased when the motor operates well below its peak capabilities. The motors will produce less heat as well, reducing the risk of failure.

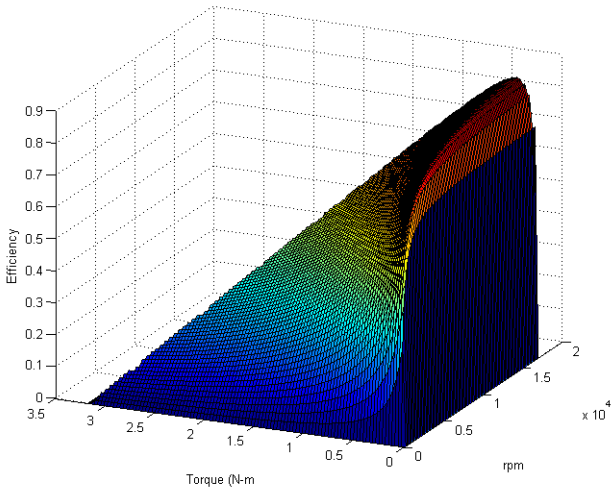

Fig. 6. The operational efficiency curve of the EC Powermax 30 motor defined by the torque load at the shaft and angular speed [3].

Additionally, the increased headroom in power of the two motors enables much more demanding activities, such as running and jumping, which do not allow as much time for energy storage from the motor as compared to walking gait thus reducing the maximum possible power amplification. Conversely, the short duration of ground contact in sprinting provides a

greater opportunity for energy storage from the impact, particularly with a higher stiffness. This principle is seen prominently in passive transtibial and transfemoral sprinting feet such as the Cheetah by Ossur. The EC Powermax 30 motor is rated at 200W of continuous output power, but is capable of much higher outputs, two to three times the continuous rating, for brief periods of time without damaging. With two such motors working together, they may be capable of 1000W or more of mechanical output power alone. Coupling this with the power amplification achievable from the robotic tendons, the SPARKy 3 design is predicted to be more than capable of producing the up to 1500W of peak output power needed for jogging and 200Nm of peak planter flexion moment for sprint starting[8], [9].

One hurdle that may yet need to be overcome is actively adjusting the stiffnesses of the springs to optimize for the significantly shorter stance phase during sprinting. Additionally, while energy savings are expected during normal walking motion compared to previous models, much greater power consumption will occur during the more agile and athletic functions of the device. Though synonymous with fatigue for the user, the device will likely require a higher capacity battery pack than is currently used on the previous models to account for the higher energy requirements, particularly for military users that are fully active and unable to recharge throughout the day.

C. CAD Design

Since SPARKy 3 was completely new, the design started around the keel. A two degrees-of-freedom joint was desired at the ankle, so a base was created to locate the plantarflexion/dorsiflexion axis, henceforth referred to as the primary axis around the biological center of rotation of a normal ankle. A couple was then designed to serve as the central part of an orthogonal custom U-joint, creating the secondary axis, for inversion and eversion. L-shaped arms, or "L-arms," were also designed to transfer the linear actuation of the actuators to the springs on the foot, using the primary axis of the ankle joint for their pivot. Due to the dimensional constraints this configuration imposes, the active lever arm through which the springs are aligned is only 4 cm as compared to the 6 cm lever arm on SPARKy 2 and the 9 cm lever arm on SPARKy 1. Because the motors are mounted 6 cm from the primary axis, an additional ratio between the motion of the actuator to the compression/extension of the springs is achieved, 1.5:1. The transmissions will be 1mm-lead roller screws similar to SPARKy 2, creating a 2/3mm effective lead between the motor and the spring. This relationship also relieves some of the load on the roller screws, as they will experience 2/3 of the force that the springs exert.

To reduce inertia effects, the mounts for the motor are fixed. Therefore, a number of additional joints are needed between the linkages to allow the device to have two degrees-of-freedom. The connection between the roller screw nut and the L-shaped arm requires two orthogonal and intersecting rotational joints to allow the motors to follow the pylon but resist the nut from turning when the roller screw shaft rotates. This was accomplished by placing a yoke reminiscent of the clevis on earlier designs on the end of the L-shaped arms and allowing it to rotate about a horizontal axis along the longer part of the arm. This interaction is shown slightly displaced from the default position to demonstrate its function in Fig. 7.

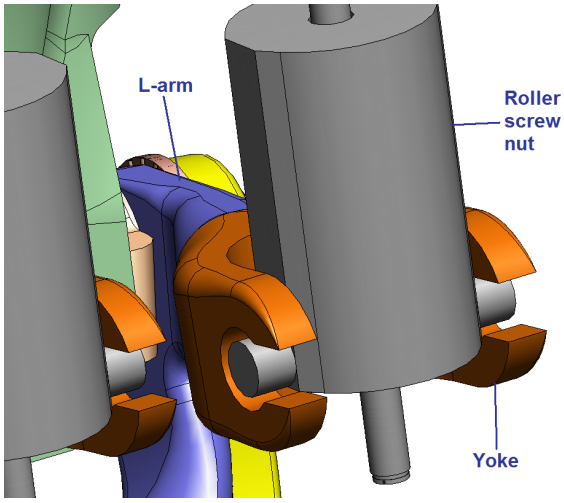

Fig. 7. The yoke swivels relative to the arm along its central axis and the roller screw wing is allowed to rotate within the yoke.

The more complex joint exists at the base of the motor mounts, as slight rotations are required to keep the roller screw shafts free from bending moments. The solution chosen involves a custom ball joint, with vertical channels on the outer race of the joint and pins on the ball to resist the torque of the motor. The ball joint was chosen due to its high load carrying characteristics without needing multiple bearings which would have cantilevered the mounts out from the pylon. The space within the ball was used to house the thrust bearings and thrust shoulder interface to reduce the size of the overall product. This portion of the design is shown from several perspectives in Fig. 8.

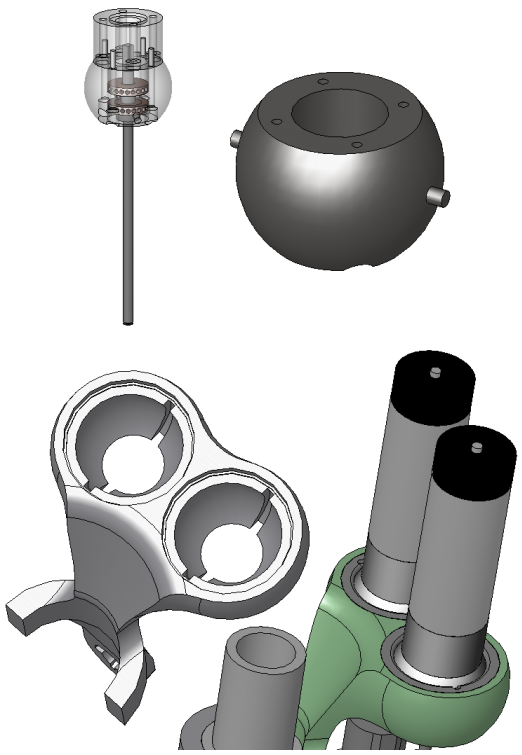

Fig. 8. The ball pieces of the ball joint interface are shown, with the actuator subassembly shown in the upper left, individual ball mount shown in the upper right, socket arm shown in the lower left, and the fully assembled ball joint interface shown in the lower right. The restricted ball joint is equivalent to two intersecting, orthogonal, rotational joints.

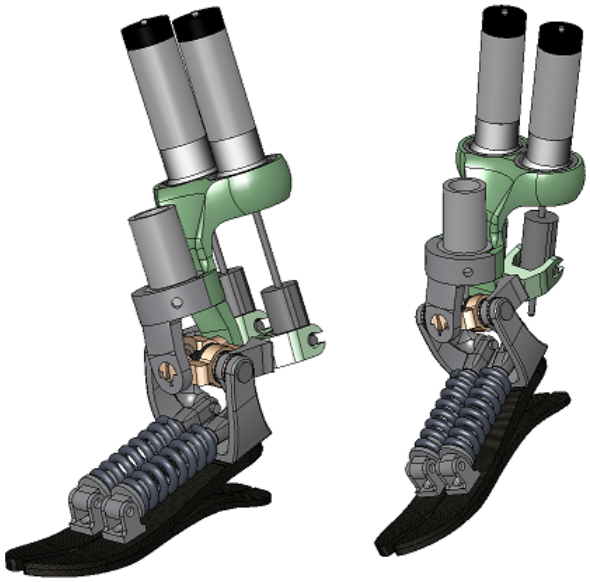

Fig. 9. The final design of SPARKy 3 in two different configurations including both coronal (frontal) and sagittal rotation from the default ankle position.

Upon completion of the design of the two additional joints, the mobility of the robotic ankle design was checked with Grubler's criterion to confirm that the foot (end effector) has two degrees-of-freedom. To perform this calculation, the mechanism had to be split into two interacting pieces, one of which operates in the plane, while the other operates in three dimensions. The current and final design of SPARKy 3 in Fig. 9 shows the device in various orientations to demonstrate its mobility. The coordination of the actuators determines the axis of motion of the device. When the actuators move in the same direction, the joint articulates about the primary axis. If the actuators move in opposing directions, the joint articulates about the secondary axis.

The geometry of the linkages means that the angular stiffness about the secondary axis is less than half that of the primary axis. Since the biological stiffness is not well documented, due to the slenderness of the human ankle, a supplemental stiffness may be necessary to increase the ankle stability about the secondary axis. It is also a safe practice to limit the motion allowed by this joint so the ankle cannot roll too far in much the same way a human ankle is rolled. The first solution was to use a hybrid torsional bearing joint manufactured by C-Flex[10]. The bearings were far too limited in both their torsional stiffness and load ratings in relation to their outside diameter and length. Instead, a custom bearing was designed. The bearing is best described visually, in Fig. 10. The torsion is achieved by adding a leaf spring between the two notches. When bent over a short length, such as the inner diameter of this bearing, a very thin leaf spring can provide a high angular stiffness, as defined by equation equation (1) from [11]. In this equation, the stiffness, K, is a function of the the modulus of elasticity of the material composing the leaf spring, E, the moment of inertia about its bending neutral axis, I, and the active length over which it is bent, L.

$$K = E * I/L \tag{1}$$

III. CONCLUSIONS AND FUTURE WORK

IV. CONCLUSIONS

Our research is focused on using springs to actively store and release energy properly during walking gait. SPARKy 1, our first regenerative ankle, was shown to store and release 16 J of energy per step. We designed and built a second device, SPARKy 2 which is lighter and more powerful using a roller screw transmission and a powerful brushless DC motor, the Maxon EC

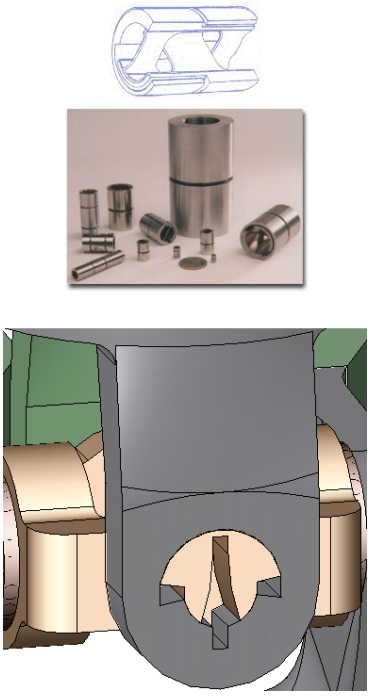

Fig. 10. The top figures are limited-motion rotational bearings manufactured by C-Flex. The bottom figure shows a custom bearing design, complete with angular limits of ± 20 degrees, torsion spring capability, and significantly higher load handling in a small and integrated package. The slot allows for the insertion of a short leaf spring to supplement the angular stiffness. Different leaf springs can be inserted for different individuals.

Powermax 30[5]. Finally, we designed and developed SPARKY 3 which is a two DOF device capable of high power for running and jumping. The design is the first to incorporate active control of both inversion and eversion as well as plantarflexion and dorsiflexion, yet will only weigh 2.1 kg (4.7 pounds) as currently designed. Combined with the power of regenerative kinetics, twin brushless DC motors, and efficient and long lasting roller screws, this device has the highest potential of returning wounded soldiers back to active duty.

V. Future Work

When SPARKy 3 is completed, subject testing will move slowly. The second degree-of-freedom and dual actuators add an element of complexity in the challenge of controlling the device. Additionally, the kinetic and kinematic data need to be analyzed for the various agile movements for which there is little or no published data. Some of this data has already been taken for basic jogging and running at various increments of speed using several rate gyros and inclinometers. Other tasks will include various lateral movements, stair and slope ascension and descension, and possibly some lateral jumping. Once these data are mated with a control system, subject testing will begin.

VI. Acknowledgments

The authors would like to acknowledge the grant that was awarded and administered by the U.S. Army Medical Research & Materiel Command (USAMRMC), under Contract Number: W81XWH-0710193. The views, opinions, findings, information and presentations made do not necessarily reflect the position of the government and no official endorsement should be made. The opinions contained in this publication are those of the authors and do not necessarily reflect those of the funding agency.

The authors would also like to thank Robotics Group Inc. and Arise Prosthetics for their participation. The authors would like to recognize Peter Rueling of the ASU Mechanical Engineering Shop for his invaluable support. Matthew Holgate, Joseph Hitt, and Kevin Hollander aided greatly in discussions about the designs.

References

[1] K. W. Hollander, R. Ilg, T. G. Sugar, and D. E. Herring, "An efficient robotic tendon for gait assistance," *Journal of Biomechanical Engineering*, vol. 128, no. 5, pp. 788–791, October 2006.

[2] J. Hitt, M. Holgate, R. Bellman, T. Sugar, and K. Hollander, "The SPARKy (Spring Ankle with Regenerative Kinetics) Project: Design and Analysis of a Robotic Transtibial Prosthesis," in *ASME International Design Engineering Technical Conference and Computers and Information in Engineering Conference*, 2007.

[3] J. K. Hitt, "A robotic transtibial prosthesis with regenerative kinetics," Ph.D. dissertation, Arizona State University, 2008.

[4] S. Au and H. Herr, "Powered ankle-foot prosthesis," in *ASME International Design Engineering Technical Conference and Computers and Information in Engineering Conference*, 2007.

[5] (2008) High precision drives and systems. Maxon Motor. [Online]. Available: http://www.maxonmotor.com

[6] (2008) Product specifications. Freedom Innovations. [Online]. Available: http://www.freedom-innovations.com

[7] (2008) Product specifications. Ossur Prosthetic Company. [Online]. Available: http://www.ossur.com/?pageid=3540

[8] M. W. Whittle, *Gait Analysis: An Introduction*, 2nd ed. Butterworth - Heineman Oxford, 1996.

[9] D. Gordon and E. Robertson. (2008) Contributions of the ankle and knee muscles to sprint starting. Sprintic Magazine. [Online]. Available: http://www.sprintic.com/articles/ankle_knee_muscles_sprint_starting

[10] (2008) Size performance and loading: Single end bearing. C-Flex Bearing Co., Inc. [Online]. Available: http://www.c-flex.com/home.html

[11] K. W. Hollander and T. G. Sugar, "Concepts for compliant actuation in wearable robotic systems," in *US-Korea Conference on Science, Technology and Entrepreneurship*, August 2004.

The SPARKy (Spring Ankle with Regenerative Kinetics) Project: Choosing a DC Motor Based Actuation Method

Matthew A. Holgate, Joseph K. Hitt, Ryan D. Bellman, Thomas G. Sugar, Kevin W. Hollander

Abstract— **The design process of a powered robotic ankle prosthesis presents many obstacles that must be overcome. To be practically implemented, such a mechanism must not only run on batteries, but sustain a long running time between recharging. Using springs to passively and actively store and supply energy to the robotic ankle, small DC motors can be optimized to perform high peak power tasks without sacrificing efficiency and net energy usage. Additional techniques are explored with the potential of substantially reducing the energy requirements as well as the size and weight of the prosthesis. The benefits of adding a unidirectional parallel spring with a Robotic Tendon are weighed and the possibility of actively varying the lever arm at which the spring force is applied is analyzed. The different actuation methods are compared to determine which methods work best in different gait regimes.**

I. INTRODUCTION

The SPARKy Project led by Arizona State University Human Machine Integration Lab with team members from Arise Prosthetics, Robotics Group, Inc. and Washington University at St. Louis is a multi-phased multi-year development effort. The project seeks to tackle several leading technical challenges that prevent the development of a truly biomimetic foot-ankle prosthetic device. This includes (1) prohibitively low power and energy density in traditional actuation schemes, and (2) development of a control methodology that translates user intent into human-like movement.

The research community has made significant improvements in prosthetic and orthotic technologies in recent years. Several prosthetic companies have produced devices that are more comfortable, provide life-like cosmeses, provide significant energy return and are now even computer controlled. New high performance composite materials and polymers have made sockets and liners more comfortable and prosthetic feet and pylons much more energy efficient. A world-class below the knee amputee sprinter using a high performance composite prosthesis can now sprint the 100 meters only one second off of the able-bodied world record [1]. Energy storage and return devices allow faster walking velocity and better terrain negotiation [2], [3], [4]. They have increased range of motion; they store and return energy; and they reduce needed energy requirements [5], [6], [7], [8], [9]. Microprocessor controller components such as the Rheo Knee use artificial intelligence to change joint angles and dampen joint motion in response to the environment and individual gait style [10]. MIT's powered foot-ankle is a microcomputer controlled prosthesis that provides power and ankle motion at normal walking speeds [11].

Hydraulic, pneumatic, direct-drive, series-elastic, electroactive polymer-based, chemical-based and many other actuation schemes are also at varying stages of research and development. Other researchers are working on wearable robot control. Embedded gait pattern control [12], EMG motion control [13][14], and state based control [15] are all in various design stages. For example, the Proprio Ankle by Ossur is a commercially available state control device that modulates ankle angle based on the environment, gait, and condition to better mimic the kinematics (opposed to both kinematics and kinetics) of the lost limb [16].

We believe that the best performance in terms of power and energy as well as system size and weight can be achieved using DC motor actuators. The purpose of this paper is to explore different methods of actuation using DC motors. The actuation methods are evaluated on their ability to give the ankle full range of motion as well as a powered push-off. The actuator must be energy efficient to extend battery life while still being able to deliver all of the necessary power for walking.

II. HUMAN GAIT

Gait is a cyclical pattern of leg and foot movement that creates locomotion[17]. To illustrate a typical pattern of gait, consider the kinematics and kinetics of a normal ankle at a self selected stride length at 1.25 m/s walking speed of an 80 kg subject, Fig. 1 and Fig. 2. Note that for different stride lengths, the curves are slightly different in magnitude and in position of peaks. The negative sign represents the physiological direction of the plantarflexing ankle, when the foot rotates downwards to push off from the ground. At the point at which the peak moment occurs, the ankle angle begins a rapid decent to its lowest overall value. The region of gait approximately between 50% and 67% of the gait cycle is known as push off. At the conclusion of push off, now considered toe off, the leg initiates swing and the foot is then positioned for the next heel strike.

The power necessary from the ankle during gait is the moment times the angular velocity of the ankle. The energy is calculated by integrating the power curve. The peak power can be up to 350 Watts and occurs during the push off portion of gait. At the beginning of gait, energy is negative as the foot resists the roll-over of the leg. During push off the energy moves sharply positive as the moment increases and

This work was supported in part by the U.S. Army Military Amputee Research Program and TATRC under Contract.

Matthew A. Holgate is with Arizona State University, Tempe, Arizona 85287 matthew.holgate@asu.edu

Joseph K. Hitt is with the US Army assigned at the Arizona State University, Tempe, Arizona 85287 joseph.hitt@asu.edu or joe.hitt@us.army.mil

Ryan D. Bellman is with Arizona State University, Tempe, Arizona 85287 ryan.bellman@asu.edu

Thomas G. Sugar is with Arizona State University, Polytechnic Campus thomas.sugar@asu.edu

Kevin W. Hollander is with Augspurger-Komm Engineering, Inc. Phoenix, Arizona 85040 kevin.hollander@asu.edu

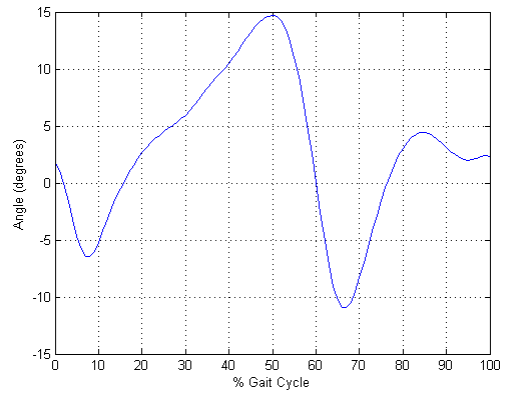

Fig. 1. The ankle angle of a normal subject walking at a self selected stride length at 1.25 m/s. 0% gait cycle corresponds to heel strike.

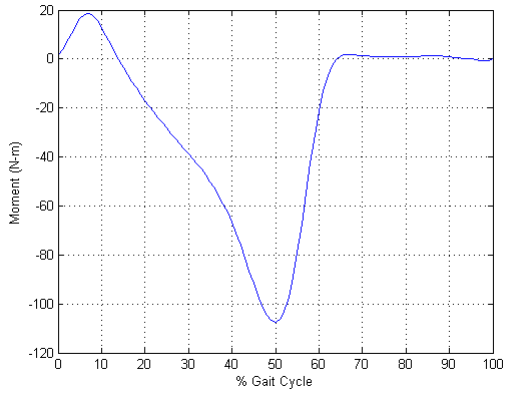

Fig. 2. The ankle moment of a normal subject walking at a self selected stride length at 1.25 m/s.

the foot propels the person. It should be noted that at self selected stride length for 1.25 m/s the net energy required is only about 10 joules per step. For slower speeds the energy becomes lower; however, for faster speeds the energy can climb to 20 joules per step or higher.

III. USING DC MOTORS

When using a DC motor actuator an important consideration is efficiency. The efficiency of a DC motor is a function of both rpm and torque. The derivation of DC motor efficiency used for this model is shown below with definitions of the symbols shown in Table I.

$$\epsilon = \frac{Trpm\frac{2\pi}{60}}{VI} \tag{1}$$

$$I = I_{nl} + \frac{T}{K_t} \tag{2}$$

$$V = \frac{rpm}{K_e} + R_m\left(I_{nl} + \frac{T}{K_t}\right) \tag{3}$$

$$\epsilon = \frac{Trpm\frac{2\pi}{60}}{\left(\frac{rpm}{K_e} + R_m\left(I_{nl} + \frac{T}{K_t}\right)\right)\left(I_{nl} + \frac{T}{K_t}\right)} \tag{4}$$

TABLE I

DEFINITIONS OF SYMBOLS SHOWN IN (1) THROUGH (4)

Symbol	Definition
ϵ	Motor Efficiency
T	Motor Torque
rpm	Revolutions per Minute
K_e	Speed Constant (rpm/Volt)
K_t	Torque Constant (N-m/Amp)
R_m	Motor Winding Resistance (Ω)
I_{nl}	Motor No-load Current (Amp)
I	Motor Current (Amp)
V	Motor Voltage (Volts)

The efficiency for a Maxon brand ECPowerMax 30 motor is plotted in Fig. 3. The highest efficiency conditions of operation are all in the low torque region of operation.

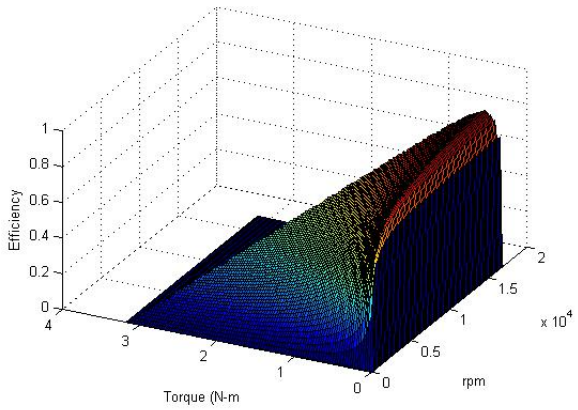

Fig. 3. Efficiency of Maxon ECPowermax30 Motor

IV. ROBOTIC TENDON

The Robotic Tendon described in [18] is a small and lightweight actuator that features an efficient DC motor used to adjust the position of helical springs using a very simple position controller. As the ankle rotates over the foot during stance phase, a lever attached to the foot pulls on the distal end of the spring. By correctly positioning the motor, which pulls on the proximal end of the spring, a desired spring deflection is obtained to store energy. A heavy, powerful motor is not needed because the Robotic Tendon stores a portion of the stance phase kinetic energy and additional motor energy within the spring. The spring releases its stored energy to provide most of the peak power required during push off. Therefore, the power requirement on the motor is significantly reduced. As described in [18], peak motor power required is 77W compared to 250W for a direct drive system in the example of a 80kg subject walking at a rate of 0.8hz. Consequently, the weight of the Robotic Tendon is just 0.95kg.

The robotic ankle consists of a spring keel for the foot; a lever arm attached to the keel; a pylon attached to the lever arm via a revolute joint; and a spring series Robotic Tendon between the pylon and the lever arm (Fig. 4). The definitions of the symbols used in Fig. 4 are shown in Table II. A defined

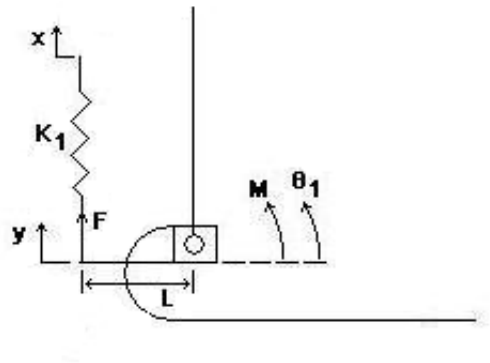

Fig. 4. Robotic Tendon Ankle Model. See Table I for definitions of symbols used. The robotic tendon nut pulls on the spring x amount, which pulls the lever arm L causing the foot to plantarflex.

TABLE II
DEFINITIONS OF SYMBOLS SHOWN IN FIG. 4

Symbol	Definition
θ_1	Lever Arm Angle (zero at horizontal)
M	Moment on the Ankle
F	Force in Spring Series Robotic Tendon
K_1	Robotic Tendon Spring Stiffness
l	Lever Arm Length
x	Robotic Tendon Spring Position
y	Lever Arm Deflection at Spring Attachment Point

moment function is given for the ankle as well as a desired angle function, shown in Fig. 1 and Fig. 2. Since the ankle has a relatively small mass and moment of inertia compared to the moments acting on it along with a limited range of motion and rotational velocity, the ankle will be assumed massless and the dynamic effects will be ignored. The motor, however, turns at a high rate and the dynamic effects can not be ignored. Using static equilibrium equations the following relationships can be developed.

$$F = K_1 (x - y) \tag{5}$$

$$y = -\theta_1 l \tag{6}$$

$$-M = lF = lK_1 (x + \theta_1 l) \tag{7}$$

$$x = -\left(\frac{M}{K_1 l} + \theta_1 l\right) \tag{8}$$

Equation (8) determines the position that the robotic tendon must follow to actuate the ankle. The spring deflection creates the ankle moment. The actuator's position is then differentiated to calculate the velocity and acceleration of the motor. Finally, the actuator velocity multiplied by the ankle moment is used to calculate power and the efficiency of the motor at every point of operation. The acceleration is used along with the inertia of the particular motor to calculate the torque necessary from the dynamic effects of the actuator. When adding the effects of inertia to the static calculations, the model matched the experimental results well.

V. PARALLEL UNIDIRECTIONAL SPRING

During the portion of the gait cycle beginning when the foot is entirely on the ground until the beginning of push off, the ankle behaves approximately like a linear spring. To illustrate this, consider the portion of Fig. 5 between points 2 and 3. Fig. 5 shows the ankle moment (Fig. 2) versus the ankle displacement angle (Fig. 1), which can be interpreted as the ankle stiffness.

If the robotic tendon series spring were chosen so that it matched the approximate linear stiffness shown in Fig. 5 between points 2 and 3 the motor would not have to move during this portion of gait. Although the motor does not need to supply any energy to the system, it still costs electrical energy because the system is backdriveable. Since the robotic tendon uses a spring in series with the motor, the moment at the ankle is transferred directly to the motor through the leadscrew transmission. If the screw were non-backdrivable, it could easily hold the load; however non-backdrivable transmissions have a large amount of friction, and thus create an inherently inefficient drive system.

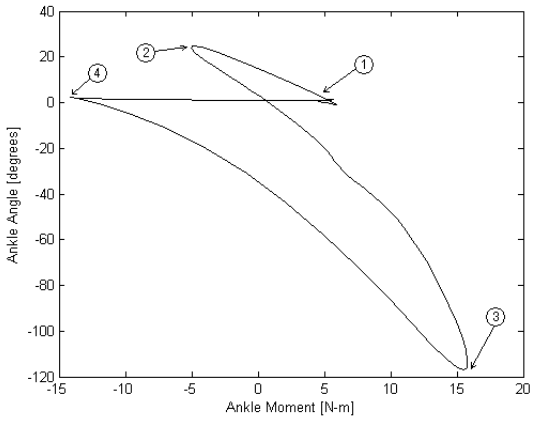

Fig. 5. Moment versus angle of the ankle for fast walking. Gait begins at point 1 with heel strike. The foot then rotates until it is flat with the ground at point 2. The tibia rolls over the ankle between points 2 and 3. Point 3 is the beginning of push off until toe off at point 4. After toe off at point 4, the foot is in swing phase until heel strike again at point 1. The slopes at different portions of gait can be thought of as the ankle stiffness and can be seen to be approximately constant during most portions.

A spring that was placed parallel to the robotic tendon could support the moment holding the load. If the parallel spring stiffness were chosen to be the ankle stiffness between points 2 and 3, then no energy would be required from the motor. However, at different speeds of walking the ankle stiffness changes. If the parallel spring stiffness was chosen to be too stiff, the motor would need to fight the spring in order to obtain the correct ankle motion. If the parallel spring was too compliant, the motor would need to add energy to the system to compensate and hold the load. A parallel spring stiffness could be fixed for a particular walking speed, and, at other speeds, the motor would need to adjust for the incorrect stiffness value.

A parallel spring is beneficial during the portion of gait shown in Fig. 5 between points 2 and 3. This portion corresponds to the portion of the stance phase when the foot dorsiflexes. When the foot plantarflexes the motor would need to fight the parallel spring and expend energy unnecessarily. To remedy this situation, the parallel spring can be configured in such a way that it is unidirectional and is only active when the foot dorsiflexes. This idea has been proven effective by researchers at MIT [11], [19]. A device with a unidirectional parallel spring can effectively lower the energy needed from the actuator especially during average and slow walking. We will show that an additional parallel spring is not beneficial for fast walking.

VI. Lever Arm

Analyzing the model for the robotic ankle shown in Fig. 4, it is reasonable to explore the possibility that the ankle could be actuated solely by changing the length of the lever arm. Solving equation (7) for l instead of x yields the following.

$$l = \frac{-xK_1 \pm \sqrt{(xK_1)^2 - 4\theta_1 K_1 M}}{2\theta_1 K_1} \tag{9}$$

If x is thought of as a constant offset on the spring, then the Robotic Tendon will not have to move during the entire gait cycle. (A non back-driveable transmission is a good choice for this design scenario.) It is apparent from the square root term in equation (9) that only certain values of x will work. For this idea to be feasible the following relationship must always be true.

$$(xK_1)^2 - 4\theta_1 K_1 M > 0 \tag{10}$$

The rest position of the spring must be set at a large offset value, larger than the range of the ankle moment so that equation (10) holds.

Another way to study this problem is to analyze the ankle as a simple torsional spring. By dividing the moment by the angle at every point of the gait cycle, a stiffness will be calculated. These values are shown in Fig. 6. It is obvious that many of the values are not attainable. However, by moving the resting equilibrium position of the spring, the stiffness values become realizable. This is modeled by adding a constant to the angle so that the resulting stiffness function is continuous. This is illustrated in Fig. 7. As the constant becomes larger, the effect of the ankle motion becomes smaller and the stiffness converges to the moment divided by the constant angle. It should be noticed that the stiffness values are both positive and negative. This can be realized by a lever arm that can go past a zero length and effectively reverse the direction of the moment.

By preloading the spring, the resting position is altered. The lever arm length needed at each point along the gait cycle is calculated using equation (9). The force on the spring is calculated using equation (5).

If a design is utilized that moves the position of the attachment point of the spring along the lever arm, the force on an actuator motor that adjusts the lever arm will be the product of the force on the spring and the sine of the angle of the lever arm. The power will therefore be the product of that force and the linear velocity along the lever arm. The motor would have to supply a large holding force unless a drive link that was not backdrivable was utilized.

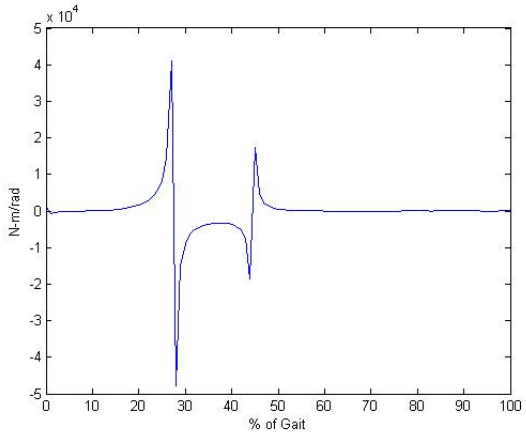

Fig. 6. Moment divided by angle. The ankle moment is divided by the ankle angle to determine a stiffness value at every point along the gait cycle. It is obvious that many of the stiffness values are not realizable.

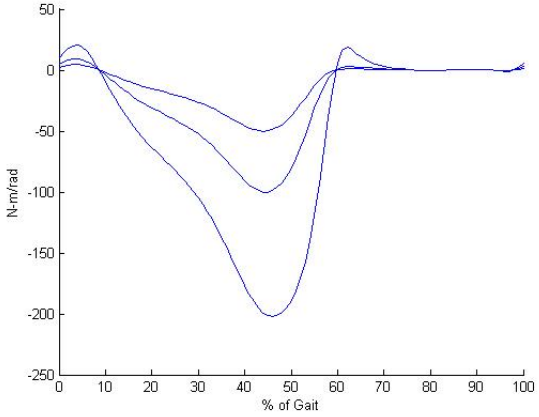

Fig. 7. Moment divided by angle with an additional positive constant offset. The moment is divided by the ankle angle with an additional constant angle to determine a stiffness value at every point along the gait cycle. Each curve represents a different constant offset. The stiffness converges to the inverse of the constant times the moment because as the constant becomes greater, the effect of the ankle motion becomes smaller.

An adjustable lever arm actuator has some advantages over the Robotic Tendon actuator. Analyzing fast and slow walking, the total energy consumed by the lever arm actuator is lower by 10-15% as compared to the Robotic Tendon. The energy is lower than the Robotic Tendon because the torque and rpm that is required is in a more efficient region of the motor shown in Fig. 3.

A pure lever arm actuator seems beneficial in simulations and theory, but in practice it creates many implementation problems. The system requires a preload of the spring of at least 3cm in practical cases. While this is a small deflection, the spring rates required are on the order of 50,000 N/m. A 3cm deflection creates a considerable force. During the entire gait cycle, forces can approach 2200 N on the spring. A structure could be designed to withstand this loading, and it would operate correctly while the foot was in contact with

the ground. Although during swing phase, the foot is not in contact with the ground and the force in the spring is still very high causing the foot to be difficult to control during this period of the gait cycle.

VII. COMBINING A ROBOTIC TENDON WITH LEVER ARM ACTUATION

While using a robotic lever arm alone might not be possible from a design standpoint, it is advantageous when it comes to saving energy. The energy savings occur because the motor is operating in a more efficient manner. Because there there can be an advantage gained by using a robotic lever arm, it seems reasonable to try and combine the actuated lever arm with a Robotic Tendon to increase the efficiency of the total system.

Analyzing Fig. 3, it is obvious that there is an area of operation over which the efficiency is very high, on the order of 85 to 90%. It is seen that the high efficiency peak roughly follows a straight line located with a low but constant torque and through almost all angular velocities. By adjusting the lever arm length, the gear ratio for the Robotic Tendon can be adjusted.

Since the moment at the ankle joint is transferred to the Robotic Tendon through a lever arm, the torque seen by the motor is proportional to the lever arm length. If the lever arm length is changed in proportion to the moment, the torque at the motor can be kept constant. The constant torque at the motor can be chosen to reside on the high efficiency peak of Fig. 3. As a result the efficiency of the Robotic Tendon motor is extremely high, almost always above 87%. Moreover, the energy required from the Robotic Tendon is reduced at all speeds as well.

However, the energy reduction does not come free; energy must be added due to the lever arm motor. Since the lever arm length must change when the lever is under load, there are times when it must compress the spring in order to shorten or lengthen the lever arm. In fact, almost all of the lever arm movements compress the spring. This is not necessarily a disadvantage, since the energy is stored in the spring and subsequently released. However, the efficiency of the lever arm actuation motor must also be taken into account. Even though lever arm actuation allows the main motor to work at very high efficiency, the lever arm motor efficiency is relatively low and the energy advantage for this motor is poor.

It can be observed that since the lever arm would need to change proportionally to ankle moment, this could possibly be accomplished by a clever mechanism. As seen in [20], using a carbon fiber keel can be beneficial in the design of a prosthetic ankle. This adds the benefit of a member of the structure which deflects proportionally to the ankle moment. A flexible keel could be linked in such a way that a deflection actuates the lever arm length eliminating the lever arm actuation motor.

VIII. PEAK POWER AND ENERGY

In this section, the peak power and energy will be analyzed for a Robotic Tendon with addition of a unidirectional parallel spring. Both spring stiffness values will be varied to determine power and energy surface plots.

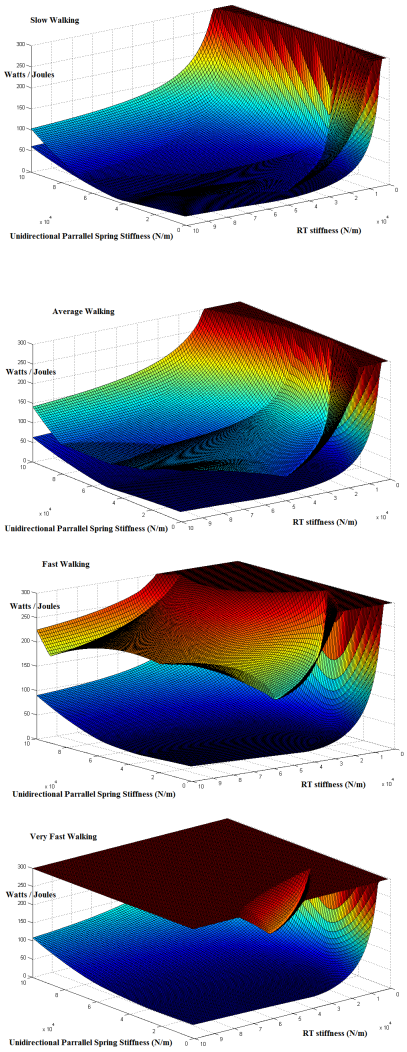

Fig. 8. Peak power and energy for different walking speeds for different stiffness values for the Robotic Tendon series spring and an additional parallel unidirectional spring. Note that values are cut off at 300 to preserve scale. The top surface is the peak power that the actuator needs to provide; the bottom surface is the energy that the actuator needs to provide. Note that most of the peak powers are above the range available for small DC motors.

As discussed in previous sections, using a unidirectional parallel spring can reduce the amount of energy needed from the actuator. This is highly beneficial for walking, especially walking at the speed for which the unidirectional spring is tuned. However, for faster walking speeds, for which the parallel spring is not tuned, additional energy from the actuator is required. Without a parallel spring the motor must hold position, but only if the series stiffness is chosen to be equal to the ankle stiffness between points 2 and 3 of Fig. 5. If a more compliant actuator series spring is chosen, the motor can continuously stretch the spring and add energy to the system as it is pulling, not simply holding position.

At slow walking speeds, the energy with a properly tuned unidirectional spring with a very stiff Robotic Tendon stiffness is slightly lower than the energy necessary for a Robotic Tendon alone. At faster speeds, however, the advantage is lost

for a constant stiffness parallel spring. At very fast walking, the lowest peak power and energy usage occurs with the correct choice of a Robotic Tendon spring.

The main advantage of the Robotic Tendon is its ability to reduce the peak power required from the motor. For average walking speeds the peak power is not as important as energy, the peak power only needs to be reduced by a small amount to stay below the maximum power of the motor. However, for fast walking speeds the peak power must be reduced if a single DC motor is used. SPARKy has shown through testing that the Robotic Tendon consistently reduces power by at least a factor of 4.5. For example, at 3 mph, the robotic tendon inputs 60 Watts peak power, but SPARKy supplies the user 260 Watts of peak power [21]. If jogging is to be achieved, peak power reduction is even more important.

Reducing peak power also increases the maximum amount of energy that the motor can provide to the ankle. Since the motor can add energy to the spring for a longer period, more energy can be released during push off. The ankle receives energy stored in the series spring during the stance phase along with additional power from the motor. With a parallel unidirectional spring the spring supplies some of the push off energy, but the motor must directly supply the remainder of the energy, which is a large portion of the energy.

IX. CONCLUSIONS

Various DC motor based actuation methods for a prosthetic ankle were investigated. These actuation methods include the Robotic Tendon alone, adding a unidirectional parallel spring to the ankle with a Robotic Tendon, controlling the length of a lever arm connected to a preloaded spring, and combining the Robotic Tendon with a robotic lever arm.

Controlling the lever arm length connected to a preloaded spring turns out to be a very efficient design, but, due to impracticalities, cannot be chosen as a realizable actuator for SPARKy. While combining lever arm actuation with the Robotic Tendon allows the system to operate extremely efficiently, the lever arm motor operates with poor efficiency and the total energy is higher than with the Robotic Tendon alone.

The Robotic Tendon operates efficiently and does not require high energy and reduces peak power by up to a factor of 6. This allows good battery life at all speeds and the ability to shrink the size of the necessary motor.

Adding a unidirectional parallel spring to the ankle can reduce the energy consumed by the Robotic Tendon by supporting its load during part of the gait cycle. This can reduce the energy slightly if properly tuned, but power amplification is lost (must choose a very high stiffness) and the motor cannot support high energy fast walking and running.

Considering performance characteristics of the motor and desired operating ranges that include walking and slow running, we have chosen the Robotic Tendon as the preferred actuation method for SPARKy.

X. ACKNOWLEDGMENTS

The authors would like to thank Greg Sawicki from the University of Michigan for providing us with invaluable gait data.

REFERENCES

[1] [Online]. Website, URL www.mshirley.com, Marlon Shirley's Personal Site, 2006.

[2] J. Casillas, V. Dulieu, and M. Cohen, "Bioenergetic comparison of a new energy-storing foot and SACH foot in traumatic below knee vascular amputations," Archives of Physical Medicine and Rehabilitation, vol. 76, pp. 39-44, 1995.

[3] S. Rao, L. Boyd, and S. Mulroy, "Segment velocities in normal and transtibial amputees: prosthetic design implications," IEEE Transactions on Rehabilitation Engineering, vol. 6, pp. 219 -226, 1998.

[4] L. Torburn, J. Perry, E. Ayyappa, and S. Shanfield, "Below-knee amputee gait with dynamic elastic response prosthetic feet: a pilot study," Journal of Rehabilitation Research and Development, vol. 27, pp. 369 -384, 1990.

[5] M Linden et la, "A methodology for studying the effects of various types of prosthetic feet on the biomechanics of trans-femoral amputee gait," Journal of Biomechanics, vol 32, pp. 877-889, 1999.

[6] J. Lehmann, R. Price, S. Boswell-Bessette, et al, "Comprehensive analysis of energy storing prosthetic feet: Flex-Foot and Seattle Foot versus standard SACH foot," Archives of Physical Medicine and Rehabilitation, vol. 74, pp. 1225-1231, 1993.

[7] P. MacFarlane, D. Nielsen, D. Shurr, and K. Meier, "Gait comparisons for below-knee amputees using a Flex-Foot versus a conventional prosthetic foot," Journal of Prosthetics and Orthotics, vol. 3, pp. 150 -161, 1991.

[8] K. Postema, H. Hermens, J. de Vries, et al., "Energy storage and release of prosthetic feet. Part 1: Biomechanical analysis related to user benefits," Prosthetics and Orthotics International, vol. 21, pp. 17-27, 1997.

[9] K. Postema, H. Hermens, J. de Vries, et al., "Energy storage and release of prosthetic feet. Part 2: Subjective ratings of 2 energy storing and 2 conventional feet, user choice of foot and deciding factor," Prosthetics and Orthotics International, vol. 21, pp. 28 -34, 1997.

[10] [Online]. Website. Rheo Knee Technical Manual, Ossur Orthopaedic Products and Services Company URL http://www.ossur.com , 2006.

[11] S. Au, "Powered Ankle-Foot Prosthesis," ASME International Design Engineering Technical Conference & Computers and Information in Engineering Conference, Las Vegas, NV, 2007.

[12] J. Ward, J. Hitt, T. Sugar, and K. Bharadwaj. "Dynamic Pace Controller for the Robotic Gait Trainer," ASME International Design Engineering Technical Conference & Computers and Information in Engineering Conference, Philadelphia, PA, 2006.

[13] S. Au, P. Bonato, and H. Herr, "An EMG-position controlled system for an active ankle-foot prosthesis: An initial experimental study," IEEE International Conference on Rehabilitation Robotics, 2005.

[14] D. P. Ferris, K. E. Gordon, G. S. Sawicki, A. Peethambaran, "An improved powered ankle-foot orthosis using proportional myoelectric control," Gait & Posture, 2005.

[15] I. Pappas, M. Popovic, T. Keller, V. Dietz, and M. Morari. ""A Reliable Gait Phase Detection System,"" IEEE Transaction on Neural Systems and Rehabilitation Engineering, vol. 9, pp. 113-125, 2001.

[16] [Online]. Website. Proprio Technical Manual, Ossur Orthopaedic Products and Services Company URL http://www.ossur.com, 2006.

[17] M. W. Whittle. Gait Analysis: An Introduction, 2 ed. Oxford: Butterworth-Heinemann, 1996.

[18] K. W. Hollander, R. Ilg, T. G. Sugar, and D. Herring. "An Efficient Robotic Tendon for Gait Assistance," *ASME Journal of Biomechanical Engineering*, vol 128(5), pp. 788-791, October 2006.

[19] Au, S. K., Weber. J., and Herr, H., "Biomechanical design of a powered ankle-foot prosthesis," Proc. IEEE Int. Conf. On Rehabilitation Robotics, Noordwijk, The Netherlands, pp. 298-303, June 2007.

[20] J. Hitt, R. Bellman, M. Holgate, T. Sugar, K. Hollander, "The SPARKy (Spring Ankle With Regenerative kinetics)Project: Design and Analysis of a Robotic Transtibial Prosthesis With Regenerative Kinetics," Proceedings of the ASME 2007 International Design Engineering Technical Conferences & Computers and Information in Engineering Conference, Las Vegas, Nevada, 2007.

[21] Joseph K. Hitt, Matthew Holgate, Thomas G. Sugar, Ryan Bellman, Alex Boehler and Kevin W. Hollander, "The SPARKy (Spring Ankle With Regenerative kinetics)Project: Power and Energy Considerations of a Robotic Transtibial Prosthesis," Submitted to Proc. IEEE Int. Conf. On Rehabilitation Robotics 2008.

A Robust Control Concept for Robotic Ankle Gait Assistance

Kevin W. Hollander and Thomas G. Sugar

***Abstract*— Previously we have developed lightweight and efficient, spring based actuators. The Robotic Tendon actuator is one such device. Testing of the earlier devices have shown good results both theoretically and experimentally in their implementation to human gait assistance. The current development is focused on a robust control methodology to support the Robotic Tendon device. This study has concluded that the stance phase of gait can be broken into five distinct zones in order to dictate controller behavior. Simulated control of these five zones have shown that simple velocity control and stiffness control meet the requirements necessary for robust gait assistance.**

I. Introduction

An effective form of robotic intervention would be a wearable system that could provide strength and performance augmentation to a person with motor disabilities. A robotic device could provide strength where there is weakness, respond to stimuli quickly rather than slowly, and a wearable robot could sense problems early, rather than after it is too late.

However, use of the term 'wearable' implies that such a robot be portable, lightweight, and safe. In order for such a device to be accessible for home use, the additional implications are that the wearable robot be economical and easy to operate. In contrast, a factory floor robot is none of these things; therefore, simple adaptation of existing technology is not possible. In order to handle the needs of people with motor disabilities, actuated wearable robots that are portable, lightweight, safe, economical and simple to operate are required[1].

Our previous work has been devoted to developing lightweight, efficient, spring based actuators to meet the challenging requirements implied by a wearable device. One such actuator is the the Robotic Tendon[2]. The Robotic Tendon features a 'tuned' spring that is positioned at the end of a linear actuator. The conceptual model of the Robotic Tendon is similar to that of the devices by Sugar and Kumar [3] and Robinson et al. [4].

In addition to needing to be lightweight and efficient, robust and intuitive control of these actuated systems is also required. A review of human gait data for ankle motion has revealed an approach to robust actuator control. The application of a specialized piecewise velocity and stiffness control scheme can be used to describe the actuator motion necessary to assist in ankle gait.

K. Hollander is a Senior Consulting Engineer with Augspurger Komm Engineering, Inc., Phoenix, AZ 85040, USA kevin.hollander@akeinc.com

T. Sugar is an Associate Professor with Arizona State University, Mesa, AZ 85212, USA thomas.sugar@asu.edu

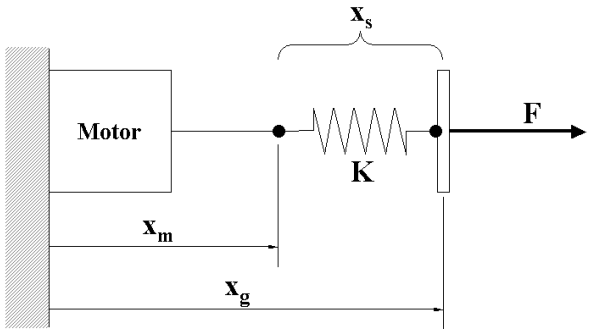

Fig. 1. Robotic tendon model: motor and spring in series

II. Robotic Tendon Model and Stiffness Control

Use of the term Robotic Tendon implies an analogy to human physiology. Mentioned earlier, the simple inclusion of a spring to a linear actuator can provide energy and power savings to the design of a wearable robotic device. The premise of the following development is that the human muscular system uses the advantages inherent in its elastic nature. Those advantages are a minimization of both work and peak power. In terms of an electric motor, minimizing both average and peak power implies the reduction of requirements for motor size and thus weight. Minimizing work implies a reduction of stored energy supply necessary to fulfill the demands of gait. Figure 1 shows the conceptual configuration of the Robotic Tendon actuator.

In the diagram, x_g represents actuator's end effector position, x_m represents the motor's position at the backside of the spring. The difference between these two measures is the dynamic length of the spring, which is dependent on free or natural length, stiffness and applied load. The relationship of all of these variables is represented in equation 1 and is easily derived from the diagram[2].

$$x_m = x_g - \frac{F}{K} - d_o \tag{1}$$

Equation 1 determines the motor position necessary to accomplish a desired actuator output force/displacement profile. The variable d_o represents the free length of the spring. Rearranging this equation for force yields equation 2.

$$F = K \cdot (x_g - x_m - d_o) \tag{2}$$

Shown previously by Sugar[5], the spring based actuator represented in Figure 1 can be used to simulate a virtual

spring. In other words, a relationship for actuator motor position, x_m, can be developed that allows the device to exhibit the behavior of any *desired* value of stiffness. From this idea, consider the equation of force for a general Hookean spring, see equation 3.

$$F = K_{des} \cdot (x_g - x_o) + f_{des} \tag{3}$$

Equation 3 can be used to describe the *desired* stiffness behavior of the actuator, where K_{des} is the desired stiffness, x_o is the virtual home position and f_{des} is the simulated preload. The *desired* force/stiffness behavior in equation 3 can be substituted into the motor position relationship, equation 1.

$$x_m = \left(1 - \frac{K_{des}}{K_{act}}\right) \cdot x_g + \frac{K_{des}}{K_{act}} \cdot x_o - \frac{f_{des}}{K_{act}} - d_o \tag{4}$$

The term K_{act} in equation 4 is the actuator's inherent, physical spring stiffness. However, following the relationship detailed in equation 4 gives the actuator the desired force behavior described in equation 3.

HUMAN GAIT

Gait is a recurring pattern of leg and foot movements, rotations, and torques. Due to its repetitive nature, the discussion of gait is done in terms of percentages of a gait cycle. A gait cycle is defined for a single leg and begins with the initial contact of the foot with the ground or 'heel strike'; the conclusion of a cycle occurs as the same foot makes a second 'heel strike'. To illustrate a typical pattern of gait, consider the kinematics and kinetics of a normal ankle[6], figure 2. Notice that the ankle moment (torque) data is normalized by body weight, kg.

In this figure, peak ankle moment occurs at roughly 45% of the gait cycle and at a value of -1.25 Nm/kg. The negative sign represents the physiological direction for which the moment occurs, and in this case, peak moment is acting to move the foot in a toes down direction. At the point at which the peak moment occurs, the ankle angle begins a rapid desent to its lowest overall value of -24^o at 60% of the gait cycle. The region of gait approximately between 45% and 60% of the gait cycle is known as 'push off'. At the conclusion of 'push off', now considered 'toe off', the leg initiates 'swing' and the foot is then positioned for the next 'heel strike'.

III. ANKLE GAIT CONTROL CONCEPT

Human ankle gait information was analyzed in terms of stiffness using methods proposed by previous researchers [7][8]. However, rather than just focusing on only the 'second rocker' phase of gait [8], the entire stance phase of the ankle was analyzed. The results of this analysis created a division of stance phase of ankle gait into five zones, illustrated in figure 3.

The analysis showed that three of these five zones can be described by linear stiffnesses, with goodness of fit values greater than 0.97. The circled number zones identify these

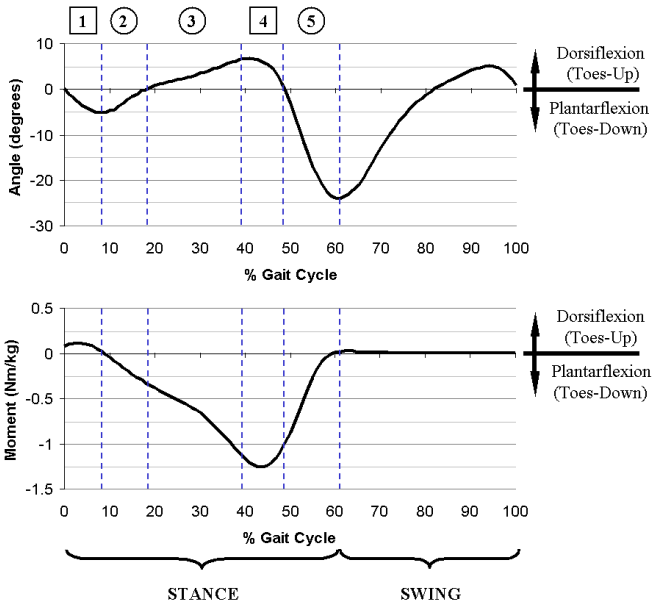

Fig. 2. Normal Ankle Gait: Kinematics and Kinetics.

linear regions in figure 3. In contrast, the remaining two zones are decidedly non-linear and are regions of constant velocity (represented by the numbers with square borders).

In terms of a robust control approach, these transitions between zones will need to be detected so that the logic of such a controller can be switched accordingly. In work by Pappas, et al. [9] a method is described for the reliable detection of phases of gait. Using a similar approach, events within streaming gait data can be observed to serve as the cues necessary for appropriate temporal control transitions. Using switching logic to change the controller behavior simplifies the controller complexity.

In our previous work [2], logic for the controlled actuator behavior rested solely on the timing of an embedded gait pattern that was scaled to match the speed of an operator (device wearer). With the present proposed method, the controller response is not dependent on timing at all. Thus the operator can update speeds and strides dynamically with no additional lag in the system's response.

A. Control Logic

The five zones of stance described can be represented using two simple control models. The first is simply a standard velocity control approach, i.e. the system is set to maintain a fixed velocity. The second model is the stiffness control relationship described in equation 4.

In the stiffness control approach, the *desired* output stiffness behavior is dictated by normative gait. However, the choice of actual stiffness must be determined by the actuator designer.

The Robotic Tendon's construction is conceptually similar to that of the human musculotendon complex in that each feature both active and passive components. A review of able

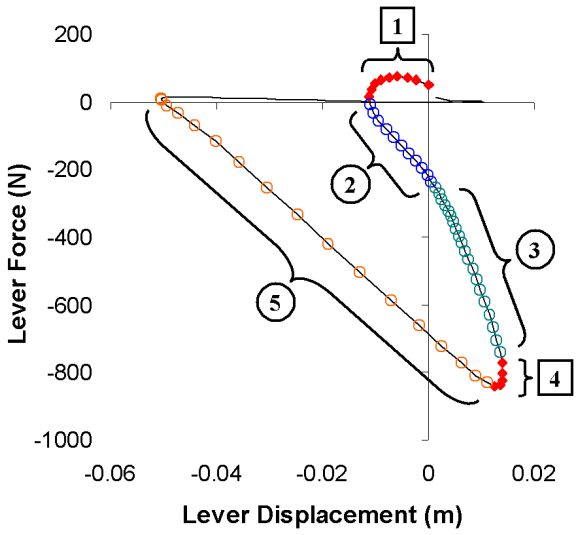

Fig. 3. Lever Force/Displacement: Normal ankle gait pattern at actuator end effector (lever length = 0.12 m).

Zone	Zone Begin	Control Mode
1.	Heel Strike (0-8%GC)	VELOCITY (match Swing velocity)
2.	$\dot{\theta} = 0$ (8-18%GC)	STIFFNESS ($K_{des} \cong 1.35 \cdot K_{act}$)
3.	$\theta = 0$ (18-39%GC)	STIFFNESS ($K_{des} \cong 3 \cdot K_{act}$)
4.	Heel Off (39-48%GC)	VELOCITY (matches Zone 3 velocity)
5.	Peak Moment (48-62%GC)	STIFFNESS ($K_{des} = K_{act} \Rightarrow$ HOLD CMD)
Swing	Near Zero Moment	RESET FOOT

TABLE I
ROBUST CONTROL CONCEPT DESCRIPTION

bodied gait literature [6][10][11][12] shows that ankle plantarflexor EMG cease activity at about 50% of the gait cycle. The same point at which peak plantarflexion power occurs. One implication of this is that the passive properties of the plantarflexors that are providing 100% of the power/energy to the last part of the stance phase of gait.

However, recent research involving ultrasound measurement of plantarflexor muscles during gait show that muscular contractions are still occurring at these later stages [13][14][15]. The difference between EMG measurements and measured muscular contraction is due to lag in electrochemical initiation and the muscle's mechanical response.

Nevertheless, using the latter idea as a guide, the robot gait motor control scheme reduces to a *stretch*, *hold* and *release* strategy. *Stretch* during loading, *Hold* at peak power, and *Release* the stored elastic energy. The Robotic Tendon actuator can operate in this way by setting the actuator's true or physical stiffness to that measured in zone five, thus setting the desired stiffness equal to the actual stiffness in equation 4. As an overview to the robust controller logic, the control method and zone transition identifiers are described in table I.

Zone 1: This zone occurs over the first 8% of the gait cycle. It begins at heel strike and ends when the ankle angular velocity, $\dot{\theta}$, crosses zero, or when the peak plantarflexion of 'weight acceptance' is reached. Constant motor velocity is maintained through this zone at a level proportional to the motor's speed achieved during the previous swing phase.

Zone 2: This zone spans from 8% to 18% of the gait cycle. Zone 2 ends just after 'foot flat' when the ankle angle, θ, returns to neutral and begins to dorsiflex. In this zone, a constant *desired* stiffness of a value 1.35 times true or actual stiffness is maintained. For example, in equation 4, the desired stiffness will be set to 1.35 times the actuator actual stiffness.

Zone 3: This zone occupies the majority of the 'loading response' from 18% to 39% of the gait cycle. The termination of zone 3 occurs as the heel lifts off (i.e. heel off) the floor. Constant stiffness is maintained with a *desired* stiffness of about 3 times actual system stiffness. It is in this region of control that over 64% of elastic spring loading is accomplished. In equation 4, the desired stiffness will be set to 3 times the actual stiffness.

Zone 4: This zone ranges from 39% to 48% of the gait cycle. Heel off begins this zone and a constant velocity is maintained that matches the motor speed achieved in zone 3. The termination of this zone ends as the peak plantarflexion moment occurs. It is this at this point in time, due to body position, that the body can no longer resist the build up of forces contained within the spring and its stored energy begins to release.

Zone 5: Within this zone, 48% to 62% of the gait cycle, the free energy release of the spring is done. It terminates at the moment the spring is completely unloaded and 'swing' begins. Stiffness control drives this part of the gait cycle. However, matching the true system stiffness to that measured in zone 5 gait data creates a motor command that simply holds its present position. So at the instance that peak plantarflexion moment begins to diminish, the actuator motor simply holds its position, thus allowing the energy release to occur.

In equation 4, the desired stiffness equals the actual stiffness and x_o is the position at the start of zone 5. The desired force in equation 4 is equal to the force at the start of zone 5 and d_o equals the natural free length of the spring. In this zone, the motor's position will be held to a constant value.

Using basic sensor information at the foot and ankle, the

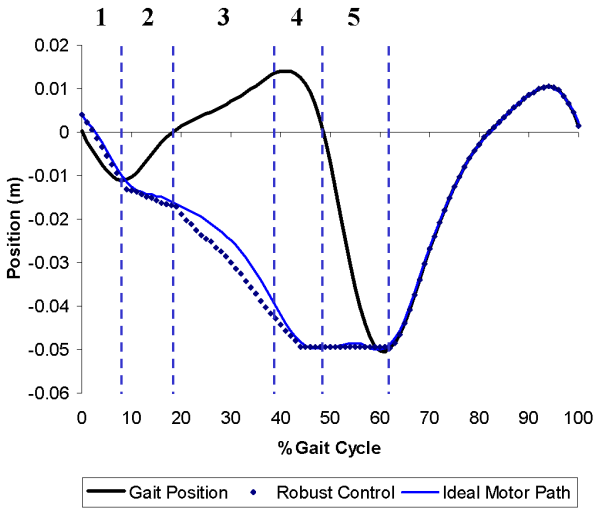

Fig. 4. Simulated Motor Position

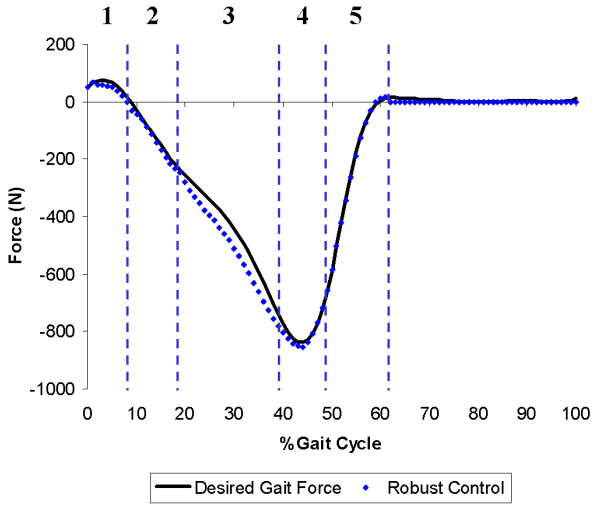

Fig. 5. Predicted Force Output

transition of stance zones can be detected. Many potential sensor methods are available. As an example a combination of a heel switch, a rate gyro, encoder and potentiometer could be used. The focus of this paper is to describe a method of robot control for the stance phase of gait. Swing was not analyzed in this paper. In our current work, the actuator follows a commanded swing profile to dorsiflex the foot.

IV. Simulation Results

The robust control concept was simulated using only normative ankle kinematics (angles) data and selected transition points as described in table I. For convenience the analysis was done with respect to the actuator's displacements and forces, rather than in terms of ankle angles and torques. Also, consistent with our previous work [2], the simulation assumed a 80kg body mass and a 0.12m lever arm acting at the ankle. These values are used to convert ankle angles and torques into simple displacements and forces.

It should be noted that following simulations results are not an evaluation of any specific controller, but rather of a conceptualized desired motor path on which a controller design shall be based. For example, in previous work by Sugar [5] a proportional and derivative position controller was used to drive the desired actuator stiffness behavior. For the current ankle control concept, slightly more complicated controller logic will be needed.

Using equation 4 to describe the stiffness control portions of the gait cycle, desired stiffnesses of 18,660 N/m, 40,957 N/m, and 13,796 N/m were used for zones 2, 3, and 5 respectively. Actual stiffness of the spring was 13,796 N/m. Figure 4 shows the resulting motor positions predicted using both constant stiffness and constant velocity control schemes.

The figure shows both ankle output position, x_g, and motor position, x_m. For convenience, the data is plotted for a zero length spring, thus the differences between ankle gait position and motor path is the deflection stored within the physical actuator spring. Comparing the simulated robust control approach (equation 4) to the ideal motor path (equation 1) shows a good correspondence. This ideal path was generated using the methods described in our previous work [2] and an actuator stiffness value of 13,796 N/m.

However, the robust control approach tends to slightly over deflect the spring during zone 3 control. Based upon the differences between gait position and the robust control simulated motor path, the resulting system forces can be calculated. The force results calculated are presented in figure 5.

The curves plotted in figure 5 are the required forces measured from normal gait data [6] and the forces calculated from the robust control simulation. Again, there is a good correspondence between these two sets of data. The deviation between the two curves in zone 3 is due to the slight over deflection observed in figure 4. The peak differences in force shown is calculate to be only about 70 N.

V. Conclusions

The simulation results of this analysis are encouraging. However, the simulations are based upon a number of assumptions. In particular, the division of stance zones described is dependent on literature sources in combination with the specific gait data set analyzed. Once testing of this technique has begun, refinement of the transition definitions maybe required.

The reason the simulation results are encouraging is that these results were driven only by measured output positions derived from human gait data. This means that for the stiffness control portion of the gait cycle, operator ankle position is the only input parameter to the model. The system will behave simply as a virtual spring during these zones until the next transition point occurs.

The next step for this work is to add in the appropriate sensors necessary to implement this control approach on our

latest Robotic Tendon prototype. Additionally, an analysis of our *structure control* actuator approaches [16] using this technique can also be done. Whereas the final goal of this work is to create an intuitive and robust control methodology for our lightweight, energy efficient actuators and wearable assistance device.

REFERENCES

[1] K. W. Hollander and T. G. Sugar, "Concepts for compliant actuation in wearable robotic systems," in *US-Korea Conference (UKC2004)*, 2004.

[2] K. W. Hollander, R. Ilg, T. G. Sugar, and D. Herring, "An efficient robotic tendon for gait assistance," *ASME Journal of Biomechanical Engineering*, vol. 128, pp. 788–791, 2006.

[3] T. G. Sugar and V. J. Kumar, "Design and control of a compliant parallel manipulator for a mobile platform," in *ASME Design Engineering Technical Conferences and Computers in Engineering Conference (DETC)*, 1998.

[4] D. W. Robinson, J. E. Pratt, D. J. Paluska, and G. A. Pratt, "Series elastic actuator development for a biomimetric walking robot," in *IEEE/ASME International Conference on Advanced Intelligent Mechatronics*, 1999, pp. 561–568.

[5] T. G. Sugar, "A novel selective compliant actuator," *Mechatronics*, vol. 12, no. 9-10, pp. 1157–1171, 2002.

[6] M. W. Whittle, *Gait analysis : an introduction*, 2nd ed. Oxford: Butterworth-Heinemann, 1996.

[7] D. J. Stefanyshyn and B. M. Nigg, "Dynamic angular stiffness of the ankle joint during running and sprinting," *Journal of Applied Biomechanics*, vol. 14, pp. 292–299, 1998.

[8] R. B. Davis and P. A. DeLuca, "Gait characterization via dynamic joint stiffness," *Gait and Posture*, vol. 4, pp. 224–231, 1996.

[9] I. P. Pappas, M. R. Popovic, T. Keller, V. Dietz, and M. Morari, "A reliable gait phase detection system," *IEEE Transactions on Neural Systems and Rehabilitation Engineering*, vol. 9, no. 2, pp. 113–125, 2001.

[10] D. A. Winter, *The Biomechanics and Motor Control of Human Gait: Normal, Elderly and Pathological*, 2nd ed. Waterloo, Ontario, Canada: Waterloo Biomechanics, 1991.

[11] J. Perry, *Gait Analysis : Normal and Pathological Function*, 1st ed. Thorofare, New Jersey: SLACK Incorporated, 1992.

[12] A. L. Hof, H. Elzinga, W. Grimmius, and J. P. K. Halbertsma, "Speed dependence of averaged EMG profiles in walking," *Gait and Posture*, vol. 16, pp. 78–86, 2002.

[13] G. A. Lichtwark and A. M. Wilson, "Interactions between the human gastrocnemius muscle and the achilles tendon during incline, level and decline locomotion," *Journal of Experimental Biology*, vol. 209, pp. 4379–4388, 2006.

[14] G. A. Lichtwark, K. Bougoulias, and A. M. Wilson, "Muscle fascicle and series elastic element length changes along the length of the human gastrocnemius during walking and running," *Journal of Biomechanics*, vol. 40, pp. 157–164, 2007.

[15] M. Ishikawa, P. V. Komi, J. Grey, Michael, V. Lepola, and G.-P. Bruggemann, "Muscle-tendon interaction and elastic energy usage in human walking," *Journal of Applied Physiology*, vol. 99, pp. 603–608, 2005.

[16] K. W. Hollander, T. G. Sugar, and D. E. Herring, "Adjustable robotic tendon using a 'jack spring'," in *IEEE International Conference on Rehabilitation Robotics (ICORR2005)*, Chicago, IL, 2005.

Proceedings of the ASME 2007 International Design Engineering Technical Conferences & Computers and Information in Engineering Conference
IDETC/CIE 2007
September 4-7, 2007, Las Vegas, Nevada, USA

DETC2007-34512

THE SPARKY (SPRING ANKLE WITH REGENERATIVE KINETICS) PROJECT: DESIGN AND ANALYSIS OF A ROBOTIC TRANSTIBIAL PROSTHESIS WITH REGENERATIVE KINETICS

Joseph K. Hitt*, Ryan Bellman*, Matthew Holgate*, Thomas G. Sugar[+], Kevin W. Hollander++

Department of Mechanical and Aerospace Engineering*
Department of Engineering[+]
Arizona State University
Tempe, Arizona 85287-6106
Email: joseph.hitt@asu.edu

Augspurger-Komm Engineering, Inc. [++]
Scottsdale, AZ 85260

ABSTRACT

Even today's most sophisticated microprocessor controlled ankle-foot prosthetic devices are passive. They lack internal elements that actively generate power, which is required during the "push-off" phase of normal able-bodied walking gait. Consequently, lower limb amputees expend 20-30% more metabolic power to walk at the same speed as able-bodied individuals. Key challenges in the development of an active ankle-foot prosthetic device are the lack of high power and energy densities in current actuator technology. Human gait requires 250W of peak power and 36 Joules of energy per step (80kg subject at 0.8Hz walking rate). Even a highly efficient motor such as the RE75 by Maxon Precision Motors, Inc. rated for 250W continuous power with an appropriate gearbox would weigh 6.6 Kg. This paper presents the first phase of the *Spring Ankle with Regenerative Kinetics (SPARKy 1)*, a multi-phased project funded by the US Army Military Amputee Research Program, which seeks to develop a new generation of powered prosthetic devices based on the Robotic Tendon actuator, that significantly minimizes the peak power requirement of an electric motor and total system energy requirement while providing the amputee enhanced ankle motion and "push-off" power. This paper will present data to show the kinetic advantages of the Robotic Tendon and the electro-mechanical design and analysis of SPARKy 1 that will provide its users with 100% of required "push-off" power and ankle sagittal plane range of motion comparable to able-bodied gait.

Index Terms – SPARKy, Ankle-Foot Prosthesis, Power/Energy Density, Powered Prosthesis, Power Amplification.

INTRODUCTION

A. BACKGROUND

The SPARKy Project is a multi-phased spiral development effort led by Arizona State University Human Machine Integration Lab with team members from Arise Prosthetics, Robotics Group, Inc. and St. Louis University Human Performance Lab. This project will develop what is most likely the first-of-its-kind smart, active and energy-storing transtibial prosthesis. The project seeks to tackle several leading technical challenges that prevent the development of a truly biomimetric foot-ankle prosthetic device. Currently a device like SPARKy does not exist because of several challenges that include (1) prohibitively low power and energy density in traditional actuation schemes, and (2) development of a control methodology that translates user intent into human like movement. The team's approach is to leverage both the vast and considerable efforts in the rehabilitation and robotics communities.

The rehabilitation community has made significant improvements in prosthetic and orthotic technologies in recent years. Several prosthetic companies have produced devices that are more comfortable, provide life-like cosmeses, provide significant energy return and are now even computer controlled. New high performance composite materials and polymers have

Copyright © 2007 by ASME

made sockets and liners more comfortable and prosthetic feet and pylons much more energy efficient. A world-class below the knee amputee sprinter using a high performance composite prosthesis can now sprint the 100 meters only one second off of the able-bodied world record [1]. Energy storage and return devices allow faster walking velocity and better terrain negotiation [2-4]. They have increased range of motion; they store and return energy; and they reduce needed energy requirements [5-9]. Microprocessor controller components such as the Rheo Knee use artificial intelligence to change joint angles and dampen joint motion in response to the environment and individual gait style [10].

Similarly, the robotic research community has made significant advances in wearable robots, control and actuation. In response to government initiatives, several exoskeleton devices that provide enhanced human performance have been developed. In addition, with renewed energy, the community has also crossed over into robotic rehabilitation devices. From large in-clinic to small portable devices that provide gait support, robots are currently at all stages of product realization. Hydraulic, pneumatic, direct-drive, series-elastic, electroactive polymer-based and many other actuation schemes are also at varying stages of research and development. Many other researchers are working on wearable robot control. From the highly publicized neuro-controlled bionic arm [11] to embedded gait pattern control [12], EMG motion control [13,14], and state based control [15] are all bearing fruit. For example, the Proprio Ankle by Ossur is a commercially available state control device that modulates ankle angle based on the environment, gait, and condition to better mimic the kinematics (opposed to both kinematics and kinetics) of the lost limb [16].

The research community has come a long way since the days of wooden pegs. Even still, today's foot-ankle prosthetic devices are still largely passive and untunable. They typically use rubber like springs or leaf springs made from carbon composite materials. They do not contain powered elements that assist in locomotion. Amputees must rely on the limited spring-back passive devices provide and modify their gait to help propel themselves forward. Amputees cannot drastically change their locomotion conditions due to the unchangeable parameters of their prostheses. Carrying heavy loads or transitioning from walking to running using a single device remains a challenge. Amputees frequently change from one device to another to meet these conditions. Even though these represent a vast improvement from the rigid and damper based systems, they are inadequate for majority of high level amputees especially the Military amputee, the intended user of SPARKy.

B. ANKLE COMPLEX DURING WALKING GAIT

Gait is a cyclical pattern of leg and foot movement that creates locomotion. Gait is commonly discussed in terms of a percentage of a single gait cycle. A gait cycle is defined for a single leg and begins with the initial contact of the foot with the ground or 'heel strike'; the conclusion of a cycle occurs as the same foot makes a second 'heel strike'. To illustrate a typical pattern of gait, consider the illustration of the ankle complex during stance phase of a single cycle of gait, figure 1 and the kinematics and kinetics of a normal ankle, figure 2. Notice that in figure 2, peak ankle moment occurs at roughly 45% of the gait cycle and at a normalized value of -1.25 Nm/kg. The negative sign represents the physiological direction of the plantarflexing ankle. The foot rotates downwards to push off from the ground. At the point at which the peak moment occurs, the ankle angle begins a rapid decent to its lowest overall value of -24 degrees at 60% of the gait cycle. The region of gait approximately between 45% and 60% of the gait cycle is known as 'push off'. At the conclusion of 'push off', now considered 'toe off', the leg initiates 'swing' and the foot is then positioned for the next 'heel strike'.

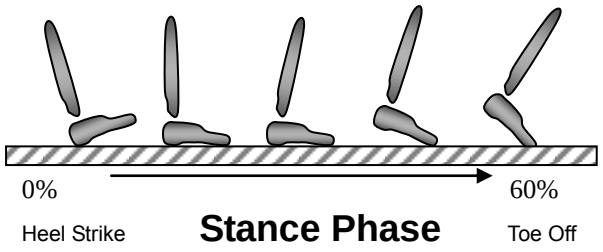

Figure 1. Stance phase of a single gait cycle. 60-100% of gait is the swing phase, not shown [17].

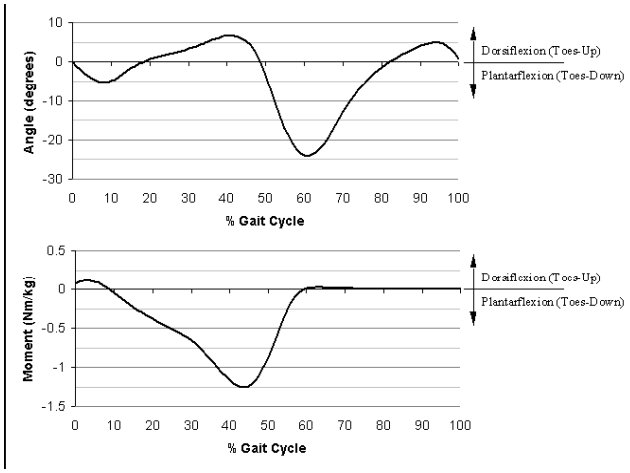

Figure 2. Normal Ankle Gait: Kinematics and Kinetics [18].

C. ENERGY AND POWER DENSITY

An ankle joint requires 250W of peak power and in the ideal direct drive scenario 36 Joules of energy per step (80kg subject at 0.8Hz walking) [19]. This is significantly more than what is required at the knee or hip joints. An actuator and transmission system that can provide the necessary peak power would most likely be an electric motor and gearbox system that under a traditional approach weights 6-7 kg. Providing 36

Copyright © 2007 by ASME

Joules of energy per step would require a significantly larger battery for a modest 8 hours of operation. Other actuator technologies that are used in gait therapy devices such as pneumatic and hydraulic actuators like the "McKibben Muscle" can provide the required power with a small device but are impractical as portable devices because they require separate pumps or other air supply [20]. Electroactive polymers have been used to demonstrate stationary bicycle pedaling and bicep movement in a human size skeleton but even the most promising of these materials, the dielectric elastomer, would require more than 5000V of electricity for operation of a much smaller 100W actuator [21].

II. THE ROBOTIC TENDON AND ESAR FEET

A. THE ROBOTIC TENDON

The Robotic Tendon [19] is a small and lightweight actuator that features a low energy motor that is used to adjust the position of the helical spring using a very simple position controller. Figure 3 illustrates how the desired spring deflection and consequently via Hookes Law the desired force is achieved using a spring. As the ankle rotates over the foot during stance phase, a lever position profile as shown in figure 3 is obtained. By correctly positioning the motor, a desired spring deflection as shown in the shaded area of figure 3 is obtained. A heavy, powerful, impedance controlled motor is not needed because the Robotic Tendon stores a portion of the stance phase kinetic energy and additional motor energy within the spring. The spring releases its stored energy to provide most of the peak power required during push off. Therefore, the power requirement on the motor is significantly reduced. As described in [19], peak motor power required is 77W compared to 250W for a direct drive system in the 80kg subject at a 0.8hz example. And consequently, the weight of the Robotic Tendon, at just 0.95kg, is 7 times less than an equivalent direct drive motor and gearbox system that is required to provide the necessary peak power. In addition, ideal energy requirements, as determined by the integration of the power curves, were reduced from nearly 36 Joules to 21 Joules per step (80kg subject walking at 0.8hz) significantly reducing battery requirements so that a commercially available battery pack worn in a fanny pack could potentially power SPARKy for 8 hours of continuous operation.

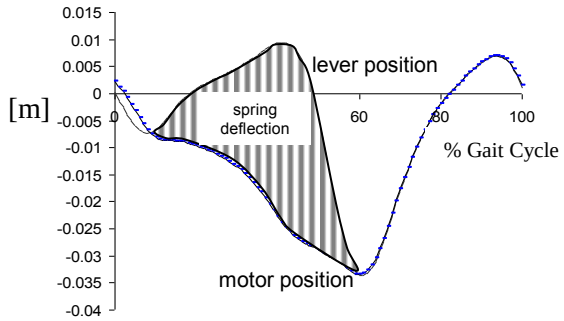

Figure 3. Desired spring deflection, shaded area, is achieved by controlling the motor position and capitalizing on the cyclical nature of gait [17]. As the tibia rotates about the stance foot, the lever extends the springs. Simultaneously, the motor extends the spring in the opposite direction to achieve the desired spring deflection and via Hooke's Law the forces required to generate the required ankle moments for walking.

B. ROBOTIC TENDON TEST DATA

In a recent experiment, we tested two able-bodied subjects (male, 60kg and female, 70kg both at 0.8hz) outfitted with an orthotic device with a Robotic Tendon on a treadmill. The device was configured to provide 50% assistance, which was done by scaling the body weight by half to determine the power requirements. The purpose was to confirm our new dynamic control scheme [12] and to confirm that by harnessing the stored elastic energy in the mechanical elements, motor requirements were significantly reduced – a critical requirement towards portability.

As described in detail in [17], a 70kg subject walking with 50% assistance with a typical gait would require a peak power of approximately 108W. Consequently, a direct drive system would be forced to provide 100% of the 108W. A tuned Robotic Tendon reduced the peak power required by the motor to be 43W. This is a significant reduction in motor requirement and therefore, size and weight.

Results of our initial evaluation can be seen in figure 4. Input power was determined by the product of the linear velocity and the force at the motor. Output power was determined by the product of the linear velocity of ankle displacement and the force acting on the spring. The measured output peak power was 131W. The corresponding input power generated by the motor was 55W. This means that the spring provided 76 W of the 131W of peak power. The output was 238% higher than the power generated by the motor – a 2.38 power amplification. This is a very positive result in terms of kinetic efficiency. This demonstrates the power of harnessing spring energy in gait assistance.

Copyright © 2007 by ASME

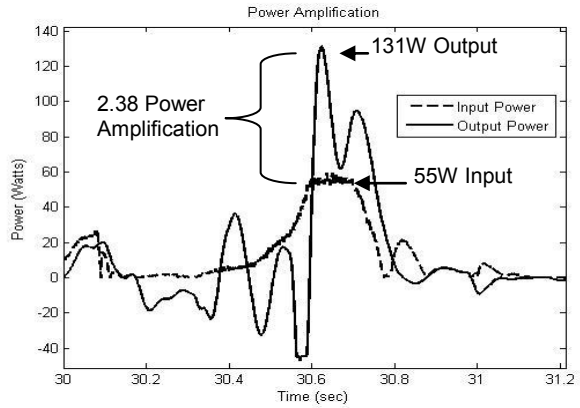

Figure 4. The input power is the power generated by the DC motor. The output power is the combination of motor and spring power. Note: output power profile includes noise due to the use of numerical differentiation method [17].

C. ENERGY STORAGE AND RETURN (ESAR) FEET

Research shows that energy storage and return (ESAR) devices compared to the SACH Foot provide better performance. When used, they allow faster walking velocity and better terrain negotiation [2-4]. They have increased range of motion; they store and return energy; and they reduce needed energy requirements [5-9]. Sienko et al in their study [22], compared the power generation capability of the several leading ESAR feet commercially available today. For example, they report that the Seattle Lite foot creates a peak power generation of 0.73 W/kg and the Genesis II Plus feet, with the largest power generation, create 1.47 W/kg. Since a typical person would generate approximately 4 W/kg, leveraging ESAR devices have the potential to supply 35% of the peak power requirement during push off. Schneider et al [23] report in their study of BK children that the Flex Foot generated 0.115J/kg and 1.36W/kg at 0.9 m/s and 0.133 J/kg and 1.90W/kg at 1.3 m/s. This report suggests that the Flex Foot may be able to provide up to 45% of the peak power and 30% of the energy required for walking gait. Therefore, SPARKy will include ESAR feet in its design.

All ESAR feet use deformable forefoot keels to store and release energy as a leaf spring mechanism [24], figure 5. Therefore keel stiffness and the amount of input energy dissipated by the foot before "push-off" becomes a significant criterion in our prosthesis selection process. Geil investigated the stiffness and hysteresis for eleven prosthetic feet [24]. The tests revealed that the feet fell in four general levels of stiffness with the most stiff at 76 KN/m, more stiff at 60.6 KN/m, less stiff at 38.4 KN/m, and least stiff at 27.7 KN/m. He also found that the least stiff foot, the College Park TruStep returned the most energy at 5.77J but was the most inefficient losing 31% of energy. Generally, the stiffest feet, 76KN/m, were the most efficient at 0.85 efficiency but the energy return was only at about 4J.

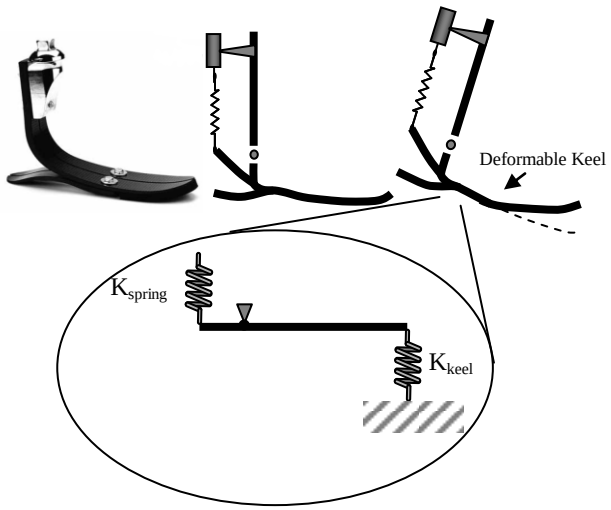

Figure 5. Flex-Foot Vari-Flex by Ossur pictured and conceptualized to illustrate the deformable keel. The spring and lever model is a simplistic view of the keel and the spring in the Robotic Tendon. The interaction between the two springs must be considered as we select both the keel and the Robotic Tendon spring [25].

III. SPARKY DESIGN

A. OBJECTIVES

As the title suggests with the term "Regenerative Kinetics," the primary objective is to develop a new generation of powered prosthetic devices based on lightweight, *energy storing* elastic elements that will significantly minimize the peak power requirement of the motor and total system energy requirement while providing the amputee enhanced ankle motion and "push-off" power.

The SPARKy Project is a multi-phased effort that will culminate with the functionality to support walking in an unstructured environment for up to 8 hours with a single charge of a wearer portable battery pack and support structured running.

This paper describes the design and analysis of the Phase 1 SPARKy. Phase 1 specifications include: (1) tabletop controls to start, stop and modulate speed on a linear walking surface, (2) capability to provide 100% of the required power for gait and sagittal plane range of motion equivalent to able-bodied gait, and (3) with use of elastic mechanical elements, mechanism design and motor control, significantly reduce the power and energy output burden on an electric motor so that the size and weight of the electric motor and batteries will be reduced to a lightweight, portable level. Phase 1 SPARKy will be tested on at least two below the knee amputees.

B. MECHANICAL DESIGN

The mechanical design of SPARKy has presented several obstacles that needed to be overcome to maximize the energy output without limiting the comfort, capability and safety of the robot. Figure 6 show two perspectives of the modeled

Copyright © 2007 by ASME

prosthetic. A new parallel two spring Robotic Tendon is attached to a custom aluminum pylon and to a commercial FS3000 Keel from Freedom Innovations via a lever. The four sensors that provide closed loop feedback are not shown in these illustrations. The computer and electronics are tethered in a table top configuration for the Phase 1 SPARKy.

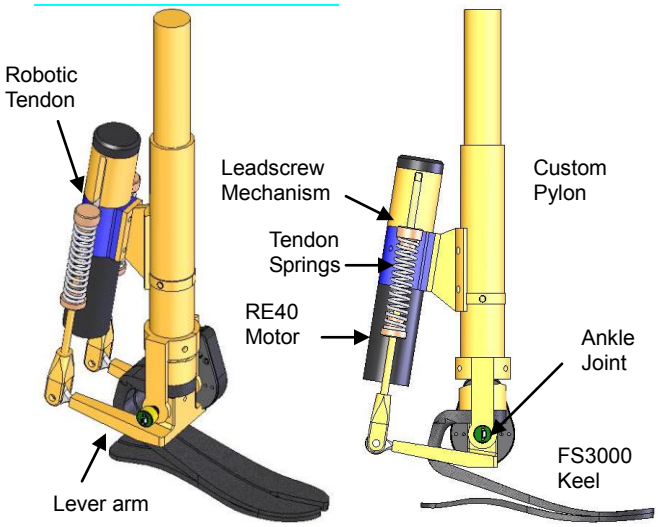

Figure 6. Isometric and side views of current design as modeled in Solidworks. The RE40 motor coupled with the robotic tendon provide a dynamic moment about the ankle joint.

While the Robotic Tendon itself was already designed and tested at the inception of this project, it was not modeled for this particular application. These designs were modified to accommodate a larger motor as well as larger forces.

For tuning purposes, there was also a great need for adjustability in many aspects of the design. As the spring stiffness requirement changes with the weight of the user, the system must incorporate interchangeability with springs. It was also desired that the lever arms have some level of adjustment, as a minute change in the length of the lever arm can have drastic effects on the power generation. This was done by using male threaded rod ends.

It was determined during the design phase that locking the ankle joint and isolating the Robotic Tendon during certain phases of gait would further increase the energy storage potential in the keel and Robotic Tendon system. The method of achieving this lock utilizes the user's body weight to cause a small compression of a spring-loaded locking pin after heel strike. The pin is then released using a solenoid.

Future possibilities were also taken into consideration in this design. A common complaint by users of such prosthetics is the discomfort associated with stepping on a laterally slanted surface due to the rigidity of the prosthetic in that dimension. While the split-keel design of this foot alleviates this to some extent, further advantage may be taken by the dual spring design of the robotic tendon. The current design has an additional axis in the ankle that would allow for the springs to operate separately in the event of an ankle "roll," allowing approximately 17 degrees in each direction. For phase 1, however, this motion will be further limited by rubber bushings on each side of the central shaft.

C. ELECTRONICS, SENSORS AND COMPUTING

SPARKy is controlled in real time using Real Time Workshop and Simulink from Mathworks. The Simulink model is compiled on to the embedded target PC with the xPC Target Operating System. An encoder at the motor, an encoder at the ankle joint, a strain gauge on the keel, and an optical switch embedded at the heel provides the necessary sensor feedback. Advantech's 650MHZ PC-104 with 512MB on board memory is selected to run the system. A multifunctional I/O board from Sensoray Co., Model 526, which is connected to the PC104 via an ISA bus, controls a RE-40 Maxon DC motor with encoder feedback. In the current prototype, the computing is done with the system mounted in a separate table top enclosure. Future prototypes will make use of batteries and a computing system to be worn by the user and eventually fully contained in the unit.

D. CONTROL

Together with power and energy density, computer control of prostheses remain a significant challenge. Efforts towards control methodology that produce biologically realistic movement in prostheses and orthoses began in the early 1960s with work such as the Belgrade Hand. However, even after a half century of work, achieving human like control is proving to be very difficult. Work by Au et al and Ferris et al in EMG position control [13-14] and by Pappas et al in state based control [15] seems promising because of its simplicity. Sugar's effort to reduce the control problem using compliant simple force control [26] is a key finding towards simplifying control methodology and served as our starting point with the Robotic Tendon.

The SPARKy controller has a predetermined gait pattern, which is based on able-bodied gait data from [18] and kinetic analysis from [19], expressed as a time-based function embedded in the controller, which drives the motor controller and thus the system. Gait is initiated at heel strike with activation of an optical switch embedded in the heel. As the user initiates gait, the motor drives the lead screw nut through a pattern predetermined for each subject with closed loop feedback. The ankle, however, is not forced to follow the specific pattern because the compliant spring is between the motor and user, safely absorbing environmental irregularities such as a rock under foot or user errors. This inherent compliance not only provides for a safer interface, but allows for a much simpler control scheme because we no longer require high bandwidth high precision force control.

Copyright © 2007 by ASME

IV. DESIGN ANALYSIS

A. Freedom Series 3000 KEEL

The FS 3000 Keel was selected for SPARKy primarily for its geometry. Its unique pylon interface allows for a robust design platform. However, as part of its selection, we conducted a force-deflection test to determine its stiffness using Geil's method [24]. The keel rated for an average walking male, plantarflexed at 12 degrees, was loaded from 0 to 600N, 0 to 800N and 0 to 1000N at 1mm/sec using the Material Testing System (MTS) SINTECH 1/S. The average of the linear slopes of the three force-deflection curves was used to approximate the equivalent keel stiffness to be 76KN/m. A finite element analysis of the foot using COSMOS revealed its deflection pattern and stress levels, figure 7, when loaded in a similar manner as the force-deflection testing. The stain gauge which will be used to determine the deflection in the keel will be placed at the highest stress area based on our FEA results.

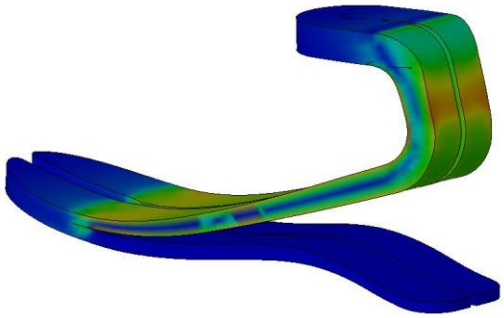

Figure 7. Finite element analysis of the FS3000. The red color represents the highest stress levels. Loading and constraint parameters replicated the condition at peak moment during the "push-off" phase.

B. KINETIC AND KINEMATIC ANALYSIS

It is understood from a pogo stick and a hopping robot example that springs alone are not enough to provide 100% of the power required for its dynamic tasks. Motors alone are too expensive in terms of power and energy. What combination of actuator, Robotic Tendon spring stiffness, ESAR keel stiffness, ankle joint motion and control scheme is optimal? To answer these questions, multiple models were derived, each with varying combinations of these design parameters. Ankle joint angle and moment data used in the simulation are from able-bodied data generated by inverse dynamics of motion capture and force plate test data published by Whittle in [18]. The remaining kinetic and kinematic analysis is derived using a quasi-static approach. MATLAB simulation of the models showed that a power amplification of up to 6 may be possible. Presented here are 2 of those models selected for SPARKy Phase 1 for their simplicity and robustness. Simulation of these 2 models showed that a power amplification of 4.26 and 3.25 is possible while maintaining gait kinematics and kinetics similar to able-bodied persons.

All of the models used the basic premise of the Robotic Tendon. As the tibia rotates over the stationary ankle (ankle rocker), the tendon spring has the potential to become extended by this motion. In addition, the keel deflects due to the dynamics of gait, figure 8. The two models presented here have different spring stiffnesses, ankle joint motion and control laws.

SIMPLE SERIES MODEL

In the simple series model, the keel and the Robotic Tendon springs are in series, therefore, the moment in the keel is equal to the moment in the Robotic Tendon. Motor position is controlled so that the moment of the Robotic Tendon matches that of the able-bodied moment data, Equation (1). Note that K_a is the keel stiffness, K_s is the spring stiffness, B is the radius of the keel deflection, d is the moment arm due to the keel deflection. See figure 9.

$$M_A(t) = M_{keel}(t) = M_{RT}(t) \quad (1)$$

$$\text{where :}$$

$$M_A \ \text{from published AB data [18]}$$

$$M_{keel}(t) = K_a Bd\varphi(t)$$

$$M_{RT}(t) = K_s(x(t) - l\theta(t))l$$

Solving Equation (1) for motor position, x(t), gives the expression in Equation (2):

$$x(t) = l\theta(t) - \frac{K_a Bd}{K_s l}\varphi(t) \quad (2)$$

The assumed force in the Robotic Tendon is given by Equation (3):

$$F(t) = \frac{M_A(t)}{l} \quad (3)$$

The ideal power generated by the motor to move to position x(t) is given by the product of the force and velocity in the tendon, Equation (4):

$$P_m(t) = F(t)\frac{dx(t)}{dt}$$

$$\Rightarrow P_m(t) = \frac{M_A(t)}{l}\left[\frac{K_a Bd}{K_s l}\frac{d\varphi(t)}{dt} - l\frac{d\theta(t)}{dt}\right] \quad (4)$$

The expression in Equation (4) represents the power required by the motor to generate the desired moment and ankle angle of able-bodied gait published in [18] given that the spring provides the majority of the required power.

Optimization of Equation (4) varying keel stiffness, K_a, and spring stiffness, K_s, showed that a minimum peak motor power profile is achieved by varying K_s as seen in Figure 10. This figure is a surface plot of the peak power at a given spring and

Copyright © 2007 by ASME

keel stiffness. It shows that a spring stiffness of 32000N/m is optimal in terms of minimum peak motor power. At this spring stiffness, the peak motor power is at its lowest value of 80W. Note that as the tendon spring becomes rigid, required motor power reaches that of a direct drive system. And as the tendon spring stiffness reaches zero, required motor power becomes asymptotic.

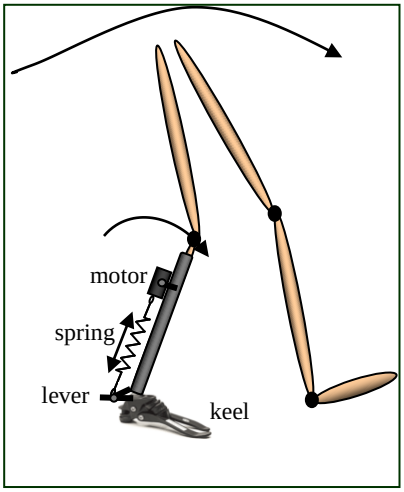

Figure 8. The ankle rocker motion extends the spring and deflects the keel. The motor increases the spring deflection to add additional energy into the spring to support push off. The spring and keel provides the majority of the peak power required during push off [25].

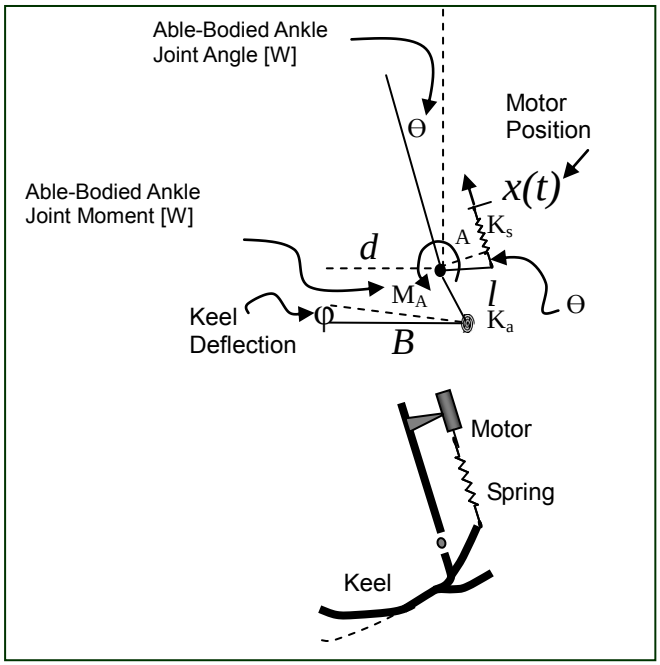

Figure 9. A 2 degrees-of-freedom model with a seismic excitation representing the motor excitation, a torsional spring for the keel and a helical spring between the lever and the motor is shown. The moment due to the keel is a function of φ(t) and the moment due to the spring is a function of x(t)-Θ(t)l. The moment at the ankle is from published information determined using inverse dynamics of motion capture and force plate test data as published in [18].

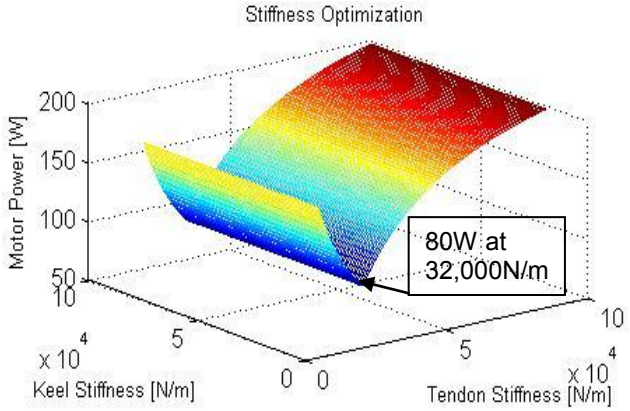

Figure 10. This is a surface plot of the peak power from Equation (4) varying K_a and K_s. Notice that at a spring stiffness of 32,000 N/m, the minimum peak motor power of 80W is achieved. Keel stiffness does not have any bearing in this optimization.

The results are significant because it shows that SPARKy with use of a keel and Robotic Tendon can achieve significant kinetic advantages similar to our previous work with the Robotic Tendon on an orthotic device. This simulation illustrates that with an input power of 80W from the motor, that SPARKy, with use of springs, can deliver the required 260W of peak gait power, which is a power amplification of 3.25. Figure 11, generated from the simulation, shows the motor, gait and keel power profiles. Notice that the motor power peaks at 80W and the gait power peaks at 260W. The keel power profile is not additive because the system is in series. However, notice that this power profile is similar to what is found in literature about ESAR keel power.

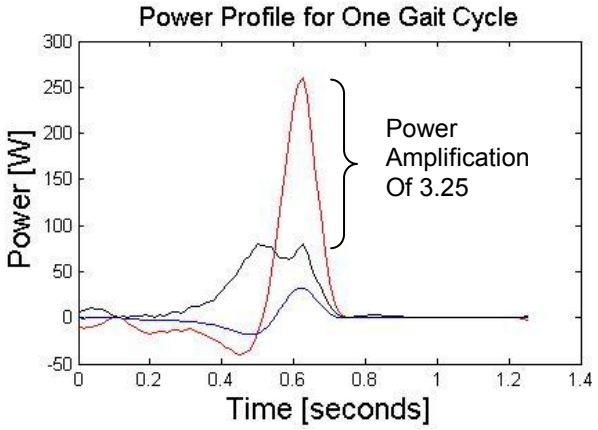

Figure 11. The power profiles for able-bodied gait in red, required motor power in black and power from the keel in blue. (From simulations.)

This series model achieves 100% of the required gait power with less than a third of input power (motor power) by harnessing the energy storage potential of springs. In addition,

Copyright © 2007 by ASME

because the system's joint motion is controlled only by the counter-moments of the tendon spring and keel, kinematics of the system is almost identical to the desired able-bodied gait, see figure 12. Note that the ankle joint motion is identical to the desired able-bodied ankle angle data as seen in figure 2 and total motion of the ankle-foot complex is the summation of the ankle joint motion and keel deflection. This total motion of SPARKy is expected to provide its user with kinematics similar to able-bodied gait kinematics representing a significant improvement from today's state of the art.

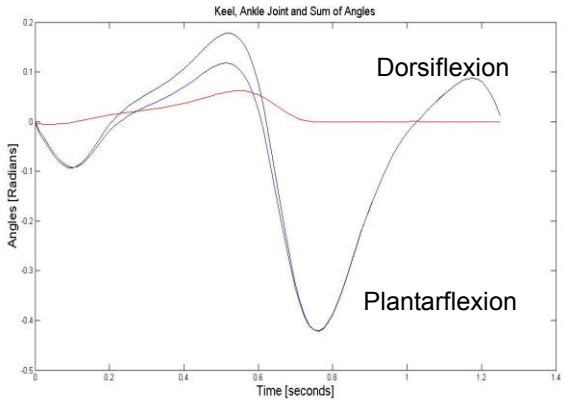

Figure 12. This figure shows the ankle joint angles in blue, keel deflection angles in red and the sum of both in black. (From simulations.)

VARIABLE STIFFNESS MODEL

In this model, through joint motion control and related control scheme, the equivalent system stiffness is varied throughout the gait cycle. And the keel and Robotic Tendon work together to store and release energy during the critical "push-off" phase. By shielding the Robotic Tendon from the dynamics of mid-stance phase of gait by locking the ankle joint, the motor is allowed to work free of external forces to store elastic energy in the tendon spring. This methodology reduces further, the motor power requirements from 80W in the simple series model to 61W in this model. See figure 13. The black line is the required motor power profile. The green line is the power generated by the Robotic Tendon that includes the motor and tendon spring. The blue line is the keel power and the red line is able-bodied gait power. Notice that the peak motor power is at 61W. Also notice that the Robotic Tendon generates a power profile very similar to that of the able-bodied power profile. Summing the Robotic Tendon and keel powers bring the power profile even closer to that of the able-bodied profile.

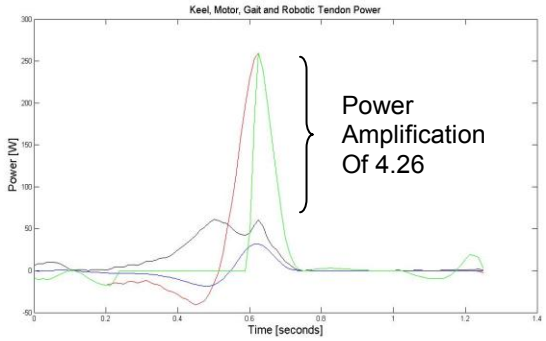

Figure 13. Gait power profile is in red. Power generated by the Robotic Tendon is in green. Motor power is in black and keel power is in blue. Keel and Robotic Tendon power are additive from 20% to 50% in this model. 61W from the motor is enough to output the required 260W for gait, a power amplification of 4.26. (From simulations.)

Simulations show that SPARKy with the variable stiffness model is able to provide 100% of the peak power required during "push-off" while maintaining a gait kinematics similar to able-bodied gait. See figure 14. This figure shows that SPARKy's total motion shown in green provides all of the required plantarflexion and most of the dorsiflexion during the stance phase and all of the dorsiflexion during the swing phase.

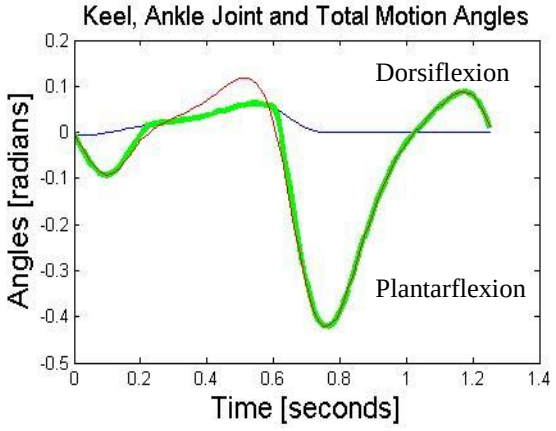

Figure 14. The red line is the ankle joint angle. The blue line is the keel deflection angle. The green line represents the motion of SPARKy as a function of ankle joint motion and keel deflection. (From simulations.)

V. CONCLUSION

Significant advances have been achieved towards computer controlled active transtibial prosthetic devices that can actively support its users in their normal environment and conditions. The Proprio Ankle [29] by Ossur and the MIT's Ankle-Foot Emulator [30] are good examples of the most recent achievements. However, low power and energy density and inadequate control methodology remain as key challenges towards realizing biomimetric devices. We presented in this paper the design and analysis of the Phase 1 SPARKy. We showed that our approach gains kinetic advantages by

Copyright © 2007 by ASME

leveraging elastic energy potential in uniquely tuned helical springs. As the tibia rotates over the stance foot ankle during walking gait, we position the spring to maximize elastic energy storage. We presented a powered orthotic example where we achieved a power amplification of 2.38 with the motor providing 55W and the spring providing the remaining 76W. We presented two models of SPARKy that achieved a power amplification of 3.25 and 4.26 in MATLAB simulation. We also show that SPARKy should be able to provide 100% of the "push-off" power required in walking gait while maintaining gait kinematics similar to able-bodied gait. This is an unprecedented finding because this level of kinetic and kinematic performance may represent the very best in today's transtibial prosthetic technology. Also, as significant is that this level of power amplification brings powered running devices within sight.

The SPARKy team has finished building its Phase 1 device, figure 15. System level subject testing will start June 2007.

Figure 15. The Phase 1 SPARKy on a treadmill during initial testing.

ACKNOWLEDGMENTS

The authors would like to acknowledge the grant that was awarded and administered by the U.S. Army Medical Research & Materiel Command (USAMRMC), under Contract Number: W81XWH-0710193. The views, opinions, findings, information and presentations made do not necessarily reflect the position of the government and no official endorsement should be made. The authors would also like to thank Robotics Group Inc. and Arise Prosthetics for their participation. The authors would like to recognize Peter Rueling of the ASU Mechanical Engineering Shop for his invaluable support. The opinions contained in this publication are those of the authors and do not necessarily reflect those of the funding agency.

REFERENCES

[1] [Online]. Website, URL www.mshirley.com, Marlon Shirley's Personal Site, 2006.

[2] J. Casillas, V. Dulieu, and M. Cohen, "Bioenergetic comparison of a new energy-storing foot and SACH foot in traumatic below knee vascular amputations," Archives of Physical Medicine and Rehabilitation, vol. 76, pp. 39–44, 1995.

[3] S. Rao, L. Boyd, and S. Mulroy, "Segment velocities in normal and transtibial amputees: prosthetic design implications," IEEE Transactions on Rehabilitation Engineering, vol. 6, pp. 219 –226, 1998.

[4] L. Torburn, J. Perry, E. Ayyappa, and S. Shanfield, "Below-knee amputee gait with dynamic elastic response prosthetic feet: a pilot study," Journal of Rehabilitation Research and Development, vol. 27, pp. 369 –384, 1990.

[5] M Linden et la, "A methodology for studying the effects of various types of prosthetic feet on the biomechanics of trans-femoral amputee gait," Journal of Biomechanics, vol 32, pp. 877-889, 1999.

[6] J. Lehmann, R. Price, S. Boswell-Bessette, et al, "Comprehensive analysis of energy storing prosthetic feet: Flex-Foot and Seattle Foot versus standard SACH foot," Archives of Physical Medicine and Rehabilitation, vol. 74, pp. 1225–1231, 1993.

[7] P. MacFarlane, D. Nielsen, D. Shurr, and K. Meier, "Gait comparisons for below-knee amputees using a Flex-Foot versus a conventional prosthetic foot," Journal of Prosthetics and Orthotics, vol. 3, pp. 150 –161, 1991.

[8] K. Postema, H. Hermens, J. de Vries, et al., "Energy storage and release of prosthetic feet. Part 1: Biomechanical analysis related to user benefits," Prosthetics and Orthotics International, vol. 21, pp. 17–27, 1997.

[9] K. Postema, H. Hermens, J. de Vries, et al., "Energy storage and release of prosthetic feet. Part 2: Subjective ratings of 2 energy storing and 2 conventional feet, user choice of foot and deciding factor," Prosthetics and Orthotics International, vol. 21, pp. 28 –34, 1997.

[10] [Online]. Website. Rheo Knee Technical Manual, Ossur Orthopaedic Products and Services Company URL http://www.ossur.com , 2006.

[11] Popular Magazine Article, "Neuro-Controlled Bionic Army," November Issue, 2005.

[12] J. Ward, J. Hitt, T. Sugar, and K. Bharadwaj. "Dynamic Pace Controller for the Robotic Gait Trainer," ASME International Design Engineering Technical Conference & Computers and Information in Engineering Conference, Philadelphia, PA, 2006.

[13] S. Au, P. Bonato, and H. Herr, "An EMG-position controlled system for an active ankle-foot prosthesis: An initial experimental study," IEEE International Conference on Rehabilitation Robotics, 2005.

Copyright © 2007 by ASME

[14] D. P. Ferris, K. E. Gordon, G. S. Sawicki, A. Peethambaran, "An improved powered ankle–foot orthosis using proportional myoelectric control," Gait & Posture, 2005.
[15] I. Pappas, M. Popovic, T. Keller, V. Dietz, and M. Morari. ""A Reliable Gait Phase Detection System,"" *IEEE Transaction on Neural Systems and Rehabilitation Engineering*, vol. 9, pp. 113-125, 2001.
[16] [Online]. Website. Proprio Technical Manual, Ossur Orthopaedic Products and Services Company URL http://www.ossur.com, 2006.
[17] J. Hitt, A. Oymagil, T. Sugar, et al. "Dynamically Controlled Ankle-Foot Orthosis with Regenerative Kinetics: Incrementally Attaining User Portability," Proceedings of the 2007 IEEE International Conference on Robotics and Automation, Roma, Italy, 2007.
[18] M. W. Whittle. *Gait Analysis: An Introduction*, 2 ed. Oxford: Butterworth-Heinemann, 1996.
[19] K. W. Hollander, R. Ilg, T. G. Sugar, and D. Herring. "An Efficient Robotic Tendon for Gait Assistance," *ASME Journal of Biomechanical Engineering*, vol 128(5), pp. 788-791, October 2006.
[20] Kartik Bharadwaj, Kevin W. Hollander, Christian Mathis, and Thomas G. Sugar. "Spring Over Muscle (SOM) Actuator for Rehabilitation Devices," IEEE International Conference on Engineering in Medicine and Biology Society (EMBS), San Francisco, CA, 2004.
[21] H. Herr and R. Kornbluh. "New Horizons for Orthotic and Prosthetic Technology: Artificial Muscle for Ambulation," The MIT Media Laboratory, 2004.
[22] S. Sienko Thomas, C. E. Buckon, D. Helper, N. Turner, M. Moor, J. I Krajbich, "Comparison of the Seattle Lite Foot and Genesis II Prosthetic Foot during walking and running"' Journal Prosthet Orthot., vol. 12, num. 1, pp. 9-14, 2000.
[23] K. Schneider, T. Hart, R. Zernicke, Y. Setoguchi and W. Oppenheim, "Dynamics of Below-Knee Child Amputee Gait: Sach Foot versus Flex Foot," J. Biomechanics, vol 26. no. 10, pp. 1191-1204, 1993.
[24] M. Geil, "Energy Loss and Stiffness Properties of Dynamic Elastic Response Prosthetic Feet," Journal of Prosthetic and Orthotic Science, vol. 13, no. 3, pp 70-73, 2001.
[25] J. Hitt, "Design and Control of a Robotic Transtibial Prosthesis with Regenerative Kinetics," PhD Proposal, Arizona State University, Tempe, Arizona, 2006.
[26] T. G. Sugar. "A Novel Selective Compliant Actuator," *Mechatronics Journal*, vol. 12, pp. 1157-1171, 2002.

Copyright © 2007 by ASME

An Efficient Robotic Tendon for Gait Assistance

Kevin W. Hollander
e-mail: kevin.hollander@asu.edu

Robert Ilg

Thomas G. Sugar

Donald Herring

Departments of Mechanical and Aerospace Engineering,
and Industrial Design,
Arizona State University,
Tempe, AZ 85287-6106

A robotic tendon is a spring based, linear actuator in which the stiffness of the spring is crucial for its successful use in a lightweight, energy efficient, powered ankle orthosis. Like its human analog, the robotic tendon uses its inherent elastic nature to reduce both peak power and energy requirements for its motor. In the ideal example, peak power required of the motor for ankle gait is reduced from 250 W to just 77 W. In addition, ideal energy requirements are reduced from nearly 36 J to just 21 J. Using this approach, an initial prototype has provided 100% of the power and energy necessary for ankle gait in a compact 0.95 kg *package, seven times less than an equivalent motor/gearbox system.* [DOI: 10.1115/1.2264391]

Introduction

An effective form of robotic intervention would be a wearable system that could provide the strength and performance augmentation to a person with motor disabilities. A robotic device could provide strength where there is weakness, respond to stimuli quickly rather than slowly, and a wearable robot could sense problems early, rather than after it is too late.

However, use of the term "wearable" implies that such a robot be portable, lightweight, and safe. In order for such a device to be accessible for home use, the additional implications are that the wearable robot be economical and easy to operate. In contrast, a factory floor robot is none of these things; therefore, simple adaptation of existing technology is not possible. In order to handle the needs of people with motor disabilities, actuated wearable robots that are portable, lightweight, safe, economical and simple to operate are required [1]. These exoskeletons would add power to the system, unlike orthoses that are typically resistive devices.

Well known projects in the area of assisted locomotion are the BLEEX (Berkely Lower Extremity Exoskeleton) robot and the HAL-3 (Hybrid Assistive Leg) robot [2–4]. Both devices are rigidly attached to the wearer and are directly driven, i.e., no compliant interface. The BLEEX robot uses hybrid hydraulic actuators to drive the system, whereas the HAL-3 robot uses dc motors and gearboxes to provide power for movement to the user. In both projects, the same solution is used providing both positive and negative forces to the user to achieve a desired movement pattern. For example in gait, sometimes the robot needs to push the user (positive) and sometimes for support the robot needs to resist the user (negative) and in either case the robot is putting power into the system. In order to meet the demanding requirements stated above, our powered ankle orthosis will include energy conservative, power reducing springs for safety, portability, and regenerative braking.

Contributed by the Bioengineering Division of ASME for publication in the JOURNAL OF BIOMECHANICAL ENGINEERING. Manuscript received August 18, 2005; final manuscript received March 22, 2006. Review conducted by Andrew A. Amis. Paper presented at the 2005 Design of Medical Devices Conference.

Robotic Tendon

Use of the term robotic tendon implies an analogy to human physiology. Mentioned earlier, the simple inclusion of a spring to a linear actuator can provide energy and power savings to the design of a wearable robotic device. The premise of the following development is that the human muscular system uses the advantages inherent in its elastic nature. Those advantages are a minimization of both work and peak power. In terms of an electric motor, minimizing both average and peak power implies the reduction of requirements for motor size and thus weight. Minimizing work implies a reduction of stored energy supply necessary to fulfill the demands of gaits. For a portable robotic system, these are both very important considerations.

The robotic tendon is similar to the devices by Sugar and Kumar [5,6] and Robinson et al. [7]. Each of these devices include a linear actuator in series with a spring. Different from these, our system features a small, lightweight, low energy motor that is used to adjust the position of the spring using a very simple conventional position controller. A heavy, powerful, impedance controlled motor is not needed because it is not the "actuator." The actuator is a spring that is tuned and dynamically positioned for normal gait. Many other mechanical solutions could be used to adjust the position of the spring. A conceptual model of the Robotic Tendon can be seen in Fig. 1.

The stiffness of the spring must be adjusted for different applications such as stair climbing and running. The authors are developing a helical spring that can be tuned dynamically.

In other works, a robotic powered knee, RoboKnee [8], and an active ankle foot orthosis, AAFO [9], have been developed to assist with an individual's gait. Each of these devices feature the linear Series Elastic Actuator [7] as the means of robotic control. The linear series elastic actuator features a helical spring in series with a ball screw mechanism. For the series elastic device, the inclusion of the spring aids greatly in force and impedance control task stability. However, even though the device uses a spring between the actuator and the environment (i.e., human), the compliance of this system is derived mostly from its controller. Based upon the geometry and length of the springs used, very little deflection or compliance would be possible and thus the stiffness of the system is nearly similar to a directly driven system comprising of a lead screw and motor.

It has been well known to the legged robot community that the inclusion of springs in robotics can effectively reduce both the power and energy requirements demanded of an actuator [10,11]. This is because a spring can store and release energy efficiently during cyclic repetitive tasks and the power released from a spring is limited only by the natural frequency and stiffness of the system.

Human Gait. Gait is a reoccurring pattern of leg and foot movements, rotations, and torques. Due to its repetitive nature, the discussion of gait is done in terms of percentages of a gait cycle. A gait cycle is defined for a single leg and begins with the initial contact of the foot with the ground or "heel strike"; the conclusion of a cycle occurs as the same foot makes a second "heel strike." To illustrate a typical pattern of gait, consider the kinematics and kinetics of a normal ankle [12], Fig. 2. Notice that the ankle moment (torque) data is normalized by body weight, kg.

In this figure, peak ankle moment occurs at roughly 45% of the gait cycle and at a value of -1.25 N m/kg. The negative sign represents the physiological direction for which the moment occurs, and in this case, peak moment is acting to move the foot in a toes down direction. At the point at which the peak moment occurs, the ankle angle begins a rapid desent to its lowest overall

 Copyright © 2006 by ASME

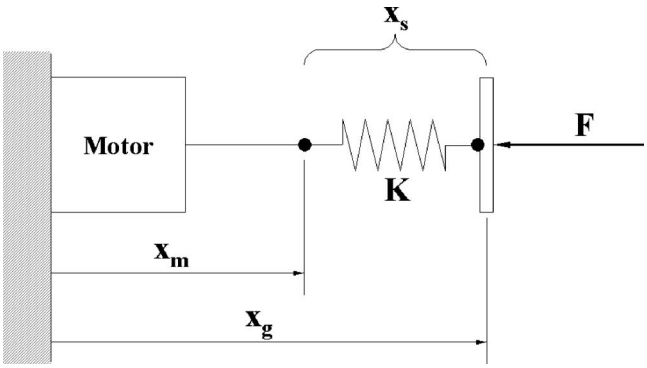

Fig. 1 Robotic tendon model: motor and spring in series

value of −24 deg at 60% of the gait cycle. The region of gait approximately between 45% and 60% of the gait cycle is known as "push off." At the conclusion of "push off," now considered "toe off," the leg initiates "swing" and the foot is then positioned for the next "heel strike."

Analysis of the Robotic Tendon. In contrast to the direct drive example, a spring based actuator design will have very different characteristics. Using the simple model of the robotic tendon in Fig. 1, comparisons to direct drive approaches can be seen. In a direct drive approach, the stiffness K can be considered nearly infinite; thus all of the environmental displacements must come from the linear actuator. In the Robotic Tendon model, the selection of K reduces the energy and peak power requirements of the motor.

From Fig. 1, a development of motor power requirements based upon stiffness K can be derived. The position of the environment, x_g, is given by converting the joint angles of the gait to linear displacement using a simple lever arm. In the model, the position, x_g can be achieved by the compression of the spring and the movement of the motor. It is thus a combination of the position of the motor, x_m, and the position of the spring, x_s, see Eq. (1)

$$x_g = x_m + x_s \tag{1}$$

However, since a spring is a passive device its position is determined by the force, F, applied to it. The force, F, is calculated by converting the moment needed in gait using a simple lever arm. Consider the basic Hookean spring shown in Eq. (2)

$$F = K \cdot \Delta x_s \tag{2}$$

where

$$\Delta x_s = d_o - x_s$$

The free undeformed length of the spring is represented by d_o and is simply an offset value. Solving Eq. (2) for x_s, yields

$$x_s = d_o - \frac{F}{K} \tag{3}$$

The length of the spring is based upon the environmental force and spring stiffness. Equation (3) can be substituted into the equation for environmental position, x_g, and solved for the required motor position, x_m. From this substitution, Eq. (4) is determined.

$$x_m = x_g + \frac{F}{K} - d_o \tag{4}$$

and taking its derivative, yields the velocity required

$$\dot{x}_m = \dot{x}_g + \frac{\dot{F}}{K} \tag{5}$$

Knowing the forces, F, required by the gait cycle and knowing the motor's required velocity, $\dot{x}_m$, the relationship for motor power, P_m, can be obtained. Power is simply force multiplied by velocity, thus multiplying F by Eq. (5) will yield a relationship for motor power,

$$P_m = \left| \underbrace{F \cdot \dot{x}_g}_{\text{gait power}} + \underbrace{\frac{F \cdot \dot{F}}{K}}_{\text{spring power}} \right| \tag{6}$$

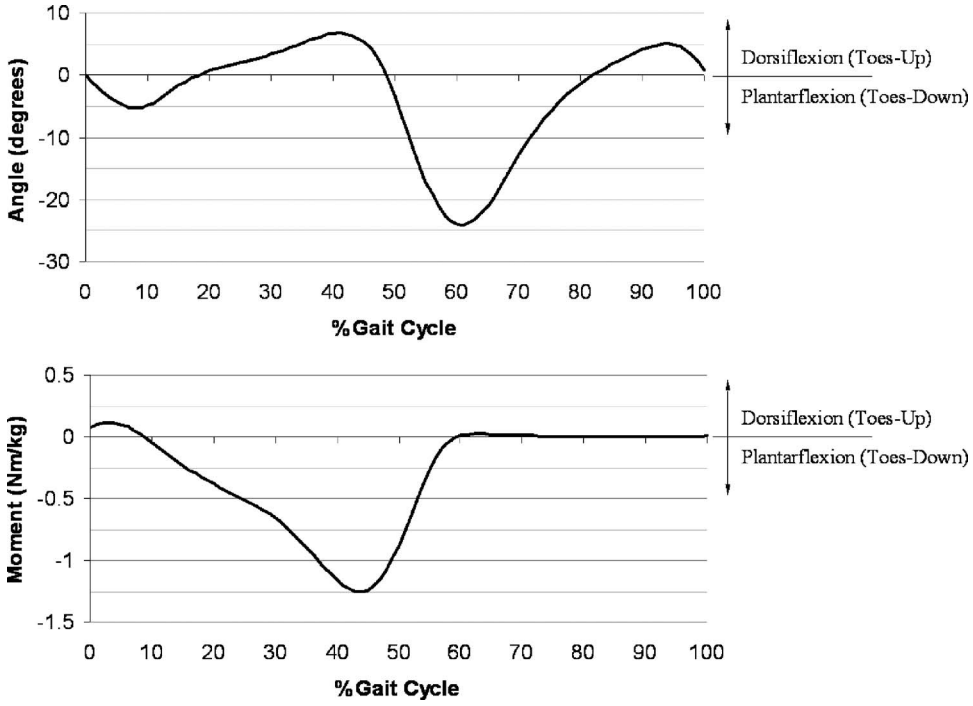

Fig. 2 Normal ankle gait: kinematics and kinetics

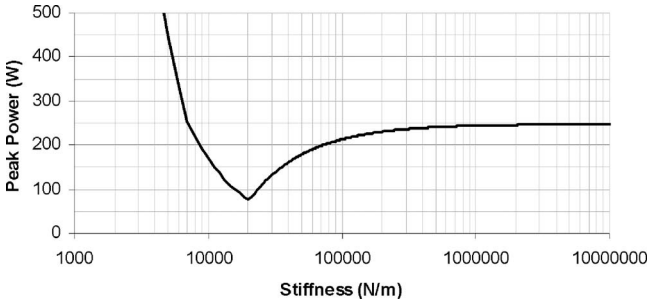

Fig. 3 Optimization of stiffness, *K*

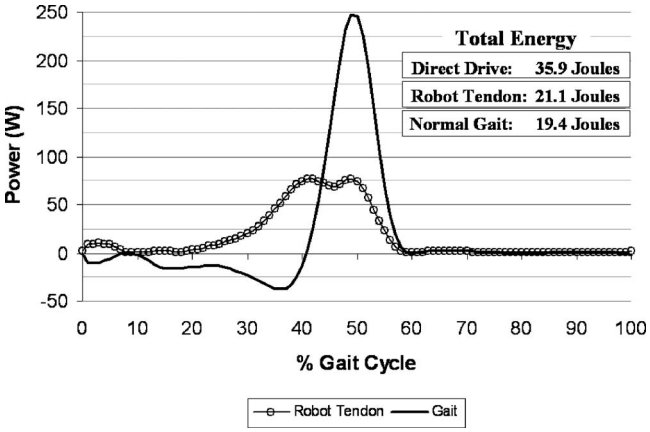

Fig. 4 The power required for the human ankle in gait versus the input power needed for the motor driving the robotic tendon

Human ankle gait power can be both negative and positive. When it is negative, a resistance motion is applied to the ankle, and when it is positive, a propelling motion is applied. A motor unit cannot typically provide negative power; therefore, it must provide power to both resist and propel human motion. For this reason, an absolute value in Eq. (6) is used. In addition, values for force, F, velocity, $\dot{x}_g$ and $\dot{F}$ can all be determined from human gait analysis data. Thus, stiffness, K, becomes the only design parameter.

Consider the case where spring stiffness, K, is nearly infinite (i.e., direct drive). In this example the spring power term drops to zero and the motor must provide the absolute value of normal gait power. In the opposite case, consider a spring with a stiffness near zero.

In this example, the power requirements tend toward infinity. If a straight line is assumed between these two cases, it would appear that a direct drive scenario is the best. Fortunately, this simplistic relationship is not the case. On the contrary, if a spring is properly selected both energy and peak power for the motor required to perform human gait can be drastically reduced compared to the direct drive analogy.

Direct Drive Scenario. In order to evaluate Eq. (6), some assumptions about the human operator and device must be made. For this analysis, consider a 80 kg person, who has a walking rate of 0.8 Hz. Also consider that the lever arm necessary to convert the rotational ankle joint characteristics to linear movements is 12 cm. With these assumptions peak power for human gait is nearly 250 W.

In the angle and moment relationships for human ankle gait, Fig. 2, it can be shown that the highest moments and highest velocities must occur at approximately 50% of the gait cycle. To match the peak power, a motor of significant size and weight would be required. As an example, the Maxon motor RE75 (Maxon Precision Motors, Inc., San Diego, CA) is rated for 250 W continuous power (rated peak power, 393 W) and weighs 2.8 kg not including the weight of a gearbox. Adding an appropriate gearbox would increase the weight by 3.8 kg; this combined weight is no small consideration for a portable wearable device. Although the peak power requirement for gait is high, it is only at this magnitude for the instant at which "push off" is initiated. For the remainder of the gait cycle the power requirements are much more modest. Because gait is a repetitive task, the manufacturer suggested that the power required be matched with the continuous rated power of a motor.

Spring Design. Based upon Eq. (6), the relationship between stiffness, K, and "peak" motor power is considered in Eq. (7).

$$(P_m)_{\text{peak}} = \max \left| F \cdot \dot{x}_g + \frac{F \cdot \dot{F}}{K} \right| \tag{7}$$

Again using the assumptions for our example person, an evaluation of Eq. (7) for a range of stiffnesses can be performed, see Fig. 3.

Figure 3 reveals an interesting relationship. Both extreme cases described earlier can be seen in this figure. At a stiffness value near zero, infinite motor power would be required.

It is seen that a high stiffness spring asymptotically approaches peak gait power near 250 W. However, rather than being a linear relationship between the two extremes, a minimum point or cusp occurs. The driving profile for this plot is determined by a $-(1/K)$ relationship with respect to power. The cusp is created as a function of the absolute value of this factor and hence a minimum is created. For the example problem, an optimal value of stiffness, K, is determined to be 20,278 N/m.

In Fig. 4, the peak motor power is significantly reduced compared to the human ankle gait demands. An optimally chosen spring reduces peak motor power requirements to just 77 W and needs only 21.1 J of energy per step. It is not hard to imagine that the human musculotendon structure may likely be doing something very similar. In contrast, consider that for a direct drive system, the power requirement must be considered as the absolute value of the normal gait curve. Integrating the power of a direct drive system yields the total energy required for each step to be 35.9 J.

The peak power of the robotic tendon actuator is only 31% of that required by the direct drive system. A comparable dc motor for this range of power would be the Maxon RE35, which is nominally rated for 90 W (rated peak power, 206 W) and weighs 0.34 kg. These savings in power, weight and energy translate favorably to requirements demanded by wearable systems.

Prototype Evaluation

Based upon the gait scenario and the design method described above, an ankle robot was constructed that could provide 100% of the strength and power necessary for normal human walking. A sketch of the second generation, powered ankle-orthosis is shown in Fig. 5. The actuator for this robot weighs just 0.95 kg, which is 7 times less than that of an equilvanent direct drive system, i.e., motor and gearbox.

Although the prototype robotic tendon was designed for an 80 kg person walking at 0.8 Hz, testing involved a 65 kg person walking at just 0.5 Hz. This slower rate of walking was chosen purely as a safety measure during initial evaluation. The ankle was immobilized and the powered ankle orthosis positions the ankle as well as supplies the required torque (see Fig. 6).

The results of this evaluation can be seen in Fig. 7. The differences between design and evaluation assumptions are reflected in a lower overall power for gait.

The measured data shown is a single step captured during a walking trial. Notice that the computed ideal power (RT ideal) and

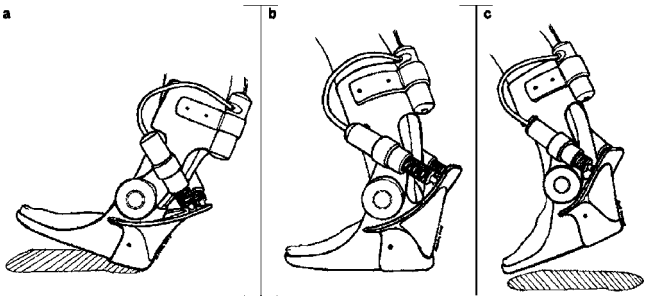

Fig. 5 A second generation, powered ankle-orthosis will be designed using a robotic tendon. In this example, the spring and the power unit are separated for compactness.

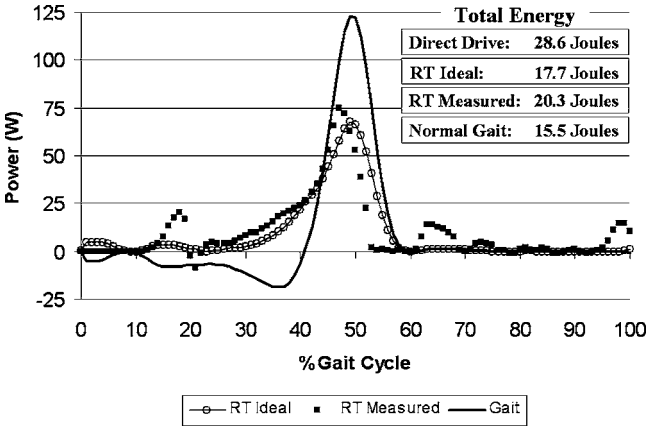

Fig. 7 Power comparison between predicted and measured power of the motor driving the robotic tendon versus the power required for the human ankle in gait

the measured power (RT measured) match very well. The difference in magnitude between these two peaks is a result of friction in the system not considered within the ideal calculations. Also, there exists a slight shift in phase for the measured peak power. This shift is a result of the wearer trying to match the timing of a simple fixed controller used to drive the robot.

Even with frictional losses, the total difference in energy between the ideal and measured cases is minimal. Had a spring stiffness been chosen for the 65 kg person (16,476 N/m), energy required for this system would have approached half of what is predicted for an ideal direct drive case.

Conclusions

To develop wearable robots for human strength and performance augmentation, devices that are *powerful, energy conservative, portable, lightweight*, and *safe* are required. These demands can be difficult to achieve using only traditional robot design approaches. In order to meet all of these listed requirements, the design of a spring-based linear actuator is necessary. In addition to providing a measure of safety, the inclusion of the "correct" spring stiffness can provide significant energy and peak power savings for such wearable robotic devices.

In an ideal example, peak *input* power required by a motor for ankle gait is reduced from 250 W to just 77 W. In addition, the ideal *input* energy requirements are reduced from nearly 36 J to just 21 J. Using the robotic tendon design approach, the initial prototype can provide 100% of the *output* power and energy necessary for ankle gait in a compact 0.95 kg package. This value of weight is 7 times less than that of an equivalent direct drive approach. Not only is weight savings a benefit of reducing motor power, but more importantly, operator safety is improved as well.

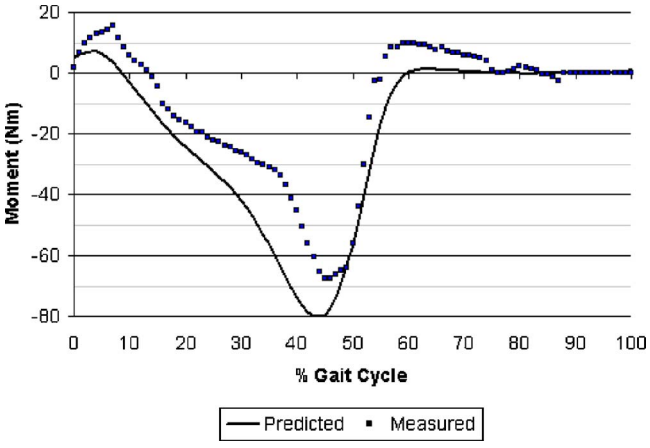

Fig. 6 The predicted moment is calculated from Fig. 2. The measured moment is calculated knowing the deflection of the spring during the gait cycle.

An experimental evaluation of the robotic tendon prototype has validated our analytical predictions. The predicted and measured behavior of an ankle gait assistance device match well, and significant peak power and energy savings are demonstrated.

The "correct" spring stiffness allows the actuator to store energy available from gait dynamics, while allowing that energy to be returned quickly when it is needed.

A robotic tendon actuator allows a wearable assistance device to become a more practical reality to people with motor disabilities. With significant benefits, a robotic tendon actuator can help make wearable robotics a more prevalent part of our near future.

References

[1] Hollander, K. W., and Sugar, T. G., 2004, "Concepts for Compliant Actuation in Wearable Robotic Systems" US-Korea Conference (UKC) CDROM.

[2] (Online), 2004, Website, BLEEX project description, Berkeley Robotics and Human Engineering Laboratory, URL http://bleex.me.berkeley.edu/bleex.htm.

[3] Kawamoto, H., and Sankai, Y., 2002, "Comfortable Power Assist Control Method for Walking Aid by HAL-3," In IEEE International Conference on Systems, Man and Cybernetics, Vol. 4, pp. 6–11.

[4] Kawamoto, H., Kanbe, S., and Sankai, Y., 2003, "Power Assist Method for HAL-3 Estimating Operator's Intention Based on Motion Information," in IEEE International Workshop on Robot and Human Interactive Communication, pp. 67–72.

[5] Sugar, T. G., and Kumar, V. J., 1998, "Design and Control of a Compliant Parallel Manipulator for a Mobile Platform," in ASME Design Engineering Technical Conferences and Computers in Engineering Conference (DETC) CDROM.

[6] Sugar, T. G., 2002, "A Novel Selective Compliant Actuator," Mechatronics, **12**(9–10), pp. 1157–1171.

[7] Robinson, D. W., Pratt, J. E., Paluska, D. J., and Pratt Gill, A., 1999, "Series Elastic Actuator Development for a Biomimetric Walking Robot," in IEEE/ASME International Conference on Advanced Intelligent Mechatronics, pp. 561–568.

[8] Pratt, J. E., Krupp, B. T., and Morse Christopher, J., 2004, "The RoboKnee: An Exoskeleton for Enhancing Strength and Endurance During Walking," in IEEE International Conference on Robotics and Automation (ICRA), pp. 2430–2435.

[9] Blaya, J. A., and Herr, H., 2004, "Adaptive Control of a Variable-Impedance Ankle-Foot Orthosis to Assist Drop-Foot Gait," IEEE Trans. Neural Syst. Rehabil. Eng., **12**(1), pp. 24–31.

[10] Raibert, M. H., 1986, *Legged Robots that Balance*, MIT Press, Cambridge.

[11] Hurst, J. W., Chestnutt, J., and Rizzi, A., 2004, "An Actuator with Mechanically Adjustable Series Compliance," Technical Report No. CMU-RI-TR-04-24, Robotics Institute, Carnegie Mellon University, Pittsburgh, PA, April.

[12] Whittle, M. W., 1996, *Gait Analysis: An Introduction*, 2nd ed., Butterworth-Heinemann, Oxford.